

An Investigation into Vibration Assisted Machining – Application to Surface Grinding Processes

Vaios I. Tsiakoumis

*A thesis submitted in partial fulfilment of the requirements of Liverpool John
Moore's University for the degree of Doctor of Philosophy*

December 2011

The following tables and figures have been omitted on request of the university –

Fig/Tab 1.1 (p.1-3)

Fig/Tab 2.1 (p.2-2)

Fig/Tab 2.5 (p.2-7)

Fig/Tab 2.6 (p.2-10)

Fig/Tab 2.7 (p.2-16)

Fig/Tab 2.8 (p.2-17)

Fig/Tab 3.1 (p.3-4)

Fig/Tab 3.2 (p.3-7)

Fig/Tab 3.3 (p.3-9)

Fig/Tab 3.4 (p.3-10)

Fig/Tab 3.7 (p.3-19)

Fig/Tab 3.8 (p.3-21)

Fig/Tab 3.9 (p.3-23)

Fig/Tab 4.1 (p.4-3)

Fig/Tab 4.2 (p.4-5)

Fig/Tab 4.8 (p.4-12)

Fig/Tab 4.9 (p.4-13)

Fig/Tab 4.20 (p.4-24)

Fig/Tab 11.5 (p.11-5)

Abstract

The purpose of this study was to apply vibrations to the workpiece during surface grinding in order to improve the performance of the process. In addition to this, further necessary parameters were examined and analysed. A first step was to design the vibrating rig and after a number of different designs the most suitable model was selected for the conduction of the preliminary studies. However, a novel-improved system was designed and manufactured in order to undertake the full volume of experimental work. A number of simulations including stress and modal analysis were carried out and all the static and dynamic characteristics of the rigs were identified. Moreover, the exact dynamic behaviour of the rigs - including their natural frequencies - was established through real experiments. Sweep - sine and impact tests were employed in order to identify these dynamic parameters and the results were compared to those of simulation with the intention to detect the amount of error between these techniques. The rigs were vibrated at their resonant frequencies in order to achieve high values of amplitude with low voltage input.

The static and dynamic characteristics of the grinding machine tool were identified. Similar methods such as sweep-sine test were employed in order to find the natural frequency of the machine tool's spindle unit. Static and dynamic stiffness of the machine tool's spindle unit as well as its compliance were identified.

The preliminary studies showed an improvement in surface quality of the workpiece as well as a small reduction in cutting forces. This reduction was getting bigger with the increase of depth of cut. The main body of experimental work followed and showed that for 25 μm depths of cut, the vibration-assisted method could decrease up to 22.5 % the tangential forces. Furthermore, the effect of vibration was getting more noticeable at higher wheelspeeds and workspeeds. At those speeds the reduction in workpiece surface roughness reached 12.6%.

Moreover, it was found that the application of vibration increased the material removal rate, reduced the cutting forces, increased the G-ratio and produced lower values of wheel wear compared to conventional grinding.

Finally, an innovative *closed-loop* vibration control system was used for the process which could control the amplitude and the frequency of vibration in the actual grinding cycle. This

system managed to control the applied values of vibration amplitude at resonant or near resonant frequencies. It was found that for higher depths of cut the *closed-loop* vibration control reduced the normal forces by 19% compared to *open-loop* control and 21% compared to conventional grinding. Furthermore, the *closed-loop* control system performed better in terms of workpiece surface quality when grinding mild steel compared to conventional grinding and open-loop vibration control.

Acknowledgements

First of all, I would like to thank my parents for their support, understanding and endless encouragement through all my studies. Their emotional contribution was vital for the completion of my work.

Special gratitude goes to my director of studies, a special person and a great engineer Dr. Andre D.L. Batako for his theoretical and practical guidance, assistance and patience through all these years. His eagerness and passion to any innovative idea led to absolute success of my project.

Thanks are due to Professor Otar Mgaloblishvili whose immense experience and engineering knowledge solved many problems of this study.

Special thanks go to all technical staff and especially Mr. Peter Moran, Mr. Thomas Scargill, Mr. Mick Noord, Mr. Steve Horan, Mr. Mark Jameson, Mr. Panagiotis Stamatopoulos and Mr. Clive Eyre. Their technical support was significant for the completion of my experimental work.

Finally, I would like to thank my fiancée for her understanding, patience and support throughout my research.

Nomenclature

Symbol	Meaning	Units
a	Applied depth of cut	m
A	Cross sectional area	m ²
a_e	Real depth of cut	m
A_o	Amplitude of forced response	m
b_s	Grinding width	m
b_w	Contact width	m
C	Damping coefficient	N s/m
Cs	Spindle compliance	m/N
d_e	Mean diameter of wheel	m
E	Modulus of elasticity	Pa
e_c	Specific energy	J/mm ³
$F(t)$	Excitation force	N
F'_n	Specific normal force	N/mm
F'_t	Specific tangential force	N/mm
$F_{cutting}$	Cutting force	N
F_H	Horizontal component	N
F_n	Normal grinding force	N
$F_{ploughing}$	Ploughing force	N
$F_{sliding}$	Sliding force	N
F_t	Tangential grinding force	N
F_{tot}	Total force	N
F_V	Vertical Component	N
h_{cu}	Uncut chip thickness	m
h_{eq}	Equivalent chip thickness	m
I	Area moment of inertia	m ⁴
k	Stiffness	N/m
K_m	Grinding machine static stiffness	N/m
K_{res}	Resultant stiffness	N/m
K_s	Wheel system static stiffness	N/m
K_w	Workpiece static stiffness	N/m
L	Flat spring length	m
l_c	Real contact length	m
l_f	Deformation contact length	m
l_g	Geometric contact length	m
m	Mass	Kg
P	Grinding power	W
Q	Material removal rate	m ³ /s
Q'	Specific material removal rate	m ³ /s
R	Coefficient of restitution	-
R_a	Surface roughness	m
R_r	Roughness factor	-
T	Period	s
t	Flat spring thickness	m
t_{gc}	Grain contact time	s
V_s	Wheel speed	m/s

Nomenclature

V_w	Work speed	mm/s
w	Flat spring width	m
$\dot{x}(t)$	Velocity	m/s
$\ddot{x}(t)$	Acceleration	m ² /s

Greek Symbols	Meaning	Unit
ω_{dr}	Driving frequency	Hz
ω_n	Natural Frequency	Hz
Δ	Clearance distance	m
ζ	Damping ratio	-
δ	Logarithmic decrement	-
π	pi	3.14
μ	Coefficient of grinding	-

Abbreviations

APS	Applied Source Method
CBN	Cubic Boron Nitride
CNC	Computer Numerical Control
DAQ	Data Acquisition
FEA	Finite Element Analysis
FEM	Finite Element Method
FFG	Form and Finish Grinding
FFT	Fast Fourier Transform
HEDG	High Efficiency Deep Grinding
HMC	Horizontal Machining Centre
HRB	Hardness Rockwell B (Ball Tip)
HRC	Hardness Rockwell C (Cone Tip)
MQL	Minimum Quantity Lubrication
NDG	Near Dry Grinding
NI	National Instrument
PI	Physik Instrument
PSD	Power Spectral Density
PZT	Piezoelectric lead Zirconate Titanate
RPM	Revolutions Per Minute
SRG	Stock Removal Grinding
Terfenol-D	Terbium(Ter)-Iron(Fe)-Naval Ordnance Laboratory(Nol)-Dysprosium(D)
UAG	Ultrasonic Assisted Grinding
VI	Virtual Instruments
VIPER	Very Impressive Performance Extreme Removal

Table of Contents

Abstract	I
Acknowledgements	III
Nomenclature	IV
Abbreviations	VI
List of Figures	XIV
List of Tables	XX
Chapter 1: Introduction	1-1
1.1 Prologue	1-2
1.2 The Importance of Grinding	1-2
1.3 Novel Grinding Techniques	1-4
1.4 Research Aim	1-5
1.5 Research Objectives	1-5
1.5.1 Anticipated Benefits of Vibration-Assisted Grinding	1-6
1.6 Research Steps	1-7
1.7 Thesis Layout	1-8
Chapter 2: Literature Review	2-1
2.1 Introduction	2-2
2.2 Grinding Types	2-2
2.3 Advanced Grinding Methods	2-4
2.4 Vibration Assisted Machining	2-5
2.5 Vibration Assisted Grinding	2-6
2.4 Ultrasonic Assisted Grinding (UAG)	2-13
2.4.1 Ultrasonic Assisted Machining	2-15

2.5 Harmful Vibrations in Grinding	2-18
Chapter 3: Grinding Background	3-1
3.1 Introduction	3-2
3.2 Grinding Wheels-Abrasives	3-3
3.2.1 Abrasive types	3-3
3.2.2 Grinding Wheel Bonds	3-4
3.2.3 Grinding Wheel Marking System	3-5
3.2.4 Wheel Dressing	3-6
3.3 Grinding Forces	3-8
3.3.1 Grinding Forces and Wheel Wear	3-8
3.3.2 Coefficient of Grinding	3-13
3.4 Process Parameters	3-14
3.4.1 Grinding Power	3-14
3.4.2 Material Removal Rate	3-15
3.4.3 Specific Grinding Energy	3-15
3.4.4 Equivalent Chip Thickness	3-16
3.4.5 Surface Roughness	3-17
3.5 Grinding Kinematics	3-17
3.5.1 Real Contact Length	3-17
3.5.2 Geometric Contact Length	3-18
3.5.3 Kinematic Contact Length	3-20
3.5.4 Contact Zone	3-23
3.5.5 Contact between Rough Surfaces	3-23
3.6 Coolant Application in Grinding	3-25
3.6.1 Types of Fluids	3-25
3.6.2 Benefits	3-26
 Chapter 4: Vibrating Rig-Theory and Design	 4-1
4.1 Introduction	4-2
4.2 Vibration Generators	4-2
4.2.1 Electrodynamical Shakers	4-2
4.2.2 Piezoelectric Actuators	4-4

4.2.3 Terfenol - D	4-6
4.3 Forced Vibration	4-7
4.4 Background to Vibro-Impact Systems	4-11
4.4.1 Dynamic Model of Vibro-Impact System	4-13
4.5 Vibrating Rig Dynamics	4-16
4.5.1 Sweep-Sine Test	4-17
4.5.2 Impact Test – Stand Alone System	4-18
4.5.3 Impact Test – Preloaded System	4-21
4.6 Observation from Impact and Frequency Analysis	4-23
4.7 System Response under Machining Load	4-24
Chapter 5: Equipment	5-1
5.1 Introduction	5-2
5.2 Grinding Machines and Components	5-2
5.3 External Sensors and Devices	5-3
5.3.1 Piezoelectric Actuator	5-3
5.3.2 Dynamometer	5-5
5.3.3 Displacement Sensor	5-7
5.3.4 Surface Roughness Measurement Device	5-9
5.3.5 Surface Texture Analysis Instrument	5-9
5.3.6 Accelerometer	5-10
5.3.7 Data Acquisition System (DAQ)	5-10
5.3.8 Closed-Loop Control System	5-12
5.4 Consumable Products	5-13
5.4.1 Grinding Wheels	5-13
5.4.2 Workpiece Materials	5-13
5.5 Experimental Configuration	5-14
Chapter 6: Design and Simulation	6-1
6.1 Introduction	6-2
6.2 Design Aspects of the Models	6-2
6.2.1 Solid Model with Flexible Hinges	6-2
6.2.2 Table with Cylindrical Springs	6-3

6.2.3 Table with Four Flat Springs	6-3
6.3 Static Analysis	6-4
6.3.1 Meshing Parameters	6-5
6.3.2 Model with Flexible Hinges	6-6
6.3.3 Model with Cylindrical Springs	6-7
6.3.4 Model with Flat Springs	6-8
6.4 Dynamic Analysis	6-9
6.4.1 Simulation Assumptions	6-9
6.4.2 Simulation Parameters for all the Models	6-10
6.5 Frequency - Amplitude Study	6-10
6.5.1 Solid Model with Flexible Hinges	6-11
6.5.2 Model with Cylindrical Springs	6-11
6.5.3 Model with Cylindrical Springs	6-12
6.6 Model Selection	6-12
6.7 Flat Springs System-Analytical Consideration	6-13
6.7.1 Connecting Rod	6-15
6.8 Design Iteration & System Improvement	6-16
6.9 Novel System-Dynamic Characteristics	6-18
6.9.1 Modal Analysis of Novel System	6-18
6.9.2 Novel System-Frequency - Amplitude Response	6-19
6.9.3 Novel System-Analytical Calculations	6-19
6.10 Remarks	6-21
Chapter 7: Grinding Machine System Response	7-1
7.1 Introduction	7-2
7.2 Dynamics in Grinding	7-2
7.3 Natural Frequency of the Spindle Unit	7-6
7.3.1 Spindle Unit Static Stiffness and Compliance	7-7
7.3.2 Dynamic Stiffness of the Spindle Unit	7-12
7.3.3 Frequency Response of the Spindle Unit - Rotating Mode	7-13
7.4 Observations	7-15
Chapter 8: Preliminary Studies	8-1

8.1 Introduction	8-2
8.2 Experimental Configuration	8-2
8.3 Experimental Parameters	8-3
8.3 Results	8-4
8.3.1 Grinding Forces and Specific Forces	8-4
8.3.2 Grinding Force Ratio	8-7
8.3.3 Surface Roughness	8-7
8.3.4 Power Consumption	8-8
8.4 Need for a Novel Design	8-9
8.5 Remarks	8-10
Chapter 9: Effect of Grinding and Vibration Parameters	9-1
9.1 Introduction	9-2
9.2 Effect of Depth of Cut	9-2
9.2.1 Grinding Forces	9-3
9.2.2 Grinding Power	9-4
9.3 Effect of Work Speed	9-6
9.3.1 Grinding Forces	9-7
9.3.2 Grinding Power	9-8
9.4 Effect of Wheel Speed	9-9
9.4.1 Grinding Forces	9-10
9.4.2 Grinding Power	9-12
9.4.3 Surface Roughness	9-13
9.5 Effect of Vibration Frequency	9-13
9.5.1 Grinding Forces	9-14
9.5.2 Surface Roughness	9-16
9.6 Effect of Vibration Amplitude	9-17
9.6.1 Grinding Forces	9-17
9.6.2 Surface Roughness	9-18
9.7 Remarks	9-19
Chapter 10: Effect of Grinding Wheels and Workpiece Materials	10-1
10.1 Introduction	10-2

10.2 Performance of Al ₂ O ₃ (454A 601 L 7G V 3) Grinding Wheel	10-3
10.2.1 Grinding Forces	10-3
10.2.2 Surface Roughness	10-4
10.3 Performance of Al ₂ O ₃ (89A 60 K 5A V 217) Grinding Wheel	10-5
10.3.1 Grinding Forces	10-6
10.3.2 Surface Roughness	10-7
10.4 Performance of Altos (Long Grain-Porous) Grinding Wheel	10-8
10.4.1 Grinding Forces	10-8
10.4.2 Surface Roughness	10-10
10.5 Process Performance by Removed Material	10-11
10.5.1 Wheel Performance in Mild Steel (BS970 080440, HRB 90.1)	10-12
10.5.2 Wheel Performance in En31 Workpiece (BS 534A99, HRC 64.2)	10-13
10.5.3 Wheel Performance in M2 Tool Steel (BS BM2, HRC 62)	10-14
10.6 Specific Material Removal Rate Results	10-14
10.6.1 Mild Steel (BS970 080440, HRB 90.1)	10-15
10.6.2 Hardened En31 (BS 534A99, HRC 64.2)	10-15
10.6.3 Hardened M2 Tool steel (BS BM2, HRC 62)	10-16
10.7 Remarks	10-17
Chapter 11: Wheel Wear	11-1
11.1 Introduction	11-2
11.2 Experimental Description	11-2
11.3 Wheel Wear	11-3
11.4 Material Removed	11-5
11.4 G-Ratio Results	11-7
11.5 Remarks	11-8
Chapter 12: Effect of Closed-Loop Control System	12-1
12.1 Introduction	12-2
12.2 Experiment Description	12-2
12.3 Preliminary Experiment- Medium Grade Wheel (454A 601 L 7G V 3)	
with Soft Steel	12-3
12.3.1 Grinding Forces	12-3

12.3.2 Surface Roughness	12-5
12.4 Soft Grade Wheel (VU33 A 602 HH 10 V B1) with Hardened Steel En31	12-5
12.4.1 Grinding Forces	12-6
12.4.2 Specific Energy	12-8
12.4.3 Surface Roughness	12-9
12.5 Remarks	12-9
Chapter 13: Discussion - Conclusions	13-1
13.1 Discussion	13-2
13.2 Conclusions	13-6
Chapter 14: Recommendations for Further Work	14-1
REFERENCES	15-1
WEB-BASED SOURCES	16-1
APPENDICES	17-1
APPE NDIX - A	17-2
APPENDIX - B	17-5
APPENDIX - C	17-12
APPENDIX - D	17-13

Figure 4. 6: Vibrating Rigs-Design Variations.	4-10
Figure 4. 7: First Concept Vibrating System Configuration.	4-11
Figure 4. 8: Various Arrangements of Vibro-Impact Dampers (Babitsky, 1978).	4-12
Figure 4. 9: Force vibrated System with a Double-Sided Impact (Masri, 1972).	4-14
Figure 4. 10: Linear Single-Sided Impact Oscillator; a) schematics of the oscillator; b) Motion with Time (Babitsky, 1998).	4-14
Figure 4. 11: Phase Portrait of System Motion with Impact (Babitsky, 1998).	4-17
Figure 4. 12: Full System Configuration for the Sweep-Sine Test of the Vibrating Rig.	4-17
Figure 4. 13: Frequency-Amplitude Characteristics for System with Four Springs and Novel System.	4-18
Figure 4. 14: Stand-Alone System Configuration.	4-19
Figure 4. 15: Stand Alone System PSD; a) Four Springs and b) Novel System.	4-19
Figure 4. 16: Stand-Alone Systems; a) Four Spring System, b) Novel System.	4-20
Figure 4. 17: Preloaded System Configuration.	4-21
Figure 4. 18: Preloaded System PSD; a) Four Spring System, b) Novel System.	4-22
Figure 4. 19: Preloaded Systems; a) Four Spring System, b) Novel System.	4-22
Figure 4. 20: Assumed System Motion (Babitsky, 1998).	4-24
Figure 4. 21: System Response under Actual Grinding a) Open-Loop Vibration Control b) Closed-Loop Vibration Control.	4-25
Figure 5. 1: Piezoelectric Actuator and Power Amplifier.	5-4
Figure 5. 2: Experimental Rig for the Dynamometer Calibration.	5-5
Figure 5. 3: Normal Component of Force Calibration Results.	5-6
Figure 5. 4: Tangential Component of Force Calibration Results.	5-6
Figure 5. 5: Displacement Sensor - Specifications.	5-7
Figure 5. 6: Displacement Sensor-Calibration Results.	5-8
Figure 5. 7: Surface Roughness Measuring Device.	5-9
Figure 5. 8: Data Acquisition Program-Front Panel of the Sensors Configuration.	5-11
Figure 5. 9: Closed-Loop Control System.	5-12
Figure 5. 10: Actual Configuration for the Full Experimental Work.	5-14
Figure 6. 1: Solid Model with Flexible Hinges-Design and Dimensions.	6-2
Figure 6. 2: Table with Cylindrical Springs-Design and Dimensions.	6-3
Figure 6. 3: Table with Four Flat Springs-Design and Dimensions.	6-3

List of Figures

Figure 2. 1: Surface Grinding Types (Source: eFunda, 2010a).	2-2
Figure 2. 2: Centred Cylindrical Grinding.	2-3
Figure 2. 3: Internal Diameter Cylindrical Grinding.	2-4
Figure 2. 4: Centreless Grinding.	2-4
Figure 2. 5: Micro-Vibration Device (Zhong & Yang, 2004).	2-7
Figure 2. 6: Schematic representation of the experimental set up (Qu et al, 2000).	2-10
Figure 2. 7: Experimental System for Ultrasonic Vibration Turning (Babitsky et al, 2003)	2-16
Figure 2. 8: Cutting Direction of Applied Ultrasonic Vibration (Moriwaki & Shamoto, 1991).	2-17
Figure 3. 1: Standard Marking System for Conventional Grinding Wheels (Alumina and Silicon Carbide).	3-6
Figure 3. 2: Single-point Dressing of a Conventional Grinding Wheel (Malkin, 2008).	3-7
Figure 3. 3: Three Stages of Chip Generation and Grinding Force Components (Chen & Rowe, 1996).	3-9
Figure 3. 4: Grinding Stages (Alfarez and Elsharkawy, 2000).	3-10
Figure 3. 5: Simple Model of Grinding Forces.	3-12
Figure 3. 6: Analyzed Model of Grinding Forces (Chen & Rowe, 1995).	3-12
Figure 3. 7: The Geometry of the Uncut Chip (Marinescu et al, 2004).	3-19
Figure 3. 8: Applied Power Source Method Configuration (Qi et al, 1997).	3-21
Figure 3. 9: Distribution of the Intensities of Different Grains Acting along the Contact Zone (Qi et al, 1997).	3-23
Figure 4. 1: Schematic Representation of an Electrodynamic Shaker (Lang & Snyder, 2001).	4-3
Figure 4. 2: Piezoelectric Actuator (Source: Physik Instrumente-PI, 2010).	4-5
Figure 4. 3: Forced Vibration of a Single Degree of Freedom Mass-Spring System on a Friction Free Surface.	4-8
Figure 4. 4: Simplified Vibrating Model.	4-9
Figure 4. 5: Frequency-Amplitude Response for Various Spring Stiffness.	4-9

Figure 6. 4: Geometric Contact Length.	6-4
Figure 6. 5: Applied Grinding Forces.	6-4
Figure 6. 6: Meshing Parameters.	6-5
Figure 6. 7: Default Axes Settings in SolidWorks.	6-6
Figure 6. 8: a) Horizontal Displacement. b) Vertical Displacement.	6-6
Figure 6. 9: Model with Flexible Hinges-von-Mises Stress.	6-7
Figure 6. 10: a) Horizontal Displacement. b) Vertical Displacement.	6-7
Figure 6. 11: Model with Cylindrical Springs- von-Mises Stress.	6-8
Figure 6. 12: a) Horizontal Displacement b) Vertical Displacement-Model.	6-8
Figure 6. 13: Model with Flat Springs-von-Mises Stress.	6-9
Figure 6. 14: Stress Analysis-Model.	6-11
Figure 6. 15: Frequency-Amplitude Plot-Model (1).	6-11
Figure 6. 16: Stress Analysis-Model.	6-11
Figure 6. 17: Frequency-Amplitude Plot-Model (2).	6-11
Figure 6. 18: Stress Analysis-Model.	6-12
Figure 6. 19: Frequency-Amplitude Plot-Model (3).	6-12
Figure 6. 20: Flat Spring System Deflection - Component Dimensions.	6-14
Figure 6. 21: Vibrating Rig for Preliminary Studies.	6-15
Figure 6. 22: Frequency Analysis of the Vibrating Rig for Preliminary Studies.	6-16
Figure 6. 23: Four Spring System Irregularity.	6-17
Figure 6. 24: Improvement of the Novel Model.	6-17
Figure 6. 25: Novel Vibrating System and its Exploded View.	6-17
Figure 6. 26: Entire Novel Vibrating System-Experimental Configuration.	6-18
Figure 6. 27: Novel System-Frequency Analysis Results.	6-18
Figure 6. 28: High Stress Concentration Areas.	6-19
Figure 6. 29: Frequency-Amplitude Characteristics.	6-19
Figure 7. 1: Experimental Configuration for Sweep-Sine Test of the Spindle Unit.	7-6
Figure 7. 2: Frequency-Amplitude Characteristics of the Machine Tool Spindle Unit	7-7
Figure 7. 3: Experimental Set-Up for Measuring the Static Stiffness of the Spindle Unit.	7-11
Figure 7. 4: Static Stiffness of the Spindle Unit.	7-11
Figure 7. 5: Dynamic Stiffness of the Spindle Unit.	7-12
Figure 7. 6: Dynamic Compliance of the Spindle Unit.	7-13

Figure 7. 7: Frequency Response of the Wheel-Spindle System at Various Wheel Speeds.	7-14
Figure 7. 8: Wheel-Spindle Vibration at 2880, 3360 and 3840 RPM.	7-15
Figure 8. 1: Four Spring System Experimental Configuration for Preliminary Studies.	8-2
Figure 8. 2: Normal Force - Preliminary Studies.	8-5
Figure 8. 3: Tangential Force - Preliminary Studies.	8-5
Figure 8. 4: Specific Normal Force - Preliminary Studies.	8-6
Figure 8. 5: Specific tangential Force - Preliminary Studies.	8-6
Figure 8. 6: Grinding Coefficient - Preliminary Studies.	8-7
Figure 8. 7: Surface Roughness - Preliminary Studies.	8-8
Figure 8. 8: Power Consumption - Preliminary Studies.	8-9
Figure 8. 9: Four Spring System Irregularity.	8-10
Figure 8. 10: New System.	8-10
Figure 9. 1: Effect of Depth of Cut - Specific Normal Forces.	9-3
Figure 9. 2: Effect of Depth of Cut - Specific Tangential Forces.	9-3
Figure 9. 3: Effect of Depth of Cut - Grinding Power.	9-4
Figure 9. 4: Effect of Depth of Cut - Surface Roughness.	9-5
Figure 9. 5: Effect of Work Speed - Specific Normal Forces.	9-7
Figure 9. 6: Effect of Work Speed - Specific Tangential Forces.	9-7
Figure 9. 7: Effect of Work Speed - Grinding Power Results.	9-8
Figure 9. 8: Effect of Work Speed - Surface Roughness.	9-9
Figure 9. 9: Effect of Wheel Speed - Specific Normal Forces.	9-10
Figure 9. 10: Effect of Wheel Speed - Specific Tangential Forces.	9-11
Figure 9. 11: Effect of Wheel Speed - Grinding Power.	9-12
Figure 9. 12: Effect of Work Speed - Surface Roughness.	9-13
Figure 9. 13: Effect of Vibration Frequency - Grinding Forces.	9-14
Figure 9. 14: Effect of Vibration Frequency - Grinding Coefficient.	9-15
Figure 9. 15: Effect of Vibration Frequency - Surface Roughness.	9-16
Figure 9. 16: Effect of Vibration Amplitude - Grinding Forces.	9-17
Figure 9. 17: Effect of Vibration Amplitude - Grinding Coefficient.	9-18
Figure 9. 18: Effect of Vibration Amplitude - Surface Roughness.	9-18
Figure 10. 1: Grinding Wheel - Workpiece Material Experimental Combinations.	10-2
Figure 10. 2: Specific Normal Force for Al ₂ O ₃ (454A 601 L 7G V 3) Wheel.	10-3

List of Figures

Figure 10. 3: Specific Tangential Force for Al ₂ O ₃ (454A 601 L 7G V 3) Wheel.	10-4
Figure 10. 4: Surface Roughness with Al ₂ O ₃ (454A 601 L 7G V 3) Wheel.	10-5
Figure 10. 5: Specific Normal Force for Al ₂ O ₃ (89A 60 K 5A V 217) Wheel.	10-6
Figure 10. 6: Specific Tangential Force for Al ₂ O ₃ (89A 60 K 5A V 217) Wheel.	10-6
Figure 10. 7: Surface Roughness with Al ₂ O ₃ (89A 60 K 5A V 217) Wheel.	10-7
Figure 10. 8: Specific Normal Force for Altos Wheel.	10-8
Figure 10. 9: Specific Tangential Force for Altos Wheel.	10-9
Figure 10. 10: Surface Roughness for Altos Wheel.	10-10
Figure 10. 11: Measurement of Real Depth of Cut Using a Micrometer Caliper.	10-11
Figure 10. 12: Real Depth of Cut Results - Mild Steel.	10-12
Figure 10. 13: Real Depth of Cut Results - En31.	10-13
Figure 10. 14: Real Depth of Cut Results - M2.	10-14
Figure 10. 15: Specific Material Removal Rate Results – Mild Steel.	10-15
Figure 10. 16: Specific Material Removal Rate Results – En31.	10-16
Figure 10. 17: Specific Material Removal Rate Results - M2.	10-17
Figure 11. 1: Wheel Wear Test Using the Razor Blade Technique.	11-2
Figure 11. 2: Wheel Wear Test Measurement Configuration.	11-3
Figure 11. 3: Wheel Wear with Porous Grinding Wheel.	11-3
Figure 11. 4: Wheel Wear with Medium Grain Medium Grade Wheel (454A 601 L 7G V 3).	11-4
Figure 11. 5: Types of Grains for Porous and Medium Wheel (Jackson, 2008).	11-5
Figure 11. 6: Material Removed with Porous Grinding Wheel.	11-6
Figure 11. 7: Material Removed with Medium Grade (454A 601 L 7G V 3) Grinding Wheel.	11-6
Figure 11. 8: G-Ratio-Porous Grinding Wheel.	11-7
Figure 11. 9: G-Ratio-Medium Grain-Medium Grade (454A 601 L 7G V 3) Grinding Wheel.	11-7
Figure 12. 1: Closed-Loop Control System Configuration.	12-2
Figure 12. 2: Preliminary Experiment-Specific Normal Force Results.	12-4
Figure 12. 3: Preliminary Experiment-Specific Tangential Force Results.	12-4
Figure 12. 4: Preliminary Experiment-Surface Roughness Results.	12-5
Figure 12. 5: Specific Normal Force Results.	12-7
Figure 12. 6: Specific Tangential Force Results.	12-7

List of Figures

Figure 12. 7: Grinding Specific Energy.	12-8
Figure 12. 8: Surface Roughness Results.	12-9

List of Tables

Table 1. 1: Surface Roughness Values for Different Machining Processes (Dagnall, 1997).	1-3
Table 3. 1: Typical Knoop Hardness Values for Abrasive Materials (Ault, 1986).	3-4
Table 3. 2: Bond Types for Different Abrasives.	3-5
Table 4. 1: Overall Results of Vibrating Rig's Natural Frequencies.	4-23
Table 5. 1: Specification of the Abwood 5025 Surface Grinding Machine.	5-3
Table 5. 2: Specifications for the P 212.8 Piezoelectric Actuator and E 472.2 Power Amplifier.	5-4
Table 5. 3: Specifications for the Accelerometer.	5-10
Table 5. 4: Measured Hardness of Workpiece Materials.	5-13
Table 6. 1: Overall Static and Dynamic Analysis Results for all the Models	6-12
Table 6. 2: Natural Frequency Overall Results.	6-21
Table 8. 1: Grinding Parameters for Preliminary Experimental Studies.	8-4
Table 9. 1: Experimental Parameters - Effect of Depth of Cut.	9-2
Table 9. 2: Experimental Parameters - Effect of Work Speed.	9-6
Table 9. 3: Experimental Parameters - Effect of Wheel Speed.	9-10
Table 9. 4: Experimental Parameters - Effect of Vibration Frequency.	9-14
Table 9. 5: Experimental Parameters - Effect of Vibration Amplitude.	9-17
Table 10. 1: Experimental Parameters - Three Grinding Wheels and Three Workpiece Materials.	10-2
Table 12. 1: Preliminary Experiment - Grinding Parameters.	12-3
Table 12. 2: Experimental Parameters Using CLOSED-LOOP Control System.	12-6

Chapter 1: Introduction

1.1 Prologue

The United States spent approximately \$150 billion annually for metal removing operations using conventional machining technology (King and Hahn, 1986). Nowadays, that estimate tends to increase significantly due to the rapid development of novel technologies and further demands for higher quality products.

There are many situations in manufacturing where some parts or products cannot be produced by certain processes due to the required dimensional accuracy for a part or the material used is too hard or too brittle to process. One of the most known methods for producing such a demanding product quality is abrasive machining or a grinding process (Kalpakjian & Schmid, 2010).

1.2 The Importance of Grinding

Grinding is one of the most important processes in the manufacturing field. It is a finishing process which is used to improve the surface finish, and tighten the tolerance on flat and cylindrical surfaces by removing a small amount of material. An abrasive material rubs against the part and removes tiny pieces of material. The abrasive material is typically on the surface of a wheel belt or in liquid suspension. On a microscopic scale, the chip formation in grinding is similar to chip formation in other machining processes such as turning and milling.

The significance of grinding lies in the fact that it can produce very high surface quality meeting almost any requirement of geometric tolerance. Furthermore, the variety of grinding wheels can cover any need for better surface finish in products with complex shape. Table 1.1 shows the values of surface roughness that can be achieved with different machining processes.

Table 1. 1: Surface Roughness Values for Different Machining Processes (Dagnall, 1997).

According to the above table, grinding can achieve lower surface roughness values than most of the processes. Also, it is one of the fastest processes to remove material from hard surfaces and achieving good surface quality at the same time.

Shaw (1996) mentioned that grinding could be divided into two regimes: a) stock removal grinding (SRG) and b) form and finish grinding (FFG). The first regime involves those processes in which the main target is to remove the unwanted material without considering the final surface quality. The second regime involves the operations in which the surface finish of the workpiece is the main concern. During the FFG the grinding wheels should be dressed regularly in order to maintain their sharp edges and form. Furthermore, in order to describe the process better, grinding could be divided into a number of subcategories in terms of the shape of the grinding wheel and the movement of the workpiece. This is presented and examined in details in another chapter.

A grinding process is at times the only method to economically machine some materials very hard to achieve very tight tolerances. Therefore, grinding is employed in construction, automotive and aviation industries for its precision as well as in optics for the production of optical lenses and giant telescope mirrors.

Nowadays, grinding accounts for 20-25% of the total expenditures on machining operations in industrialised countries. But despite its industrial importance, this process is often held in low esteem. Finishing grinding is usually found to be more costly than other machining processes, per unit volume of material removal. Certainly, as stock allowances for material removal continue to decrease, because of the development of precise casting and forging closer to the final configuration, grinding becomes more economical as a single process for machining directly to the final dimensions without the need for prior turning or milling (Malkin, 1989).

1.3 Novel Grinding Techniques

Current manufacturing processes demands for higher machining speeds as well as better quality of the final product have become increasingly challenging. A number of researchers around the world are trying to develop new techniques that accelerate any machining process without sacrificing the quality of the workpieces. All methods that try to enhance the parameters and the performance of each process constitute a new type of machining processes named modern machining. In grinding, because of the complexity and the required accuracy of the process these techniques can be proved vital for the final result. In conventional shallow grinding the work speed varies from 0.5 to 300 mm/s with small depths of cut up to 25 μm . In creep-feed grinding the depth of cut is up to 25 mm but the work speed is as low as 0.1-20 mm/s. However, there is another grinding technique which combines large depths of cut with particularly high work speeds.

Batako and Koppal (2007) using a novel high efficiency deep grinding (HEDG) machine managed to reach 950 mm/s work speed while achieving over 1000 $\text{mm}^3/\text{mm/s}$ material removal rate without damaging the workpiece surface. Nevertheless, they had to employ essential cooling methods in order to avoid high extensive temperature rise and wheel wear.

Cooling and lubrication are two, very essential, aspects in grinding processes. In order to reduce the temperature in the grinding zone without using a large amount of fluid new

cooling methods have been introduced. Minimum quantity lubrication (MQL) (Near Dry Grinding-NDG) method inserts a small amount of fluid into the machining area in the form of an aerosol with the purpose of improving the grinding parameters without wasting huge volumes of coolants and lubricants. It is worth mentioning that in past years MQL has been employed for other machining (e.g. drilling, turning) processes with great success.

Recently studies made by Barczak et al, (2010) and Tawakoli et al, (2010) proved that this technique can be efficient in terms of reducing temperature, grinding forces and grinding power as well as enhancing the surface roughness of the final workpiece.

Finally, one of the latest developments in improving the performance of the process-which is also the purpose of this study-is to introduce micro-vibrations during grinding. The frequency of these vibrations varies from a few Hz to a few kHz in the case of ultrasonic vibrations which will be examined separately later. This vibration can be applied either to the workpiece or to the tool and provides satisfying results in terms of wheel wear, reduction in cutting forces and better surface quality of the workpiece. All these aspects are described thoroughly in the following chapters.

1.4 Research Aim

The main aim of the present research was to investigate and examine the effect of low-frequency superimposed vibration on the workpiece during shallow surface grinding process in order to achieve a better surface quality, higher material removal rates and improved coolant delivery.

1.5 Research Objectives

In this study, the objectives to be achieved in order to characterise the whole process are the following:

- To carry out a basic study of vibration-assisted machining and especially its application in grinding processes. Along with this, a study of various actuators such
-

as piezoelectric actuators, electrodynamic shakers and Terfenol-D materials was necessary.

- Before applying vibration to the machine tool a deep knowledge of its dynamic characteristics was essential. Therefore, a thorough experimental study of the machine tool dynamics was needed.
- Select the range of values of excitation frequencies in order to meet the desired requirements.
- Research and development of the vibrating rig. The rig would accommodate and vibrate the workpiece during the process and its design was based on a number of parameters.
- Static and dynamic characterisation of the vibrating rig.
- Full scale experimental work on vibration assisted surface grinding.
- Vibration-assisted grinding process characterisation.

1.5.1 Anticipated Benefits of Vibration-Assisted Grinding

At this point, the hypothesis put forward is that the introduction of vibration should provide the following benefits:

- Reduction in cutting forces.
- Better coolant delivery over the entire contact zone. The periodic disengagement of the wheel and the workpiece allows the coolant to reach this critical zone.
- Better heat removal from the grinding zone.
- The oscillations of the workpiece allow the grains to cut with more than one edge which can be beneficial to the shelf-sharpening process of the grinding wheel.
- Reduction of the load per grain and therefore, therefore reduced wheel wear.
- Better surface finish due to lapping/polishing effect.

1.6 Research Steps

In order to achieve the present study's desired target a number of specific steps should be followed. A review on the literature as well as a deep knowledge on vibration-assisted machining and vibro-impact theory was carried out. Also, a detailed study on grinding theory was completed in order to recognize the efficiency and limitations of the process. An elaborate study on how the superimposed vibration could enhance the performance of the process and diminish its limitations was made.

The dynamic characteristics of the grinding machine tool as well as its frequency response were identified experimentally using the sweep-sine test while a piezoelectric actuator was exciting the spindle unit. The purpose was to reveal the natural frequencies of the spindle unit and identify the frequency range values where the spindle produced the lowest displacement amplitude. Therefore, the vibrating rig mechanism should be designed with the intention to vibrate at frequencies at the notch of the spindle unit in order to avoid any resonance phenomena.

After a number of different vibrating rigs design the most appropriate for the specific application was selected. The mechanism was designed with the purpose to vibrate at its resonant frequency in order to achieve high values of displacement with low power consumption. Moreover, it was manufactured with the aim to be simple, subject to any modifications and be adaptable to any grinding machine tool. Initially, a number of computational simulation analyses were made in order to examine the behavior of the system under varying loading conditions as well as frequency analyses.

The resonant frequency of the vibrating rig was identified experimentally using different methods such as sweep-sine test and impact test. Next, after choosing and calibrating all the necessary devices and instruments, an experimental set-up was made and the first set of preliminary vibration-assisted grinding experiments were initiated. The aim was to observe the effect of superimposed vibration on the reduction of grinding forces, grinding power and improvement of surface quality. The first results were satisfying but due to some

technical irregularities of the vibrating rig design a novel-improved one was developed and selected to undertake the full volume of experimental work.

In summary in order to achieve the desired research output the following steps were made:

- Obtain a deep knowledge on vibration-assisted machining and especially grinding.
- Justify the potential effects of vibration on the performance of the process.
- Identify the dynamic characteristics of the machine tool in order to choose the desired frequency and amplitude bandwidth for the vibrating mechanism.
- Design the vibrating rig in order to meet the above requirements.
- Conduct experimental work and analyze the results.
- Characterize the process.

1.7 Thesis Layout

The work undertaken in this investigation is presented in fourteen chapters. Chapter 2 presents a comprehensive literature review of grinding process and especially the work of other authors on the subject of vibration-assisted grinding.

In chapter 3 a basic study of the background of grinding is carried out. The most important parameters of grinding are analysed in this chapter in order to obtain a good knowledge of the subject.

Chapter 4 initially describes devices and material that can produce vibration as well as their basic principle of work. Also, chapter 4 introduces how vibration theory can be applied to the present study. Here, the dynamic characteristics of the vibrating rigs designed particularly for the present work are identified.

Chapter 5 presents the equipment employed during the experimental work. This includes the grinding machine, sensors, transducers as well as consumable products such as grinding wheels and workpiece materials. In this section, the actual experimental configuration of this study is illustrated.

Chapter 6 investigates a number of different design models and concludes to the selection of the most suitable for this specific application. Also, a full scale finite element analysis (FEA) as well as a frequency analysis for the chosen model is conducted in SolidWorks and ANSYS software packages.

The machine tool characteristics such as static, dynamic stiffness and natural frequencies are investigated in chapter 7. A number of tests have been conducted to identify the natural frequency of the vibrating rig and its response under varying loading conditions.

In chapter 8 the results of the preliminary tests of the vibration assisted grinding process are presented. This first set of results revealed the positive and negative aspects of the selected oscillating rig. This led to further modification of the design.

A new improved design of vibrating rig was developed and a full scale experimental programme was undertaken.

The main volume of experimental work employing the new vibrating rig is presented in chapter 9. It is shown how grinding and vibration parameters affected the process.

In chapter 10 three different workpiece materials and three different grinding wheels were used to characterise grinding with superimposed vibration.

The next chapter (chapter 11) investigates grinding wheel wear under vibratory grinding.

A closed-loop control system was employed to carry out the last set of experimental work in chapter 12. The results were compared to those of open-loop control and the differences were established.

Chapter 13 provides a detailed discussion of all the experimental work including the simulation results. Key conclusions are drawn here.

Chapter 14 suggests a number of recommendations for further work.

Chapter 2: Literature Review

2.1 Introduction

Despite the wide use of grinding machines and the importance of this process in the machining field, many key problems remain unsolved. The use of micro-vibration on the workpiece, on the tool or on the tool-bed during a machining process and especially in grinding can bring positive results in terms of wheel loading, temperature rise, grinding forces reduction and better surface quality. The studies of this subject are not many but they are very promising and referable. The purpose of this chapter is firstly to explain some basics of grinding as well as to give an insight into the work of key researchers in the area of vibration-assisted machining and especially grinding. Secondly, it is needed to emphasise the problems and disadvantages of this new method and focus on them in order to enhance the performance of the process.

2.2 Grinding Types

There exist various types of grinding depending on the wheel and workpiece shape as well as the motion of the workpiece and the spindle unit.

- *Flat surface grinding*: This type of grinding is used for flat surfaces. While the wheel rotates the workpiece is moving either parallel to the spindle axis (traverse) or across it (plunge). Some other more complex configurations of surface grinding are shown below (Figure 2.1).

Figure 2. 1: Surface Grinding Types (Source: eFunda, 2010).

➤ *Cylindrical Grinding*: This method is used to grind cylindrical parts and is divided into centred and centreless cylindrical grinding. Also, with different wheel configuration it is possible to grind internal cylindrical surfaces. These three subcategories are presented and explained below.

- **Centred**: This type of process is used to shape the outside surface of a cylindrical part which must rotate about its central axis. Depending on the movement of the wheel this process can be divided into traverse or plunge grinding (Figure 2.2).
- **Internal Grinding**: this process is used to grind internal holes of cylindrical parts. Both part and wheel are rotating (Figure 2.3).
- **Centerless Grinding**: This is a cylindrical type of grinding where the workpieces do not require centre holes or fixtures. Only a blade supports the workpieces and they can be inserted and removed with automatic feeding system. However, this process requires a regulating wheel as illustrated in Figure 2.4.

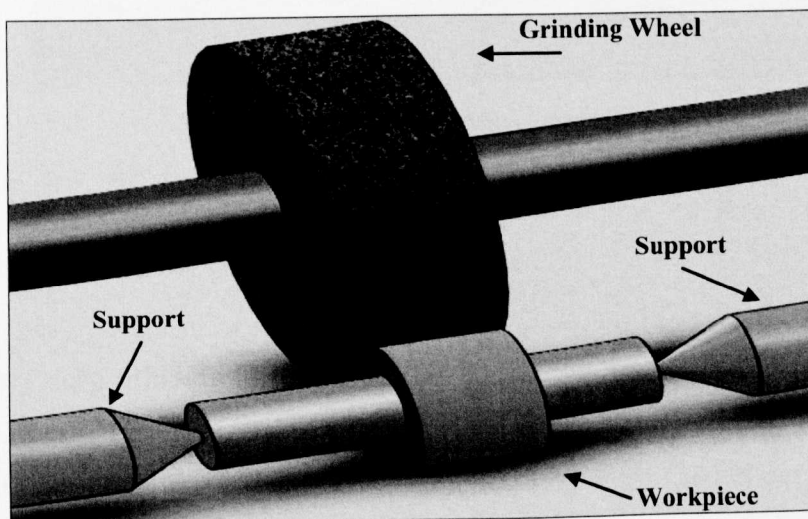


Figure 2. 2: Centred Cylindrical Grinding.

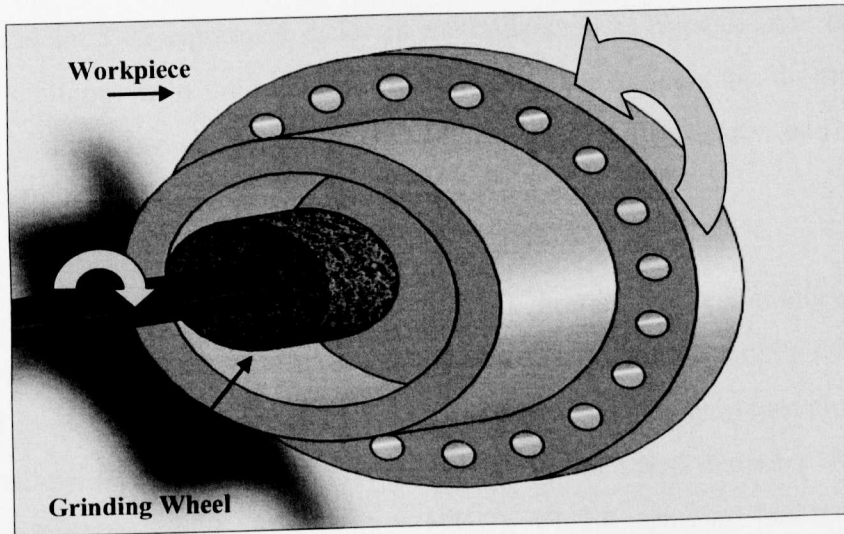


Figure 2. 3: Internal Diameter Cylindrical Grinding.

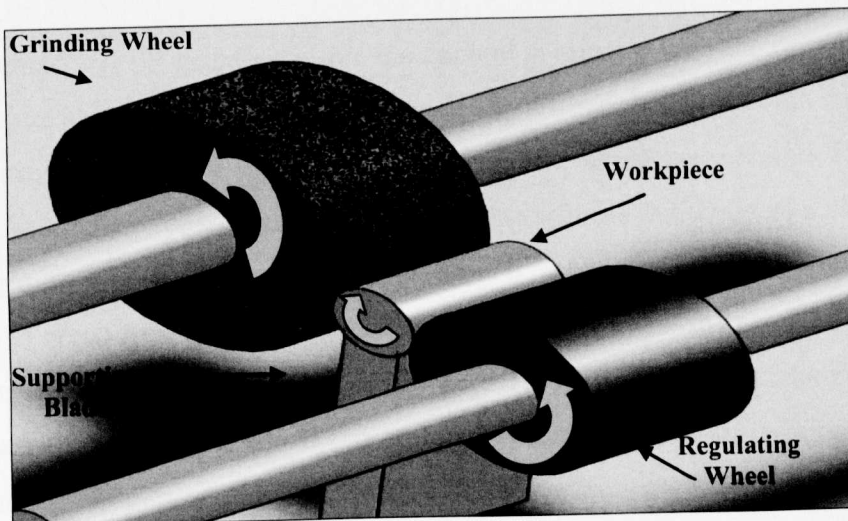


Figure 2. 4: Centreless Grinding.

2.3 Advanced Grinding Methods

High efficiency deep grinding (HEDG) is a novel grinding method which combines very large depths of cut, similar to those of creep-feed grinding, with extremely fast work-speeds and high removal rates. A number of studies have been carried out in this subject area in order to describe this process. Tawakoli (1990) discussed the technological requirements and theoretical principles for this application. According to his experimental results proved that previous practical findings from conventional grinding could not be applied to HEDG because of the complexity of the process.



Also, Batako et al in 2005 employed different methods such as optical, fibre optics and thermocouple techniques with the intention of measuring the temperature during HEDG. Some of these methods proved very accurate when comparing measured and predicted grinding temperatures but others needed further investigation.

Another novel technique is the VIPER grinding (Very Impressive Performance Extreme Removal); developed by Rolls Royce in collaboration with the Grinding Division of Makino-NCMT as a replacement for creep feed grinding of Inconel and other nickel-based alloys. Using inexpensive vitrified aluminum oxidewheels of small diameter mounted in the spindle of a horizontal machining centre (HMC), VIPER grinding has been shown to be 10 times faster at removing metal than milling (Venables, 2006).

The principle behind VIPER grinding is that the coolant is injected onto the grinding wheel under high pressure ahead of the grinding, and centrifugal force then moves the coolant out of the wheel during the grinding, cleansing the wheel and cooling the material. Regarding the wheel, Tyrolit has developed a grinding wheel that performs optimally in a continuous dress VIPER grinding process. Continuous dressing is a process enhancement that was developed for the creep feed grinding process and resulted in increased productivity up to 90 percent over normal and intermittent dress creep feed grinding. Continuous dressing maintains constant pressure between the dressing roll and the grinding wheel, which is adjustable to ensure the proper amount of wheel, is exposed during each revolution. This emergent method can achieve from 150-300 mm³/mm/s specific metal removal rates. (Radical Departures-Advanced Techniques in Aerospace Manufacturing, 2003).

2.4 Vibration Assisted Machining

In 2007 a review of vibration-assisted machining was presented by Brehl and Dow. They mentioned that this procedure combined precision machining with small-amplitude tool vibration to improve the fabrication process. Furthermore, this periodic separation between the tool rake face and the material was related to the observed reductions of chip thickness and of machining forces, which led to improvements in surface finish and extended tool life. Evidently, in their paper they mentioned the effects of this method when the vibration was applied only on the tool in two cases; i.e. one directional when the tool tip was driven

in small reciprocating motion and bi-directional when the tool tip was driven in elliptical motion. In the case of cutting systems where vibration was applied, the frequencies ranged from a few Hz to 40 kHz with amplitudes from 2 μm to 100 μm . In the majority of tests the operating frequency was 20 kHz and the result was a decreased machining time. The machining time is inversely proportional to the material removal rate.

An example of how this method can improve surface roughness and extend the cutting tool life is the work of Chern and Chang (2006) where they applied two-directional vibrations during micro-milling. They combined two piezoelectric actuators with two linear guideways in order to vibrate the worktable along with the workpiece (aluminium alloy). The applied frequency ranged from 500 Hz to 10 kHz with amplitudes of 0, 4, 7 and 10 μm . After a number of micro-milling tests they found that the slot centre and slot surface roughness was improved using mills of 1mm diameter by minimizing the slot width error. Also, the tool life was improved by 22% when vibration cutting applied due to the reduction of heat generated during end milling. However, vibration at high frequencies did not extend the tool life.

2.5 Vibration Assisted Grinding

One of the most recent works was the one of Zhang et al, (2006) where they designed and fabricated a piezo-table that consisted of a parallelogram and a piezo-electric actuator and utilized the piezo-table for vibration-assisted grinding of ceramics. The main aim of their work was to investigate the problems caused by wheel loading and the rise of the temperature in the grinding zone. To prevent the loading phenomenon two techniques were used: a) a high-speed grinding and b) vibration assisted grinding which tends to stop wheel loading and the formation of micro-welding phenomena, reduction friction, facilitate a better coolant delivery to the grinding zone so as to reduce sliding friction and enhance cooling effect.

Syoji (1999) described a very low wheel wear in grinding mild steels at a speed of 200m/s or higher. Mild steels are difficult-to-grind materials which usually wear the grinding wheel out at a rate of over 15 times higher than tool steel when ground with a CBN wheel at conventional speeds.

Zhang's piezo-table was driven by a piezoelectric actuator embedded underneath the top platform of the table and elastic hinges were used to support the platform. During the experimental work the piezoelectric actuator produced 10 μm table displacement at 200 Hz. The final results showed that with the presence of vibration the normal grinding force was reduced as well as the surface roughness. These two variables increased with the increase of depth of cut regardless the vibration assistance. For example the grinding normal force reduced from 50 N to 25 N for a 30 μm depth of cut.

This reduction in normal forces also lead to improved surface integrity and reduced subsurface damage to ceramic materials since increased normal grinding force may initiate and propagate median cracks. (Zhang & Meng, 2003).

It has to be emphasized the fact that the results were obtained after the grinding wheel was used to grind an important amount of work-piece material and was considered to be almost in the 'dull' condition. However, the vibration-assisted grinding did not show an obvious improvement for the freshly dressed grinding wheel in terms of grinding forces.

In 2004, Zhong and Yang also developed a device that could produce micro-vibration to the work-piece during a grinding process. It consisted of two mechanical systems generating micro-vibration in the vertical and horizontal directions. The vertical vibration system had a sample plate and a base plate that was driven by three piezoelectric actuators. The horizontal vibration system had a moving platform and it was also driven by one piezoelectric actuator. The moving platform was fixed on the movable blocks of three linear motion guides and it could vibrate horizontally.

Figure 2. 5: Micro-Vibration Device (Zhong & Yang, 2004).

For vertical vibrations they applied 114 Hz with a 3.3 μm displacement, in the table feed direction they applied 80 Hz with a 5 μm displacement and in the cross feed direction the oscillations were at 66 Hz with a 9.1 μm displacement. A resin bond diamond wheel rotating at 27 m/s (1450 RPM) was used. The results showed that the surface finish of the ground workpiece had been improved and the surface roughness heights of the sample ground with micro-vibration in the table feed direction were better than those without vibration. Specifically, the highest percentage of improvement in surface roughness was observed when the applied vibration had the same direction with the table speed and they were 33 % to 48 % better than those values achieved in conventional surface grinding.

One year later in 2005, Zhong and Rui attempted to improve the performance of the process using the same device (Zhong & Yang, 2004) and modifying some of its parameters. They increased the stiffness of the device and added a new, better power amplifier. The workpieces were single-crystal silicon samples. They applied 90° horizontal, 45° horizontal, 0° horizontal and vertical vibrations at 70 Hz and 30 Hz with displacement values of 3 μm and 6 μm (where 0° is the direction of table-speed). Their study was focused on increased the surface quality of the workpieces. The final results showed that the best surface roughness values were obtained when horizontal vibrations were applied at 70 Hz and amplitude of 6 μm perpendicular to the grinding direction (90°). These results lied on the fact that grinding with microvibrations can produce more ductile streaks than conventional grinding. Increased number of ductile streaks can help reduce the polishing time needed.

Zhang's device (2006) and Zhong and Yang's device (2004) seemed to be similar, however, it is essential to mention that Zhong and Yang's device oscillated the work-piece in vertical and horizontal directions. In Zhang's device the vibrations took place only in one direction along the spindle axis. In that case the excitation force produced by the actuator forced the wheel to cut with two more edges. Also, at this axis neither normal nor tangential force was applied whereas in Zhong and Yang's device the vibration actuators had to push against normal and tangential forces. However, the vibrations applied to three axes but not simultaneously. That is the reason the following work by the same author Zhong along with Rui increased the stiffness of their device and used higher power

amplifiers for their piezoactuators. Also, in Zhang's experiments the work-piece material was ceramic material while Zhong and Yang used silicon samples for his tests.

Vibration-assisted grinding can be proved helpful to avoid any wheel loading phenomena. Zhang and Miller in 2003 examined the loading of the wheel by applying vibration at different frequencies with various amplitudes during dry grinding. They adopted a simple approach for quantifying wheel loading that utilized microscope images and image analysis software. A microscope was used to capture wheel surface images along the wheel circumference. With the help of the software they determined the percentage of chip loading. There are also other methods of measuring the wheel loading such as magnetization, spectroscopy and x-ray fluorescence (Srivastava et al, 1984).

During Zhang and Miller's experiments two different types of aluminium oxide wheel were used at different grinding conditions. The amplitude of vibration was set at $5\mu\text{m}$ while the frequency was increased from 500 Hz to 2 KHz. The depth of cut was set at $25\mu\text{m}$ and $20\mu\text{m}$ while the feed rate was set at 65 mm/s and 50 mm/s respectively for each wheel with a 1018 steel workpiece. They used software to calculate the percentage of chips accumulated in different areas of the wheel.

Their results showed that as the vibration frequency was increasing the wheel loading was decreasing. However, when they tried to increase the amplitude of vibration to $7.5\mu\text{m}$ no serious change at wheel loading results was shown. This may indicate there was a threshold beyond which no additional benefit occurred.

Reviewing Zhang and Miller's work it can be said that the results of their work showed that vibration assisted grinding is beneficial for the life of the tool as it reduces the wheel loading. Nevertheless, in their study, they did not mention how they produced this kind of vibration. They did not present any additional information regarding the exact place where the vibration applied. Also, they did not mention the direction of the external vibrating force. That information could be very useful in understanding the whole process spherically and deriving data for any further work in the future.

In 2000, Qu et al, developed a technique for reducing subsurface damage and/or increasing material removal rate in ceramics grinding. A magnetostrictive actuator adjusted to the workpiece to create the intermittent unloading; although, a damage model showed that intermittent unloading could produce a lateral crack before the median crack fully develops.

Figure 2. 6: Schematic representation of the experimental set up (Qu et al, 2000).

In Figure 2.6 a Pyrex-glass workpiece was vibrated in the Z-direction by the actuator, and a 90° “pencil-point” diamond cutting nib was mounted on the spindle. The table moved in the Z-direction as well. The maximum frequency produced by the actuator was 4.5 kHz and they used low cutting velocities on the order of 100 mm/s. In order to make one scratch with intermittent unloading the actuator extended, modulated and retracted within one spindle rotation. The entire experiment was based on the shielding effect. When the grit first contacts the workpiece the first median crack is produced. After the grit unloads the lateral crack initiates. Reloading the workpiece produces the second median crack. At this instant the lateral crack acts as a barrier against further penetration of the median crack.

Their experimental observations showed a 62% increase in material removal rate (MRR) with minimal associated increase in depth of penetration of the median crack. Alternatively, the experimental results showed that modulations could be used to reduce the depth of median crack penetration by 24% at the same material removal rate (MRR). Additionally, the damage depth increased with an increase in the ratio of cutting speed to

modulation frequency. Finally, both depth of cut modulation and cutting direction modulation were effective in reducing subsurface damage

(Qu et al, 2000).

Wang et al, (1996) implemented a high-frequency micro-actuation system for vibratory modulation in the grinding process of ceramic materials. This vibratory movement of the workpiece in the cross feed direction reduced the surface roughness in this direction and therefore the overall surface roughness. The tests carried out in a conventional surface grinding machine to demonstrate the viability of this method. The results showed that the workpiece quality was improved as well as the grinding efficiency.

Orynski and Bechcinski in 2003, in their attempt to avoid wave regeneration effect in plane surface grinding, introduced a high frequency external forced vibration on the spindle of the machine in a parallel direction to the cutting speed V_w . Their aim was to determine the influence of forced vibration with different parameters on workpiece surface roughness and waviness. The frequency of vibration was 100 Hz for 20 μm depth of cut. The amplitude of vibration was set to 30 μm and the workspeed velocity was 166.6 mm/s. The study consisted of measurement of roughness and waviness of surface in grinding with and without sparking out.

The obtained results did not show any major difference in surface roughness and waviness during grinding without spark out. However, with spark out grinding, the application of vibration had been proved beneficial for the surface waviness which was decreased by half.

In 1994, Hanasaki introduced vibration in a creep-feed grinding process in order to prevent formation of burn marks on the work-piece. The vibration frequency that introduced was low (30Hz) and the amplitude was in range of 0 to 1.5 mm. The tests showed that vibratory creep-feed grinding is effective for the prevention of the burn mark. However, the wheel wear in vibratory creep feed grinding became larger than that in the conventional method. Also, in down-cut grinding, more grinding fluid was supplied to the wheel work-piece contact area and both, radial wheel wear and vertical grinding forces increased with the increase of depth of cut.

A higher vibration frequency (400Hz) was applied by Poletav and Khrul'kov in 1990 during their study in intermittent grinding method of hardened nickel alloy. Their main target was to reduce thermal stressing of the workpiece cracking and surface burning.

Another considerable use of vibration is in automatic precision polishing. Yin and Sinmura in 2007 developed three modes of vibration-assisted magnetic abrasive polishing process. The principle of working of this process was simple. The magnetic pole rotated while the work-piece was vibrated. First the magnetic abrasives were brought in the machining clearance between the tip of the magnetic pole and the workpiece. Next, these abrasives were attracted by the magnetic pole and rotated together. A cam was used to vibrate the table beneath the workpiece. The target of the work was to present and illustrate the effects of vibration of the workpiece on the magnetic field, and the polishing pressure. Also, they tried to produce better finish surfaces. Their results were based on three set of experiments. The first was with vibration in the vertical axis, the second in the horizontal axis and the third in both axes simultaneously. For their third set of experiments they applied a vibration of 3 mm horizontally and 1 mm vertically amplitude in a frequency of 6 Hz for both directions. The workpiece material was stainless steel SUS304 38 x 60 mm and 1.2 mm thickness. The results showed that when the vibration was applied horizontally and vertically simultaneously the surface was improved from 0.35 μmRy to 0.25 μmRy in X direction and 0.32 μmRy in Y direction. When the vibration was applied only in the vertical axis the surface was rougher than the one without vibration. Regarding the polishing pressure they found that when the vibration was applied only vertically the pressure was increased with higher polishing efficiency but with a rougher surface. Also, the vertical directional vibration could help to promote the relative motion of magnetic abrasives against the mechanical surface and pressure distribution uniformity in the polishing zone a smoother surface may be obtained. However when the vibration was applied both vertically and horizontally a better surface finish was achieved with high polishing efficiency.

Similar work has been presented by Sinmura and Takeshi in the past (1997) introducing horizontal vibration-assisted magnetic abrasive polishing in which the workpiece was vibrated in the horizontal direction only. After obtaining some promising results from that work, they continued their tests by applying vibration into more than one axis.

Also, Natsume (1998) used the same method to polish grooves of stainless steel in order to explore surface polishing characteristics and mechanisms of the polishing mode.

2.4 Ultrasonic Assisted Grinding (UAG)

Another effective way to apply micro-vibrations either on the workpiece or the tool is the use of ultrasonic technology. It is widely used not only for grinding but for other machining processes such as turning and milling. The process begins with converting a high-frequency electrical signal into a vibratory motion. This motion is transmitted through a metal tool-holder and cutting tool assembly. Many authors have worked upon this subject with exceptional results.

One of the most recent works was carried out by Liang et al (2010) where they induced two-dimensional ultrasonic vibrations (close to 22 kHz) in grinding with the purpose of achieving high material removal rate and better quality of the final surface of monocrystal silicon samples. They combined and synchronised two ultrasonic vibrators to accomplish an elliptical motion of the workpiece. Also, when they applied two alternative current voltages with a different phase the system could also, vibrate vertically (bending vibration). The piezoelectric ceramic devices they used, were excited at the resonant frequency of the vibrator. They achieved up to 20% reduction in cutting forces with axial ultrasonic assistance and up to 50% decrease in cutting forces with vertical vibration mode than conventional grinding. Moreover, the surface roughness was decreased by 10-30 % in the presence of ultrasonic vibration. Frictional effects were reduced due to interrupted contact of the grains and the workpiece.

In 2008, Tawakoli and Azarhoushang developed an ultrasonic vibration system in order to improve the performance of the grinding process. Their set-up consisted of a transducer with piezoceramic rings which was driven by an ultrasonic power supply that converted 50 Hz electrical supply to high frequency electrical impulses. These impulses are fed to the transducer and transformed into mechanical vibrations of ultrasonic frequency (23 kHz). The vibration amplitude was amplified by a booster and transmitted to the workpiece through a horn. All their experiments were carried out in a dry grinding environment. The

reason was that they intended to decrease the negative environmental impact of the cutting fluids and reducing manufacturing cost. Some of the machining parameters they used were: Al_2O_3 grinding wheel, soft steel (100Cr6) workpiece material, depth of cut 10-30 μm , feed speed at 500-1000-1500-2000 mm/min and cutting speed of 60 m/s. Regarding the vibration parameters they applied a 23 kHz frequency with a 10 μm amplitude. Their final results showed 70 % reduction in normal forces and up to 50 % in tangential grinding forces. Also, a significant improvement in surface roughness and in grinding wheel wear was achieved.

Zhang, Zhang and Huo, (2006) used ultrasonic technology to produce vibration during a grinding process along the axial direction. The reason of using this method was because many materials appear high performances such as high hardness, wear ability and brittleness and most of the times it is very difficult to machine them by traditional machining methods. The results showed that higher vibration amplitude and frequency was helpful in decreasing the grinding force. Also, the reduction in grinding forces was proportional to the wheel speed.

Spur and Holl (1996) also applied ultrasonic assisted grinding technology for ceramic materials using frequencies from 20 to 25 Hz. For creep feed grinding this method provided reduced normal forces at slightly increased wheel wear and surface roughness. Moreover, it served to increase the impact effect and accelerate the material removal rate as well as it could effectively improve the ground surface quality and reduce subsurface damage. During their experiments the high contact pressures had also a positive effect on the material removal rate for ultrasonic assisted grinding. This was because of the longer and effective contact between the grit and the workpiece. However, they observed that a contact pressure greater than 2 N/mm^2 could cause chatter during the process resulting in a disastrous failure of the tool. High contact pressures led to increased pulse duration which produced more cracks that resulted in higher material removal rates.

Another author who worked on the ultrasonic creep-feed grinding of ceramic materials is Uhlmann in 1998. He applied vibrating active motion on the workpiece where the motion changes its direction at amplitude of about 4 μm sinusoidally in relation to time with an ultrasonic frequency of approximately 22 kHz. The wheel speed was set at 35 m/s and the

table speed feed was set at 300 mm/min with a 1mm depth of cut. He analysed scratch structures of the Nitride and Zirconium Oxide materials with and without the presence of ultrasonic vibration. Scratching without ultrasonic assistance revealed complete traces with display predominantly areas of plastic deformation on the bottom of the scratch, while traces of various single cutting edges are partially visible. With ultrasonic vibration the trace divided into local single scratches due to repeated periodic oscillations of the workpiece and they are characterised by plastic deformations. Also, the friction effects on the active areas were clearly reduced at the same time. This led to a significant decrease in thermal loads and a reduction in process forces.

Close to the surface, the ground ceramic materials showed in all cases compressive residual stresses parallel to the grinding direction, with higher values measured for ultrasonic assistance. This could be explained by higher mechanical impulse-like alternating loads and partially higher depths of indentation, as well as lower thermal loads. Compressive residual stresses were seen as positive in this context, because they counteracted to a crack extension (Spur & Holl, 1997).

2.4.1 Ultrasonic Assisted Machining

The application of ultrasonic vibration is widely used not only during grinding but in other machining processes such as turning, drilling and milling. One of the most referable works is the work of Babitsky et al, (2003) in which they applied ultrasonic vibrations to the tool during turning process of aviation materials. The vibration was applied to the cutting tool along the feed direction. In previous works of the same authors the vibration was applied on the tangential and radial direction as well with excellent results. The next picture (Figure 2.7) shows the configuration of the ultrasonic transducer).

Figure 2. 7: Experimental System for Ultrasonic Vibration Turning (Babitsky et al, 2003).

In that case when the applied vibration was along the feed direction they had to consider the fact that the feed velocity should be less than the critical feed velocity a parameter which is determined by the frequency and amplitude of the vibrating system. For that reason when they applied 0.05 mm/rev feed rate and 20 m/min cutting speed for a 38 mm diameter workpiece the feed velocity became 0.0084 m/min. The critical feed velocity of the vibrating system was 25.64 m/min. The frequency of the ultrasonic vibration was 17 kHz with a 20 μm peak to peak tool displacement during turning of mild steel, Inconel-718 and C-263. Their results showed serious improvement of 25-40% in surface roughness and up to 40% improvement in workpiece roundness compared to conventional turning.

Another discussed work is this of Moriwaki and Shamoto (1991) where they applied ultrasonic vibration in for diamond turning of stainless steel. The vibration could be applied to three possible directions. These were the cutting direction, the thrust direction and the feed direction. In their experiments they applied ultrasonic vibration only in the cutting direction. Figure 2.8 depicts the cutting direction where vibration was applied. The cutting speed is (v) and (a) is the amplitude of vibration. Moreover, the ultrasonic vibration was applied at various feed rates.

Figure 2. 8: Cutting Direction of Applied Ultrasonic Vibration (Moriwaki & Shamoto, 1991).

Because of the excessive wear of diamond tools they could not be used as tools for machining steel. However, Masuda (1986) used single crystal and sintered CBN tools to achieve ultra-precision turning of steel. These types of tools have low chemical activity with iron. Their efforts did not lead to satisfy long tool life and good surface quality.

Moriwaki and Shamoto, applied 40 kHz vibration frequency to the diamond tool tip, which is twice as high as that of conventional ultrasonic vibration cutting in order to reduce vibration marks of the finished surface. The amplitude of the vibration was 3 μm and the tool tips were made of synthetic crystal diamond and precisely ground. The maximum vibration speed was 45 m/min. regarding

Their results revealed that the tool wear was not significant through a series of tests and obtained with the same cutting tool. The better surface finish was obtained at the smaller feed rates and a quality surface of 0.026 μm R_{max} was reached at feed rate of 3 $\mu\text{m}/\text{rev}$. However, the regular vibration marks were still visible as well as the feed marks.

Mitrofanov et al, (2003) created a finite element model and induced a high frequency vibration of 20 kHz with amplitude of 10 μm in order to simulate ultrasonic vibration during turning process. The main aim of their study was to improve the process and decrease the cutting forces, heat, and noise radiation. The developed finite element model

showed the formation of the chip and the von-Mises stresses along the surface of the workpiece during conventional and ultrasonic vibration.

During their experiments, they designed a prototype of ultrasonically assisted cutting device with auto-resonant control system (Babitsky, 1995) for turning Ni- and Ti-base super-alloys. The auto-resonant control provided the possibility of self-tuning the system to keep the resonant mode of oscillations under variable conditions. A 60 mm/s cutting speed and a 0.1 mm depth of cut were applied in Ni-base cutting process. After conventional turning a transformed surface layer about 25 μm thick was observed, whereas there were no visible alterations in the surface layer structure for ultrasonic turning.

2.5 Harmful Vibrations in Grinding

In the grinding process - as in other machining processes - vibration is considered as detrimental to the cutting process and causes undesirable results in surface quality and loading phenomena in grinding wheels. There are two types of unwanted vibration, forced and regenerative vibration.

Forced vibrations are caused by unbalanced and out of eccentricity of the wheels. Other possible sources of forced vibrations could be from hydraulic devices and from floor vibrations which are difficult to detect and eliminate (Gawlak, 1984).

The regenerative vibration (chatter) in cylindrical grinding is caused by the rotational motion of the workpiece. The generated waves on the workpiece surface are caused by the relative vibration of the wheel and the workpiece. This phenomenon leads to the change in depth of cut after one revolution of the workpiece and also can make the process critically unstable (Marinescu et al, 2007). A number of authors have tried to detect analyse and suppress these types of vibrations with satisfying results.

There seems to be general agreement with Oczos et al, (1986), and Chen and Rowe (1996) that this vibration influences the quality parameters of machined surface spoiling its finish or increasing the values of shape error. Also, it is particularly harmful because it changes the local cutting conditions and produces an error which is very difficult to measure, although well seen with a naked eye.

In centreless grinding Albizuri et al. (2006) presented a method to reduce vibrations which cause the instability for the machining process, bad surface quality and a serious wheel wear. They developed a system using piezoelectric actuators which gives a fast response in the presence of cutting force variations during the process. After several tests it was concluded that the active control system could be used to modify the dynamic characteristics of the machine increasing the stable operating range and reducing the vibration.

Another very important consequence of vibration during grinding process is chatter. Mannan et al. in 1999 presented a time domain model of plunge grinding operation and allowed for the effects of three modes of vibration. The simulation results confirmed that torsion could be very significant. However, the torsion mode involving the workpiece showed that the build up of vibration was affected but not stopped. In fact, they developed a model which could be proved useful for future work in suppressing chatter on grinding process.

A similar model has been developed by Taskesen and Ercan in 2003 - in two different studies - with one and two degrees of freedom to analyze the machine tool vibrations. Two years later, they developed a software package that could analyze machine tool chatter vibrations. The software using data inputs such as tool geometry, machine tool properties, workpiece material and cutting parameters could predict cutting forces, tool vibrations shear angle and chatter in turning, milling, drilling and grinding process (Taskesen & Ercan, 2005).

Chapter 3: Grinding Background

3.1 Introduction

Manufacturing makes ever increasing demands for higher machining speeds. This is particularly true in car and aircraft production but also for cutting tools. Parts such as high-speed cutting tools crankshafts, turbine blades and drill bits are all manufactured by grinding. Abrasive machining is a major element in manufacturing, making up approximately 20-25% of all processes. Grinding wheels are mainly made from aluminium oxide and cubic boron nitride (CBN) abrasives. The production of aluminium and silicon oxide for grinding wheels is one of the most energy intensive processes known. Therefore the basic process itself, before any cutting is even undertaken, represents a considerable environmental cost. In shallow and creep-feed grinding, the specific grinding energy is often high even at modest material removal rates; (e.g. in creep-feed grinding of nickel-based alloy the specific energy is 400 J/mm^3 for $150 \text{ mm}^3/\text{mm}$ of material removal). Much of this power is converted into heat. Therefore, to avoid high temperatures and ensuing workpiece damage, effective coolant supply to the contact zone between the wheel and the workpiece is critical. High pressure, and hence high power, coolant supply systems are used to penetrate the air barrier around the grinding wheel. This coolant also requires energy in its manufacture and poses serious environmental issues in its disposal. Recent research by the UK government (Envirowise, 2007) has shown that the purchase, management and disposal of metal working fluids (including processes other than grinding) accounts for approximately 15% of the overall manufacturing costs. This statistic shows that the efficient use of coolant can be an effective cost saving tool as well as being environmentally responsible. Further to this, 10% of the UK total oil sales for 1999 (approximately 1,000,000 tonnes a year) can be attributed to the metalworking industry, (e.g. £26 to dispose of 200 litres of used coolant). So it can be seen that a 5% reduction in machining coolant would save approximately 7,200 tons a year with the associated impact on the environment. Current grinding practice, whilst a vital manufacturing process, is clearly not environmentally friendly.

3.2 Grinding Wheels-Abrasives

Grinding wheels consist of small grains of abrasive material bonded together in different ways according to the requirements of the application. Currently on the market there exist a wide range of abrasive materials as discussed below.

3.2.1 Abrasive types

There are two main types of abrasives, natural and synthetic.

Natural abrasives

Emery, sandstone, garnet, flint, corundum and diamonds belong to natural abrasives. Generally most of these abrasives are not used in grinding wheels due to their lack of durability to withstand grinding pressures, except diamond. Emery is often preferred for use as an abrasive on coated cloth and paper as well as in many buffing compositions and it is no longer used in making grinding wheels.

Diamond is classified as both natural and synthetic abrasive. Natural stones that are unsuitable for gems are entitled as borts. Next, they are crushed down into a series of sizes for abrasive use. Diamonds have the highest hardness and require a unique bond which is more specialized than that of conventional grinding wheels.

Synthetic abrasives

Conventional: These are artificial abrasives that are mostly used in industry covering almost all the needs for grinding wheels.

- Aluminium oxide (Al_2O_3) belongs to conventional abrasives and it is the most commonly used. It is the softest of this group and is used to grind ferrous materials.
- Silicon Carbide (SiC) is commonly used for grinding non-ferrous materials. It is the hardest of the conventional abrasives but it has less impact resistance than aluminium oxide.

3. Grinding Background

- Zirconia alumina is used for rough grinding metals and particularly ferrous alloys as it has the highest impact resistance of all the conventional abrasives.

Superabrasives: Diamond and cubic boron nitride (CBN) belong to this group of abrasives.

- Diamond has the highest hardness of all the abrasives and is used to grind carbides, ceramics, glass and other materials.
- Cubic Boron Nitride (CBN) is a man-made abrasive. It is used to grind ferrous materials such as steels and alloys. Compared to diamond abrasives it is impact resistant, heat resistant and chemically less active (Ault, 1986).

The table below (Table 3.1) shows the typical Knoop hardness value for each type of synthetic abrasive.

Table 3. 1: Typical Knoop Hardness Values for Abrasive Materials (Ault, 1986).

3.2.2 Grinding Wheel Bonds

There are different ways that the grains of these abrasives are held together to form the shape of the wheel. The significance of the bond lies on in the fact that is must be strong to withstand the grinding forces pressures and temperatures. There are different groups of bonds for conventional abrasive wheels and for superabrasive wheels. The table next (Table 3.2) depicts these types of bonds used for both groups.

Conventional Abrasive Wheels	Superasbrsives Wheels
Resinoid	Resinoid
Shellac	Vitrified
Oxychloride	Metal
Rubber	
Silicate	
Vitrified	

Table 3. 2: Bond Types for Different Abrasives.

Most of the conventional wheels have either vitrified or resinoid bonds. Nearly half of the grinding wheels used today are vitrified. Vitreous bonds are made of mixtures of feldspar, clay and a frit and generally used for Alumina wheels. Resinoid-bonded wheels are produced by mixing abrasive grains with phenolic thermosetting resins and plasticizers, molding to shape and curing at 150-200°C. Rubber bonds consist of vulcanised natural or synthetic rubber. Silicate-bonded wheels are manufactured by mixing sodium silicate with abrasive, tamping in a mold, drying and baking. Shellac is a natural organic material which is rarely used as a bond material. Oxychloride is cold-setting cement, from a mixture of magnesium oxide and an aqueous solution of magnesium chloride (Malkin & Guo, 2008).

Superabrasive wheels also use vitrified and resinoid bonds. However, metal bonds are used only with superabrasive wheels. The most common are from sintered bronze, which are produced by powder metallurgy methods. Another type of metal bond is electroplated. The electroplated wheels consist of a single layer of diamond or cubic boron nitride (CBN) held in place on a form or hub by an electroplated nickel binder. These wheels have become widely used especially in automotive and aerospace industries for grinding metallic parts (Malkin & Guo, 2008).

3.2.3 Grinding Wheel Marking System

Every grinding wheel has its own identification marks consisting of letters and numbers. The purpose of these symbols is to identify and characterize the wheel in terms of its material, bonding type, grain size etc. According to the American national standard system

3. Grinding Background

of the wheel, the cutting edges of the grains become dull, the surface of the wheel becomes flat and it rubs more against the material workpiece instead of cutting.

In truing, material is removed from the surface of the wheel in order to correct the eccentricity of the wheel shape. Also, during this process the metal stuck on the surface of the wheel – clogged wheel – is cleaned out and new sharp cutting edges of the grains are obtained. Dressing method is truing the wheel and conditioning the surface of the wheel in order to cut according to the process requirements. In conventional abrasive wheels, both truing and dressing are usually done by the same process called dressing. However, in superabrasives truing and dressing may be different kind of operations and in some types of superabrasives no dressing is required. The picture below (Figure 3.2) illustrates schematically a single point dressing operation of a conventional wheel.

Figure 3. 2: Single-point Dressing of a Conventional Grinding Wheel (Malkin, 2008).

Where a_d is the dressing depth, v_d is the crossfeed velocity of the dressing tool, d_s is the wheel diameter and V_s the wheel speed. There are also different methods of dressing such as multipoint diamond dressing and rotary diamond dressing for specific applications.

3.3 Grinding Forces

3.3.1 Grinding Forces and Wheel Wear

Many theoretical models have been developed to represent the grinding forces on the work piece. These models were based on the fact that grinding is a chip removal process in which the cutting tool was an individual abrasive grain and chip formation during grinding process consisted of three stages: a) sliding stage b) ploughing stage c) cutting. In this process, cutting was not the only mechanism that produced forces on the grain. In addition to cutting, there was sliding of the cutting edge formed by the grain where both the cutting edge and the work piece were elastically deformed. Then, as the stresses on the cutting edge formed by the grain and the workpiece were increased beyond elastic limit, plastic deformation occurs. At this stage, the cutting edge penetrated into the plastic matrix and ploughing or plastic flow to the front and the side of the grain will form a groove. All these stages increased the forces and the specific energy in the grinding process (Alfarez and Elsharkawy, 2000). These stages are illustrated in the second sketch of Figure 3.4. Figure 3.4 shows the indentation and side flow of the material.

The total grinding force vector \vec{F}_{tot} exerted by the wheel on the work piece could be determined into a horizontal F_H and a vertical component F_V (see Figure 3.3).

$$\vec{F}_{tot} = \vec{F}_{sliding} + \vec{F}_{ploughing} + \vec{F}_{cutting} \quad (\text{Younis et al, 1987}) \quad (3.1)$$

Figure 3. 3: Three Stages of Chip Generation and Grinding Force Components (Chen & Rowe, 1996).

During the grinding process, the sharp grains will start to develop wear flats as a result of the grinding operation (similar to flank wear in cutting tools) while the already flattened grains became enlarged due to the overall grinding wheel wear and adhesion of metal particles. The overall grinding wheel wear, was considered as the sum of grain fracture, bond fracture, and attritious wear (See Figure 3.4).

Most of the grinding wheel wear is due to grain and bond fracture, while attritious wear constitutes an insignificant portion of the total grinding wheel wear. Though insignificant, the attritious wear is the most important form of wear since it is directly related to the size of the wear flat and hence the grinding force. As the grinding process progresses, the wear flat slides along the surface being ground, causing friction and consumes energy for sliding. The larger the wear flat, the higher the grinding force is (Malkin and Cook, 1971; Chen et al, 1998).

Figure 3. 4: Grinding Stages (Alfarez and Elsharkawy, 2000).

In precision grinding operations the issue of cutting forces is significant since it is associated with the problem of achieving the desired accuracy and workpiece quality.

Various methods have been suggested to determine the magnitude of cutting forces based on the mechanics of chip removal and properties of the material being ground. However, all these theoretical methods depend on a number of parameters such as the tool geometry that are not constant as in the case of milling and turning. Investigations have shown that the abrasive grains in a grinding wheel act as miniature cutting tools with an average negative rake angle of 45° . The combination of the angle, orientation of the grains and low depth of cut can lead to high normal (radial) forces during grinding (Saint-Gobain Abrasives, n.d.).

In grinding, there are two components of grinding forces: normal and tangential. These forces can be influenced by a number of factors such as down feed, table speed, depth of cut and grinding fluids. A related and important factor is the specific grinding energy

3. Grinding Background

defined as the energy per unit volume of removal material. In general, the grinding forces and the specific energy increase with the hardness of the workpiece and they are both influenced by the grinding fluid and the factors mentioned before (Jahanmir et al, 1995).

The normal grinding force F_n has an influence on the surface deformation and roughness of the work piece, while the tangential force F_t mainly affects the power consumption and service life of the grinding wheel (Eiji, 1982).

The ratio of the normal (F_n) to the tangential component (F_t) is usually around $F_n/F_t=2$ during grinding with a free cutting wheel. This ratio increases as the wheel glazes and may reach a value of 4 to 5. The nature of distribution of cutting forces in grinding differs radically from other metal-removal processes. This poses various problems in designing the machines and achieving the necessary levels of accuracy (Saint-Gobain Abrasives, n.d.).

Chen and Rowe (1996) in their work presented an analysis of the grinding process including a simulation of the grinding force. The force could be separated in F_n and F_t or into a horizontal component F_h and a vertical component F_v (Figure 3.3) .When the diameter of the grinding wheel was much larger than the depth of cut, the angle α was very small. Under these conditions the horizontal component could be assumed to be identical to the tangential component and the vertical component identical to the normal component. The total force could be found by summing the grinding force for each individual grain in the grinding zone. However, the identification of the real number or the orientation of the grits in the grinding zone was difficult because of the random distribution of the grains in grinding wheel. Their model differs from a simple one in a way of representing and analyzing the grinding forces. The two figures below depict this differentiation.

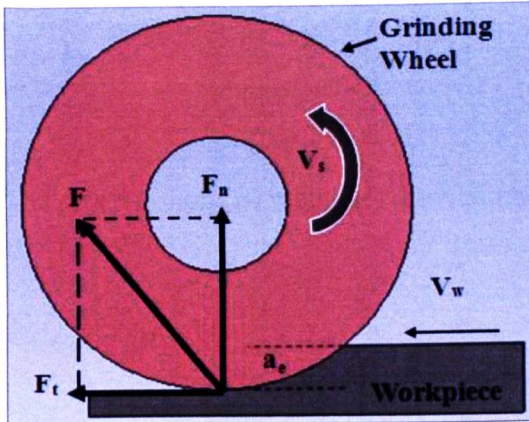


Figure 3. 5: Simple Model of Grinding Forces. (Chen & Rowe, 1995).

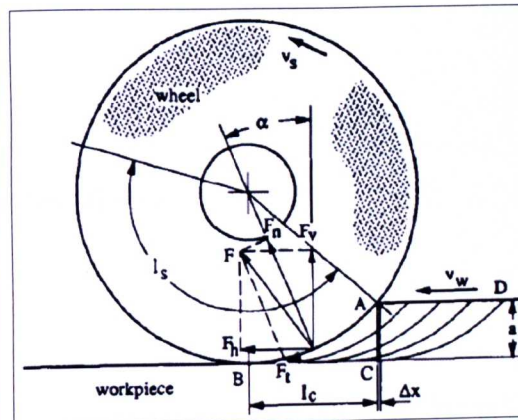


Figure 3. 6: Analyzed Model of Grinding Forces

V_w is the workspeed - also called table speed or traverse speed - of the table and is usually measured in mm/s or m/min. V_s is the speed of the grinding wheel and is measured in meters/second (m/s). Lastly, a_e is the depth of cut of the workpiece. It is usually measured in μm but it can take values of few millimeters in case of high material removal operations such as creep-feed grinding and high efficiency deep grinding (HEDG).

G-Ratio

The wheel life is an economic issue that should be taken seriously into account in order to achieve high quality results with no additional costs. There are many parameters which affect the wheel life. These include:

- Poor surface integrity.
- Extreme grinding forces and power.
- Lack of dimension accuracy
- Surface damage due to high temperatures.
- No continuous dressing and truing operations.
- Incorrect use of grinding fluids.

A traditional way of describing the wear of the grinding wheel is a performance index called G-ratio. It is the ratio of volume of material ground per unit wheel width (U_w) to volume of wheel worn per unit wheel width (U_s).



$$G = \frac{U_w}{U_s} \quad (\text{Malkin, 1989}) \quad (3.2)$$

The radial volume of material removed from the wheel is:

$$U_s = \pi d_e \Delta r_e b_s \quad (3.3)$$

Where d_e is the mean diameter of the wheel before and after grinding, Δr_e is the measured decrease in wheel radius and b_s is the grinding width (Malkin, 1989).

$$U_w = b_w \alpha_e l \quad (3.4)$$

Where b_w is the contact width, l is the contact length and a_e the real depth of cut.

The G-ratio values vary from <1 for some soft alox creep feed vitrified wheels to as high as 100,000 for vitrified CBN wheels (Marinescu et al, 2007).

3.3.2 Coefficient of Grinding

The coefficient of grinding μ is the ratio of tangential force to normal force.

$$\mu = \frac{F_t}{F_n} \quad (3.5)$$

This value of this coefficient can vary from 0.2 in cases of low stock removal such as grinding hard steel to 0.8 when the material removal stock is high such as grinding soft steel or grey cast iron. High stock removal leads to higher grinding power consumption which is proportional to tangential grinding force. Higher tangential force means higher coefficient of grinding. However, this coefficient is affected by the use of coolant as it changes the hydrodynamic pressure created by high wheel speeds and this effect is very obvious with high viscosity straight oils (Marinescu et al, 2007).

3.4 Process Parameters

In grinding operation there is a number of parameters and factors such as power energy that affect the performance of the process. These parameters are explained and described below.

3.4.1 Grinding Power

The grinding power P is a direct function of the tangential grinding force, thus it is usually expressed as follows:

$$P = Ft (Vs \pm Vw) \quad (3.6)$$

Where Vs is the wheel speed and Vw is the workspeed (or tablespeed). The plus sign is referred to up-grinding operations with the wheel and the workpiece velocities in opposite directions and the minus sign is referred to down-grinding processes when both velocities have the same direction, or internal or external for cylindrical grinding. In cases where the wheel speed is much higher than workspeed, the previous equation (3.6) can be simplified to:

$$P = Ft Vs \quad (3.7)$$

Knowing the specific energy and the specific material removal, the grinding power can be derived in the following equation (3.8)

$$P = e_c Q' b_w \quad (3.8)$$

Where e_c is the specific grinding energy, Q' is the specific removal rate and b_w is the contact width.

3.4.2 Material Removal Rate

The material removal rate in grinding is an important factor for applications in industry as it describes better the performance of a wheel or a whole process. The material removal rate Q is given from the following expression (3.9):

$$Q = b_w a_e V_w \quad (3.9)$$

Where a_e is the real depth of cut, b_w is the contact width and V_w the workspeed.

The specific material removal rate Q' is defined as the removal rate per unit grinding contact width and allows the results to be presented in a generic way. The units are in $\text{mm}^3/\text{mm}/\text{s}$.

$$Q' = a_e V_w \quad (3.10)$$

3.4.3 Specific Grinding Energy

The specific grinding energy (e_c) determines the ability of the grinding wheel to remove material. It depends on the sharpness of the grinding wheel and the grindability of the workpiece material (Rowe, 2009). It is defined as the ratio of grinding power to the material removal rate. Specifically, it is the work required to convert a cubic volume of metal into chips.

$$e_c = \frac{P}{Q} \quad (3.11)$$

The units of specific grinding energy are J/mm^3 and it is proportional to the grinding power and hence proportional to the tangential force. Also, it can be said that specific energy is useful for estimating the machine power requirements.

3.4.4 Equivalent Chip Thickness

The equivalent chip thickness (h_{eq}) is considered as another way of measuring the efficiency of the process. It actually represents the thickness of the chip that leaves the wheel after grinding. This value is proportional to the workspeed (V_w) and real depth of cut (a_e) and inversely proportional to the wheelspeed (V_s). The description of this factor is given by the following equation:

$$h_{eq} = a_e \frac{V_w}{V_s} \quad (3.12)$$

However, the equivalent chip thickness does not take into account the spacing between the grains at the surface of the wheel. For that reason a better way of looking at the details of material removed during grinding is the uncut chip thickness (h_{cu}). With reference to Marinescu et al (2007), the magnitude of h_{cu} is derived from various standard parameters for grinding and the surface morphology of the wheel. Uncut chip calculations are based on representations of the material removed in the grinding process as a long, slender, triangular shape with a mean thickness h_{cu} . The equation for the uncut chip thickness is defined as:

$$h_{cu} = \sqrt{\frac{V_w}{V_s} \frac{1}{C r} \sqrt{\frac{a_e}{d_e}}} \quad h_{cu} \ll a_e \quad (3.13)$$

Where C is the active grit density; r the grit cutting point shape factor which is equal to the ratio of grain width to grain thickness; d_e - the equivalent wheel diameter and a_e - the real depth of cut. Grit shape factor r is the ratio of chip width to chip thickness.

In high removal rate precision applications such as peel grinding with vitrified CBN or rough grinding with plated CBN the uncut chip thickness is inversely proportional to grinding specific energy (Marinescu, 2007).

$$e_c \propto \frac{1}{h_{cu}} \quad (3.14)$$

3.4.5 Surface Roughness

Surface roughness is a factor that measures how smooth a surface is; the smaller this value, the better surface quality. There are various surface roughness parameters such as Ra , Rz , and Rt . The most commonly used is the Ra which is the arithmetic average of all profile ordinates from a mean line within a sampling length after filtering out form deviations (Marinescu, 2007). This parameter of surface roughness will be used later in this research to characterize the final surface quality of the workpiece after grinding tests.

3.5 Grinding Kinematics

In manufacturing processes the mechanics of surfaces in contact are of particularly interest. An important aspect that should be considered during the grinding process is the contact between the wheel and the workpiece. This contact affects different parameters such as the force, the temperature and the wheel wear. Many authors work on this subject and predominantly in contact behaviour in grinding.

3.5.1 Real Contact Length

Referring to Rowe et al, (1993), the real contact length (l_c) between the wheel and the workpiece can be represented as the combination of the deformation contact length (l_f) and the geometric contact length (l_g).

$$l_c^2 = l_f^2 + l_g^2 \quad (3.15)$$

Contact length in grinding is consistent with the effects of elastic/plastic deformation between the rough surface of the grinding wheel and the surface of the workpiece. Development of expressions for the deformation contact length based on rough surfaces in contact for the geometric contact length yields:

$$lc = [R_r^2 8F'_n (K_s + K_w) d_e + \alpha_e d_e]^{0.5} \quad (3.16)$$

where:

$$K_s = \frac{(1 - \nu_s^2)}{\pi E_s}, \quad K_w = \frac{(1 - \nu_w^2)}{\pi E_w} \quad (3.17)$$

E_s and E_w are the moduli of elasticity of the grinding wheel and the workpiece and the ν_s , ν_w are the Poisson ratios of the grinding wheel and the workpiece. F'_n is a specific normal force, α_e is the real depth of cut, d_e is the equivalent diameter of the grinding wheel and R_r is the roughness factor (Qi et al, 1994)

3.5.2 Geometric Contact Length

The length of the uncut chip is equal to the length of contact between the wheel and the workpiece. With reference to Marinescu et al, (2004) the geometric contact length is defined as the arc length $AB=A'B'$ as shown in Figure 3.7. For surface grinding, the geometric contact length is:

$$l_g = \frac{d_s}{2} \vartheta_s \quad (3.18)$$

However, l_g is usually evaluated from the chord length AB rather than the arc length, so that

$$l_g = \sqrt{DB^2 + AD^2} = \sqrt{(d_s^2 \sin^2 \vartheta_s) / 4 + a_e^2} \quad (3.19)$$

These two expressions give the same result if θ_s is small, and DB can be found from the principle of intersecting chords.

Figure 3. 7: The Geometry of the Uncut Chip (Marinescu et al, 2004).

$$DB = \sqrt{(d_s - a_e)a_e} \quad (3.20)$$

If a_e/d_e is small

$$l_g = \sqrt{a_e d_s} \quad (3.21)$$

More generally, for surface and cylindrical grinding processes, the following form can be used:

$$l_g = \sqrt{a_e d_e} \quad (3.22)$$

Where the effective wheel diameter is given as the sum of the curvatures of the wheel and the workpiece. (Marinescu et al, 2004)

$$\frac{1}{d_e} = \frac{1}{d_s} \pm \frac{1}{d_w} \quad (3.23)$$

The effective diameter is used because the contact length depends on the relative curvature of the wheel and the machined surface. The effective diameter is an inverse measure of relative curvature. Contact length has a particular significance for the concentration of energy and forces in the contact zone and for rubbing wear of the abrasive grains.

If $a_e = 0.1d_s$ which is a very large depth of cut for most operations, the error in the simplified expression for l_g is about 1%. This expression is a very good approximation even when the depth of cut is large. It was assumed that the arc of contact was circular and still a good approximation in conventional grinding operations, if the grinding wheel remains circular (Marinescu et al, 2004).

3.5.3 Kinematic Contact Length

At high work speeds, the contact length as derived by geometry is increased. When the grinding wheel centre O_s , has moved forward a distance, s to O'_s in Figure 3.7 a succeeding cutting edge comes into contact with the workpiece at B' sweeping out the path $B'A'$. The cutting edge exits from the workpiece at a point halfway between A and A' . The cutting edge is in contact for an extra angular rotation (θ'_s) so that the total arc of contact on the wheel is $\theta_s + \theta'_s$. The relative horizontal speed between the wheel and the workpiece is $v_s \pm v_w$ where the plus sign is for up-grinding and the minus sign is for down-grinding. The extra distance to be travelled by the grain is $s/2$. The grain contact time is therefore,

$$t_{gc} = \left(l_g + \frac{s}{2} \right) \frac{1}{v_s} \quad (3.24)$$

The kinematic contact length is given by the distance travelled at the relative speed, $v_s + v_w$, during the grain contact time t_{gc} (Marinescu et al, 2004).

$$l_{gc} = \left(l_g + \frac{s}{2} \right) \frac{1}{v_s} \quad (3.25)$$

The contact length is increased for up-grinding and reduced for down-grinding. At higher work speeds, the uncut chip is shorter and fatter for down-grinding than for up-grinding. Also, the shock loading on the grain is greater in down-grinding. This implies a greater tendency for grain fracture in down-grinding and less tendency to dull, if the speed ratio is sufficiently large (Marinescu et al, 2004).

3. Grinding Background

In order to obtain the real size of the grinding zone and the real contact length between the wheel and the workpiece, several techniques have been implemented by different authors. Because of the difficulty of the process, some techniques are more efficient than others. According to Qi, (1995) the Applied Power Source method (Zhou and Lutterwelt, 1992) estimated as the most appropriate for this application. According to this method a single chromel foil probe was inserted into the workpiece. The two portions of the workpiece were insulated from the probe to prevent a short circuit. A grain forced the workpiece into contact with the probe by a cutting action which caused the top layer of the workpiece and the top of the probe to plastic deformation. The workpiece material which adhered on the surface of the grain formed a bridge between the workpiece and the probe. The following picture (Figure 3.8) depicts the configuration of this method.

Figure 3. 8: Applied Power Source Method Configuration (Qi et al, 1997).

The time interval in which the wheel moved from O to O1 was recorded and knowing all the other parameters such as length of the workpiece and width of the surface they managed to measure the real contact length. Moreover, it is essential to mention that a number of measuring devices have also been employed such as power function meters and data acquisition systems for the conduction of the experiment.

3. Grinding Background

NiCr-NiAl standard thermocouples were used to measure the temperature and contact time signal. Workpiece temperature was obtained by the thermocouple method. The measurement of grinding temperature provides useful information for further analysis of the relationship between the contact length and workpiece temperature. The overall thickness of the hot junction was 0.1 mm and the width 0.2 mm. Grains on the grinding wheel lead to temperature spikes as the grains pass over the thermocouple. The presence of spikes in the temperature trace was therefore indicative of contact (Qi, 1995).

Taking notice of the previous considerations, Qi et al, in 1997 adapted a measuring system on the grinding machine. The workpiece was housed in a jig in which an amplifier was embedded to amplify and compensate the temperature signal. The contact length signal and the thermocouple signal were recorded, displayed and stored, along with the normal, tangential grinding forces and the contact time.

The measured contact length (l_c) is obtained from the contact time t_c and the table speed v_w .

$$l_c = t_c v_w = t_c L / t_w \quad (3.26)$$

Where the table speed v_w was obtained from the force signal interval t_w and the workpiece length L .

The value of the contact time t_c was obtained from the contact signal by the Applied Power Source (APS) method. The method is characterised by the magnitude of the signal and the occurrence of the spikes. The intensity of the contact is represented by the magnitude and contact with individual grains is indicated by the spikes. The spikes occur as grains contact the top of the transducer foil and the workpiece and the frequency of contact between active grains and the workpiece is represented by the density of the spikes (Qi et al, 1997).

3.5.4 Contact Zone

The contact area between the wheel and the workpiece can be divided into three zones:

1. The cutting zone l_{cut} where the cutting action dominates
2. The cutting and ploughing zone l_{c-pl} where plastic deformation dominates
3. The rubbing (or sliding), ploughing and cutting zone l_c , which includes the whole contact length. The tail part of the contact zone, l_{rub} , generates the final surface texture of the workpiece. At the sparkout stage, l_{rub} will gradually dominate the whole contact zone (Malkin, 1989)

Figure 3. 9: Distribution of the Intensities of Different Grains Acting Along the Contact Zone (Qi et al, 1997).

The results of Qi's work (1997) revealed that the contact length in grinding is much larger than the predicted value (geometrical contact length). Moreover, due to the higher normal force, a higher table speed in surface grinding increases the contact length ratio (le/lg) - le being the measured contact length and lg is the geometric contact length. Also, the contact length in wet grinding is longer than the contact length in dry grinding. Furthermore, grinding geometry, grinding force and the roughness of the grinding wheel have independent effects on the contact effects.

3.5.5 Contact between Rough Surfaces

It is well known that the contacting surface of the grinding wheel is very rough. Bowden and Tabor (1986) assumed that solids are in contact only at isolated points. In this case the

3. Grinding Background

real contact area was determined by assuming that the asperities were deformed plastically. Also, Lo in 1969 used the same approach to solve the problem of contact between two parallel cylinders. It was shown that for rough surfaces the apparent contact area may be about 500 times larger than the real contact area. In grinding, it has been suggested that the apparent contact area of the grinding contact zone is about 100 times the real contact area. The average contact length due to the depth of cut is not directly influenced by the topography of the two contact surfaces, although the contact length for a particular grain contact may be either lengthened or shortened. However, the contact length due to elastic/plastic deflection is greatly influenced by the roughness of the contacting surfaces (Qi et al, 1994)

The contact length between rough surfaces can be expressed as l_{fr} :

$$l_{fr} = R_r l_{fs} \quad (3.27)$$

Where l_{fs} is the contact length which would apply for smooth surfaces and R_r is a roughness factor.

The main parameters influencing the contact length are:

- The real depth of cut.
- The elastic deflection of the grinding wheel.
- The surface topography of the grinding wheel.

However, the contact length in grinding is consistent with the effects of elastic/plastic deformation between the rough surface of the grinding wheel and the surface of the workpiece (Qi et al, 1994).

Particularly, one of the factors that influences the roughness factor R_r is the workpiece hardness. The greater the workpiece hardness is the lower penetration of the active grains into the workpiece for a particular force level. As a result, the ratio of contact lengths of rough surfaces and smooth surfaces will be reduced. There are several other factors such as speed ratio, grinding wheel dressing conditions, stiffness and vibration characteristics of

the grinding machine and measurement method which may also influence the roughness factor R_r . It is suggested that workpiece hardness has the greatest significance of these factors (Qi et al, 1994).

3.6 Coolant Application in Grinding

One of the main characteristics of grinding process is the excessive heat developed in the grinding zone. The generated heat leads to poor surface quality of the product, inadequate removal rates, high wheel wear and thermal damage of the workpiece. The energy that enters the workpiece must be removed quickly to prevent high local temperatures and phase transformations, and to prevent high residual stresses. Therefore, the application of coolant is necessary to any type of grinding process. The aim of these fluids is to cool and lubricate the workpiece and the wheel during grinding.

Another purpose of the fluid is to flush away the chips created from the grinding process. Any failure to remove these chips can lead to dullness of the grinding wheel which can result in high energy consumption and heat generation on the surface of the workpiece (Ge et al, 2003).

3.6.1 Types of Fluids

According to DIN 51385 the cutting fluids are divided into two categories; oil-based coolants and water-based coolants.

Oil-Based Coolants

These types of coolants normally consist of 80-95% basic oil and are used to decrease friction, high pressures and temperatures during the process by creating separation films (consisting of coolant and specific additives) between the solid surface of the tool and the workpiece. Oil-based coolants normally provide enhanced corrosion resistance and lubrication effect in comparison to water-based coolants. Also, low viscosity oils have a better crack penetration ability compare to higher viscosity oils (Brinksmeier, 1999). It was

3. Grinding Background

found that during face grinding of steel the oil-based coolants proved better than water-based due to higher evaporation temperature (300°C). The water-based coolants started to evaporate at depths of cut more than 35 µm and temperatures in excess of 100°C. (Marinescu, 2007).

Water-Based Coolants

The water-based emulsions contain 20-70% basic oil (mostly mineral oil). They are used for high cooling effects and washing capabilities. Water-based solutions consist of inorganic and/or organic substances and water and very seldom contain mineral oils. Their main disadvantage is susceptibility to leakage oils and micro organisms making high maintenance costs unavoidable. Also, the water and oil phases must be separated before disposal (Brinksmeier, 1999). These types of coolants are used in creep-feed grinding where the coolant becomes the primarily source of heat removal and maintains the workpiece surface at a temperature at or below 130°C, the boiling point of the coolant under sufficient pressure (Howes, 1990).

3.6.2 Benefits

The overall benefit of the application of coolant fluids are:

- Reduced dressing frequency, due to less loading with work material and reduced abrasive grain wear.
- Thermal damage of the workpiece material is reduced, allowing higher removal rates.
- More of the applied flow rate will be effective, allowing the overall applied flow rate to be reduced.
- No need to reduce wheel speed or soften wheel grade to alleviate burn.

(Webster, 2008).

There exist several types of nozzles for effective coolant delivery to the grinding zone. Numerous works have been carried out in order to improve the understanding of the fluid flow in the nozzles and the interaction of the coolant and the wheel. Baines-Jones in 2010

3. Grinding Background

performed a number of CFD and CFX analysis of fluid flow inside and outside nozzles in order to improve the coolant delivery during grinding process.

Each nozzle is made for a specific application depending on the grinding parameters such as wheel speed and type of material to be ground and also the type of coolant. The faster the workpiece and the wheel cool down the better surface quality, and lower wheel wear can be achieved.

Chapter 4: Vibrating Rig - Theory and Design

4.1 Introduction

In engineering vibration various equipment and devices are used to generate oscillation for specific purposes. These purposes are: testing, vibrating conveyors, vibro-impact systems, vibration assisted machining etc. This chapter gives a report about these devices and describes their principle of work, with the intent to identify the suitable one to be employed for the conduct of the experimental work in the present study.

4.2 Vibration Generators

The vibration is generated from devices that are especially made for this purpose. The weight, shape, material and performance of each device depend on the type of application. Some of them are described below.

4.2.1 Electrodynamic Shakers

These devices are force generators or transducers which produce vibration or shock for testing and analysis purposes. They are used to determine the performance of the component under vibration or shock loads, detect flaws through modal analysis, verify product designs, measure structural fatigue of a system or material or simulate the shock or vibration conditions found in aerospace, transportation or other areas. There are several types of shakers such as mechanical shakers which use a motor with an eccentric shaft to generate vibration. However, the most common in use are the electrodynamic shakers (Globalspec, 2010).

At the heart of the electrodynamic shaker is a coil of wire, suspended in a fixed radial magnetic field. When a current is passed through this coil, an axial force is produced in proportion to the current. Referring to Figure 4.1 below, the coil is attached to a work table and the alternate flow of the current produces an oscillatory motion of the coil and this is transmitted to the table structure to which the test piece may be attached. Figure 4.1 shows

a sketch of an electromagnetic shaker. A permeable (ferrous) inner pole piece transmits flux from one end of an axially magnetized permanent magnet or electromagnet (north face). A permeable “back structure” conducts flux from the opposite pole of the magnet to a permeable disk with a hole in its centre surrounding the inner pole piece. This creates a radial flux field in the air gap between the round face of the north-polarized inner pole piece and the round hole in south-polarized outer pole piece. The air-gap between these pole pieces is minimized to reduce the reluctance of the magnetic circuit thus maximizing the intensity of the fixed magnetic field.

Figure 4. 1: Schematic Representation of an Electrodynamic Shaker (Lang & Snyder, 2001).

The three functional limits to an electrodynamic shaker performance are displacement, velocity and acceleration. Displacement limits shaker operation at the lowest frequencies, and acceleration limits the shaker performance at the highest frequencies. Velocity limits shaker performance in a band between the other two limits. Displacement of an electrodynamic shaker is a function of how far up and down the armature is capable of travelling. Velocity is the speed at which the armature can move. Velocity limits for electrodynamic shakers can reach 2.54 meters per second. The higher the velocity limit, the

greater the shaker's capability of attaining a wider range of shock pulses. Acceleration is expressed in terms of gravitational units or g 's.

Some of the main disadvantages of the electrodynamic shakers are their huge mass and their poor performance in terms of pushing forces. Their stroke can reach a few millimetres but the generated forces do not exceed 100 N. Much higher forces can be produced by massive and particularly expensive shakers which sometimes are not suitable for limited size applications.

4.2.2 Piezoelectric Actuators

The principle of work of these devices is based upon the piezoelectric effect which is a property of some crystalline materials. When these materials are compressed they produce a voltage proportional to the applied pressure. Conversely, when these materials are subjected to an electric or electromagnetic field they have the ability of modify their shape. In other words, they convert electrical energy to mechanical energy and vice – versa. Nowadays, most of the devices made for producing some kind of vibration use these materials and especially polycrystalline ceramics, such as lead zirconate titanate (PZT). This is a ferroelectric material with piezoelectric properties. These devices are driven by the output voltage of a power amplifier that amplifies a small sinusoidal input signal from a function generator. The picture next (Figure 4.2) depicts a typical piezoelectric actuator and its components.

Figure 4. 2: Piezoelectric Actuator (Source: Physik Instrumente-PI, 2010).

The maximum operating voltage is proportional to the thickness of the disks. Most high-voltage actuators consist of ceramic layers measuring 0.4 to 1 mm in thickness. Stacked elements can withstand high pressures and exhibit the highest stiffness. Standard designs which can withstand loads up to 100 kN are available, and preloaded actuators can also be operated in push-pull mode.

One of the main features of piezo actuators is that they can perform sub-nanometer moves at high frequencies moving extremely high loads up to several tons. Also, because they do not have any moving or sliding parts they cannot cause any type of friction. Hence, they require no maintenance.

The stiffness of the actuator is an important parameter for forces generated, resonant frequency and full-system behaviour, etc. The stiffness of a solid body depends on Young's modulus of the material. Stiffness is normally expressed in terms of the spring constant k_T , which describes the deformation of the body in response to an external force.

In most applications, piezo actuators are used to produce displacement and forces. High force generation is always coupled with a reduction in displacement. The maximum force (blocked force) a piezo actuator can generate depends on its stiffness and maximum

displacement. At maximum force, the displacement drops to zero (Physik Instrumente, 2010).

The difficulty of investigating the characteristics of piezoelectric actuators has occupied a number of researchers who tried to identify these parameters with various methods. Pomirleanu and Giurgiutiu (2002) developed static and dynamic linear models of a specific large stroke piezoactuator and analysed experimentally the dynamic characteristics of this actuator at high displacements as well as its blocked force. They found that the blocked force was consistent for voltages up to 70% of the maximum voltage. Above this value its performance starts to become non-linear.

Also, Huang and Sun (2006) employed piezoelectric actuators to generate elastic waves in order to monitor damage of composite materials. Therefore, they had to identify the characteristics of this actuator. Their numerical results of the created model were compared with those of finite element analysis. The numerical results showed that the efficiency of the actuator depended on its geometry, material and the loading frequency.

An additional use of piezoelectric actuators is the control of vibration in a number of structures. Kermani et al, (2005) studied the active vibration control of large scale flexible structures using piezoactuators. They designed a mechanism that converts the force produced by the actuator to a bending moment. The closed-loop vibration they applied was superimposed on free vibrations and they concluded that the actuator could suppress the vibrations of the structure successfully.

4.2.3 Terfenol - D

Terfenol-D is also called giant magnetostrictive material (GMM). It is an alloy of terbium (Ter-), Iron (Fe-) and dysprosium (D-). The last three letters (nol-) refer to Naval Ordnance Laboratory where it was initially developed. In comparison with other active materials, it has a very large force and displacement with a fast response time which makes it suitable for high-frequency applications.

It is also called smart material as it can produce five to ten times more strain than piezoceramics and it has the ability to transform the energy inputs into different types of energy with minor losses. This material generates more force and a larger stroke distance than can be achieved with piezoceramic materials of the same size and shape. It offers a broad range of operating temperatures (-51.1°C to 71.1°C), which has benefits in vehicle applications (Ashley, 1998).

Many studies have been devoted to the behavior of Terfenol-D. Dapino et al, (2006) focused on characterisation of the Terfenol-D properties under magnetic bias mechanical preloads, AC drive fields, frequencies of operation, and mechanical loads typical of many dynamic transducer applications. They also proved that because of the number of repeated tests under fixed operating conditions the properties of the Terfenol-D were changed.

Kondo in 1997 applied a $5\ \mu\text{s}$ pulse current at 200 A to a coil twisted on a Terfenol-D rod. This produced magnetostriction propagated in the axial direction of the rod as an elastic wave with a velocity of 1700 m/s and $1\ \mu\text{m}$ displacement. Also, he found experimentally that higher displacements could be obtained by superimposing the displacements produced by two coils.

There are many advantages of Terfenol-D material as it can be used in a number of applications with high success. However, due to its high cost and uniqueness, it is considered unnecessary for the present study whereas a piezoelectric actuator was adequate for this specific application.

In this study a piezo actuator was used to produce forced vibration. Therefore, the following section will focus on forced vibration as most relevant to this study. This will help with the selection of adequate system configuration of the vibrating jig and its dynamic response.

4.3 Forced Vibration

In this type of vibration an external dynamic force is applied to the system. In the present study only the case of a harmonic excitation was examined where the external applied

force to the system is sinusoidal and acted at a specific frequency. The system under examination for the present study is assumed to be a mass-spring system vibrating under the effect of an external force and can be schematically illustrated as shown in Figure 4.3 in a generic form.

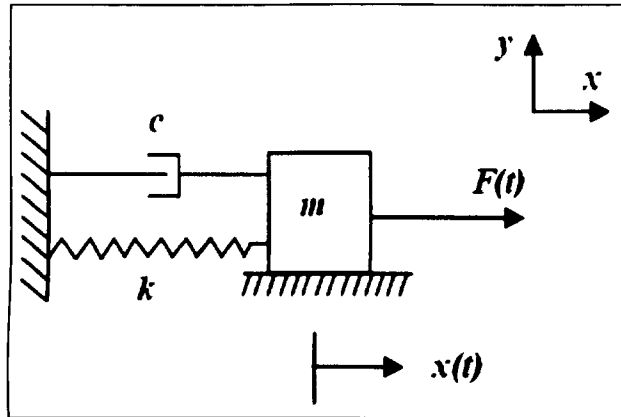


Figure 4.3: Forced Vibration of a Single Degree of Freedom Mass-Spring System on a Friction Free Surface.

Here, m is the mass; C is the damping coefficient; k is the stiffness of the spring $x(t)$ the displacement and $F(t)$ is the driving force.

To simplify the design in this study the damping was neglected at the beginning and the driving force is given a sine wave form. Thus the force is expressed in the following form:

$$F(t) = F_0 \cos \omega_{dr} t \quad (4.1)$$

Where F_0 is the magnitude of the excitation force and ω_{dr} is the driving frequency of the force and t is time. It is considered that the forces in the vertical direction are in equilibrium thus they have no significant effect on the motion of the system in that direction. With these assumptions the following simplified model in Figure 4.4 is obtained.

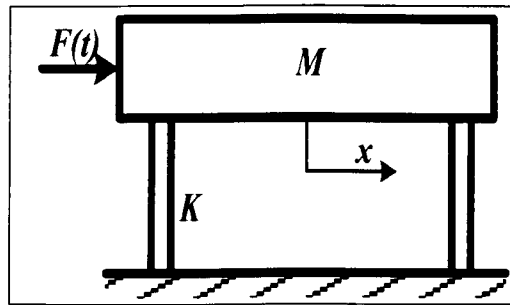


Figure 4. 4: Simplified Vibrating Model.

After this theoretical consideration, an initial concept of the configuration of the oscillating system emerged.

The model in Figure 4.6 was used without accounting for machining interaction. Four flat springs were used to model the system response characteristics with six different thicknesses namely: 2mm, 3mm, 4mm, 5mm, 6mm and 8mm. This was done by using Matlab-Simulink software where a programme was developed to study the response of the system under various driving forces and different spring stiffness.

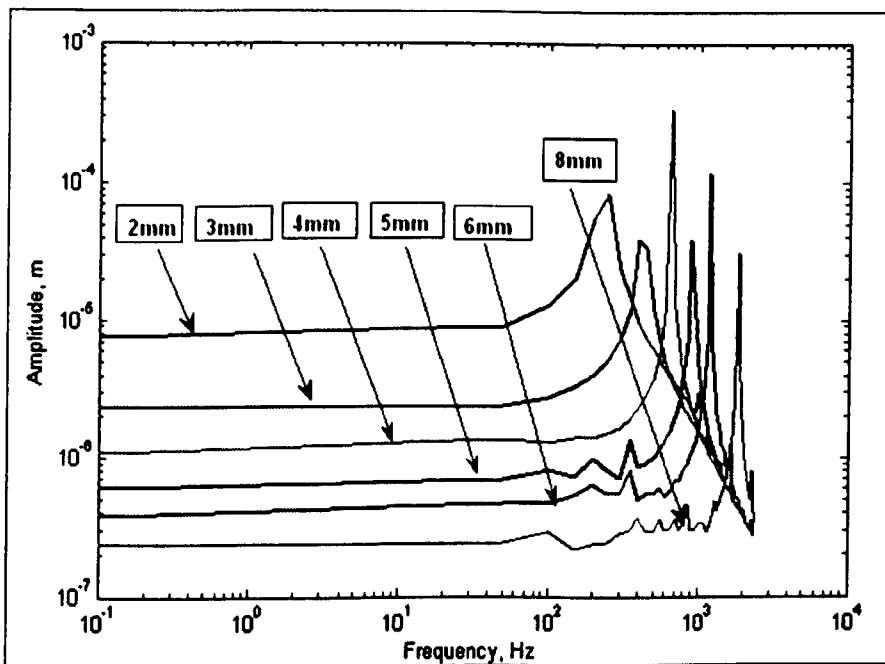


Figure 4. 5: Frequency-Amplitude Response for Various Spring Stiffness.

4. Vibrating Rig - Theory and Design

The results obtained (illustrated in Figure 4.5) though not fully accurate due to crude assumptions provided the confidence that this approach could be used to develop an oscillating rig that could operate at various resonant frequencies by changing the springs as required by the process. The main objective of this exercise was to obtain an estimate of system displacement amplitude as prime parameter of concern and the resonant frequency. Based on this initial result a further two variations of similar configuration were developed as illustrated in Figure 4.6

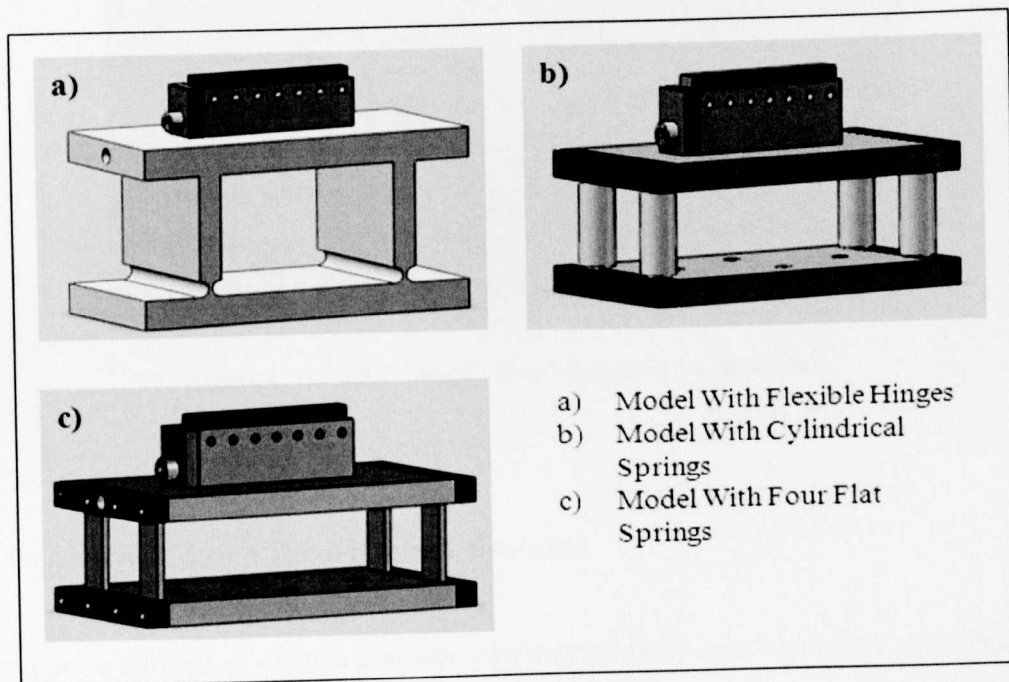


Figure 4. 6: Vibrating Rigs-Design Variations.

These three models were thoroughly studied as presented in chap 6 for their static and dynamic behaviour. This allowed for selecting the suitable model for the intended application. However, as it will be shown in relevant section the most appropriate and fit design for this application will only emerge after actual preliminary test grinding.

After the selection of a suitable model a first generation prototype was manufactured. Having the real rig in hand allowed for determining the damping in the system. Figure 4.7 illustrates the first concept of the system and its elements. The intent was to use an electromagnetic shaker to drive an oscillating rig at its resonant frequency. The flexibility



and re-configurability of the rig was the main purpose of the chosen design as it allowed for changing various spring stiffness as a function of machining conditions.

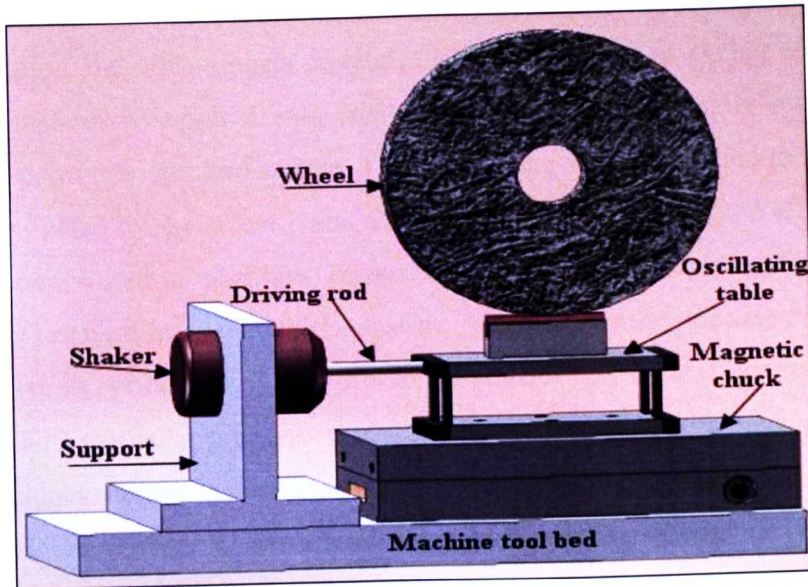


Figure 4. 7: First Concept Vibrating System Configuration.

4.4 Background to Vibro-Impact Systems

An impact is defined as a single collision of a moving body against another one which may be in motion or at rest, Harris, (1988). The following types of impact are possible: direct, oblique, central, eccentric, tangential and meeting. The collision develops through two major phases: loading and unloading. The loading stage goes from the instant of contact of bodies to maximum deformation; the unloading phase starts at maximum deformation and ends at the separation of the bodies. However, in constrained oblique impact with friction, Babitsky, (1978) noticed that the loading phase could be apportioned into two stages due to the change in sign of tangential velocity within this phase.

A vibro-impact system is defined as a mechanical system with systematic impact interactions of its elements, Babitsky (1978). Any two members of the system that are involved in a single impact are treated as an impact pair. There exist impact pairs with



single-sided impact (see Figure 4.8a) and double-sided impact (see Figure 4.8b) depending on the number of surfaces involved in one-dimensional impact on each member. There are also certain vibration machines in which impact does not occur. Independently of their purpose, vibration and vibro-impact machines have an actuator or exciter and a vibration system. The actuator is supplied with energy to generate a periodically oscillating force which is applied to the vibration system. The ratio of the energy supplied to the process to the energy dissipated by the actuator and the vibrating system defines the efficiency of the machine. Among vibration machines, resonant machines have a higher efficiency as they operate near the natural frequency of the system. Resonance is the selective response of the vibration system to periodic excitation at a frequency near the natural frequency, Astashev et al, (2000). This particular property of resonant machines affects the practical application of these machines because of the complexity of keeping resonance in conditions of unpredictable loads to observe the requirement of the operating system.

Many theoretical and experimental studies of vibro-impact systems are devoted to understanding impact vibration absorbers. Figure 4.8 illustrates various arrangements of vibro-impact dampers. These consist of a small mass attached to the main body with a clearance that allows for the collision between both elements. In Figure 4.8b the impact vibration absorber, the “free absorber” has a loose mass set at a clearance Δ to produce a double-sided impact. Figure 4.8a shows a single-sided vibro-impact absorber with an elastic element. A linear double-sided impact absorber with two restoring elastic elements is shown in Figure 4.8c. Similar absorber with visco-elastic bumpers is illustrated in Figure 4.9.

Figure 4. 8: Various Arrangements of Vibro-Impact Dampers (Babitsky, 1978).

Figure 4. 9: Force vibrated System with a Double-Sided Impact. (Masri, 1972).

4.4.1 Dynamic Model of Vibro-Impact System

Dynamic behaviour of vibro-impact systems is often studied by investigating the motion and the amplitude-frequency response of an oscillator colliding with a rigid stop. The model of such an impact oscillator (see Figure 4.10a) is made of a mass M on a spring of stiffness k and the stop is placed with clearance at a distance Δ .

If there is no stop on the path of the mass M , the motion of the system under harmonic excitation is defined by a sine wave. Assuming that both the mass and the stop are made of perfectly elastic materials, their coefficient of restitution is theoretically equal to unity. Therefore, after impact the mass will bounce with a velocity equal by value to the velocity before impact.

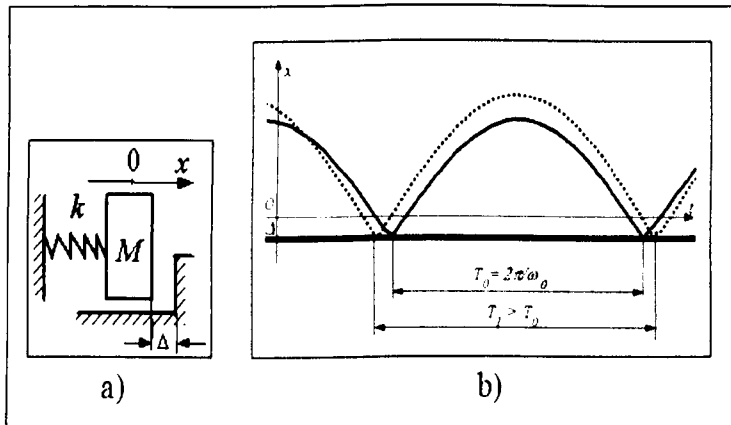


Figure 4. 10: Linear Single-Sided Impact Oscillator; a) schematics of the oscillator; b) Motion with Time (Babitsky, 1998).

In a vibro-impact system, the impact pair can be set with negative, positive or zero clearance. If in the system, the impact pair is set with interference (preload), the clearance Δ is considered as negative. The motion of a system with impact interaction is illustrated in Figure 4.10b where, for any different initial condition, the period T_I is greater than T_0 . However, the period of the free vibro-impact regime cannot exceed the period of the linear system without stop. Figure 4.11 displays the phase plot of a vibro-impact system with different settings of the clearance Δ .

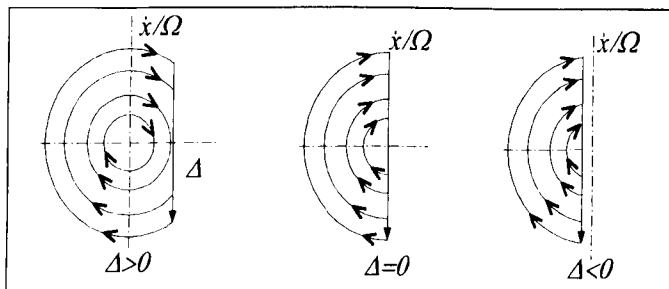


Figure 4. 11: Phase Portrait of System Motion with Impact (Babitsky, 1998).

Several studies have been devoted to the process occurring in-between two bodies during their impact in order to determine the coefficient of restitution, the impact force and the

duration of impact. Considering a straight central impact of bodies with masses m_1, m_2 and velocities \dot{x}_1, \dot{x}_2 ; ($\dot{x}_1 > \dot{x}_2$), and using the law of conservation of momentum, the coefficient of restitution is expressed as follows

$$R = \frac{\dot{x}_{2+} - \dot{x}_{1+}}{\dot{x}_{1-} + \dot{x}_{2-}} \quad (4.2)$$

Where, $\dot{x}_{1-}, \dot{x}_{2-}$ are the velocities of bodies before a collision; $\dot{x}_{2+}, \dot{x}_{1+}$ are the velocities of bodies after a collision.

In a recent publication, Babitsky and Vepruk, (1998), investigating the evolution of collision, used a lumped body of mass m that collides with a visco-elastic (Kelvin-Voigt element) bumper mounted on a wall. The bumper is made of a spring and dashpot (with viscous damping c) mounted in parallel. An accelerometer attached to the mass records the acceleration during the collision. The equation of system motion was solved for time τ , which is the duration of impact and was obtained as

$$\tau_1 = -\frac{1}{\omega_n \sqrt{1-2\zeta^2}} \arctan \left(\frac{2\zeta \sqrt{1-\zeta^2}}{1-2\zeta^2} \right) \quad (4.3)$$

It is observed that the impact duration depends only on system natural frequency and damping loss factor. During the evolution of the impact, the peak acceleration (i.e. max impact force) occurs at time τ_1 , which is expressed as follows:

$$\tau_1 = -\frac{1}{\omega_n \sqrt{1-2\zeta^2}} \arctan \left(-\frac{(4\zeta-1)\sqrt{1-\zeta^2}}{\zeta(3-4\zeta^2)} \right) \quad (4.4)$$

4.5 Vibrating Rig Dynamics

As explained in the design chapter, the model with four flat springs was selected and manufactured to undertake the preliminary tests of vibration assisted grinding as described in the preliminary studies. However, the results obtained from the preliminary tests led to the development of a second generation design (novel model) which was used for full scale experimental work.

Before any actual vibration assisted grinding experiment, the identification of natural frequencies and the amplitude of oscillation of each model was undertaken. After obtaining the frequency-amplitude characteristics of both first and second generation models it was possible to observe how the systems responded at lower, higher and resonant frequencies and the values of deflection they could reach. Two experimental methods were used for this study: the sweep-sine test and the impact test. Furthermore, the results from the impact test were compared to those of a frequency analysis, performed in another section of the work, in order to compare those two methods and detect any possible errors between simulation and experimental tests proving the validity of the software. The second impact test of the structure was performed when the system was attached only to the magnetic chuck of the tool-bed to keep conformity with simulation software environment. Here, the vibration transmitted from a piezoelectric actuator to the vibrating rig through a steel rod. The role of the rod was also to preload the piezoelectric actuator as requires from the manufacturer. It was attached to the exciter and therefore it belonged to the impact pair vibrating rig-grinding wheel.

4.5.1 Sweep-Sine Test

A piezoelectric actuator was used to excite the rig with frequency increasing from 50 to 400 Hz. As illustrated in Figure 4.12 below, the actuator was located on the machine tool moving axis but outside the enclosure for safety measures; thus a steel rod was used to transmit the vibration to the jig. The length of the rod was dictated by machine tool configuration rather than a design parameter where it should have been a function of the wave length. The isolation of the piezoelectric actuator was to protect it from coolant and debris during the grinding process according to the manufacturer's safety precautions. A high resolution, water resistant displacement sensor - which was also calibrated - was attached to the other end of the jig and it was used to take real-time measurements during the test. The acceleration was recorded through an accelerometer in order to obtain the frequency domain characteristics of the system. The rig was mounted on a dynamometer hence setting the system as it would be used for the experimental work. Figure 4.12 shows the full configuration of the system for this particular test. The displacement sensor and the accelerometer were connected to a Data Acquisition (DAQ) system in order to observe and record all the results in real time during the experiment. The data were collected and post-processed using the Labview 8.5 software package.

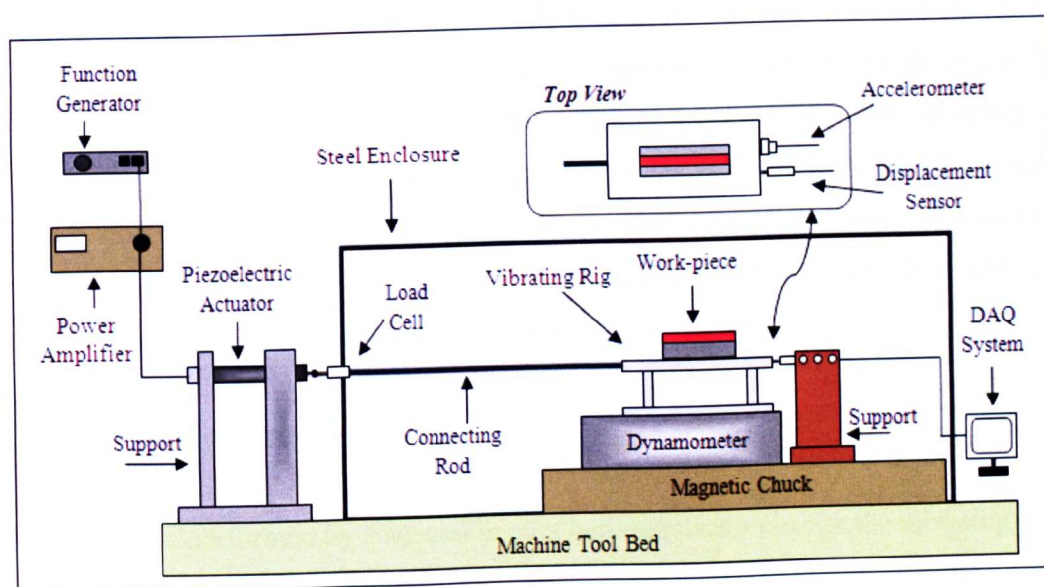


Figure 4. 12: Full System Configuration for the Sweep-Sine Test of the Vibrating Rig.



Applying a pushing force of 100 N with rising frequencies from 50 Hz to 400 Hz, a frequency- amplitude characteristic for both rigs was obtained.

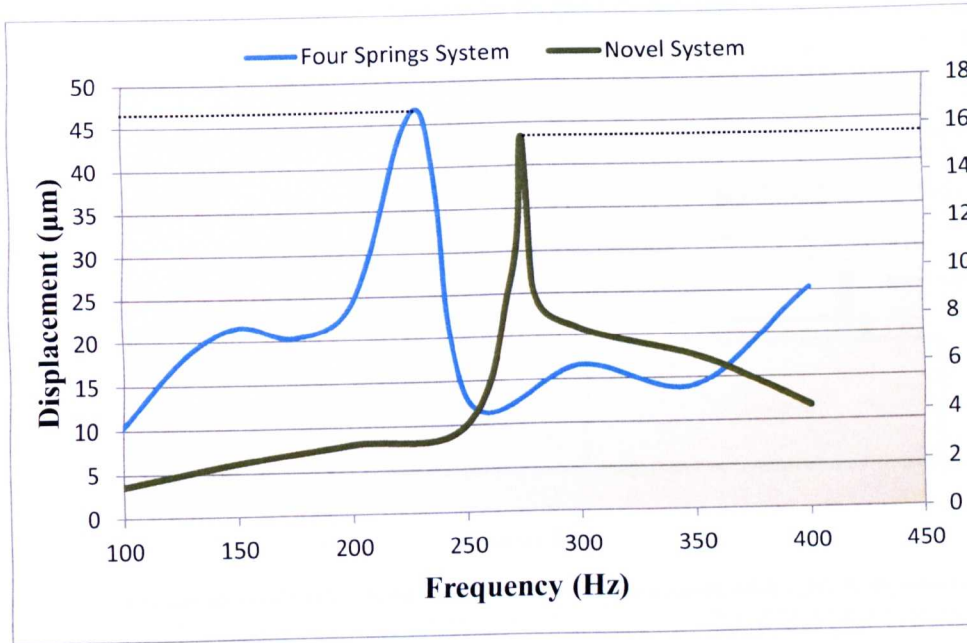


Figure 4. 13: Frequency-Amplitude Characteristics for System with Four Springs and Novel System.

Figure 4.13 displays the frequency-amplitude graph, of both models showing the natural frequency of the system with four springs at 230 Hz with a maximum deflection at 46 µm and for the novel model a resonance at 275 Hz with 15.6 µm maximum displacement. It must be mentioned the fact that the magnitude of displacement depends on the value of the applied static force from the piezoelectric actuator and the stiffness of the structure. It is observed here that the new jig made of two flat spring is stiffer thus deflects less with its resonance shift to higher value. This is because the thickness of the spring was increased from 3 to 4mm and the length increased from 48mm to 78mm in order to match some constraints imposed by the working envelop of the machine tool.

4.5.2 Impact Test- Stand Alone System

This process was performed by a special impact hammer used to excite the vibrating jig via an impulse. An accelerometer was placed at the back end of the rig and recorded the response of the system. The impact test was performed for two different cases: a) when the



4. Vibrating Rig - Theory and Design

systems were stand alone (see Figure 4.11) and b) when the systems were preloaded, connected to the piezoelectric actuator (see Figure 4.17). A fast Fourier transform (FFT) algorithm was used to analyse this signal in the frequency domain.

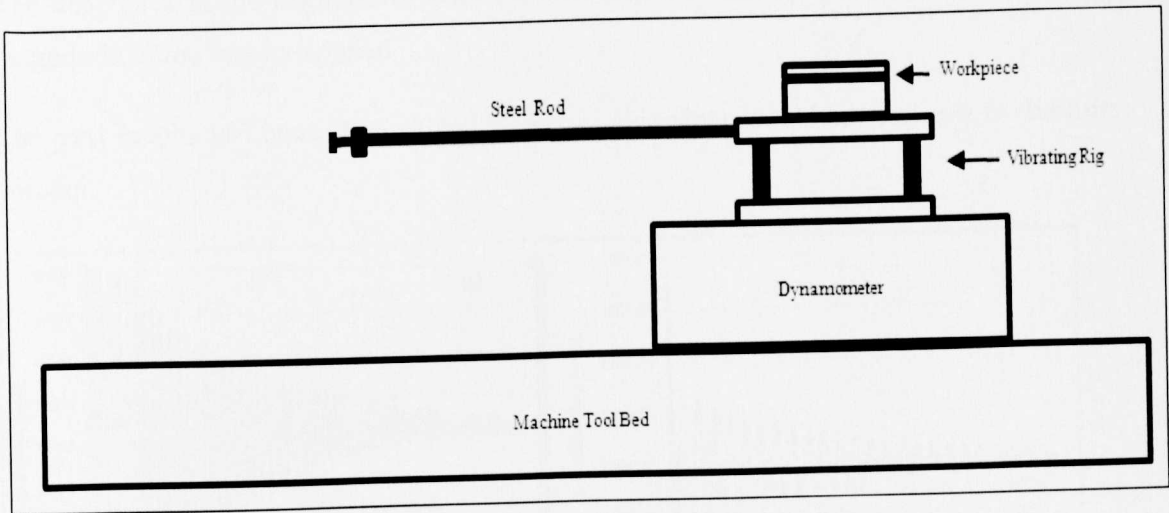


Figure 4. 14: Stand-Alone System Configuration.

For this case, the vibrating rigs were only fixed at their base on the top of the dynamometer which was mounted on the tool-bed by the magnetic chuck as illustrated in Figure 4.14. Figures 4.15 a) and b) represent the response of both rig assemblies under impulse excitation for single impact.

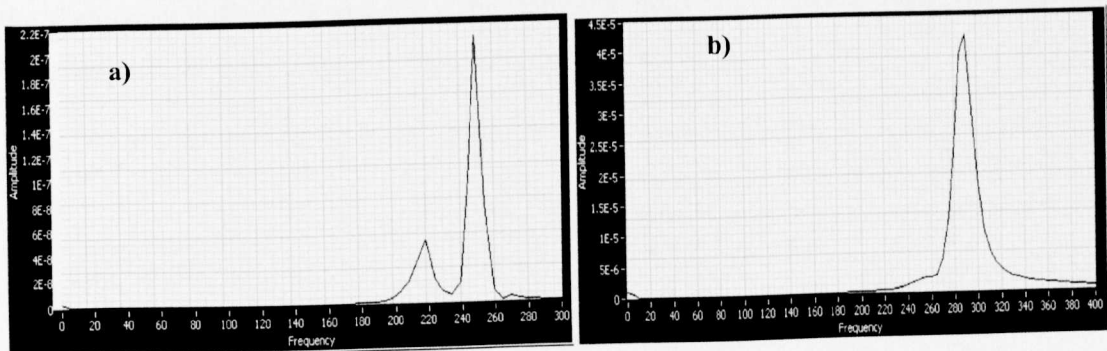


Figure 4. 15: Stand Alone System PSD; a) Four Springs and b) Novel System.

In Figure 4.15 (a) it is observed that the natural frequency for the system with four springs is 250 Hz, however the first peak at 220 Hz shows that this system in standalone mode



exhibits two degree of freedom response. The four spring system was a bit loose and during the impact test the accelerometer picked a second frequency of another component. This might be the rod or one of the clamping plates. However in Figure 4.15 (b) the novel system displays a clear single degree of freedom response with its resonance at 290 Hz. The difference in the response of both systems may be related to the discrepancy of the magnitude of the impact applied.

The next graphs in Figure 4.16 a) and b), show the response of both systems in the time domain.

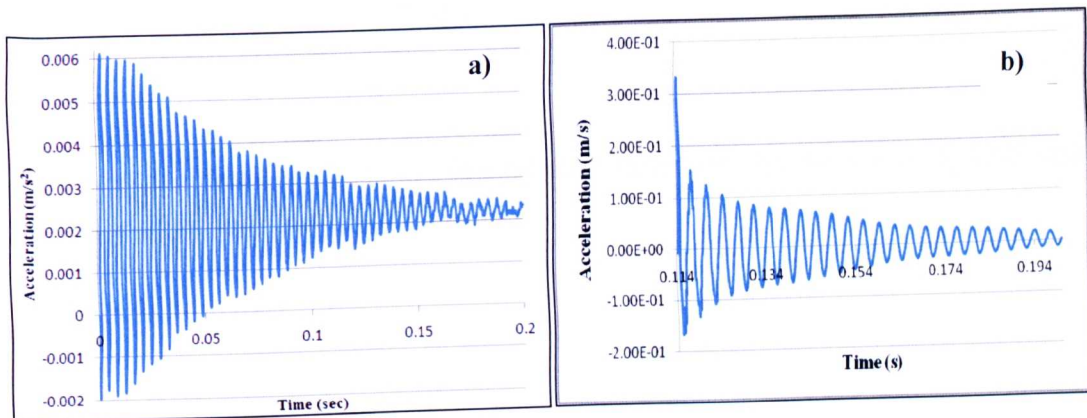


Figure 4.16: Stand-Alone Systems; a) Four Spring System, b) Novel System.

The data collected from these graphs were used to calculate the logarithmic decrement and the damping ratio of the systems. The damping ratio is calculated using the following equations.

$$\zeta = \frac{\delta}{\sqrt{4\pi^2 + \delta^2}} \quad (4.5)$$

The logarithmic decrement is:

$$\delta = \ln \frac{x_1}{x_2} \quad (4.6)$$



Where

And x_1 and x_2 two successive amplitudes peaks of the recorded signal

When these amplitudes are n periods away the formula of the logarithmic decrement is:

$$\delta = \frac{1}{n} \ln \frac{x_1}{x_2} \quad (4.7)$$

Therefore, with the four spring system the damping ratio is as follows

$$x_1 = 0.0051 \text{ m/s}^2 \text{ and } x_2 = 0.0046 \text{ m/s}^2$$

$$\text{Hence } \delta = 0.103 \text{ and } \zeta = 0.016$$

Following the same method, the logarithmic decrement for the novel system and the damping ratio are respectively:

$$\delta = 0.125 \text{ and } \zeta = 0.02$$

4.5.3 Impact Test - Preloaded System

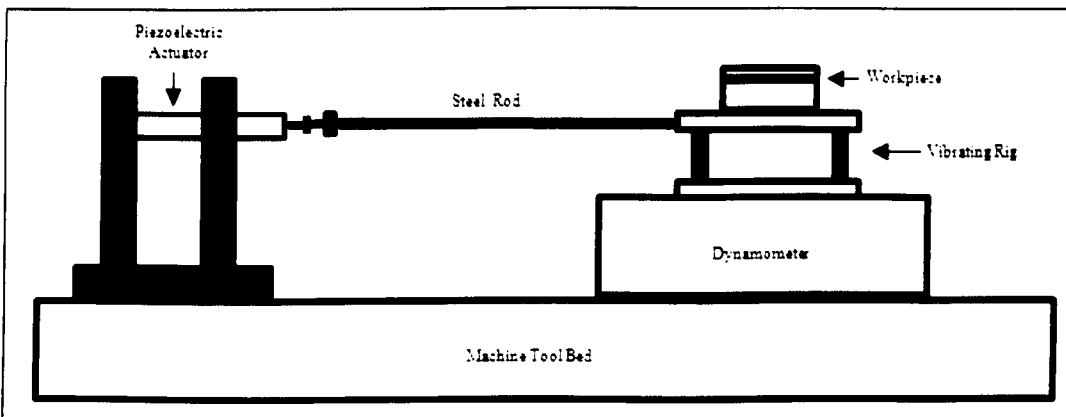


Figure 4. 17: Preloaded System Configuration.

In this case the rigs were assembled as in the working configuration i.e. fixed at their base while the end of the rod was attached to the piezoelectric actuator. The following graphs in Figures 4.18 a) and b) depict the response of both models.

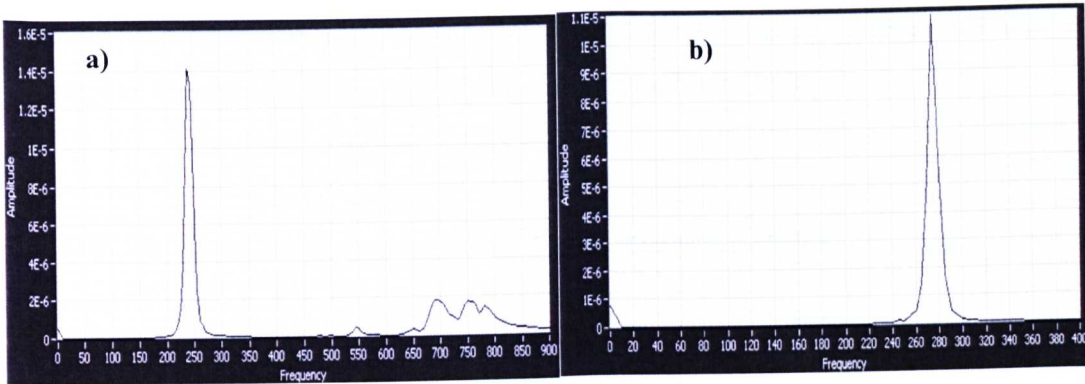


Figure 4.18: Preloaded System PSD; a) Four Spring System, b) Novel System.

As the rigs were assembly in working configuration, it was structurally identical to the setting used for the sweep sine test. Therefore, the impact test in this case produced the same results i.e. 235 Hz for four-spring system and 275 Hz for the novel design. Figures 4.19 a) & b) show the impulse response of the rigs in the working set up.

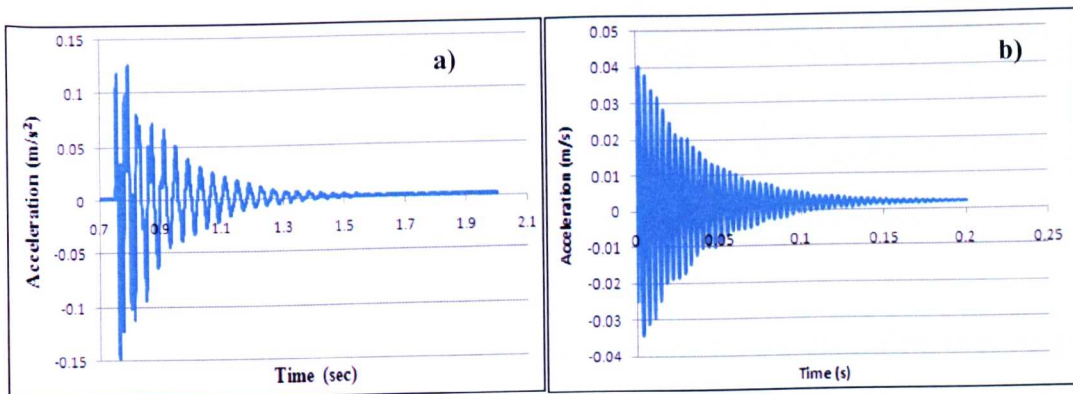


Figure 4.19: Preloaded Systems; a) Four Spring System, b) Novel System.

Assembled in the working configuration, the damping ratio in both systems is now redefined as follows.

System with Four Springs $\rightarrow \delta = 0.28$ and $\zeta = 0.044$

Novel System $\rightarrow \delta = 0.213$ and $\zeta = 0.034$



The obtained values of damping ratio show that the preloaded systems in the working situation exhibit more damping due to more losses in the assembly.

4.6 Observation from Impact and Frequency Analysis

A number of computational simulations and frequency analysis for the systems have been performed in respective chapters. The overall results of all methods for both rigs are presented in the following table.

Vibrating Rigs	Theoretical modelling		Actual rig test	
	Analytical Calculations	Frequency Analysis (ANSYS)	Impact Test	Sweep Sine
Four Springs System	407 Hz	385 Hz	235Hz	230Hz
Novel System	307 Hz	294 Hz	275 Hz	275 Hz

Table 4. 1: Overall Results of Vibrating Rig's Natural Frequencies.

- The table shows that the results are in agreement in pairs depending of the methods. However, the theoretical modelling had overestimated the natural frequencies of the actual four spring rig though the discrepancy is in an acceptable range. It was then set to use the following natural frequencies: System with four Flat Springs Natural frequency: 235 Hz
- Novel System Natural Frequency: 275 Hz. This value of natural frequency was obtained from impact test results of the actual system. The vibrating rig was preloaded-attached to the piezoelectric actuator ready for actual grinding. Therefore, this value of natural frequency was considered as the most representative.

4.7 System Response under Machining Load

Observation from initial grinding tests suggested that in order to achieve an adequate performance of the design selected and to avoid drastic wear of the grinding wheel, the impact pair i.e. tool/workpiece must be configured as illustrated below in Figure 4.20.

Figure 4. 20: Assumed System Motion (Babitsky, 1998).

If the clearance Δ between the tool (wheel) and the workpiece were greater than zero, this would lead to a hammering process against the friable wheel with subsequent rapid wear of the wheel. It was decided to preload the oscillating rig by deflecting it to the right from its free standing position as illustrated in Figure 6.20. The actual magnitude of the deflection due to preloading was not quantified. Therefore, in this study it is assumed that between the impact (wheel/workpiece) there is no clearance ($\Delta=0$) or the clearance is a negative i.e. $\Delta \leq 0$. However, depending on the table feed rate, the clearance Δ has been negative for most of the experiments undertaken in this study.

When $\Delta < 0$, a vibro-impact regime can occur only when an additional hard excitation is supplied. In the present study this excitation was provided by the piezoelectric actuator. In this case the vibration velocity was lower than the workspeed. Thus, there was no disengagement of the wheel and the workpiece in the most of experiments. However, the superimposed vibration let the workpiece to restore from the elastic deformation occurred

during the process and the wheel grains could remove more material due to their high wheel speed. In conventional grinding due to the constant contact (wheel-workpiece) the workpiece does not have the time to restore from elastic deformation and that is the reason of the applied depth of cut is always lower than the actual depth of cut value achieved at the end of the process.

The present study is based on the principles of vibro-impact theory which has been used in ultrasonic assisted machining in past years with exceptional results. However, the applied frequency in this work is much lower than this of ultrasonic at a range of few hundreds Hz. This constitutes an alternative approach that can be proved useful and enhance the performance of machining processes and particularly grinding.

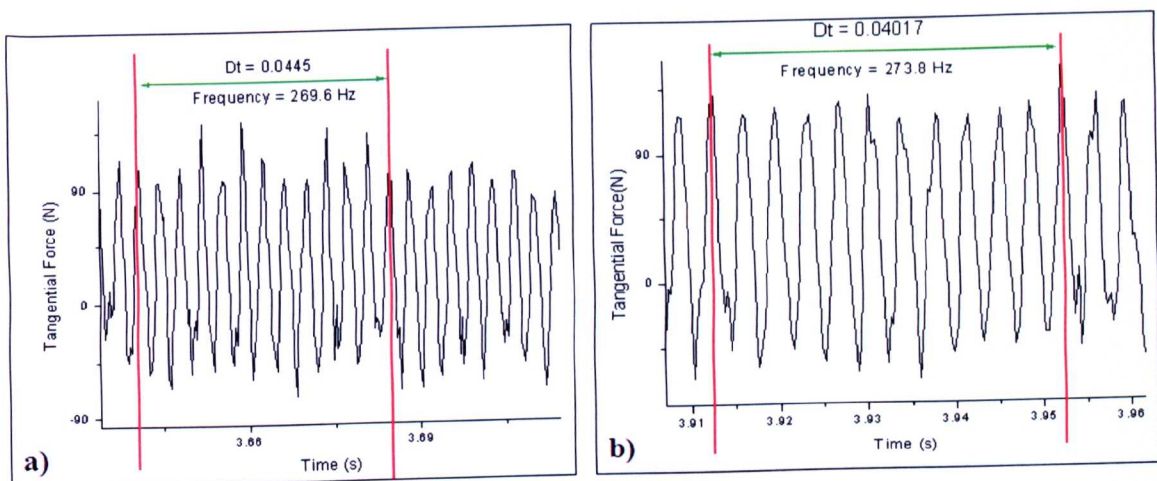


Figure 4. 21: System Response under Actual Grinding a) Open-Loop Vibration Control b) Closed-Loop Vibration Control.

Figure 4.21 illustrates the response of the vibrating rig under machining load. It shows that the oscillation of the system is not suppressed by the applied cutting normal and tangential forces. Figure 4.21a) gives the frequency response of the rig in open loop (270 Hz); whereas the system vibrates at 274 Hz in closed loop control. The driving frequency was 275 Hz and it is seen that the grinding process did not affect too much the performance of the rig (error: 1-5 Hz); therefore it was assumed that the design of the rig was adequate



4. Vibrating Rig - Theory and Design

enough to undertake the bulk of the experiments in this study. The direction of vibration coincided workspeed direction as well as the tangential grinding force. This constitutes the first stage of vibration-assisted surface grinding studies. Future studies will aim at the effect of vibration at different directions.

Chapter 5: Equipment

5.1 Introduction

During this study, several pieces of equipment have been utilized for the experimental work. This chapter describes the features of the equipment used in three subcategories. The first one concerns the basic grinding machine and its components, the second illustrates all the external sensors, devices and any additional mechanisms that have been employed depending on the requirements and the third one relates the consumable products that have been used during the tests.

5.2 Grinding Machines and Components

The experimental work was carried out on the Abwood Series 5025 grinding machine - a conventional surface grinder with analogue pneumatic controls for the automatic traverse cycles. It has a 1.5 kW motor for the wheel head ensuring rapid stock removal. A self-contained hydraulic pump system was built as a separate unit and was housed at the base of the machine. The tank could hold up to 36 liters of oil. The unit operated at a maximum pressure of 0.833Mpa and required low pressure pipes which connected to the hydraulic actuators of the machine. The traverse speed could reach 200 mm/s. The wheel speed was controlled through an AC servo motor giving variable control up to 5000 RPM. The machine specification is shown in Table 5.1.

5. Equipment

Parameter	Value
Spindle motor power	1.5 kW continuous power
Spindle speed	Variable up to 5000 RPM
Cross traverse of head, via headstock <ul style="list-style-type: none">• Resolution	260 mm 10 μm
Longitudinal traverse, via workpiece <ul style="list-style-type: none">• Resolution	530 mm 10 μm
Vertical traverse of head, via headstock <ul style="list-style-type: none">• Resolution	350 mm 1 μm
Automatic Feed	Pneumatic control in X,Y and Z axis
Maximum wheel size	400 mm x 25 mm

Table 5. 1: Specification of the Abwood 5025 Surface Grinding Machine.

5.3 External Sensors and Devices

There were several sensors and devices used in this study including:

5.3.1 Piezoelectric Actuator

This device can produce a small displacement at high frequencies with a high force when an alternated voltage is applied to it. The piezo-elements (ceramic discs) inside are based on modified lead zirconate titanate (PZT) and barium titanate. These elements can produce oscillations by their expansion and contraction depending on the applied voltage.

The actuator was driven by a power amplifier that amplifies a small sinusoidal input signal from a function generator. The piezoelectric actuator employed for the present study was a high performance P212.8 suitable for static and dynamic applications. It could produce up to 2000 N peak force with a 120 μm maximum displacement.

The amplifier was a two channel E 472.2 (Physic Instruments) high power amplifier with a 110 W average output power for dynamic open loop operation and it could generate up to

1100 Volts output. Moreover, there was a DC offset potentiometer in order to add a constant to the analogue control input in such a way the input being 1/100 of the desired output. The full specification of the piezoelectric actuator is illustrated in the table below.

Parameters	Values
Dimensions	
• Length	139 mm
• Diameter	18 mm
• Translator Diameter	8 mm
Pushing Force Capacity	2000 N
Pulling Force Capacity	300 N
Open – loop Travel	120 μ m
Piezoelectric Actuator Mass	0.21 Kg
Power Amplifier Channels	2
Power Amplifier total Output	1100 Volts
Amplifier Average Output Power	110 Watts

Table 5. 2: Specifications for the P 212.8 Piezoelectric Actuator and E 472.2 Power Amplifier.

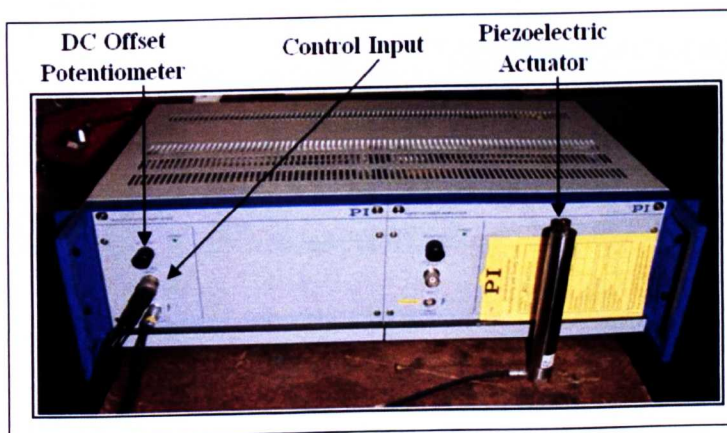


Figure 5. 1: Piezoelectric Actuator and Power Amplifier.

A ball tip was placed at the end of the translating shaft with the intention of decoupling torque and off-centre forces from the load. The main function of the piezoelectric actuator was to oscillate the workpiece during the grinding process, horizontally opposing to the



tangential grinding force. Therefore, it was mounted in a special structure, manufactured according to the test requirements and the piezoelectric actuator assembly is shown in Appendix A2.

5.3.2 Dynamometer

Grinding forces were measured with a 3-axis Kistler dynamometer type 9257A. It allows measurement up to 5000 N in X, Y, and Z coordinates. It has a resolution of $<0.01\%$ of full scale, great rigidity, high natural frequency and insensitivity to temperature influences. However, the initial calibration was only carried out up to 200 N normal and tangential directions (X, Y directions) as illustrated in Figure 5.2. This was done in both loading and unloading modes as recommended by the manufacturer in an ambient temperature of $\sim 20^{\circ}\text{C}$. The calibration arrangement for both normal and tangential components can be seen schematically in Figure 5.2.

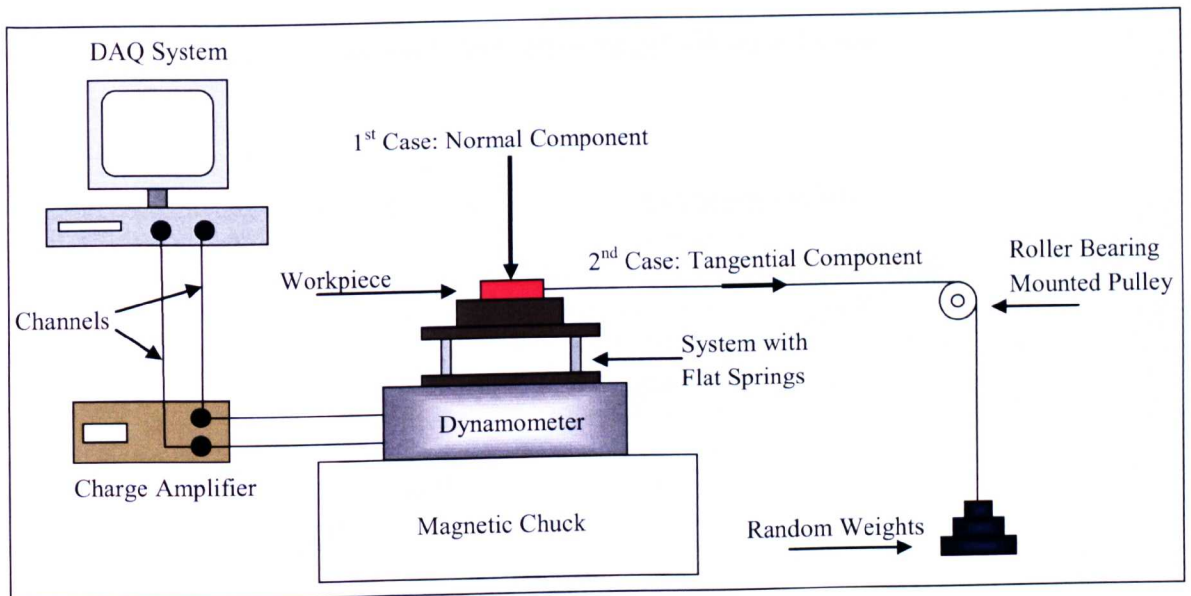


Figure 5. 2: Experimental Rig for the Dynamometer Calibration.

For the tangential force component the charge amplifier was set at a sensitivity of 8.015 pC/N and the scale was set at 100 units per volt; for the normal force component 3.755 pC/N and the scale as 100 units per volt. The graphs below (Figure 5.3 and 5.4) represent



the calibration results for both normal and tangential components. Moreover, a linear approximation and an equation for each graph have been derived in order to convert voltage into force.

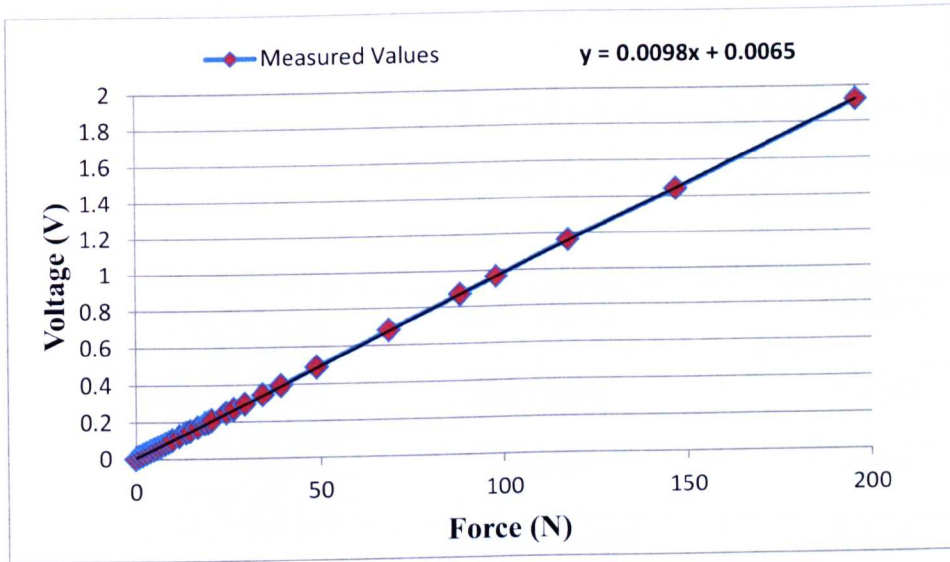


Figure 5. 3: Normal Component of Force Calibration Results.

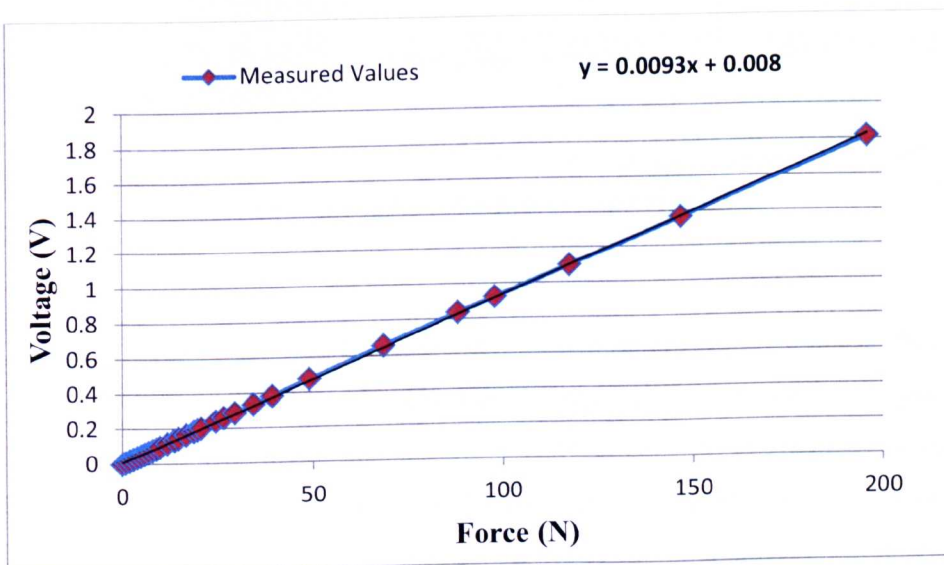


Figure 5. 4: Tangential Component of Force Calibration Results.



It is observed from fig. 5.3 and 5.4 that the response of the dynamometer is linear over the calibration range and no hysteresis was observed.

5.3.3 Displacement Sensor

A water proof displacement sensor (HSG-DVRT-6) from Technimeasure with high resolution of 0.6 μm was used during these studies. The picture in Figure 5.5 depicts the actual device and its specifications.

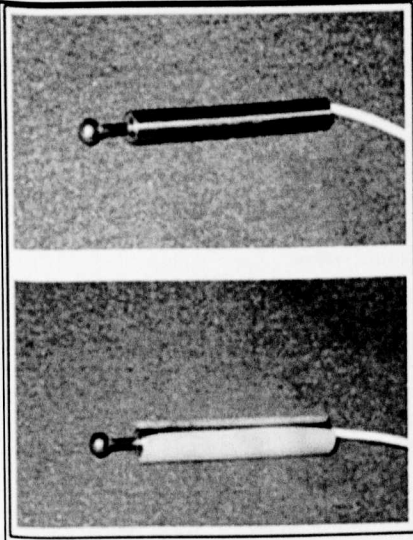
	Parameter	Value
	Resolution	0.6 μm
	Stroke	6 mm
	Overall Length	50.5 mm
	Outer Diameter	6 mm
	Frequency Response	800 Hz
	Operating Temperature	-55 $^{\circ}\text{C}$ - 175 $^{\circ}\text{C}$

Figure 5. 5: Displacement Sensor - Specifications.

Any movement of the ball guide modifies the core's position which is detected by measuring the coils differential reluctance using excitation and a synchronous demodulator. This differential detection method provides a very sensitive measure of core position while cancelling out temperature effects. All the experimental tests were carried out on the top of the magnetic chuck of the grinding machine. A special rig was manufactured with the purpose of holding the displacement sensor according to the nature of the experiment. For that reason, the sensor was accommodated in an acrylic enclosure in order to be isolated from any magnetic forces that could affect its inside core and therefore



the output voltage readings. The demodulator was encapsulated into a steel box sealed with a silicon rubber gasket for better isolation against any liquid or humidity during the grinding process.

For the calibration process, the sensor was held by a steel support mounted to the magnetic chuck. The ball guide was attached to a second immovable steel plate. A set of feeler gauges with various thicknesses has been used. Different gauges were placed between the sensor and the plate giving each time an alternation in output voltage respectively. A Data Acquisition System (DAQ) was used in order to obtain all the voltage output values. This test was carried out several times in order to obtain more accurate results. Thus, a relationship between the output voltage and the sensor's displacement has been established. The calibration graph below (Figure 5.6) describes this relationship.

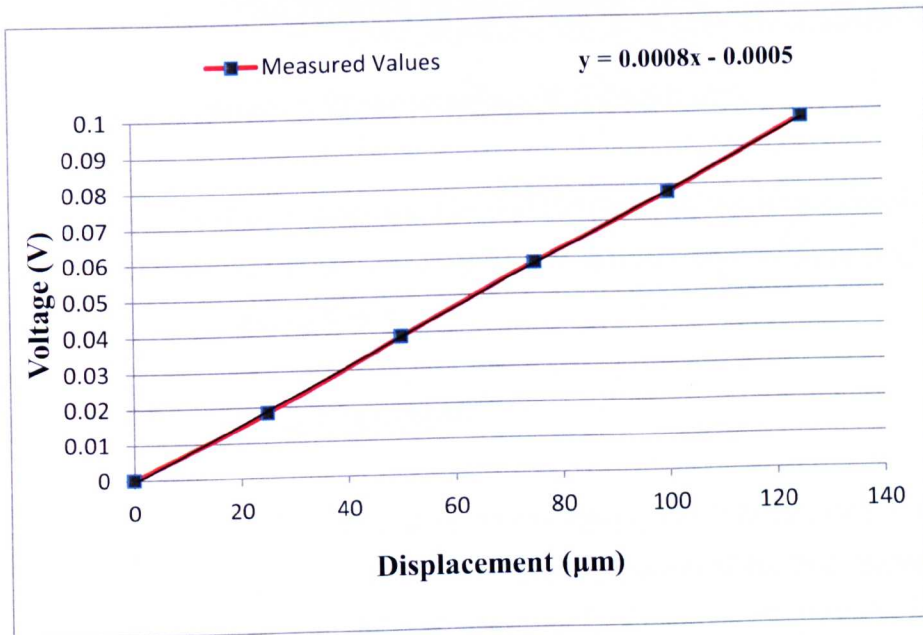


Figure 5. 6: Displacement Sensor-Calibration Results.

The sensor response was linear as expected in low noise environment. However in the grinding condition when the high frequency inverter of the grinding machine operates, there was very high level of noise. This made it difficult to extract the displacement signal.



5.3.4 Surface Roughness Measurement Device

The Sutronic Duo of Taylor-Hobson illustrated in Figure 5.7 was used to measure the roughness of the workpiece surface after a grinding experiment. It could measure key roughness parameters such as Ra Rz and Rt as well as Rp, and Rv.



Figure 5. 7: Surface Roughness Measuring Device.

At the bottom half of the device there is a diamond stylus which was drawn across the part. The traverse mechanism was a cam driven to ensure that the required horizontal distance was travelled for adequate measurement.

5.3.5 Surface Texture Analysis Instrument

The Form Talysurf Series 120 surface analysis instrument was also used for in this study because it is computerised and provided a wide range of functionality. This equipment was used to measure the wear of the grinding wheel as explained in Chapter 11. The Form Talysurf Series 120 consists of a traverse unit on which a stylus beam and a skid are attached to it, a column which provides a stable mounting for the traverse unit and also allows for precise height and angle adjustment and an epoxy granite base to ensure a firm support of the column and workpieces. All the moving parts are connected to a control module for manual control of the units. The whole configuration of this instrument is shown in Appendix A3.



5.3.6 Accelerometer

The accelerometer used for the present work was a Kistler 8704B100 low impedance with ultra low base strain and low thermal transient response. The specification of this device is shown in Table 5.3.

Parameter	Value
Range	± 100 g
Sensitivity $\pm 5\%$	50 mV/g
Frequency Response $\pm 5\%$	0.5 kHz – 10 kHz
Operating Temperature	-54 °C – 100 °C
Housing Base	Titanium
Weight	8.6 grams

Table 5. 3: Specifications for the Accelerometer.

The accelerometer was fixed to the vibrating jig through a special mounting threaded stud. The acceleration was recorded using a NI 9233 four-channel dynamic signal acquisition module which was sited to a NI cDAQ 9172 chassis.

5.3.7 Data Acquisition System (DAQ)

In order to record the acquired data from the dynamometer, displacement sensor and accelerometer, a data acquisition system has been used. Because the experiment was carried out in a workshop where several machine tools run concurrently there was high noise and electrical interference that was picked up together with the desired signal from the sensor. Relevant measures were taking to reduce the noise level however filtering was used during the post-processing of the acquired data.

For all the experimental requirements a National Instruments NI-6250 data acquisition card with 8 analogue inputs (16-bit) ADC was used. It allowed a single channel of data to be sampled at a rate of 1.25×10^6 samples/sec or multiple channels at a rate of up to 1×10^6

5. Equipment

samples/sec in total. In order to control the hardware LabView 8.5 software package was used. Data were sampled continuous at a frequency of 10 kHz for the accelerometer and 3 kHz for the dynamometer and displacement sensor. The following signals were recorded: a) acceleration b) displacement c) normal force and d) tangential force. For this system, the software was designed to give a visual display of the current values in graphical and numerical way. The data stream was written continuously into a file saved and then post-processed. Figure 5.8 below shows the full configuration of the program set up for all the devices.

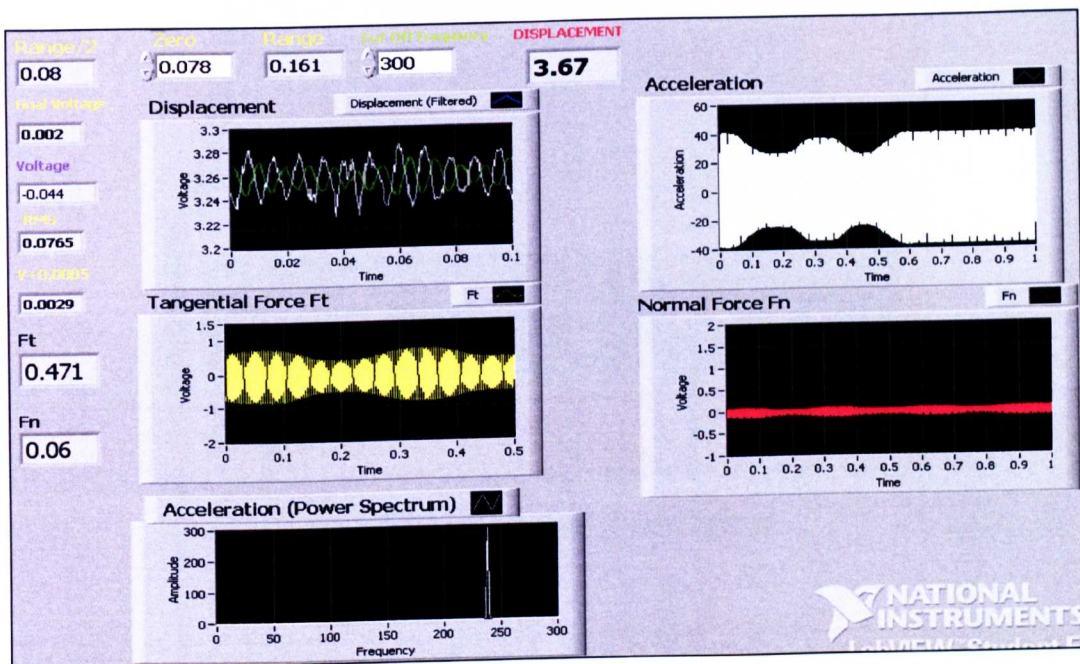


Figure 5. 8: Data Acquisition Program-Front Panel of the Sensors Configuration.

For the displacement sensor a low-pass Butterworth filter with a cut-off frequency at 300 Hz has been added. Using the calibration results obtained initially for the sensor, an equation that describes the relationship between the voltage and displacement was inserted to the LabView program. Thus, the actual numerical value of displacement could be illustrated on the front panel of the software in real time. The full program can be seen in Appendix A4



5.3.8 Closed-Loop Control System

The main purpose of this device was to control a given vibration parameter by keeping it constant during vibration-assisted grinding. A VibPilot from M+P International was used as it provides a dynamic signal analysis as well as vibration testing using integrated software. Figure 5.9 depicts the VibPilot.

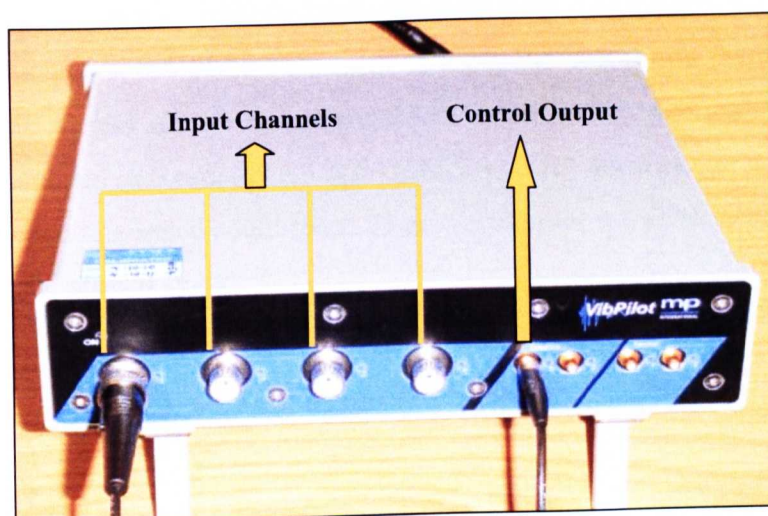


Figure 5. 9: Closed-Loop Control System.

The VibPilot could record the data of 4 or 8 input signals (4-channel version used) but it could control only one. Acceleration, velocity or displacement of the vibration could be controlled at one given time. In the present work the vibration displacement was controlled using an accelerometer. The power amplifier of the piezoelectric actuator was connected to the control output of the system in order to maintain the preset displacement constant regardless of external factors



5.4 Consumable Products

5.4.1 Grinding Wheels

The experimental work was conducted using aluminum oxide wheels with vitrified bonds. A custom manufactured alumina wheel (Altos wheel) with 54% porosity and high aspect ratio, in the region of 10:1 was used. Three other aluminum oxide wheels were used for the grinding experiments. The first one was a vitrified medium grade, medium grain wheel (454A 601 L 7G V 3) with a maximum nominated speed of 40 m/s. The second one was a vitrified medium-soft grade, medium grain, grinding wheel (89A 60 K 5A V 217) with a maximum nominated speed of 50 m/s. Both of them had a 200 mm diameter. The third wheel used was a viper ultra vitrified aluminum oxide soft-medium wheel with mixed grain size and an open structure (VU33 A 602 HH 10 V B1). Its diameter was 220 mm and the maximum operating speed could reach 64 m/s. Appendix A1 illustrates all the grinding wheels used in the present study.

5.4.2 Workpiece Materials

The experimental work involved three types of materials: mild steel (BS970 080440), En 31 (BS 534A99) and M2 tool steel (BS BM2). The mild steel is hard to grind but it was used to simulate aspects of grinding very ductile materials. M2 is a high carbon tool steel and the En31 is a bearing steel. The hardness of all the three workpiece materials is presented below (Table 5.5).

Workpiece Material	Hardness Rockwell
Mild Steel (BS970 080440)	90.1 HRB
En 31 (BS 534A99)	64.2 HRC
M2 Tool Steel (BS BM2)	62 HRC

Table 5. 4: Measured Hardness of Workpiece Materials.

5.5 Experimental Configuration

Figure 5.10 depicts the actual arrangement of the above described devices during the experimental work.

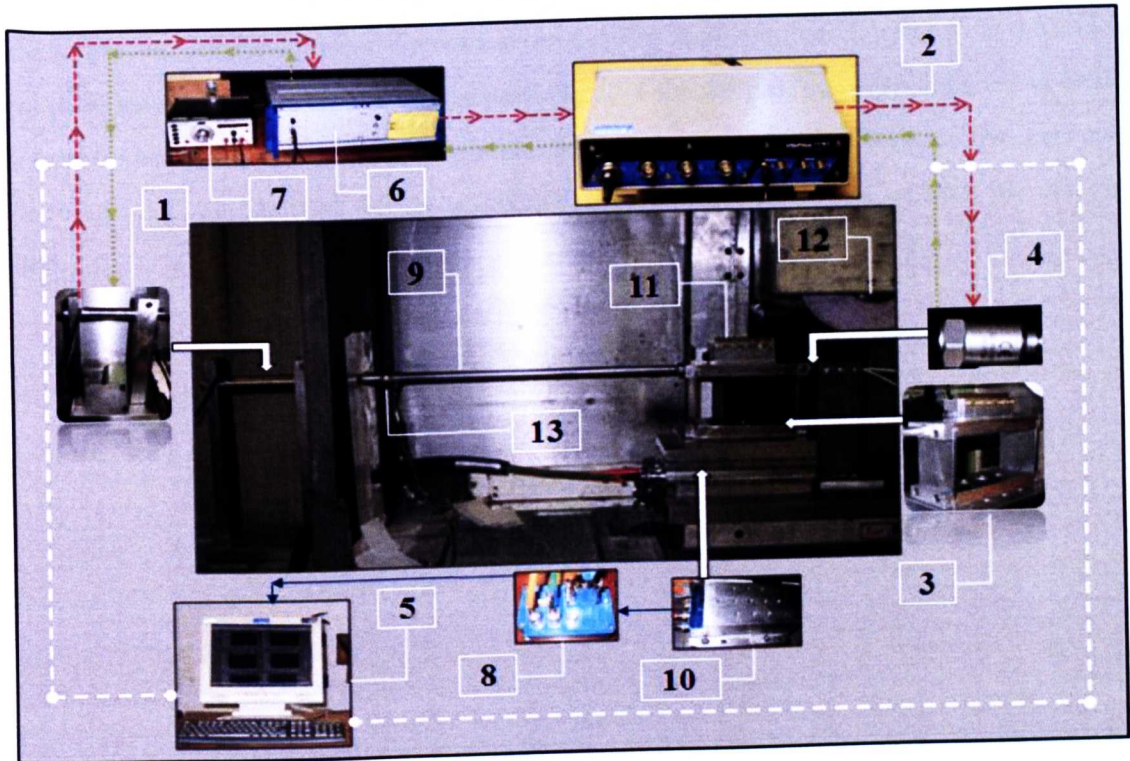


Figure 5. 10: Actual Configuration for the Full Experimental Work.

- | | |
|-------------------------------|---------------------|
| 1) Piezoelectric Actuator | 8) Charge Amplifier |
| 2) Closed-Loop Control System | 9) Connecting Rod |
| 3) Two-Spring Vibrating Rig | 10) Dynamometer |
| 4) Accelerometer | 11) Workpiece |
| 5) Data Acquisition System | 12) Grinding Wheel |
| 6) Power Amplifier | 13) Load cell |
| 7) Function Generator | |



5. Equipment

The design criteria were defined by the distance between the rig and the grinding wheel. During the experiments in open-loop, the frequency and the amplitude of the applied vibration were set from the function generator connected to the power amplifier of the piezoelectric actuator. However, for the experiments in closed-loop the frequency and the amplitude of the vibration were specified in the control system of the closed-loop (2) which determined the performance of the piezoelectric actuator using the signal from the accelerometer. All the data were recorded through the data acquisition system. In the end it has to be said that at the end of the connecting rod a special part has been attached in order to connect the system with the piezoelectric actuator and preload it. Between that part and the rod a load cell has been added but its use and performance do not concern the present study.

Chapter 6: Design and Simulation

6.1 Introduction

To undertake the planned programme of experiments, an oscillating rig was developed using a 3D solid modelling package. Three computer models of the rig were designed and two different types of analysis have been performed: static analysis and dynamic analysis which is explained below in more details. All the dimensions were selected in a manner that the vibrating rig to fit on the top of a dynamometer. Finally, the most appropriate design for this application was selected and used for the preliminary experimental tests.

6.2 Design Aspects of the Models

The system was designed taking into account the machining work envelop. Therefore, the device must be accommodated within the space available between the wheel and the worktable of the grinding machine.

6.2.1 Solid Model with Flexible Hinges

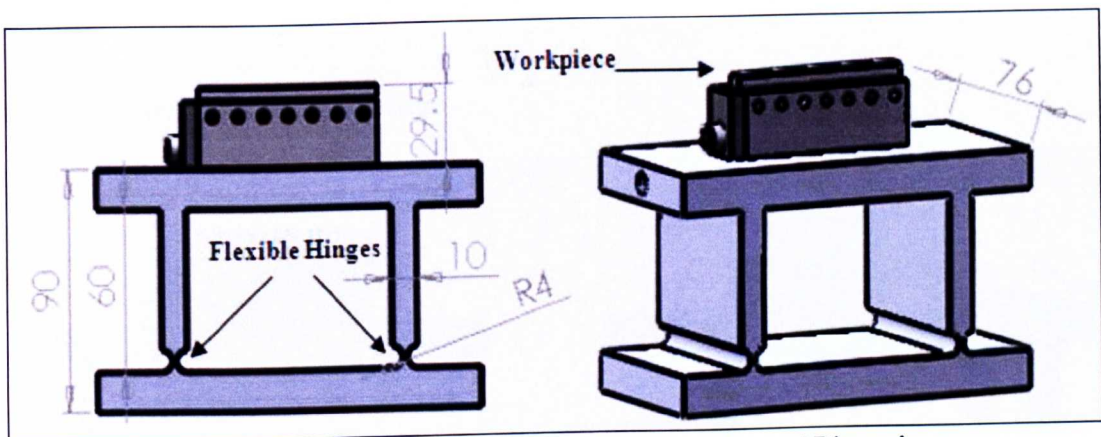


Figure 6. 1: Solid Model with Flexible Hinges-Design and Dimensions.

This was a rigid solid model designed to be machined from a single piece to the required shape (Figure 6.1). It consisted of a bottom plate two flexible hinges 10 mm thick and a top plate similar to the bottom one where the workpiece holder and the workpiece could be accommodated.



6.2.2 Table with Cylindrical Springs

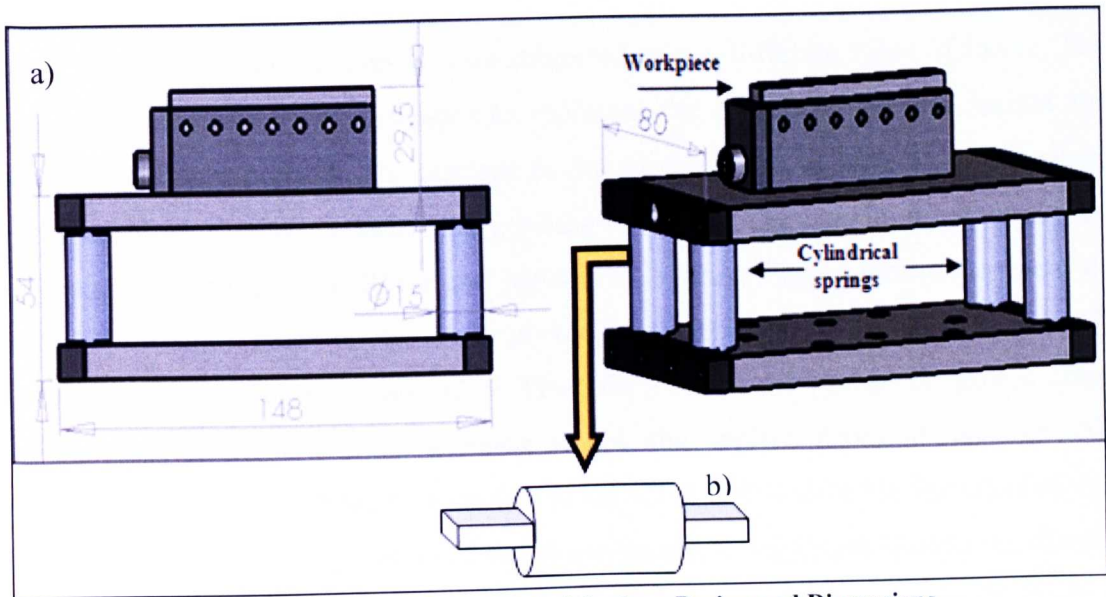


Figure 6. 2: Table with Cylindrical Springs-Design and Dimensions.

The system in Figure 6.2 consisted of two parallel steel plates which were connected to each other via four cylindrical springs as shown in Figure 6.2b. The workpiece was mounted to the top plate. Four clamps were used to keep the springs in position between the bottom and the top plate.

6.2.3 Table with Four Flat Springs

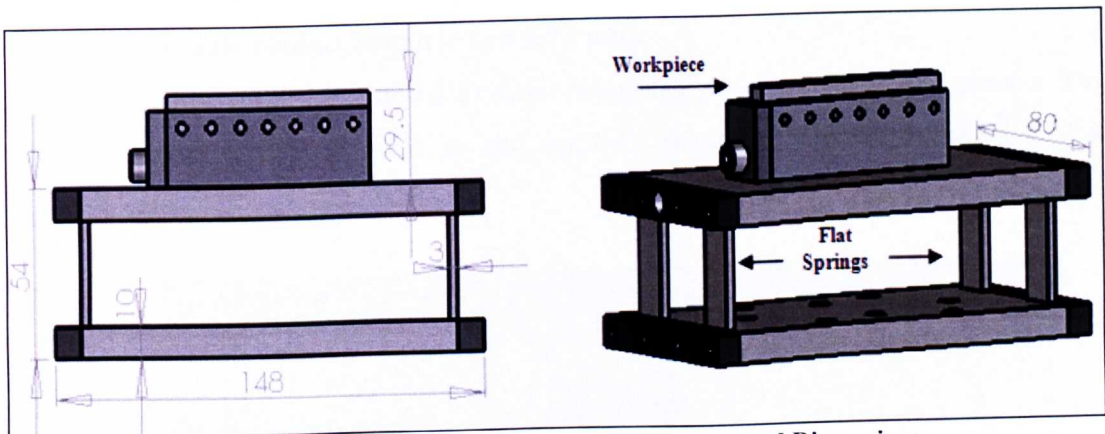


Figure 6. 3: Table with Four Flat Springs-Design and Dimensions.

The model Figure 6.3 is similar to the previous one but with four flat springs contrary to cylindrical ones. The differences between all of the models are explained further.



6.3 Static Analysis

During this analysis all the models were subjected to two different types of forces. These forces were applied to the workpiece to represent the tangential and the normal force during the grinding process. The purpose of this analysis was to have an initial view of how all the models respond during the grinding operation. The magnitude of those forces were taken according to Qi, Rowe and Mills (1997) where during their experiment they found that for $15\mu\text{m}$ depth of cut in a mild steel workpiece, the tangential force was 47 N and the normal grinding force was 72 N. Thus, for a mild steel workpiece ground using a medium grain aluminium oxide grinding wheel, the applied depth of cut was $15\mu\text{m}$ (assumed to be the real depth of cut) which is the value that is used for the calculations in this section of work. Taking notice all the above parameters and considering the diameter of the wheel, the geometric contact length of the workpiece was derived from the following formula:

$$l_g = \sqrt{a_e \times d_e} \quad (\text{Marinescu et al, 2004})$$

l_g : Geometric contact length.

a_e : Actual Depth of cut.

d_e : Diameter of the grinding wheel.

In the present case the $d_e = 199.86 \text{ mm}$, $a_e = 0.015 \text{ mm}$

Hence, the geometric contact length is $l_g = 1.73 \text{ mm}$

The pictures below (Figure 6.4 and 6.5) show in a closer view the geometric contact length of the workpiece (WP) as well as the applied grinding forces (Normal \downarrow and Tangential \leftarrow).

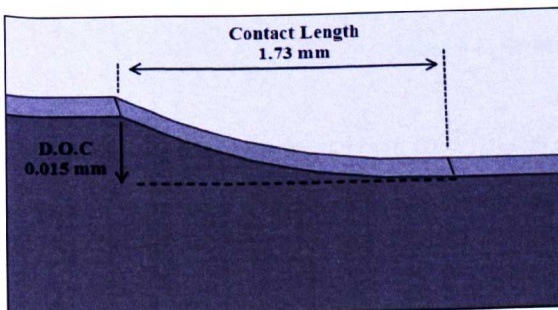


Figure 6. 4: Geometric Contact Length.

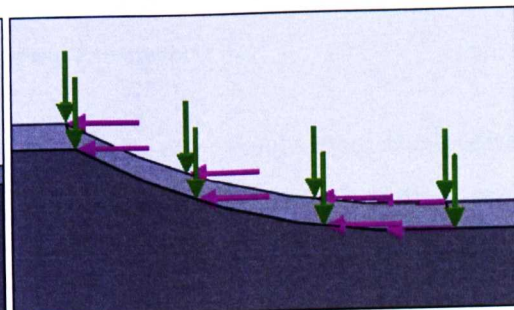


Figure 6. 5: Applied Grinding Forces.



The material used for this analysis was a Mild Steel with a density of 7800 Kg/m^3 , modulus of elasticity of 200000 N/mm^2 and Coefficient of Thermal Expansion per degree C from 20° C : 11.6×10^{-6} . Figure 6.4 does not represent the real design of the workpiece as it is used to illustrate the parameters such as contact length and depth of cut. Also, Figure 6.5 does not represent the design of the real workpiece but it was used to depict the direction of applied grinding forces. The real contact length had the shape of an arc due to the grinding wheel.

6.3.1 Meshing Parameters

A standard fine mesh was applied to the three models with identical elements size for the static analysis. However, it was necessary to apply different mesh parameters (mesh control) on the area where the grinding forces were applied. The full details for all the meshing parameters are shown below in Figure 6.6.

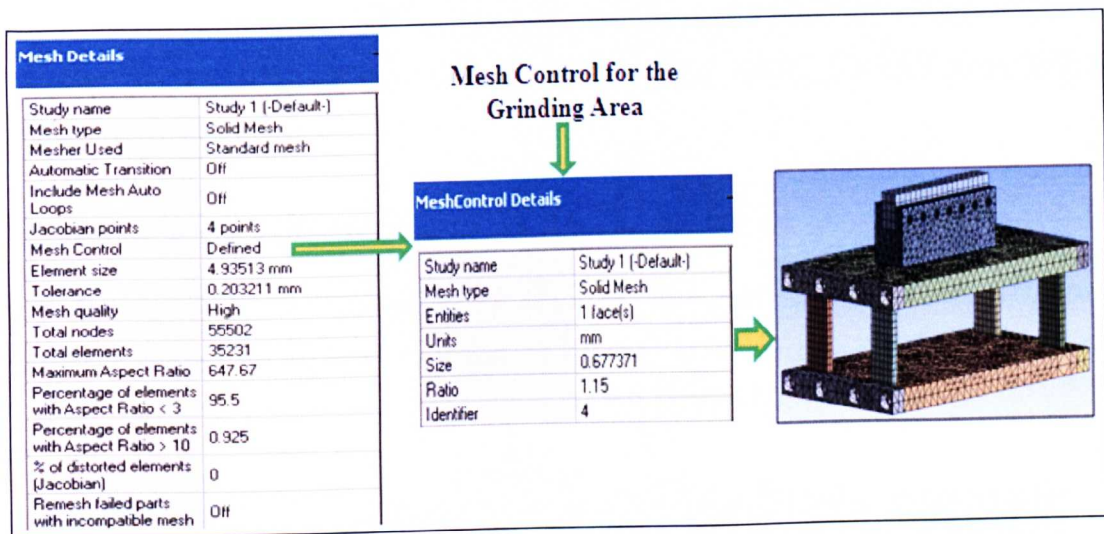


Figure 6. 6: Meshing Parameters.

Referring to the results given in Figures 6.8 - 6.11, one should note the positive and negative orientation of axes set up as default in Solidworks. This default setting (see Figure 6.7) makes the results of these simulations look inverse to what it should be. Consequently, in all models the bottom plate is displayed in red colour. Due to these default settings in SolidWorks software, the positive values were from left to right and the negative from right to left with reference to "0". Regarding the vertical axis Y the positive values were



set from up to down whether the negative ones were from down to up. Figure 6.7 shows the default setting in Solidworks.

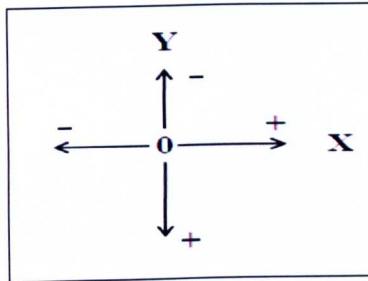


Figure 6. 7: Default Axes Settings in SolidWorks.

The direction of the tangential grinding force applied on the workpiece was from right to left. Therefore, the top plate moved to the left direction and the displacement appeared in blue colour. However, the blue areas of the models had the largest displacement and the minus sign indicated the direction of the deflection. The red areas appeared on the bottom plates of the models moved in the opposite direction as they had positive values. However, these values of displacement were in the scale of nanometres and they were considered as negligible. Therefore, one should bear this in mind when reading the simulation diagrams in the results given below.

6.3.2 Model with Flexible Hinges

The following results are showing the maximum displacement in vertical and horizontal axis as well as the von-Mises stress together with high stress concentration areas.

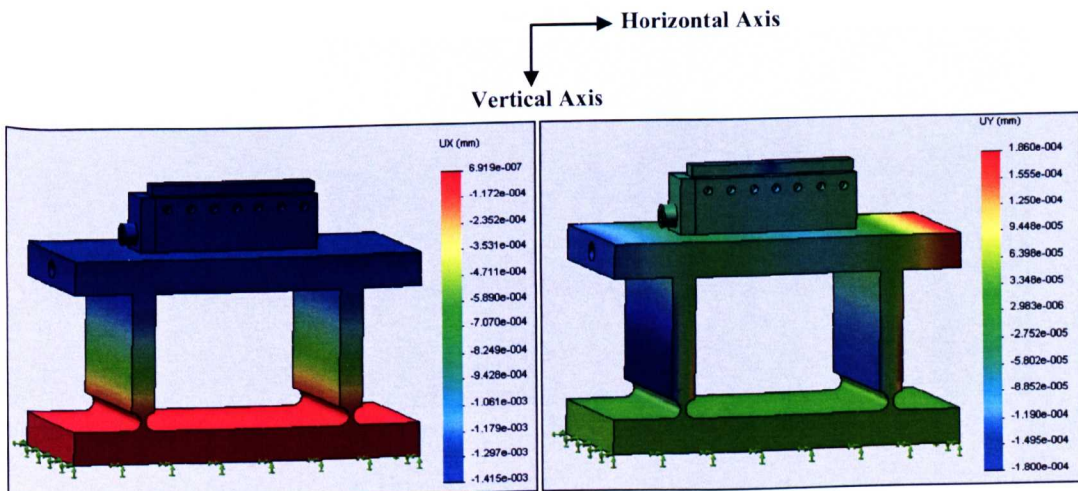


Figure 6. 8: a) Horizontal Displacement. b) Vertical Displacement.



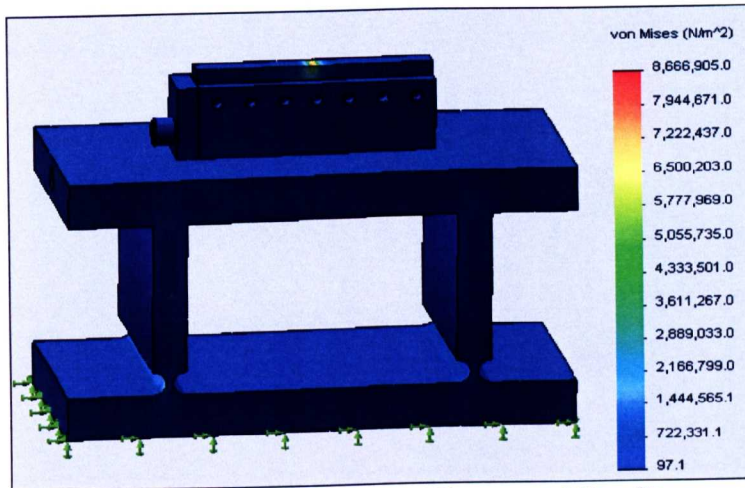


Figure 6. 9: Model with Flexible Hinges-von-Mises Stress.

As it can be seen from the results above (Figure 6.8a) the maximum displacement in the horizontal axis due to the tangential force for the model with the flexible hinges was $1.41 \mu\text{m}$ whereas in the vertical axis the maximum displacement - due to the normal grinding force - was $0.18 \mu\text{m}$. Both values were low and did not cause any serious motion of the system. This shows that the system has high rigidity thus; it did not deflect too much. The maximum stress (Figure 6.9) was found to be at the workpiece where both forces were applied and it was 8.6 MPa . It is essential to mention the fact that in the vertical axis, the displacement was extremely small thus, it can be neglected.

6.3.3 Model with Cylindrical Springs

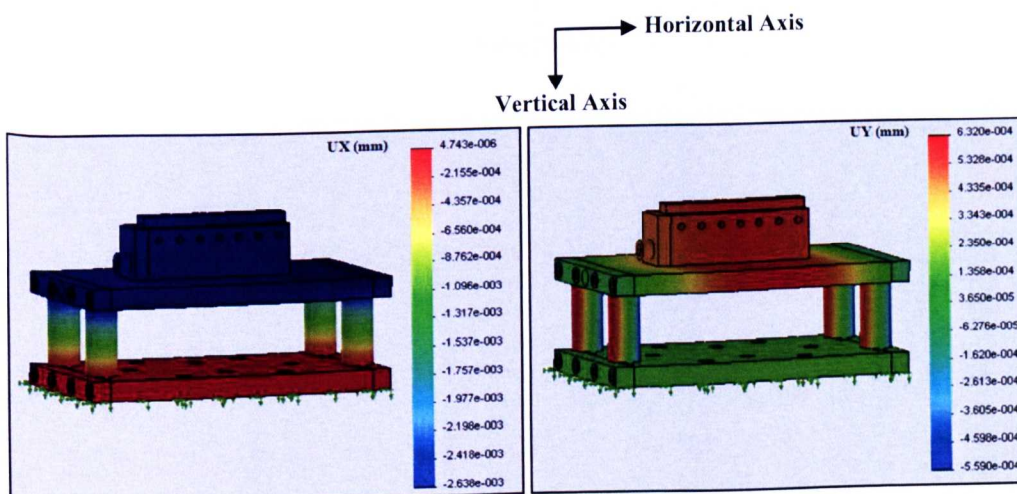


Figure 6. 10: a) Horizontal Displacement.

b) Vertical Displacement.



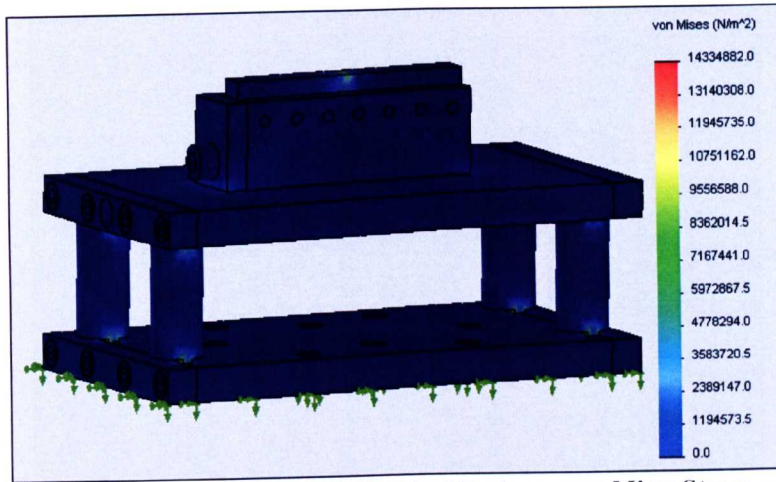


Figure 6. 11: Model with Cylindrical Springs- von-Mises Stress.

For this model the maximum displacement in the horizontal axis was $2.63 \mu\text{m}$ whereas in the vertical axis is $0.63 \mu\text{m}$. The highest value of stress was 14.3 MPa and appeared at the top and bottom end of the springs as well as at the area of workpiece where the forces were applied. This model appeared to be a lot stiffer and more rigid than the previous one. Also, in this case the value of displacement in the vertical axis was very small- $0.63 \mu\text{m}$ and could be neglected.

6.3.4 Model with Flat Springs

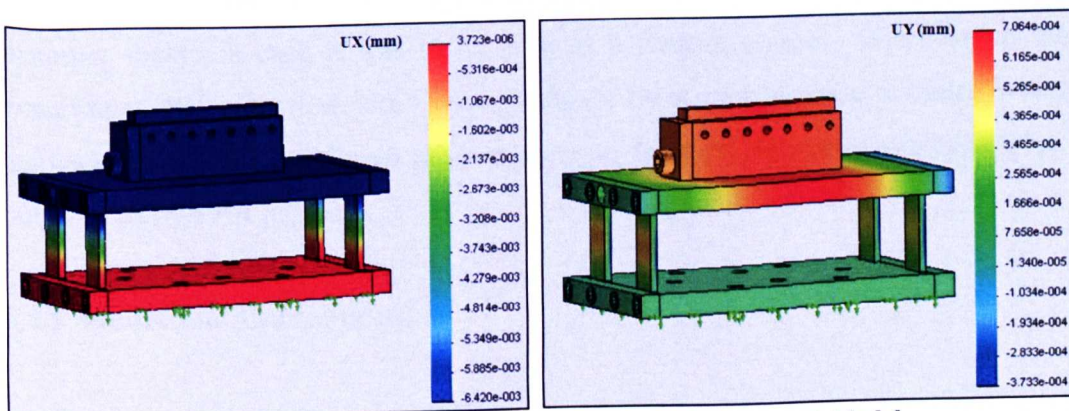
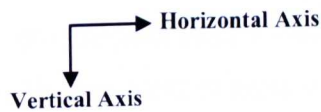


Figure 6. 12: a) Horizontal Displacement

b) Vertical Displacement-Model.



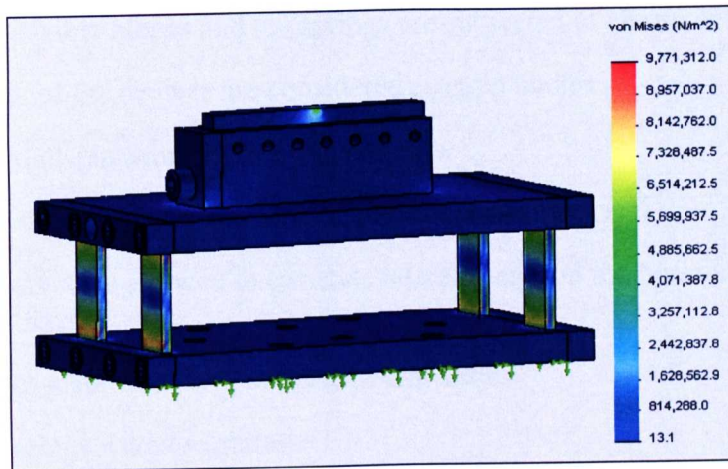


Figure 6. 13: Model with Flat Springs-von-Mises Stress.

This model provided the highest displacement in both axes compared to previous ones. In the horizontal axis the displacement reached $6.4 \mu\text{m}$ and $0.7 \mu\text{m}$ in the vertical. Moreover, the highest value of stress was 9.7 Mpa and appeared at the top and bottom of flat springs as well as on the area where grinding forces were applied. It was observed that in all models the displacement in the vertical axis was very low and it could be neglected.

6.4 Dynamic Analysis

The aim of this analysis is to obtain the response of each model under simulated loading conditions that are changing in time. For the preliminary study a sinusoidal force of 100N amplitude was applied horizontally to the top plate of each model at different frequencies. Here the magnitude of 100N was simulating the maximum force of a small electrodynamic shaker in case it was to be used as a backup option. However, in the actual experiment the excitation force was produced by a piezoelectric actuator which could theoretically reach a maximum pushing force of 2000 N . All the simulations were carried out in ANSYS FEA package.

6.4.1 Simulation Assumptions

The following assumptions were made in order to characterise the simulation process and to describe all the boundary conditions of the models during the analysis.



- Only the flexible hinges and the springs are subjected to elastic deformation.
- Other parts of the devices are considered as rigid bodies.
- There is no displacement in the vertical axis.
- The force was applied to the top plate horizontally (X-Axis).
- The systems were allowed to translate laterally only in the horizontal axis under the excitation force.
- The bottom plate was fixed to the grinding table.
- The flat springs were weightless.
- Damping in the system was considered as internal friction and was neglected.

6.4.2 Simulation Parameters for all the Models

- Material used: Low carbon steel En9.
 - Modulus of Elasticity 200000N/mm^2
 - Density: 7800 Kg/m^3
 - Poisson's Ratio: 0.3
 - Coefficient of Thermal Expansion per C from 20 C: 11.6×10^{-6}
- Meshing: Mechanical medium mesh. The full mesh of each model can be seen in Appendix B1.

6.5 Frequency-Amplitude Study

The following results depict the high stress concentration areas of all three models at 200Hz frequency. Also, a frequency- amplitude characteristic has been created in order to observe the response of each one under dynamic loading conditions as well as find their natural frequencies. The results revealed the high stress concentration areas of each model at 200Hz which was chosen randomly. Also, the natural frequency and the peak value of displacement each model can reach under the effect of this force have been identified. Equally, a frequency- amplitude characteristic of each system has been plotted.

6.5.1 Solid Model with Flexible Hinges

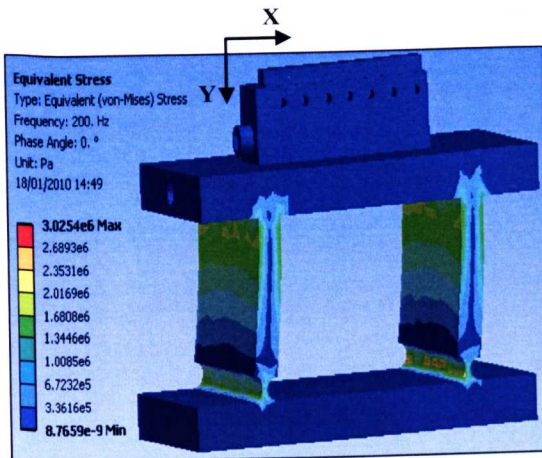


Figure 6.14: Stress Analysis-Model.

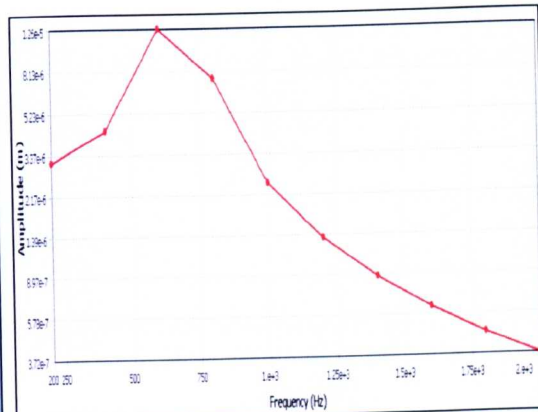


Figure 6.15: Frequency-Amplitude Plot-Model (1).

In Figure 6.14 it is seen that higher stress of about 3 MPa appears at the bottom curved area of the hinges. At 200 Hz the system had a displacement of $3.17 \mu\text{m}$ (Appendix B2) whereas at its natural frequency 683.37 Hz (Figure 6.15) the deflection reached $12.6 \mu\text{m}$ under 100 N applied force.

6.5.2 Model with Cylindrical Springs

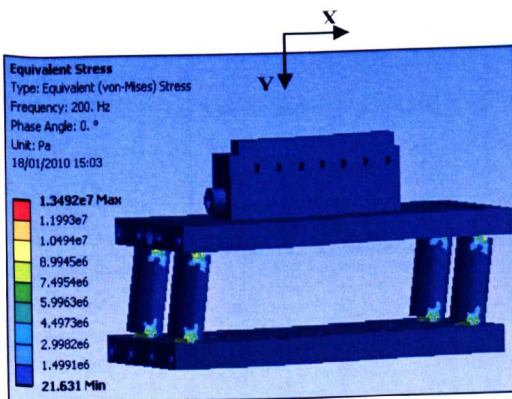


Figure 6.16: Stress Analysis-Model.

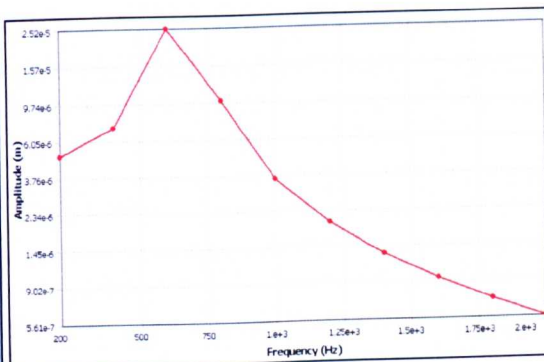


Figure 6.17: Frequency-Amplitude Plot-Model (2).

The model with cylindrical springs gave higher stress of 13.4 MPa (Figure 6.16). The stress concentrated at the top and the bottom area of the springs. At 200 Hz frequency the displacement was $5 \mu\text{m}$ (Appendix B3) but at its natural frequency - 624.32 Hz- the maximum deflection was $25.2 \mu\text{m}$ as shown in Figure 6.17.



6.5.3 Model with Cylindrical Springs

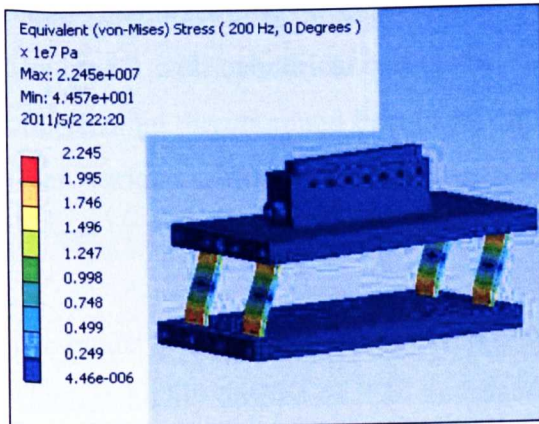


Figure 6. 18: Stress Analysis-Model.

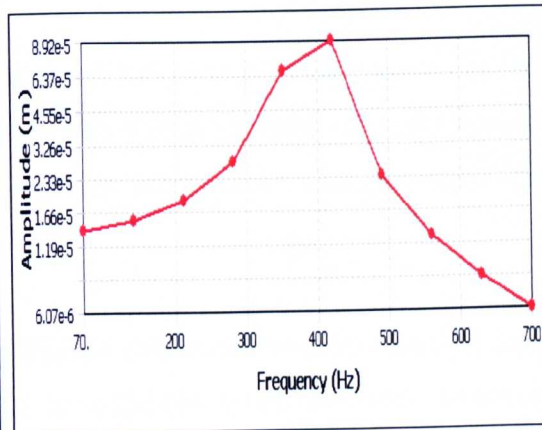


Figure 6. 19: Frequency-Amplitude Plot-Model (3).

With the flat spring model stress reached 22.4 MPa (Figure 6.18). As seen in the same Figure, the stress concentration areas are on the flat springs. At 200 Hz this model provided the highest displacement 18.92 μm (Appendix B4) with 89.2 μm deflection at its resonant frequency (425 Hz) as illustrated in Figure 6.19.

The Table 6.1 below presents the overall results of the static and dynamic analysis for the three models.

	Static Analysis			Dynamic Analysis			
	Displacement X-Axis (μm)	Displacement Y-Axis (μm)	von-Mises Stress (MPa)	Displacement X-Axis (μm) (200Hz)	Von-Mises Stress (MPa) (200Hz)	Natural Frequency (Hz)	Maximum Displacement (μm)
Model with Flexible Hinges	1.41	0.18	8.6	3.17	3.0	683.3	12.6
Model with Cylindrical Springs	2.63	0.63	14.3	5.0	13.4	624.3	25.2
Model with Flat Springs	6.4	0.7	9.7	18.9	22.4	425	89.2

Table 6. 1: Overall Static and Dynamic Analysis Results for all the Models

6.6 Model Selection

The study undertaken above showed the performance of each model with their merits and disadvantages.

It was observed that the model with flexible hinges was very stiff as it was a solid model. This model had low stresses during the dynamic analysis and showed no buckling



phenomena. However, such a device would be relatively not suitable for manufacturing and interchangeability purposes. This because if other stiffness were needed this would require manufacturing the entire device.

The model with cylindrical springs has a clear advantage in providing good displacement in horizontal direction and being stiff enough. This model provides room for modification when various stiffness is needed, as this could be achieved by changing the cylindrical springs.

The model with the flat springs secure the highest displacement at its resonant frequency which is highly desired as it is envisaged to drive the system at resonance. However, this model had relatively high level of stress, which could lead to high buckling risk under high forces.

Considering the performance, interchangeability and manufacturing aspects of the three systems, the model with the flat spring was selected as the most suitable for this kind of application without excluding the possibility of using the model with the cylindrical springs if needed. Therefore the model was manufactured and used only for the preliminary studies.

6.7 Flat Springs System-Analytical Consideration

The model depicted in Figure 6.22 represents a sketch of the vibrating system with the four flat springs. When a force $F(t)$ was applied on the top plate horizontally, it caused the mass M to translate only in the horizontal axis. According to the previous assumptions only the flat springs were subjected to any elastic deformation. Figure 6.20 illustrates how the system is deflected due to the external applied force as well as the dimensions of each element.

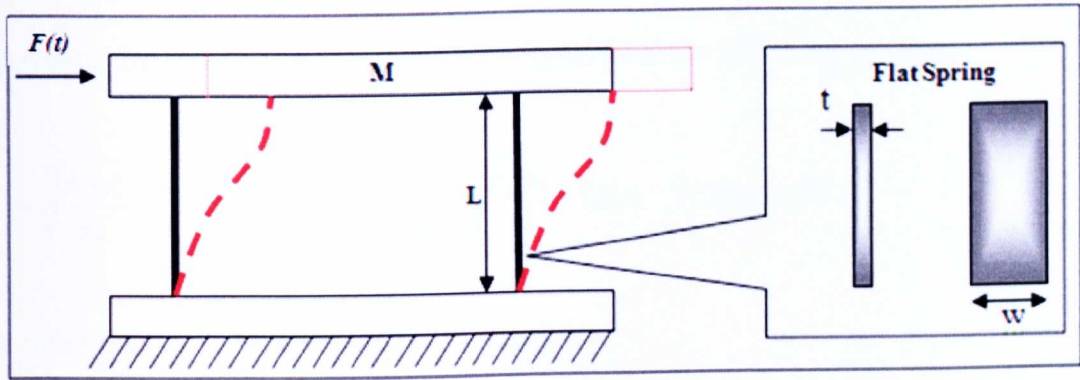


Figure 6. 20: Flat Spring System Deflection - Component Dimensions.

The structure consisted of four springs mounted vertically and it assumed the springs are aligned squared and parallel. Hence, the effective spring stiffness of the structure was four times the lateral stiffness of each flat spring and is therefore:

$$K_{tot} = 4 \times K \quad (\text{Smith, 1988}) \quad (6.1)$$

$$K \text{ is the stiffness of one flat spring and it equals to: } K = \frac{12 \times E \times I}{L^3} \quad (6.2)$$

The material used was cast carbon steel with a modulus of elasticity $E = 200 \times 10^9 \text{ N/m}^2$
 E : Modulus of elasticity of the material.

I : Area moment of inertia

$$I = \frac{1}{12} \times w \times t^3 \quad (6.3)$$

For this specific case the values for the dimensions were:

$$w = 15 \times 10^{-3} \text{ (m)}$$

$$t = 3 \times 10^{-3} \text{ (m)}$$

$$L = 34 \times 10^{-3} \text{ (m)}$$

$$I = \frac{1}{12} \times 15 \times 10^{-3} \times 27 \times 10^{-9} \rightarrow I = 3.375 \times 10^{-11} \text{ (m}^4\text{)}$$

The total stiffness of the system can now defined as:

$$K_{tot} = 4 \times \frac{12 \times 200 \times 10^9 \times 3.375 \times 10^{-11}}{(34 \times 10^{-3})^3} \rightarrow K_{tot} = 8243435.7 \text{ (N/m)}$$



The natural frequency of the system can be found from the following equation:

$$\omega_n = \sqrt{\frac{K_{tot}}{M}} \quad (rad/s) \quad \text{or} \quad \omega_n = \frac{1}{2\pi} \times \sqrt{\frac{K_{tot}}{M}} \quad (Hz) \quad (\text{Chan, n.d})$$

The vibrating mass of the system is $M = 1.258 \text{ Kg}$

$$\omega_n = \frac{1}{2\pi} \times \sqrt{\frac{8243435.7}{1.258}} \rightarrow \omega_n = 407.6 \text{ (Hz)}$$

The difference between the analytical calculations and the harmonic analysis results obtained from ANSYS, is not big, thus the error between the two methods is 4%. The analytical results of the natural frequency of the model confirm the validity of the finite element method.

6.7.1 Connecting Rod

In order to drive the vibrating rig, the oscillation from the piezoelectric actuator was transmitted through a metallic rod connected to the top plate. The transmission of the vibration via the rod was designed to keep the actuator out of the grinding zone. This is because the actuator is susceptible to damage by the cutting chips wheel debris and the cutting fluid. The picture in Figure 6.21 shows the actual configuration of the whole vibrating rig.

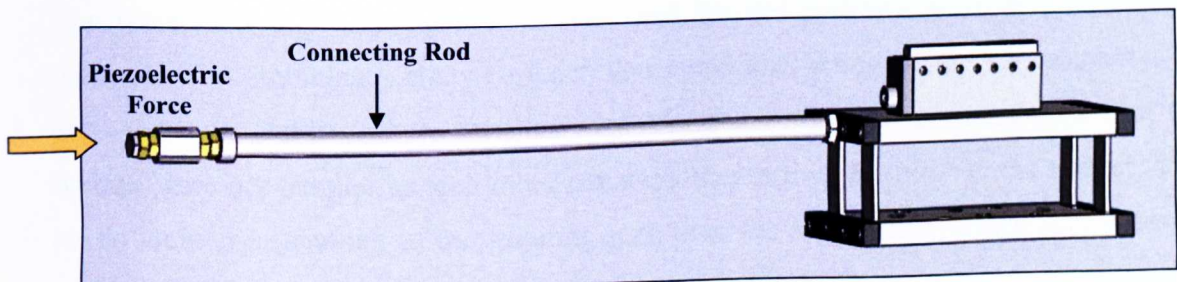


Figure 6. 21: Vibrating Rig for Preliminary Studies.



However by adding the rod, the mass of the vibrating system now increased to 1.655 Kg. Consequently, the system natural frequency shifted and system resonated at one of the rod modes rather than the rig frequency. Therefore, further analytical and FEA studies were undertaken and the natural frequency of the model was found to be 385.8 Hz. Figure 6.22 shows the results of the new frequency analysis performed and illustrates different modes of the system response.

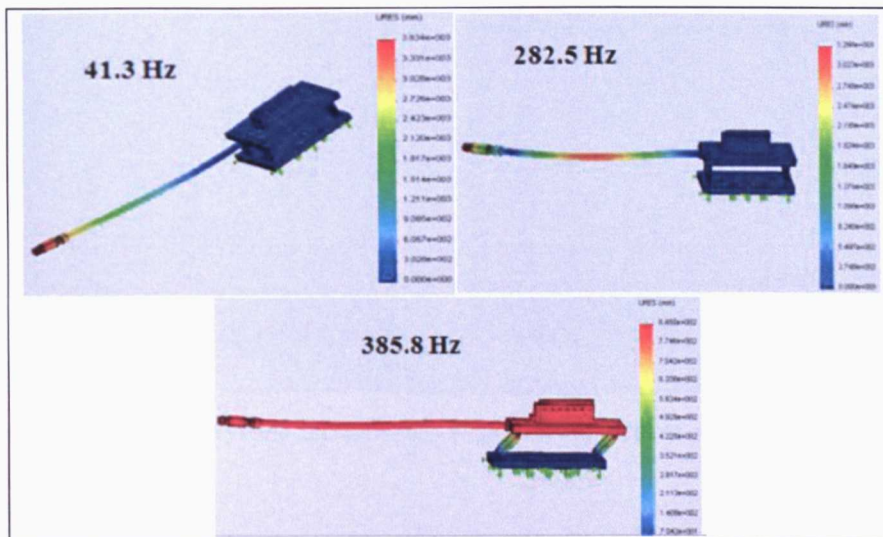


Figure 6.22: Frequency Analysis of the Vibrating Rig for Preliminary Studies.

Figure 6.22 shows three modes of vibration of the rig assembly. It is seen that the first two modes are related to the rod whereas the third mode, which is the most representative is the rig itself where the error is 5.3%. The connecting was part of the impact pair vibrating rig-grinding wheel as it was connected to the piezoelectric actuator.

6.8 Design Iteration & System Improvement

The selected four flat spring system was used for the preliminary studies during this research. The preliminary study revealed some malfunctioning of the rig assembly. As expected in assemblies where parts are manufactured with loose tolerances, the four flat springs were not parallel to each other nor were they orthogonal (90° to the plates). This led to arching or slanting of the grinding path over the workpiece. There was a design problem i.e. the round profile at the edges of the springs (see Figure 6.23 below) that led to the rocking of the spring and the slot in the plate was not manufactured with tight tolerance.



To resolve this problem and achieve desired results, a novel design was introduced with two flat springs with no round ends that were ground flat to mate tight with the plates (see Figure 6.24). There were no fillets from the milling tools as there are no slots. The initial idea did not change entirely but the model converted to a smaller and more stable one.

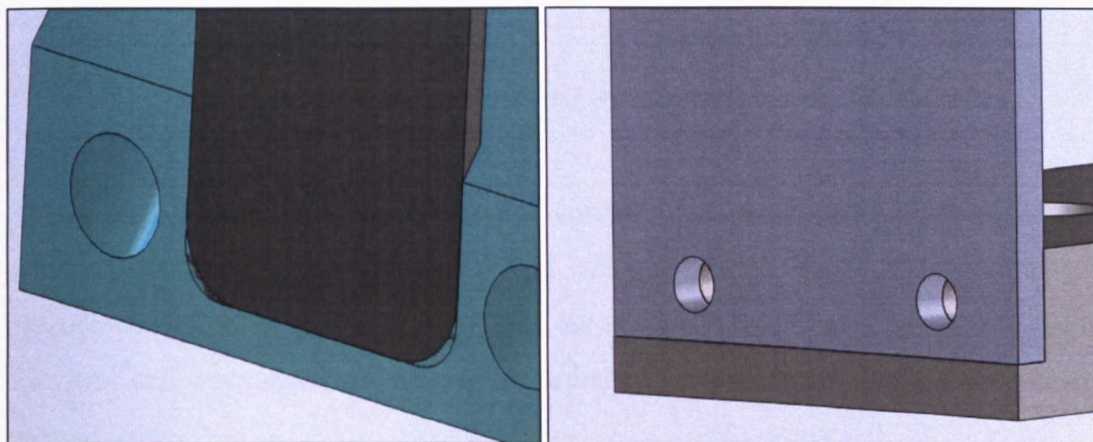


Figure 6. 23: Four Spring System Irregularity. Figure 6. 24: Improvement of the Novel Model.

The new model was stiffer than the previous one and it consisted of two flat springs made of high speed steel and could be replaced with thinner or thicker ones to vary the stiffness of the whole system if needed. Figures 6.25 and 6.26 below illustrate the details of the novel system as well as the entire assembly of the vibrating rig. This new system was used for the main body of vibration-assisted grinding study. Further detailed representation of the novel design is depicted in Appendix B5 where all the drawings of each part are shown.

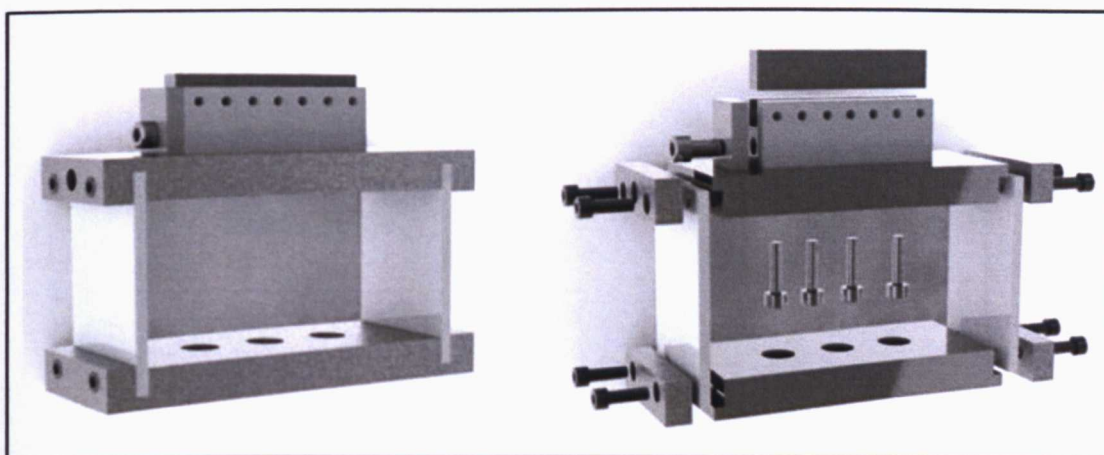


Figure 6. 25: Novel Vibrating System and its Exploded View.

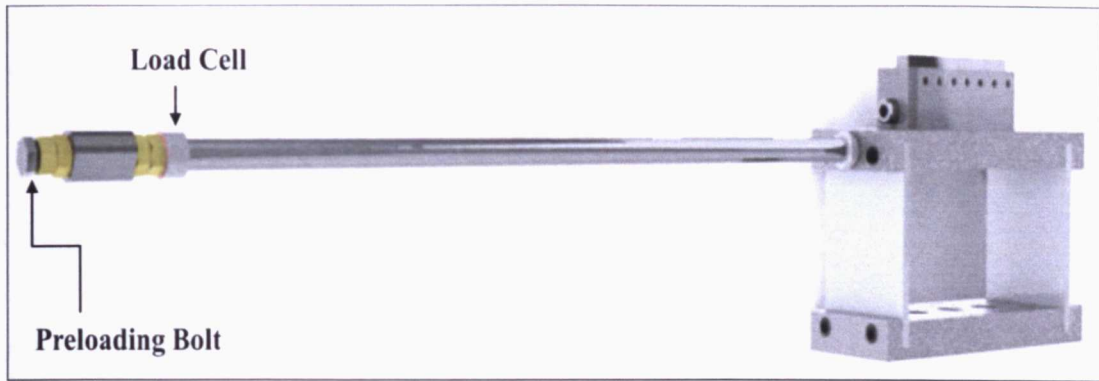


Figure 6. 26: Entire Novel Vibrating System-Experimental Configuration.

At the end of the steel rod a special arrangement was added. The purpose of this arrangement was to accommodate a load cell and a bolt. The bolt was attached to the piezoelectric actuator and used to preload the system before any grinding trial takes place. The load cell was used for obtaining a number of measurements that are not related to the present study.

6.9 Novel System - Dynamic Characteristics

It was expected that the system would behave differently due to changes in its mass which mainly affect the system natural frequency. Therefore, a full frequency analysis of the new system was undertaken.

6.9.1 Modal Analysis of Novel System

A frequency (modal) analysis of the vibrating rig has been carried out as previously in ANSYS the following results in Figure 6.27 show the mode of the system response.

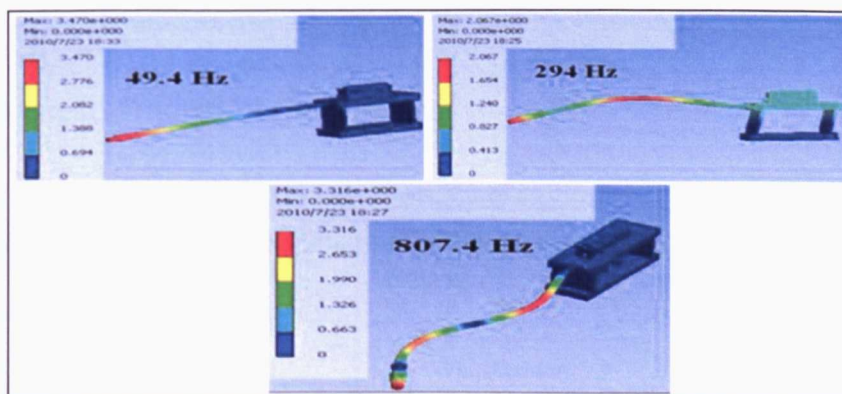


Figure 6. 27: Novel System-Frequency Analysis Results.



In Figure 6.27 it is observed that the new system displays three modes 49.4 Hz, 294 and 807 Hz. Here, the second mode is close to the calculated value (see Figure 6.29) – 294 Hz.

6.9.2 Novel System - Frequency-Amplitude Response

The purpose of this analysis was to observe the response of the system under dynamic loading conditions as well as to inspect the stress concentration areas of the model. A dynamic force of 100N amplitude was applied to the model. Also, a frequency – amplitude characteristic for the system has been obtained.

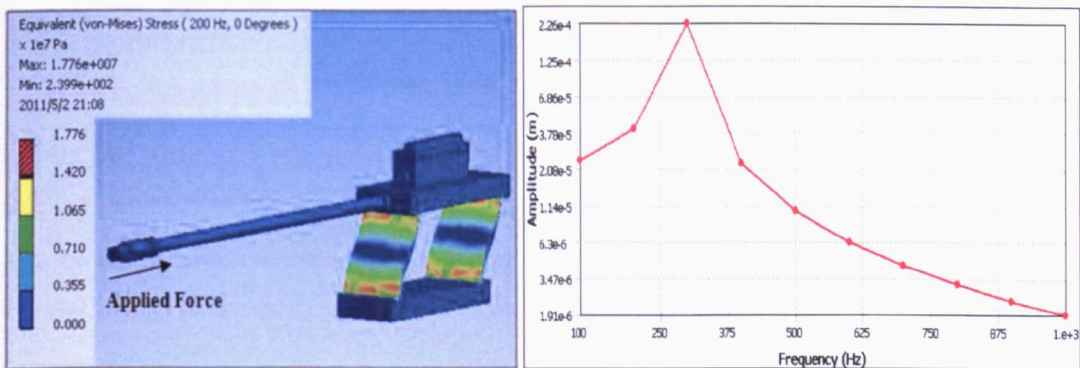


Figure 6. 28: High Stress Concentration Areas. Figure 6. 29: Frequency-Amplitude Characteristics.

Figure 6.28 depicts the stress areas of the model at a specific frequency of 200 Hz. The higher values of stress appeared at the top and bottom (clamped area) of the two springs. Furthermore, the natural frequency of the model was found to be at around 310 Hz which agrees with the value of the modal analysis performed earlier in this study and the manual calculation with an error of 5.1%.

6.9.3 Novel System - Analytical Calculations

Similar analytical calculations were made to obtain the natural frequency of the new model.

$$K = \frac{12 \times E \times I}{L^3}$$



The material used was high speed steel with a modulus of elasticity $E = 180 \times 10^9 \text{ N/m}^2$

E : Modulus of elasticity of the material.

The value of modulus of elasticity was derived from the tensile test performed particularly for that material because its properties were not clear. The Experimental procedure for this test is given in Appendix B6.

I : Area moment of inertia

$$I = \frac{1}{12} \times w \times t^3$$

For this case the values for the dimensions were:

$$w = 50 \times 10^{-3} \text{ (m)}$$

$$t = 4 \times 10^{-3} \text{ (m)}$$

$$L = 58 \times 10^{-3} \text{ (m)}$$

$$I = \frac{1}{12} \times 50 \times 10^{-3} \times 64 \times (10^{-3})^3 \rightarrow I = 2.666 \times 10^{-10} \text{ (m}^4\text{)}$$

The total stiffness of the system derived as two times the stiffness of one spring and is therefore:

$$K_{tot} = 2 \times \frac{12 \times 180 \times 10^9 \times 2.666 \times 10^{-10}}{(58 \times 10^{-3})^3} \rightarrow K_{tot} = 5902825 \text{ (N/m)}$$

The natural frequency of the system can be found from the following equation:

$$\omega_n = \sqrt{\frac{K_{tot}}{M}} \text{ (rad/s)} \quad \text{or} \quad \omega_n = \frac{1}{2\pi} \times \sqrt{\frac{K_{tot}}{M}} \text{ (Hz)}$$

The vibrating mass of the system is now $M = 1.587 \text{ Kg}$



$$\omega_n = \frac{1}{2\pi} \times \sqrt{\frac{5902825}{1.587}} \rightarrow \omega_n = 307 \text{ (Hz)}$$

Using analytical calculation, the natural frequency of the system is in agreement with the frequency analysis performed earlier. The overall results of the three methods for determining the natural frequency of the system are presented on the next table (Table 6.2).

Method	Natural Frequency Results (Hz)
Analytical Calculations	307
Frequency Analysis	294
Harmonic Analysis	310

Table 6. 2: Natural Frequency Overall Results.

As seen the highest error detected was between the frequency analysis and the harmonic analysis and it was 5.1%.

6.10 Remarks

After the completion of the design and simulation a number of conclusions were drawn:

The simulation results showed how each model behaved under loading conditions in static and dynamic mode. This helped to select the suitable model for this application. The two chosen final models were used in real grinding for preliminary and main experimental work in this study.

The frequency analysis conducted in the present chapter - which was in match with analytical calculations - showed that the selected models are capable of withstanding the vibration induced during grinding.



The FEA analysis showed that the model with two flat springs had lower stresses than that of four springs. Thus, the range of simulations gave the results needed for the continuation of this study.



Chapter 7: Grinding Machine System Response



7.1 Introduction

An essential part of this work was the understanding and identification of static and dynamic characteristics of the machine tool. Equally important was the investigation of the vibrating jig's static and dynamic behaviour. Due to the nature of this work dealing with vibration, it was prudent to explore how the machine tool as well as the rig, performs under external dynamic loading conditions. Stiffness and natural frequencies of each component examined experimentally in this chapter in order to obtain a full understanding of the system response.

7.2 Dynamics in Grinding

All the machining processes require a given level of accuracy and consistency. In order to accomplish this, an insight into the dynamic characteristics of each machine is necessary. However, each machine has its own characteristics and responds differently depending on the specific application. A number of papers have been published describing and characterising the dynamic characteristics of different machines such as milling, drilling etc. One of the most recent works is the one of Filiz et al, (2009) where they tried to predict the frequency response of a tool-holder-spindle-machine system using an innovating model, which could describe most of the machining applications.

In terms of grinding, many theoretical studies have been carried out in order to determine and verify the parameters that characterise this process. Some of these parameters are the natural frequencies, the effective grit pass and the grinding wheel contact dynamics.

In Jiang et al, (2007) they utilised modal experiments to describe the dynamic characteristics of a cylindrical grinding machine. Their target was to collect typical vibration signature produced by the machine and attempt to avoid those values of vibration during the grinding process. They set 25 measuring points on the machine using accelerometers and non-contact displacement sensors. Their first experiment was to identify the natural frequencies of the machine in static mode where the excitation was produced by an impact hammer. The second one was to find critical frequencies - that should be avoided - while the wheel was rotating from 70 to 700 RPM. Finally, they



performed the same test but in real grinding processes. Hence, they revealed the critical vibration frequencies during the process and they analysed the relationship between the workpiece spindle speed and surface coarseness. They concluded that the increase of spindle speed led to an improvement of surface roughness of the ground workpiece. For that reason, in order to improve the surface roughness, the work-piece should be ground at high speeds.

In 2005, Gao and Tse evaluated the dynamic parameters of a modulator based grinding machine system which was under-damped. Their target was to identify the natural frequency of the wheel system and the damping ratio. They derived the theoretical response of the wheel system displacement $y(t)$ to a unit step input as follows:

$$y(t) = 1 - \frac{1}{\sqrt{1-\zeta^2}} e^{-\zeta\omega_n t} \sin\left(\omega_n \sqrt{1-\zeta^2} t + \cos^{-1} \zeta\right) \quad (\text{Dorf and Bishop, 1998}) \quad (7.1)$$

Where ζ is the damping ratio; ω_n is the undamped natural frequency and t is time.

Zhang et al, 2005, performed a dynamic analysis of the grinding process, in order to reduce the surface roughness of the workpiece caused by vibration. They tried to determine the frequency-amplitude characteristics of the grinding process. Thus, they developed a model and the following grinding condition have been considered: Grinding Wheel: 250mm (Synthetic Aluminium Oxide), cutting speed: 30-35 m/s, depth of cut: 0.005-0.03 mm, amplitude of vibration: 0.001- 0.002mm, frequency of vibration: 0-120 Hz, grain size: 0.40-0.50mm. The results showed that the developed model was valid in the considered range of frequency of vibration and the qualitative behaviour of the machine changed for different frequencies.

Kirpitchenko et al, (2002) developed a non-linear model for the analysis of dynamic characteristics of the grinding process such as frequency and amplitude. That research, focused on grinding kinematics and was based on the relative movements that are performed by every cutting grain of the grinding wheel and the ground component. Two possible force control systems for grinding operations were considered. The first was used



to minimize the bending moment (static and dynamic) in the bearing units of the spindle of the grinding machine. The key benefit of the system was that it did not depend on the frequency of the exciting force. However, such systems do not minimize the relative displacement of the grinding wheel and the work-piece. The second control system was to minimize the relative deformation at the contact between the grinding wheel and the workpiece. The results showed that the proposed control system is dependent on the frequency of the exciting forces. This work also aimed at reducing the surface waviness and roughness induced by vibrations, and to achieve a machine higher accuracy.

One of the most recent models for cylindrical grinding developed by Orynski and Pawlowski in 2002 in order to analyse the dynamics of a grinding machine tool. Their model consisted of the grinding wheel headstock with hydrostatic slideways, the headstock drive system, the hydrostatic bearings of the wheel spindle, the grinding wheel, force interactions of the grinding process, the workpiece supported in dead centres and the grinding table on hydrostatic slideways. The purpose of this model was to analyse the dynamics of the grinding wheel headstock in idle. Using computer simulation, Orynski and Pawlowski managed to find the influence of the grinding process on vibration of the table in the perpendicular direction to its hydrostatic slideways as well as the influence of the grinding process on vibration of the grinding wheel spindle and grinding wheel headstock with hydrostatic slideways.

Chiu and Malkin (1993), tried to describe a cylindrical plunge grinding operation using a computer simulation. Their simulation could predict both the grinding behaviour during the cycle and the final part quality including grinding forces, power, actual material removal, thermal damage, thermal expansion, wheel wear, surface roughness and roundness. The beneficial aspect of their simulation was that the program was developed to predict the time-dependant grinding behaviour and the finished part quality. The simulation was fed by process inputs including the job requirements, grinding fluid, wheel specifications, spindle vibrations, workpiece material, dressing parameters, system stiffness and control infeed. The operation was then performed by execution of a virtual grinding machine constructed from physical models, which took into account both the process and the machine. (Xiao et al, 1992) used computer simulation to evaluate optimization strategies for intelligent control of plunge grinding cycles.



Garcia-Gardea et al, 1980) used a Dynamic Data System (DDS) approach to reveal the dynamic characteristics of the grinding process based on the cutting force signal. They assumed that the cutting force signal during grinding should have all pertinent features of the grinding dynamics. This approach was a new tool for modelling and analysis and was different from the conventional modelling procedures. The DDS approach could provide a new methodology for the analysis of the dynamics of the grinding process. Since this approach evolved from the data coming from an operation, it was expected that the methodology, besides its simplicity, would be closer to the reality. The experimental work provided all the data needed for the modelling and for the development of cutting force models.

In 2007, Cheng et al, tried to describe the frequency response of a tool holder spindle of a milling machine. In order to determine the frequency response function (FRF) of the unit they used the impact test using a low-mass accelerometer. Their experiment carried out while the spindle was not rotating. That method provides acceptable data and reliable predictions for the system response. However, for some spindles the response varies with their speed (Tian and Hutton, 2001, Xiong et al., 2003, Schmitz et al., 2004, Movahhedy and Mosaddegh, 2006). According to the aforementioned authors the predictions based on the non-rotating frequency response functions (FRF) may not be sufficient. When the spindle was rotating at 10,000 RPM they developed another measuring method (reacceptance coupling substructure analysis) and they discovered that the response was quite different.

Using the finite element method Kang et al (2001), completed a harmonic response and static, a modal, and stability analysis of their model. The identified natural frequencies and modal shapes of the jigs allowed them to obtain the speed threshold of operational instability. However, the computational aided engineering (CAE) strategies cannot provide a complete solution for the design of spindle-bearing systems.

Taking into account the works done on this subject, it can be said that identifying the dynamic characteristics of a system is not simple. Computational methods and simulation analysis cannot be 100% accurate because they do not take into account any external



factors that can affect the stability and the performance of the system. However, from their results a clearer view of the response of the system was achieved.

7.3 Natural Frequency of the Spindle Unit

The natural frequency of the equipment was determined before any vibration experiment. The spindle unit of the grinding machine was subjected to a continuous harmonic excitation force produced by a piezoelectric actuator. In the present study, the spindle unit of the surface grinding machine is tested, in non-rotating mode (in idle mode), in order to identify its natural frequency. A sweep-sine test was used with a piezoelectric actuator exciting the spindle with a specific force, while the frequency was increasing. A high-resolution displacement sensor was used to measure the deflection of the unit at each frequency. Figure 7.1 below depicts the full configuration of the experimental set up. A real representation of the system is illustrated in Appendix C1.

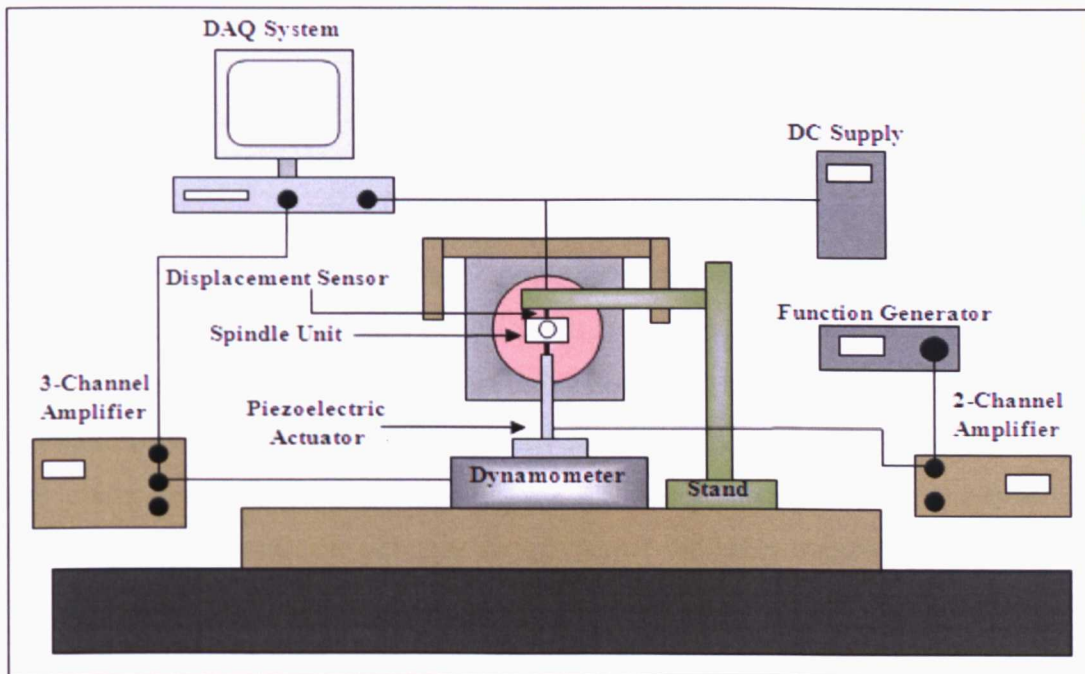


Figure 7. 1: Experimental Configuration for Sweep-Sine Test of the Spindle Unit.

The oscillation was applied to the spindle in the vertical direction; hence, only vertical movement was recorded. The piezoelectric actuator was mounted on a steel block fixed to the magnetic chuck of the tool bed. The actuator was driven by an amplifier which can produce up to 1100 Volts output. The initial electronic signal was generated by a function generator which allowed controlling the system by modifying the characteristics of the



output voltage such as the frequency and amplitude. The displacement sensor was held by a steel stand that maintained the sensor in vertical position allowing for measurements of spindle deflection in vertical direction as shown in Figure 7.1. A DAQ (Data Acquisition) system used to record the signal from the sensors. Keeping the applied force constant, the frequency was increased step-wise over a range of frequencies. The graph in Figure 7.2 shows the amplitude frequency characteristics of the spindle unit.

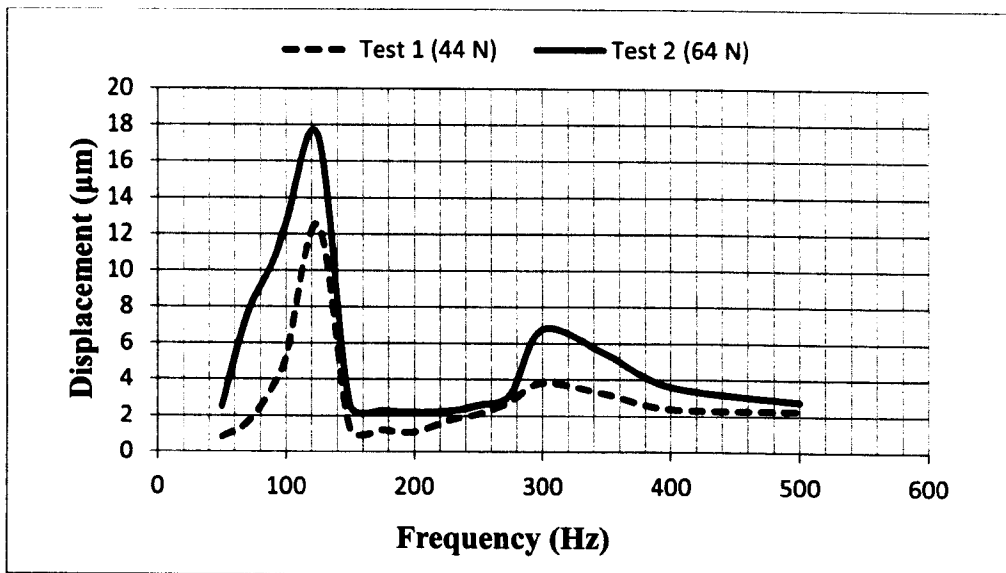


Figure 7. 2: Frequency-Amplitude Characteristics of the Machine Tool Spindle Unit.

Two excitation forces with different magnitudes applied to the spindle unit via a piezoelectric actuator. The sweep-sine test results revealed that the natural frequency of the spindle unit was 125 Hz with a maximum deflection at 12.5 μm and 17.4 μm depending on the excitation forces who were 44 N and 64 N respectively. However, at around 300 Hz a second mode observed. According to Figure 7.2, the frequency of the excitation force produced by the piezoelectric actuator during actual vibration-assisted grinding shall not match the areas with the highest amplitude peaks. However, the areas with low displacement must be considered as the most appropriate to operate a piezoelectric actuator during vibration-assisted grinding process.

7.3.1 Spindle Unit Static Stiffness and Compliance

The dynamic stiffness is important in machine tool design as it can improve the quality of the work-piece, and it increases the machine tool life. Machine tool stiffness affects the



repeatability of the part being manufactured. Another essential aspect of grinding machine dynamic behaviour was the determination of the spindle unit stiffness and compliance.

Orynski and Pawlowski in 2002 described the dynamics of a cylindrical grinding machine using a physical model. One of the main features of their work was to measure the static rigidity of the grinding wheel headstock, the workpiece and the grinding wheel itself.

Zaruba (2005) determined the static stiffness and compliance of a cylindrical grinding system. He examined the forces in both static and dynamic conditions. The static forces were related to zero frequency relevant to slow changes in the relative position of wheel and workpiece during the grinding cycle. In the second case, the forces were related to the working frequency of the rotating wheel.

Trying to produce a better surface quality of a work-piece, Jenkins and Kurfess in 1996 tried to determine the dynamic stiffness of a spindle unit of a grinding machine. Their model consisted of a three servomotors and an electromagnetic shaker to excite the system at different frequencies - from 30 to 5000 Hz they observe the response of the spindle unit particularly at resonant frequencies performing a stepped sine sweep test. They used accelerometers, force sensors and an eddy current probe for the measurement of the actual displacement. Using this configuration, the tool-end displacements were determined as a function of the applied force frequency. That is because the dynamic stiffness $K_d(s)$ is dependent on the frequency ω of the applied force as well as the system physical constants.

$$K_d(s) = \left. \frac{F(s)}{X(s)} \right|_{s=j\omega} \quad (7.2)$$

where $F(s)$ is the applied force; $X(s)$ the displacement and s is the Laplace operator.

The experiments were carried out in three directions and a number of natural frequencies at each direction were identified. Their results revealed that there were several significant resonant frequencies of the spindle unit at which the dynamic stiffness was reduced.

Regarding the surface finish effects and the influence of the force on the system, they used different wheel speeds at different work-speeds. Hence, at 9600 RPM wheel speed at feed rates of 4 mm/s and 5.33 mm/s the system produced larger forces compared to the 7200



RPM wheel speed case. Those two feed-rates were used to maintain a constant theoretical surface finish for both cases. Finally, they proved that grinding at the resonant mode may be beneficial in attaining smoother surface finishes. Moreover, the interaction between the tool and the work-piece may cause variations in the resulting frequencies. However, the effects of regenerative chatter should be taken into consideration in order to improve the understanding of the process at resonant frequencies (Jenkins and Kurfess, 1996). This type of chatter can be caused by the workpiece (cylindrical grinding) or by the wheel (cylindrical and surface grinding). In this case the waves generated on the surface of the wheel grow rather slowly due to wear resistant of the wheel. When this vibration amplitude builds up to a certain limit, the wheel has reached the end of its re-dress life. Therefore, these waves should be removed through truing and dressing (Marinescu, 2007).

In 1988 Lee and Furukawa tried to define the static and dynamic stiffness of a cylindrical grinding machine. Firstly, they referred to the contact stiffness between the wheel and the work-piece. This stiffness depends on the grain size and the hardness of the wheel. After a number of experiments, they derived the contact stiffness (K_{con}) as expressed below:

$$K_{con} = 1.5 \times F_n^{0.8} \tag{7.3}$$

Where F_n is the normal force per unit width (N/mm).

According to them, ‘The value of K_{con} under full power grinding, can be calculated with the normal grinding force obtained from a specific spindle motor power’.

Furthermore, a static stiffness of a grinding machine K_m consists of a workpiece static stiffness K_w and wheel system static stiffness K_s and is determined by the following equation:

$$\frac{1}{K_m} = \frac{1}{K_w} + \frac{1}{K_s} \tag{7.4}$$

Next, they determined the resultant stiffness K_{res} as:



$$\frac{1}{K_{res}} = \frac{1}{K_m} + \frac{1}{K_{con}} \quad (7.5)$$

The last parameter for their calculations was the recommended resultant static stiffness $K_{res\ rec}$ which was obtained from the relation between spark-out time and resultant static stiffness. Finally, after a number equations and substitutions the minimum static stiffness of the grinding machine was found to be:

$$K_m = \frac{1}{\frac{1}{K_{res\ rec}} - \frac{1}{K_{con}}} \quad (\text{Lee and Furukawa, 1988}) \quad (7.6)$$

In the present work only the static stiffness and compliance of the spindle unit of the surface grinding machine were determined. In order to measure the static stiffness, an external force has been applied to the centre of the spindle unit as illustrated in Figure 7.3. The direction of the external force was along the normal component of the grinding force and was produced from a hydraulic jack. The static compliance of the grinding system was established as the compliance due to the normal grinding force. The jack was placed on the top of a dynamometer (KISTLER 9257A) - which was already calibrated - in order to measure the applied forces. For the measurement of the deflection, a dial gauge indicator was positioned on the top of the spindle unit supported by three steel bars attached to the machine tool bed. The measurements of the deflection were relative to the machine bed. Regarding the applied force, a Data Acquisition System (DAQ) was used to record the loads. A schematic diagram of the experimental settings is shown in Figure 7.3 below.



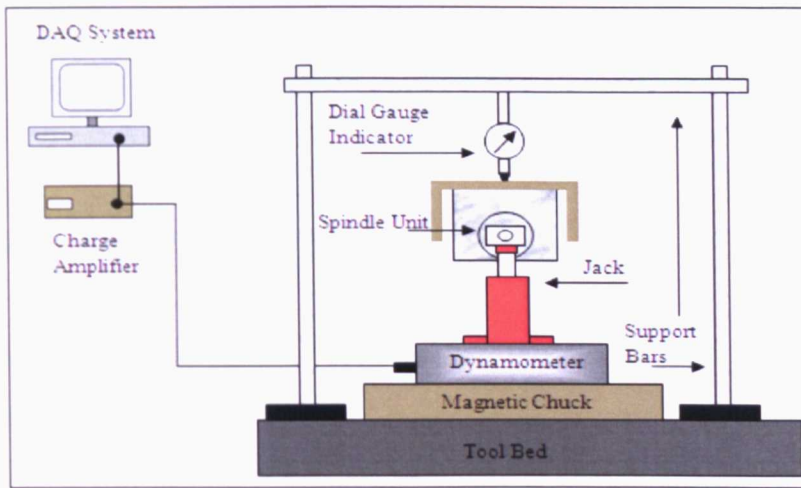


Figure 7.3: Experimental Set-Up for Measuring the Static Stiffness of the Spindle Unit.

Over twelve readings of different loads were recorded. The force-deflection relationship is given in the graph below in Figure 7.4

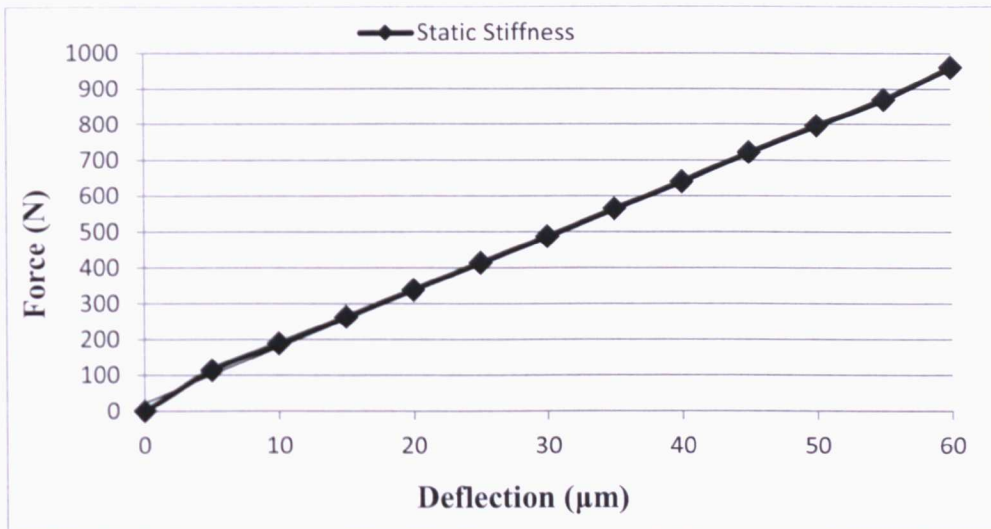


Figure 7.4: Static Stiffness of the Spindle Unit.

The force-deflection- relationship is seen to be linear. The average value of the stiffness according to the linear approximation was calculated as:

$$K = 16.67 \text{ N}/\mu\text{m}.$$

The compliance of the spindle unit can be defined as the reciprocal value of the stiffness. Hence, the compliance C_s was:



$$C_s = 1/k = 1/16.67 = 0.059 \mu\text{m/N} \quad (7.7)$$

7.3.2 Dynamic Stiffness of the Spindle Unit

To identify the dynamic stiffness of the machine, the method in Jenkins and Kurfess's work (1996) was adopted.

In this case the spindle unit was excited under a force produced by a piezoelectric actuator. At forced vibration, the system tended to vibrate at its own natural frequency as well as to follow the frequency of the excitation force. The spindle unit was assumed to be a single degree of freedom damped system with forced vibration. However, in this study the effect of damping was neglected, thus the spindle was considered as a simple mass-spring system.

According to vibration theory (Jenkins and Kurfess, 1996) the dynamic stiffness of a system depends on the driving frequency of the excitation force. In the current work, during the sweep-sine test of the spindle unit, the frequency of the excitation force varied from 50 Hz to 500 Hz. Taking notice of the spindle's resonant frequency (125 Hz). The graph below (Figure 7.5) depicts the magnitude of the system's dynamic stiffness as a function of frequencies. Each value of dynamic stiffness was calculated using the formula (7.2). More details on the configuration of the present experiment is depicted in Appendix C2.

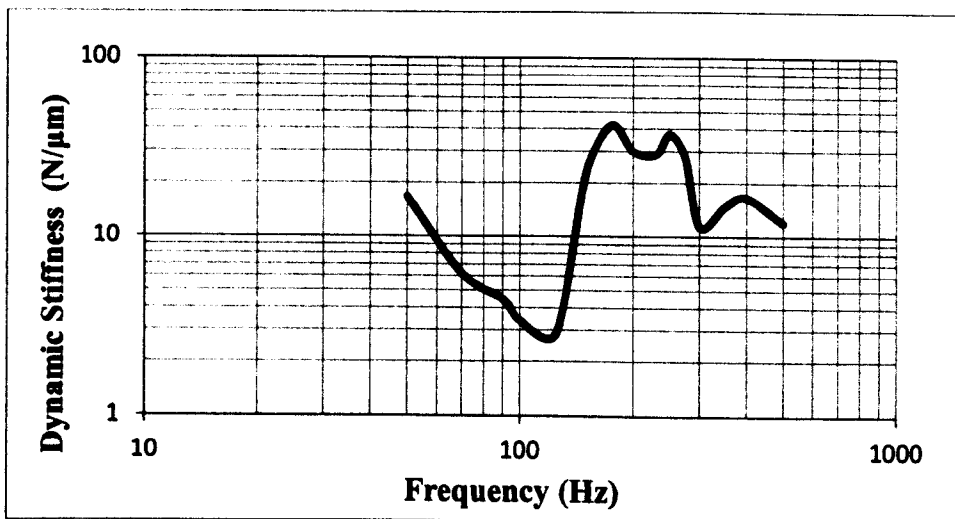


Figure 7. 5: Dynamic Stiffness of the Spindle Unit.



It can be clearly seen that as the excitation frequency approaches the resonant frequency (125 Hz), the system tends to be less stiff. At this point, the compliance of the machine tool reaches its highest value. After this point, the dynamic stiffness of the machine is increased again with small fluctuations at higher frequencies. One of the most beneficial aspects of this experimental work was that the knowledge of the system's dynamic stiffness might contribute to the identification and avoidance of any resonant modes.

Using the equation (7.2), the dynamic compliance of the machine tool is calculated and illustrated below. In this case, each value of compliance was calculated using the formula (7.7). Figure 7.6 depicts the dynamic compliance of the system as function of frequency.

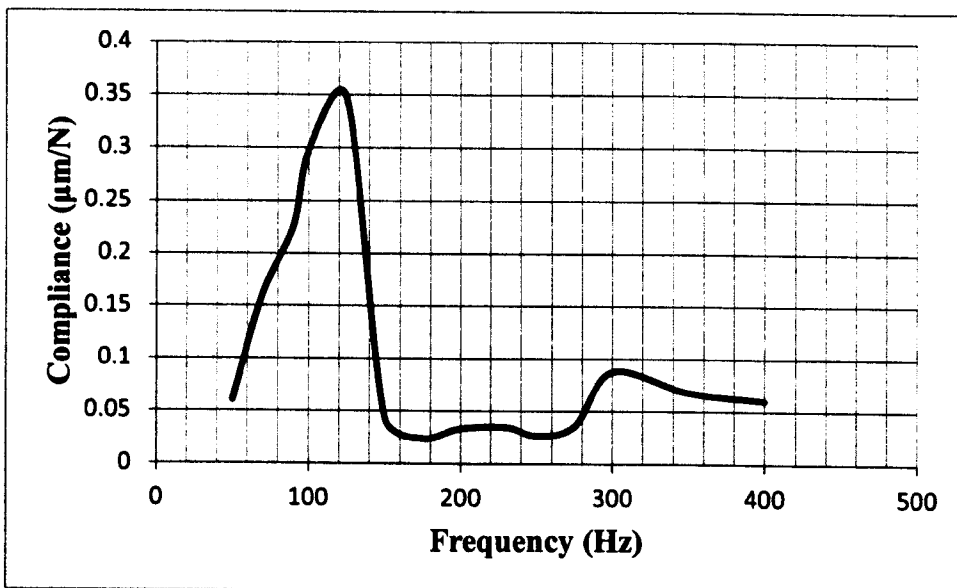


Figure 7. 6: Dynamic Compliance of the Spindle Unit.

As shown in the graph above, at the resonant frequency of the spindle unit (125 Hz) the compliance of the system rises reaching $0.36 \mu\text{m/N}$.

7.3.3 Frequency Response of the Spindle Unit – Rotating Mode

The purpose of this experiment was to observe the behaviour and the frequency response of the wheel-spindle system in rotation mode. The main target was to identify at which wheel speeds the system exhibits large amplitudes of vibration in terms of acceleration. An accelerometer was mounted on the top of the grinding wheel guard in order to record any



data and establish the frequency domain of the system. The data was recorded in the Labview data acquisition environment and analysed using a power spectral density (PSD). The overall results of vibration for each value of wheel speed are shown in Figure 7.7.

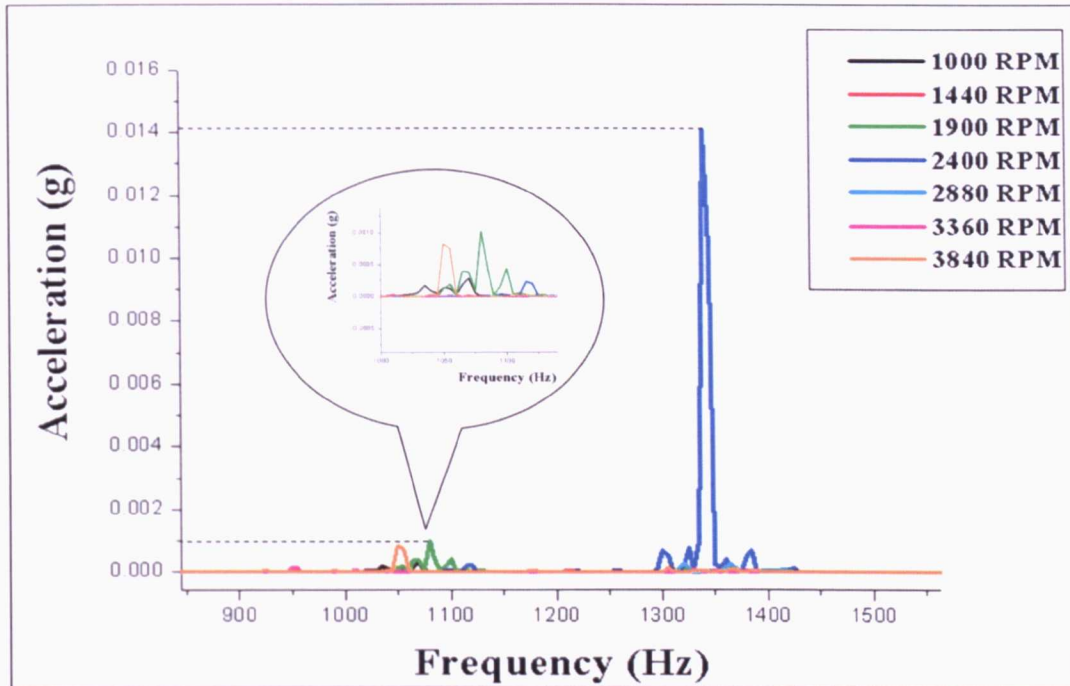


Figure 7. 7: Frequency Response of the Wheel-Spindle System at Various Wheel Speeds.

From the graph in Figure 7.7, it is observed that at a wheel speed of 2400 RPM (the system vibrates at 1360 Hz with the highest amplitude of 15×10^{-3} g's. Moreover, there are also some small amplitude rises at around 1080 Hz for 1900 RPM and 3840 RPM. In addition, the peak at 1900 RPM is the 9th harmonic of the system and the peak at 2400 RPM is the 11th harmonic. In this study, the most frequently used wheel speeds were 2880 RPM and 3360 RPM. Figure 7.8 shows a close look at the vibration of the wheel-spindle system at 2880 and 3360 RPM.



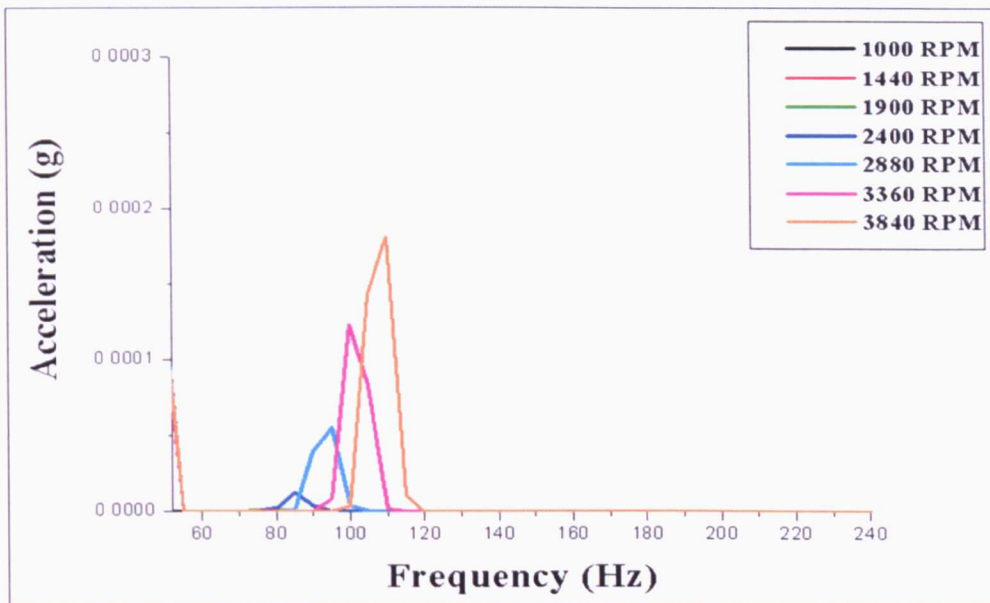


Figure 7. 8: Wheel-Spindle Vibration at 2880, 3360 and 3840 RPM.

Comparing graphs in Figures 7.7 and 7.8 the amplitude of vibration for 2880 RPM and 3360 RPM is 5×10^{-5} and 10^{-5} g's respectively. Comparing those values to the one of 2400 RPM (15×10^{-3}), they can be considered negligible and harmless for the further experimental works.

7.4 Observations

After a review of the literature on the subject of machine tool dynamics, experimental work on the identification of the grinding machine dynamic characteristics has been carried out. The static stiffness of the grinding machine's spindle unit has been identified as well as its compliance. Furthermore, according to the dynamic analysis the natural frequency of the spindle has been found to be at 125 Hz. This test indicated that during vibration-assisted grinding the frequency of the excitation force should not match the resonant or near resonant frequencies of the spindle unit. The results of the dynamic stiffness showed that when the spindle was vibrating at 125 Hz its stiffness decreased significantly. The last test performed while the grinding wheel was rotating at different speeds and it intended to show at which speeds, the spindle exhibits the highest deflection. The test showed that at 2400 RPM the spindle unit vibrated the most but at a very high frequency. Moreover, more peaks appeared at various wheel speeds but their amplitude was much lower and it was considered negligible and harmless for the process.



Chapter 8: Preliminary Studies



8.1 Introduction

This section of the research presents the preliminary experimental tests employing the vibration-assisted grinding process. Here, the oscillating rig with four flat springs which was designed and analysed in chapter 6 is employed. The purpose of the preliminary tests was to acquire a first clear view of the performance of this method and identify any problems that could affect the normal functioning of the system.

8.2 Experimental Configuration

The experimental set up, consisted of the system with four flat springs, a dynamometer, a displacement sensor, an accelerometer and a piezoelectric actuator. The picture below (Figure 8.1) depicts the full arrangement of these elements.

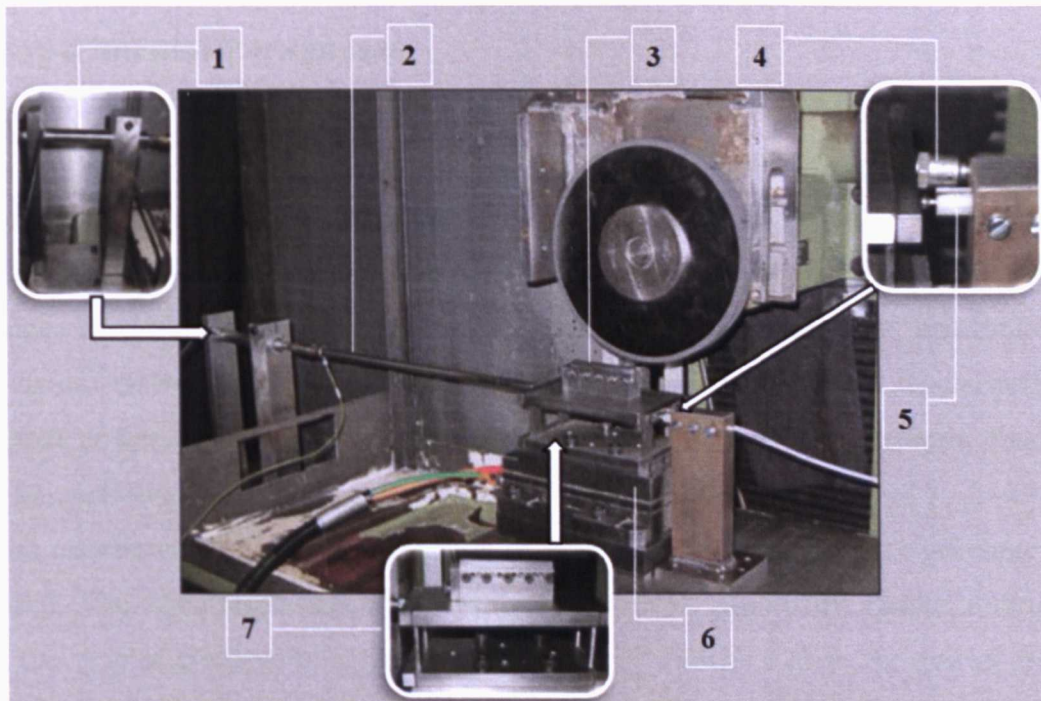


Figure 8. 1: Four Spring System Experimental Configuration for Preliminary Studies.

- | | |
|---------------------------|------------------------|
| 1. Piezoelectric Actuator | 5. Displacement Sensor |
| 2. Connecting Rod | 6. Dynamometer |
| 3. Workpiece | 7. Four Spring System |
| 4. Accelerometer | |



The system with four flat springs (vibrating rig) was mounted on a three-axis Kistler dynamometer which was connected to a data acquisition system (DAQ). A displacement sensor was placed at the back end of the vibrating rig (7) in order to measure the amplitude (displacement) of vibration generated by the piezoelectric actuator. The displacement sensor was used during the calibration process when the machine tool was switched off. However, it was removed before the grinding process for technical reason and also due to poor noise to signal ratio caused by the high frequency inverter of the machine tool.

The excitation was produced by the piezoelectric actuator which was connected to the vibrating rig through the steel rod. The actuator was set to vibrate the rig horizontally in the direction of table motion. The actuator was fixed outside the machine tool working envelop on a custom made steel support as illustrated in Figure 8.1. The DAQ (Data Acquisition) system recorded all the signals from the dynamometer, displacement sensor and the accelerometer. Labview 8.5 software controlled the DAQ system and saved the data for post-process and analysis.

8.3 Experimental Parameters

This set of experimental work was conducted on the Abwood surface grinding machine in dry conditions. No coolant or lubricant was used in any experimental work in this research. For the vibration assisted grinding, the piezoelectric actuator was set to drive the rig at its resonance frequency which was 235 Hz. This frequency has been found and established with various methods in chapters 6 and 7. This allowed achieving high displacements at low input power. It also has to be mentioned that the preliminary tests were conducted using an open-loop control.

In these experiments, the Altos aluminium oxide (Al_2O_3) - a custom made grinding wheel was used. The wheel had a high aspect ratio grain with 54 % porosity. Further information about this type of grinding wheel is given in chapter 5. Table 8.1 gives the overall grinding parameters for the preliminary experimental work where the effect of vibration with different depths of cut during grinding was examined.



Grinding Parameter	Value
Grinding Wheel Type	Altos (Al_2O_3)
Wheel Speed (V_s)	25 m/s
Work Speed (V_w)	30 mm/s
Grinding Condition	Dry
Workpiece Material	Mild Steel (BS970 080440) (90.1 HRB)
Wheel Feed	Traverse
Vibration Frequency	235 Hz
Vibration Amplitude	15 μ m (Peak)
Depth of Cut	5 – 25 μ m

Table 8. 1: Grinding Parameters for Preliminary Experimental Studies.

8.3 Results

Ten identical workpieces were used for this set of tests. The first five were ground in conventional mode applying 5, 10, 15, 20 and 25 μ m depth of cut and the other workpieces were ground at the same depths of cut in vibration assisted mode. Here, the depths of cut were set using the dial of the machine tool but not measured after grinding. The real depth of cut depends on a number of parameters such as workpiece and wheel deformation, thermal expansion, and wheel wear as explained clearer in the next chapter in formula 9.1. Therefore, the real depth of cut in grinding process is always less than the applied one.

8.3.1 Grinding Forces and Specific Forces

The following graphs in Figure 8.2 and Figure 8.3 depict the results of normal (F_n) and tangential (F_t) forces of grinding in conventional and vibration mode. The specific forces (F'_n) and (F'_t) are defined as grinding forces per unit grinding width. In this study the width of the workpieces was smaller than this of the wheel. Hence, the grinding width was equal to the width of workpieces - 8 mm. The data of the forces were recorded using a DAQ system in Labview 8.5 software environment. A low-pass, 200 Hz, 3rd order, Butterworth filter was employed to reduce the noise content of the signals. The cut frequency was selected just above the driving frequency in order to preserve the integrity of the signal.



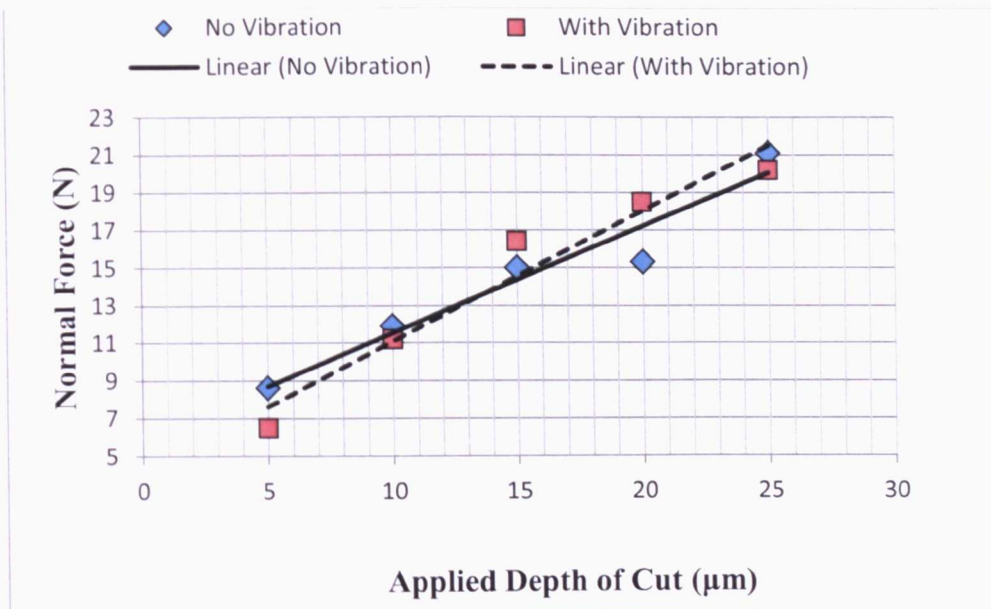


Figure 8. 2: Normal Force - Preliminary Studies.

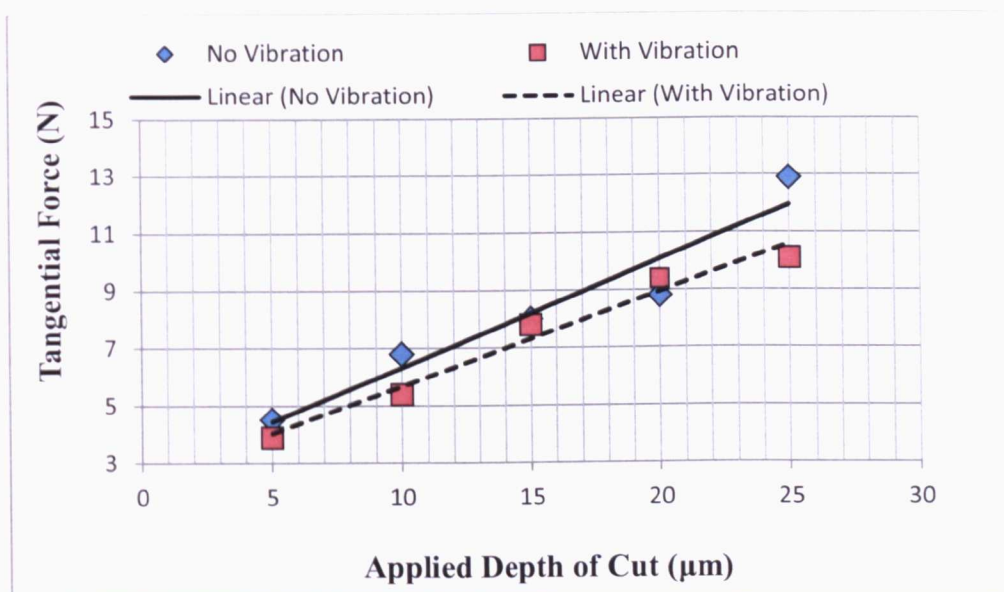


Figure 8. 3: Tangential Force - Preliminary Studies.

Referring to the results shown in Figures 8.2 and 8.3 a difference in grinding forces between the vibration and non-vibration mode is observed. The application of vibration decreased both normal and tangential forces contrary to conventional. Moreover, the tangential forces decreased more than 10.9% when vibration was applied and particularly at 25 μm depth of cut where the decrease reached 21.7%.



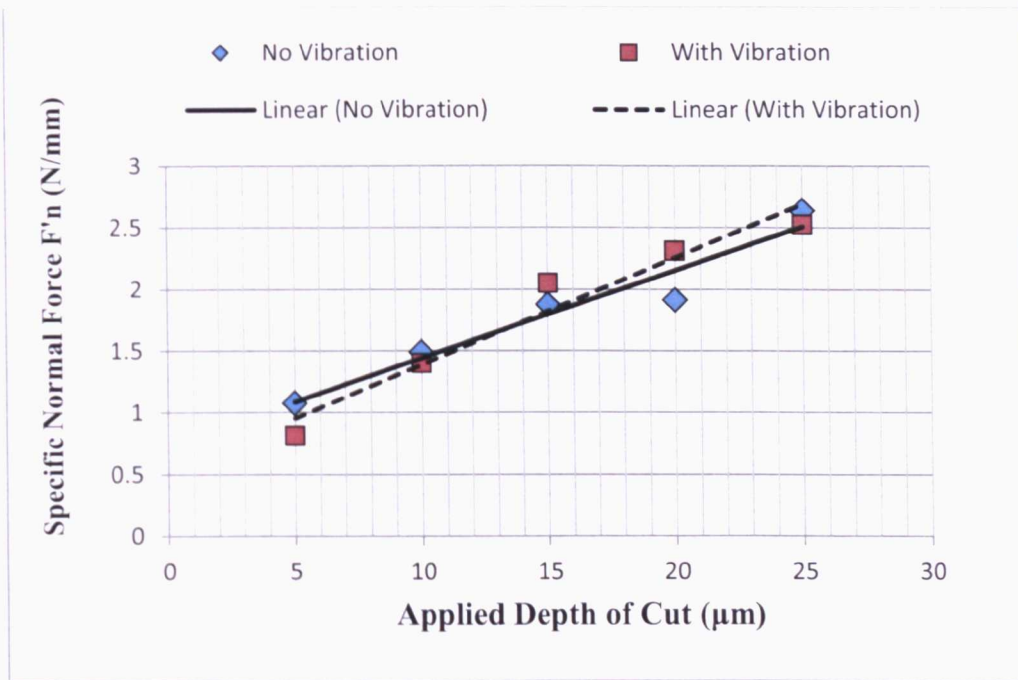


Figure 8. 4: Specific Normal Force - Preliminary Studies.

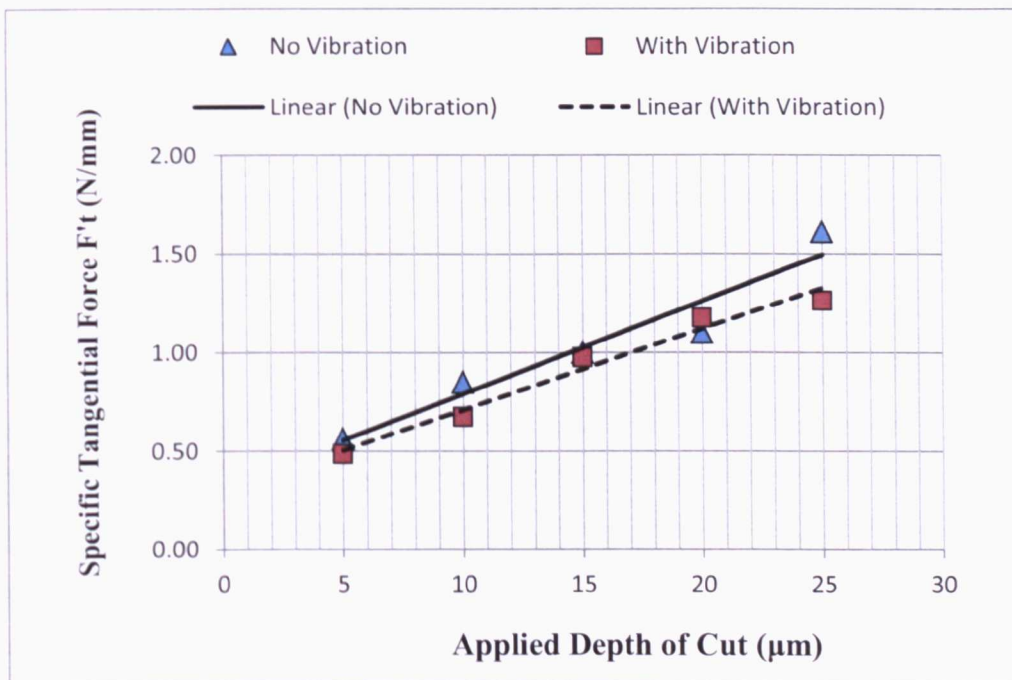


Figure 8. 5: Specific tangential Force - Preliminary Studies.

Similar decrease is detected for both specific normal and tangential forces when vibration was applied according to Figures 8.4 and 8.5.



8.3.2 Grinding Force Ratio

The next set of results represents the grinding force ratio or coefficient of grinding. Generally the ratio of tangential force to normal force is termed *coefficient of grinding* or *grinding force ratio*.

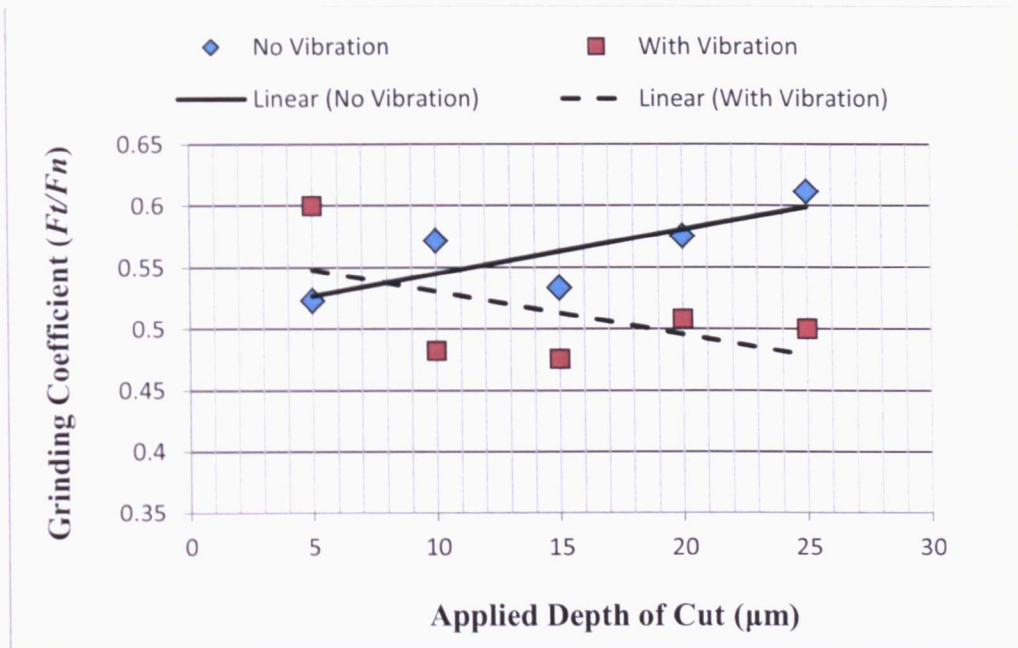


Figure 8. 6: Grinding Coefficient - Preliminary Studies.

Referring to Marinescu et al, (2007), high grinding force ratio means high material removal stock. However, here a mild steel was used and in terms of grinding process, mild steel is difficult to grind because of its ductility and it clogs the wheel rapidly. This leads to frequent wheel dressing and consequently to high wheel wear. However, the application of vibration reduced the grinding coefficient by more than 8.9% reaching 18% reduction at 25 μm depth of cut.

8.3.3 Surface Roughness

After completing a set of grinding trials the surface finish of each workpiece was measured using a surface roughness measurement machine. The values of R_a were derived using an average of four measurements at different points on the surface of each workpiece. The obtained results are presented in Figure 8.7.



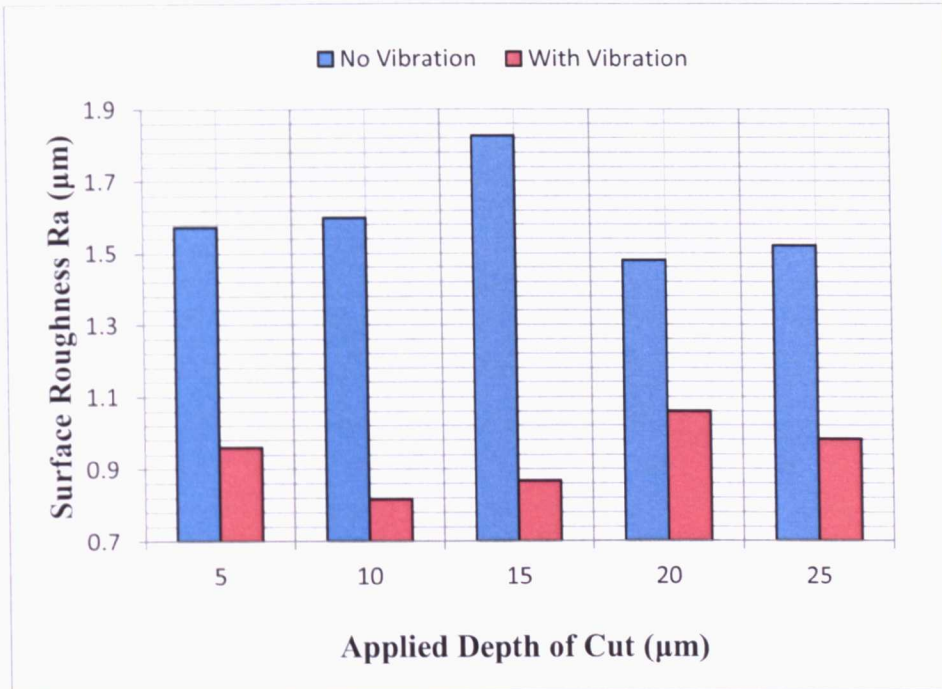


Figure 8. 7: Surface Roughness - Preliminary Studies.

The difference in surface roughness between vibration and conventional grinding is obvious for all depths of cut according to Figure 8.7. For most depths of cut the reduction in workpiece surface roughness reached more than 41.25%. The application of vibration contributed to the improvement of the surface due to the lapping process. Regardless of middle steel being hard to grind, the superimposed vibration provided a considerable improvement in surface finish.

The wheel rotated at 2400 RPM and produced high values of displacement at 1360 Hz which is the 11th harmonic of the spindle's natural frequency (Figure 7.7). Taking into account that parameter, the surface roughness results come in agreement with Jenkins and Kurfees work (1996) where they proved that grinding at resonant modes maybe helpful in attaining smoother surface finishes.

8.3.4 Power Consumption

The grinding power consumption (P) during conventional and vibration-assisted grinding was determined using the equation (3.7) $P = Ft Vs$ where Ft is the tangential force and Vs is the wheel speed. The results are presented below in Figure 8.8.



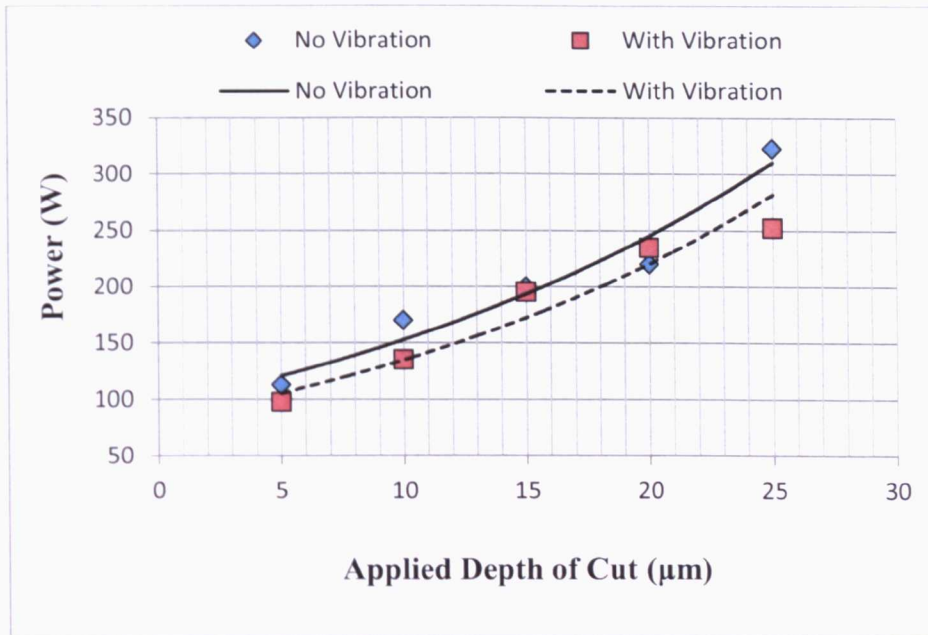


Figure 8. 8: Power Consumption - Preliminary Studies.

As expected a reduction in grinding power is observed during vibration-assisted grinding due to the reduction of cutting forces F_t . The system spent less energy during cutting in vibration mode than in conventional grinding..

8.4 Need for a Novel Design

The system with the four flat springs was selected amongst a number of designs as the most appropriate for this specific application. The first set of experimental tests revealed that this novel technology of superimposed vibration has a potential of improving the grinding performance. However, some technical issues appeared during the preliminary grinding test using the four-spring rig. The main problem encountered was the misalignment in the rig assembly cause by the design to manufacture. It was observed that the slots housing the flat spring had radii that caused a tilting and swing of the top platform. Therefore, flatness and consistent depth of cut could not be achieved during the preliminary tests. This led to the re-design of a new and stable vibrating rig. The new design consisted of two flat springs grounded flat and two ground plates. The following picture (Figure 8.9) depicts these irregularities of the four spring system and Figure 8.10 illustrates the new system.



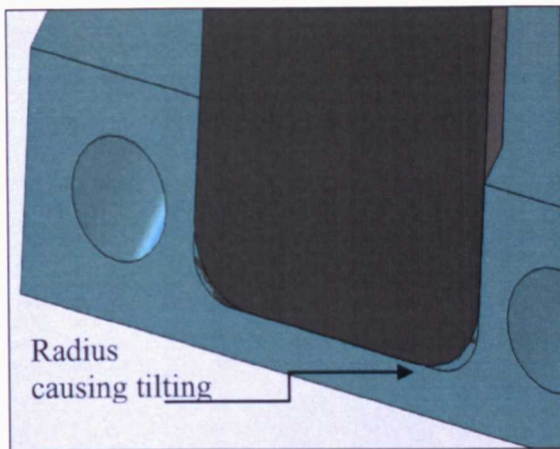


Figure 8. 9: Four Spring System Irregularity.

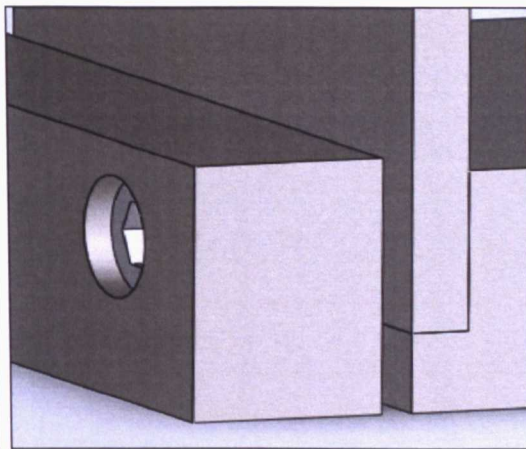


Figure 8. 10: New System.

The re-designed system was used for the remaining experimental work. The static and dynamic characteristics of this model are presented in chapters four & six.

8.5 Remarks

The first set of experimental work has been carried out employing the system with four flat springs. The results showed an improvement in grinding forces as well as in force ratio when vibration was applied. Considerable improvement was achieved in the surface quality of the workpiece. Also, less grinding power was consumed while grinding in the presence of vibration due to the reduced cutting forces. However, due to misalignment the model with four flat springs needed to be replaced with a novel one. The main problem of the system with four springs was the corner radius of the springs. Their round edges did not allow for proper positioning on the plates thus, affecting the parallelism and the flatness of the top plate and so the workpiece (Figure 8.9). Consequently, before any grinding trial each workpiece had to be ground flat. The novel design had all its parts ground flat along with the two flat springs which were perfectly squared with no round edges. Their geometry ensured the flatness between the base and the top plate and thus the flatness of the workpiece. The re-designed rig will be used for full scale experimental work reported in the next chapters.



Chapter 9: Effect of Grinding and Vibration Parameters



9.1 Introduction

After the preliminary studies a full scale of experimental work with vibration-assisted grinding was undertaken. The experimental configuration was explained in detail in chapter 5. This is a comparative study which puts side by side the results of conventional grinding and vibration-assisted grinding processes. Grinding forces, grinding coefficient, power consumption and surface roughness of the workpieces are presented in this set. In each test, one grinding parameter such as depth of cut, work speed, wheel speed or frequency of vibration was varied while keeping the other parameters constant. This allowed observing the effect of each parameter on vibration assisted grinding.

9.2 Effect of Depth of Cut

The following table (Table 9.1) shows in details the parameters of the experiment while using a hard material (En31). The applied depth of cut was 5, 10, 15, 20, 25 μm and was set by the dial of the handle on the machine tool and does not represent the actual depth after machining. The vibration frequency was chosen to be the resonant frequency of the vibrating rig in order to achieve high displacements.

Grinding Parameter	Value
Grinding Wheel Type	Al ₂ O ₃ (454A 601 L 7G V3)
Wheel Speed (Vs)	35 m/s
Work Speed (Vw)	25 mm/s
Grinding Condition	Dry
Workpiece Material	En 31 (BS 534A99) HRC 64.2
Wheel Feed	Traverse
Vibration Frequency	275 Hz
Vibration Amplitude	15 μm (Peak)
<i>Applied Depth of Cut</i>	<i>5 – 25 μm</i>

Table 9. 1: Experimental Parameters - Effect of Depth of Cut.



9.2.1 Grinding Forces

The following graphs (Figure 9.1 and 9.2) represent the specific normal and tangential forces for conventional and vibration-assisted grinding.

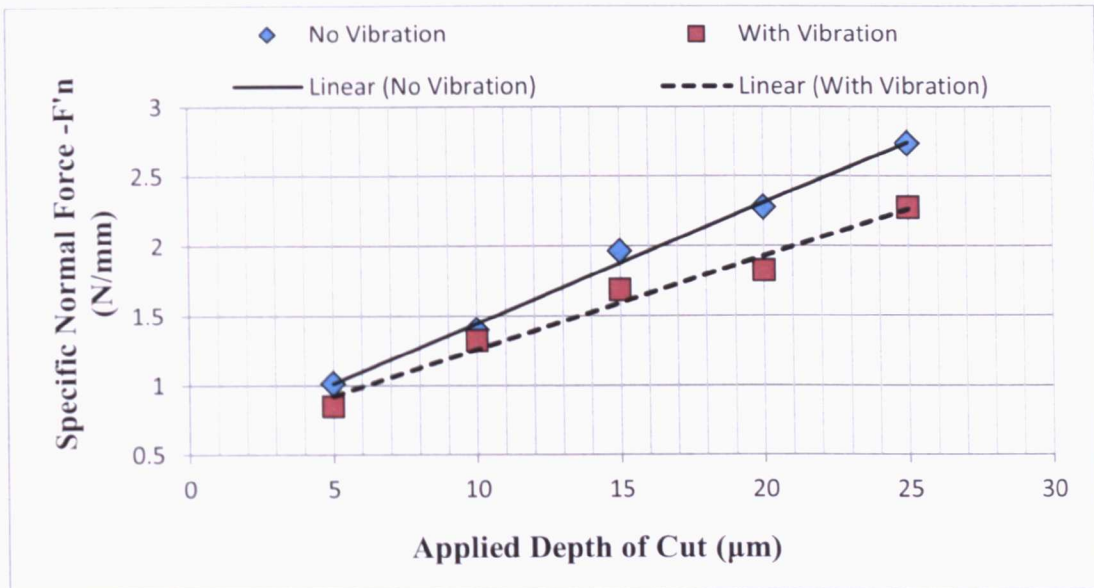


Figure 9. 1: Effect of Depth of Cut - Specific Normal Forces.

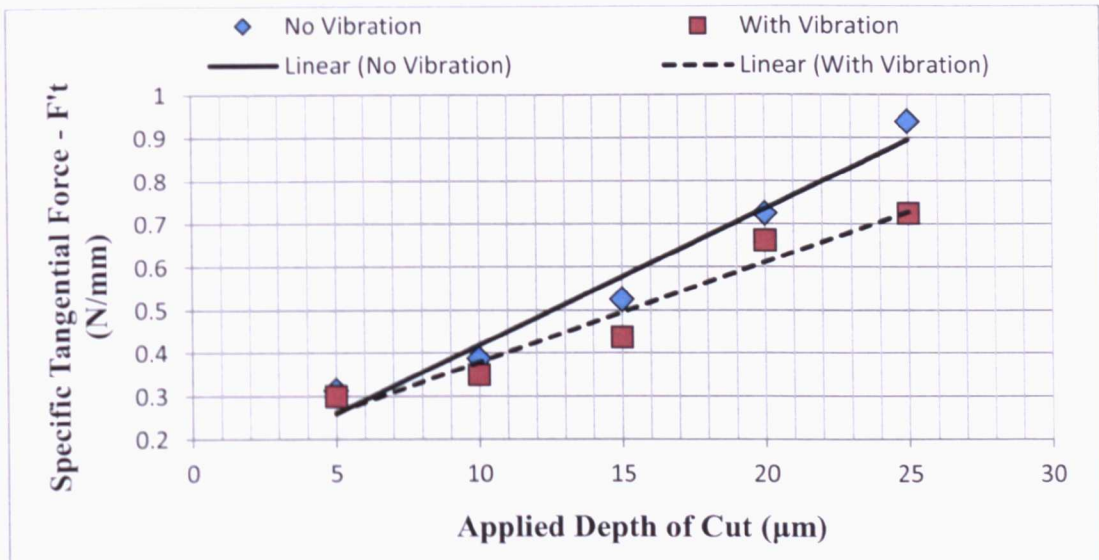


Figure 9. 2: Effect of Depth of Cut - Specific Tangential Forces.



Figure 9.1 and 9.2 show a decrease in both normal and tangential force when vibration was applied to the grinding process. However, it is observed from these results that for small depths of cut, the application of vibration did not bring any reduction in cutting forces. This does not mean that the added vibration does not have any effect. The small effect is due to this specific machine tool configuration because cuts below 10 μm are in the range of the backlash of the spindle unit. Thus the wheel does not remove enough material from the workpiece due to the lack of stiffness. However, as the depth of cut increases, the effect of the superimposed vibration became noticeable. For example at 20 μm depth of cut a reduction of 20% was observed in normal forces per width ground. Reduction in normal force in grinding is important as it affect wheel wear and the load on the wheel and the workpiece. Low normal forces are very desirable in industry when grinding slender workpieces. Also, the tangential forces per width ground reached a decrease of 22.5% for 25 μm depth of cut. Tangential forces also affect the service life of the wheel. It is observed from the graphs that the advantage of the superimposed vibration increased with the increase of depth of cut.

9.2.2 Grinding Power

The graph in Figure 9.3 illustrates the grinding power consumption during conventional and vibration-assisted grinding.

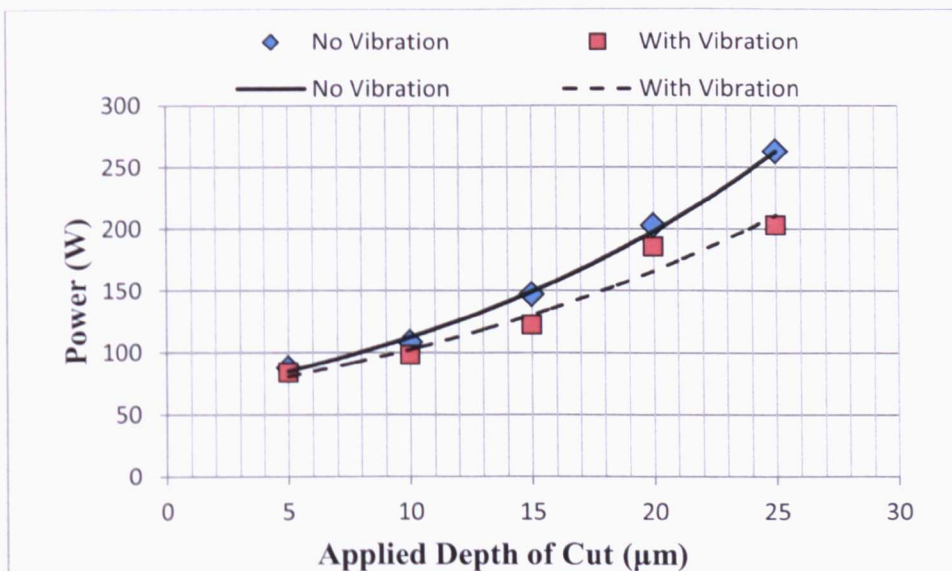


Figure 9. 3: Effect of Depth of Cut - Grinding Power.



The decrease of tangential forces during vibration-assisted grinding led to proportional decrease in power consumption of the process, which is seen in Figure 9.3. It is observed in this graph that with the increase of depth of cut the power drawn for the process decreases.

The surface roughness of the workpiece was measured after each test. It was measured at five points and the average value was considered as the representative value of roughness (Ra) of each workpiece. As mentioned above in this set all grinding trials were performed in a single pass in dry condition with no coolant. The surface roughness for this experiment is presented in Figure 9.4.

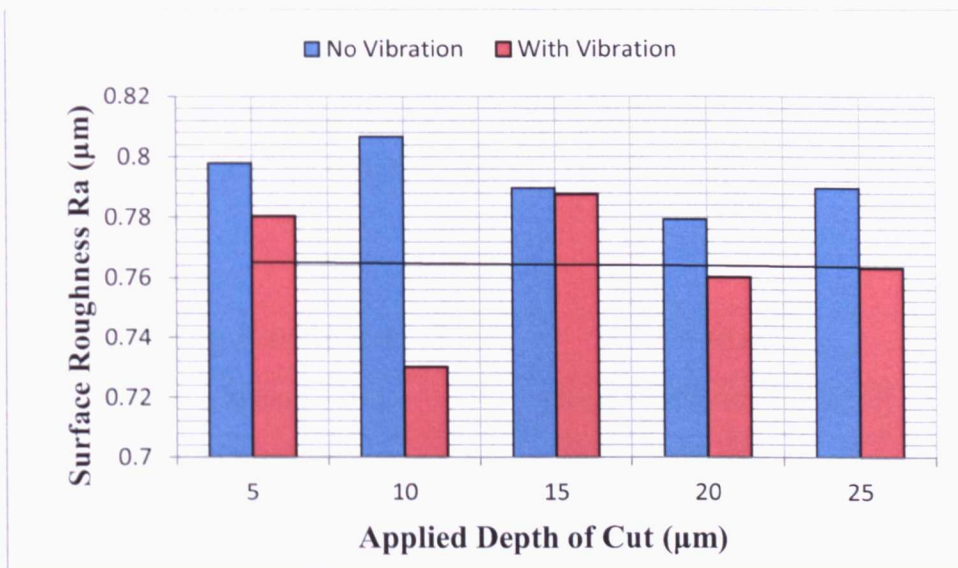


Figure 9. 4: Effect of Depth of Cut - Surface Roughness.

From the graph in Figure 10.4 it can be seen that the added vibration provided an improvement of the quality of the workpiece surface finish. The measured surface roughness was lower in vibration assisted grinding than in conventional. The improvement was about 3.8% and particularly for 10 μm depth of cut it reached 8.8%. Normal grinding forces generally affect the quality of surface roughness and this is supported by the findings in Figure 9.1 with the reduction in normal forces in vibratory mode.

The unexpected reduction in roughness at 10 μm depth of cut is due to the fact that the actual depth of cut was not measured in this specific experiment. According to Marinescu (2004) the actual depth of cut is given from the following formula:



$$\alpha_e = \alpha - \delta - \alpha_{sw} + \alpha_t \quad (9.1)$$

Where α_e is the actual depth of cut, α is the applied depth of cut, δ is the deflection of the wheel and the workpiece, α_{sw} is the wheel wear and α_t is the thermal expansion

Therefore, due to the nature of the process it was unknown the exact amount of material removed on each pass.

9.3 Effect of Work Speed

The table below (Table 9.2) depicts the parameters used during this test while the speed of the table was changing. Here, five workspeeds were used namely 10, 20, 50, 100 and 200 mm/s. A depth of cut of 20 μm was chosen because at higher depths of cut the vibration effect was more obvious and the surface roughness was more affected.

Grinding Parameter	Value
Grinding Wheel Type	Al ₂ O ₃ (454A 601 L 7G V3)
Wheel Speed (V_s)	35 m/s
<i>Work Speed (V_w)</i>	<i>10-200 mm/s</i>
Grinding Condition	Dry
Workpiece Material	EN 31 (BS 534A99) HRC 64.2
Wheel Feed	Traverse
Vibration Frequency	275 Hz
Vibration Amplitude	15 μm (Peak)
Depth of Cut	20 μm

Table 9. 2: Experimental Parameters - Effect of Work Speed.

In this experiment the work speed (table speed) was the variable whilst the other parameters remained constant. Figures 9.5 and 9.6 present the grinding forces per width ground as a function of work speed.



9.3.1 Grinding Forces

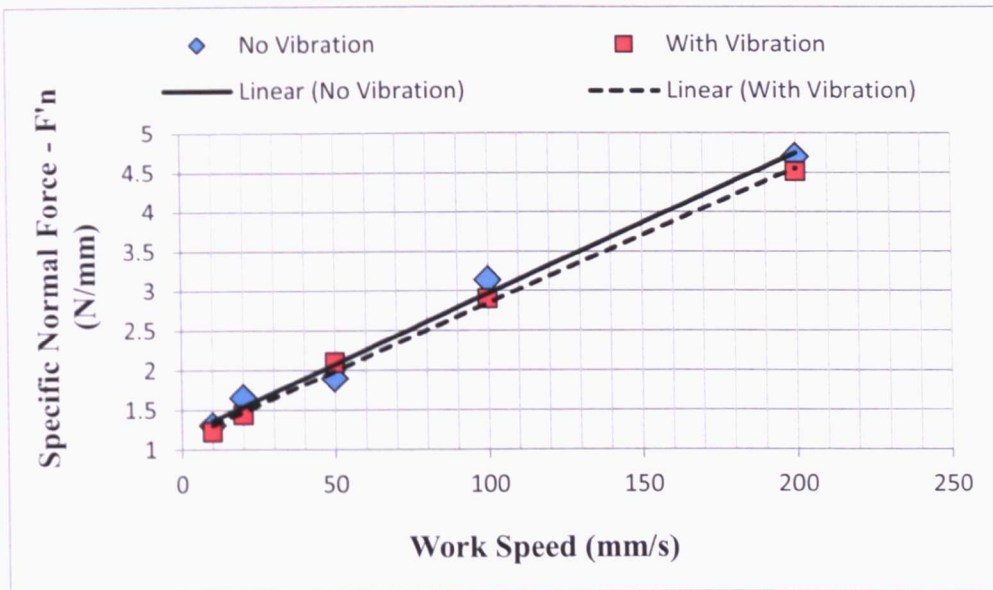


Figure 9. 5: Effect of Work Speed - Specific Normal Forces.

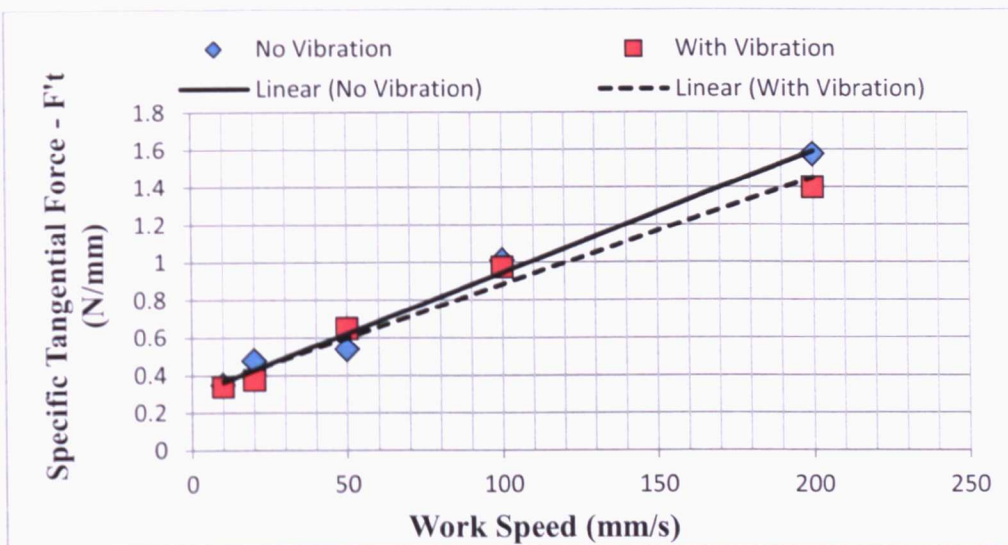


Figure 9. 6: Effect of Work Speed - Specific Tangential Forces.

As in any other tests, it can be seen that vibration-assisted grinding secured lower forces than the conventional process. The cutting forces increased with the increase of work speed. This is because with a fixed wheel speed the increase of work speed (feed rate) leads to the increase of the load on individual cutting edge. This results in an overall increase of tangential cutting force. In this set of tests, the reduction in tangential forces reached 11.1% at 200 mm/s and 4% in normal forces. From the results in Figure 9.5 and



9.6 it can be stipulated that the effect of vibration becomes stronger with the increase of work speed, though there is a limited effect on normal forces.

9.3.2 Grinding Power

Figure 9.7 represents the grinding power consumption for this set of tests.

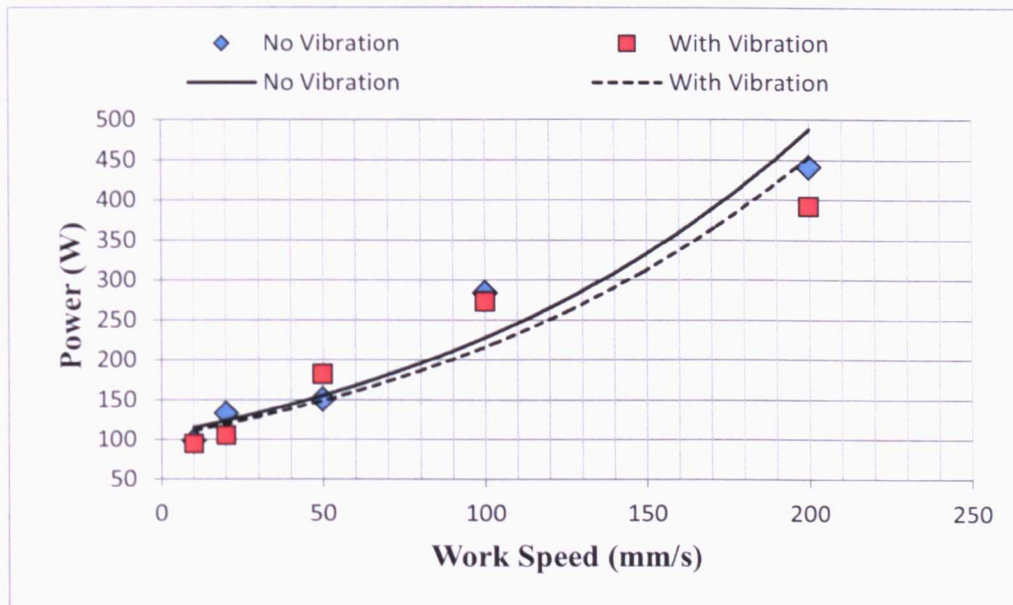


Figure 9. 7: Effect of Work Speed - Grinding Power Results.

It is shown here that the application of vibration reduced the power consumption though the gain is not significant. This result is in agreement with the cutting forces. For this particular machine and experimental configuration this result shows that at low work speed the vibratory grinding performed at the same level as conventional grinding in terms of power requirements.





Figure 9. 8: Effect of Work Speed - Surface Roughness.

The surface roughness of the workpiece was measured after each grind and the results are presented in Figure 9.8. Though the reduction in grinding forces was very limited, this result shows that with the increase of work speed, the surface roughness improves with the application of vibration. The reduction of surface roughness was more than 7% reaching 10.7% and 12.6% for work speeds of 100 mm/s and 200 mm/s respectively.

9.4 Effect of Wheel Speed

During this experiment only the peripheral speed of the grinding wheel was changed up to 40 m/s, whereas the other parameters remained constant. The wheel speeds used were 20, 25, 30, and 35 and both specific normal and tangential forces were measured during conventional and vibration-assisted grinding operations. The experimental parameters of this set of tests are given in Table 9.3.



Grinding Parameter	Value
Grinding Wheel Type	Al ₂ O ₃ (454A 601 L 7G V3)
<i>Wheel Speed (Vs)</i>	<i>20 - 35 m/s</i>
Work Speed (Vw)	25 mm/s
Grinding Condition	Dry
Workpiece Material	En 31 (BS 534A99) HRC 64.2
Wheel Feed	Traverse
Vibration Frequency	275 Hz
Vibration Amplitude	15 μm (Peak)
Depth of Cut	20 μm

Table 9. 3: Experimental Parameters - Effect of Wheel Speed.

9.4.1 Grinding Forces

Figures 9.9 and 9.10 give the grinding forces per width ground as a function of wheel speed. Taking notice of the experimental tests carried out for different depths of cut it was observed that for small values of depth of cut there was no difference in the performance between conventional and vibro-grinding. Therefore, in this set of experiment the depth of cut was set to 20 μm where the effect of vibration is strong.

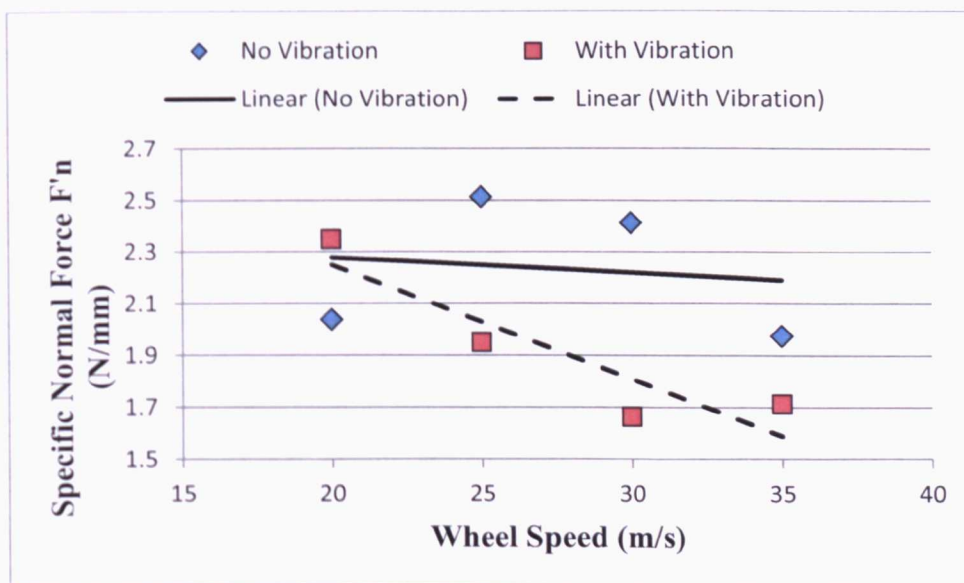


Figure 9. 9: Effect of Wheel Speed - Specific Normal Forces.



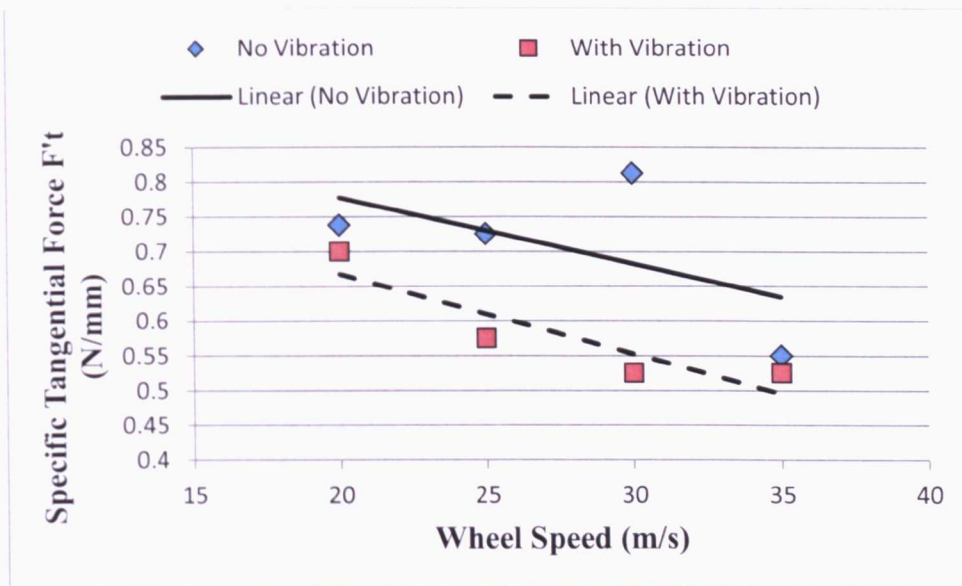


Figure 9. 10: Effect of Wheel Speed - Specific Tangential Forces.

The results in Figure 9.9 and 9.10 show that with the increase of the wheel speed the tangential cutting force decreases and this is in agreement with the finding of Ebbrell (2003) in high speed grinding with Cubic Boron Nitride (CBN) wheels. With the increase of wheel speed, each individual cutting edge has a shorter travel time and this reduces the load on the edge and leads to the reduction in tangential force.

Also, the wheel speed is inversely proportional to equivalent chip thickness. Higher wheel speed lead to smaller chips which means lower depth of cut and thus less grinding forces. Moreover, according to the results the application of vibration reduced both grinding forces for all values of wheel speeds. The reduction - which was more noticeable at higher wheel speeds - exceeded 19.3% for normal forces reaching 33.3% and more than 20.8% for tangential forces. Linear averaging (dotted line) shows that the benefits of vibration become more significant with drastic decrease in tangential forces with the increase of wheel speed whereas for conventional grinding there is only a slight decrease.

Observation from Figure 9.9 shows that in conventional grinding the normal forces increased contrary to the decreasing trend in vibro-grinding. The fluctuation of the points in Figures 9.9 and 9.10 during conventional grinding depends on the fact that for some wheel speeds the real depth of cut was higher or lower whereas vibration-assisted grinding



secured a smooth decrease of all the different values of wheel speeds. Moreover, the increase of wheel speed was proportional to the reduction of cutting forces for that specific range of wheel speed values.

9.4.2 Grinding Power

The results in Figure 9.11 depict the effect of vibration on grinding power consumption.

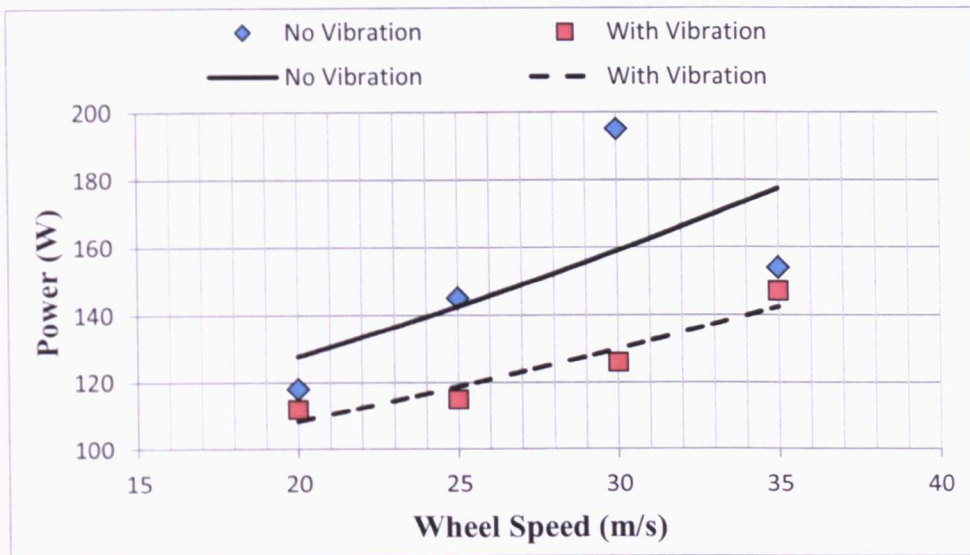


Figure 9. 11: Effect of Wheel Speed - Grinding Power.

It is observed here that the vibration-assisted grinding required less power than conventional. The reduction was more than 21.8%; it increased with the increase of wheel speed and reached 30.6% for 40 m/s wheel speed. The increase of the wheel speed led to increase of grinding power as power and wheel speed are proportional. Also, for small wheel speeds no significant difference between the two methods was observed but as the wheel speed increased the vibration secured a net reduction in grinding power consumption. Knowing that the stress of the wheel increases as the square of the wheel speed and reaches its maximum value at the bore (Shaw, 1996) the contribution of vibration in reducing the power at high wheel speeds becomes extremely important.



9.4.3 Surface Roughness

Figure 9.12 depict the measured surface roughness of the workpieces during conventional and vibration-assisted grinding.

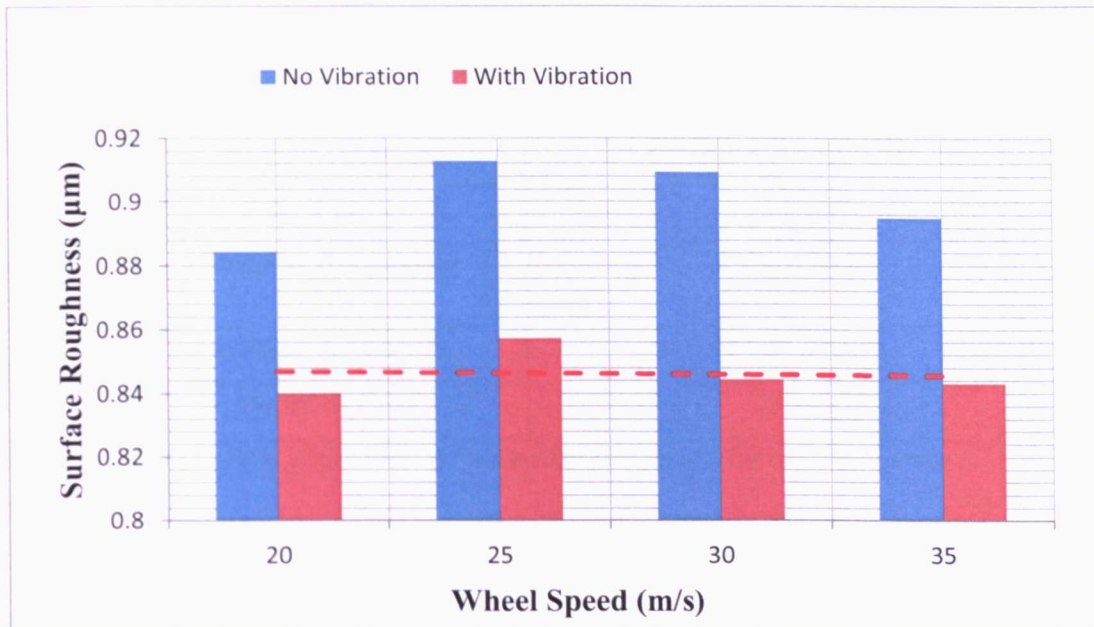


Figure 9. 12: Effect of Work Speed - Surface Roughness.

This result shows that the surface roughness decreases with the increase of wheel speed. A similar trend was observed in the case with increasing work speed but on a different scale. Figures 9.8 and 9.12 portrait that increasing work speed provides a better surface finish (0.75-0.85) whereas increasing wheel speed gives a good finish (0.79-0.84). Here a reduction of more than 5.6% was achieved with vibration. However, it is desirable, though outside this scope of work to undertake grinding tests at speeds higher than 35 m/s to seek for consistency with the findings in this test.

9.5 Effect of Vibration Frequency

In this section of experiment only a vibration-assisted grinding process was carried out. The purpose was to investigate how the vibration frequency affected the performance parameters such as grinding forces and workpiece surface roughness. The frequencies were in a range from 150 Hz to 400 Hz including the resonant frequency of the vibrating rig. Table 9.4 below describes the experimental parameters for this specific test.



Grinding Parameter	Value
Grinding Wheel Type	Al ₂ O ₃ (454A 601 L 7G V3)
Wheel Speed (Vs)	35 m/s
Work Speed (Vw)	25 mm/s
Grinding Condition	Dry
Workpiece Material	En 31 (BS 534A99) HRC 64.2
Wheel Feed	Traverse
Vibration Frequency	150 - 400 Hz
Vibration Amplitude	15 μm (Peak)
Depth of Cut	20 μm

Table 9. 4: Experimental Parameters - Effect of Vibration Frequency.

9.5.1 Grinding Forces

The following graphs in Figures 9.13 and 9.14 depict the variation of grinding forces at different frequencies as well as the grinding coefficient respectively.

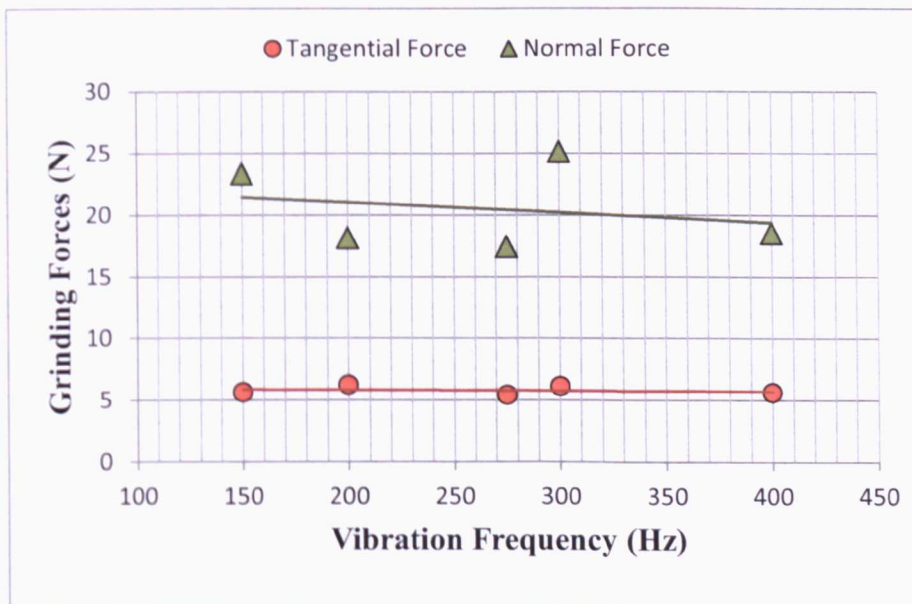


Figure 9. 13: Effect of Vibration Frequency - Grinding Forces.



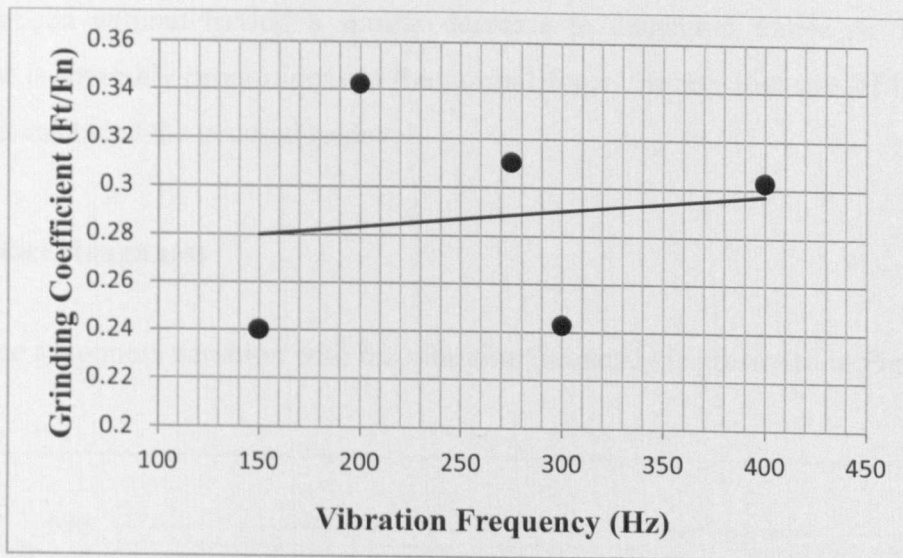


Figure 9. 14: Effect of Vibration Frequency - Grinding Coefficient.

In Figure 9.13 there is a fluctuation in normal forces as vibration frequency rises. The interesting observation is that the normal force reaches its minimum value at 275 Hz, which is the resonant frequency of the vibrating rig. This suggests that driving the rig at its resonant frequency provides a three-fold benefit, namely: low driving power, increased amplitudes of oscillation and low normal forces. It is also observed that at 150, 300 Hz pick forces were recorded, and these frequencies are the resonant of the spindle unit. This finding implies the avoidance of spindle natural frequency is important in vibration-assisted machining in order to reduce potential damage to the spindle unit and to keep low normal forces.

The variation in tangential forces was negligible. However, its minimum value was also recorded at 275 Hz. This suggests that though the normal forces increased, the actual force needed to remove the material remained the same and did not depend on the frequency. The rise of grinding forces at the frequency of 300 Hz and 150Hz is due to the fact that the excitation frequency matched the resonant frequency of the spindle unit.

In Figure 9.14 grinding coefficient is low at the spindle resonant modes. However, the trend shows that the grinding coefficient increases as the frequency is increased. There



was an increase at frequencies of 200 Hz and 275 Hz. The reason was that the normal forces dropped without having a similar decrease in tangential forces as the grinding coefficient is inversely proportional to the normal force. Hence, that rise of the grinding coefficient enhanced the material removal.

9.5.2 Surface Roughness

The surface roughness variation with the vibration frequency is presented in Figure 9.15.

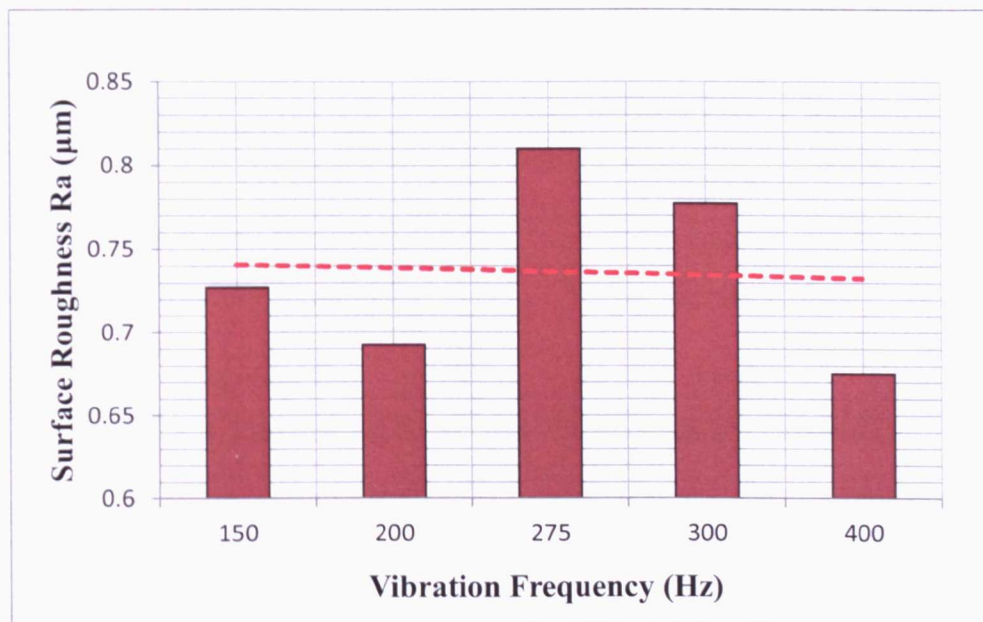


Figure 9. 15: Effect of Vibration Frequency - Surface Roughness.

As expected from the grinding coefficient results the surface integrity of the workpiece was poor at 275 Hz. Figure 9.15 shows that due to the higher material removal at the frequency of 275 Hz the surface roughness also increased. At 300 Hz the improvement in surface roughness was slight but the lowest value was found at 400 Hz. In general if the rig resonant and its surrounding frequencies are avoided then the surface finish improves (decreases) with the increase of driving frequency.



9.6 Effect of Vibration Amplitude

In this section the effect of vibration amplitude on the process is examined. During this experiment the frequency of vibration remained constant at 275 Hz while the peak amplitude varied from 5 μm to 25 μm . Table 9.5 gives the parameters of the test.

Grinding Parameter	Value
Grinding Wheel Type	Al ₂ O ₃ (454A 601 L 7G V3)
Wheel Speed (Vs)	35 m/s
Work Speed (Vw)	25 mm/s
Grinding Condition	Dry
Workpiece Material	En 31 (BS 534A99) HRC 64.2
Wheel Feed	Traverse
Vibration Frequency	275 Hz
<i>Vibration Amplitude</i>	<i>5 – 25 μm (Peak)</i>
Depth of Cut	20 μm

Table 9. 5: Experimental Parameters – Effect of Vibration Amplitude.

9.6.1 Grinding Forces

Figure 9.16 and Figure 9.17 show the grinding forces and grinding coefficient as functions of vibration amplitude.

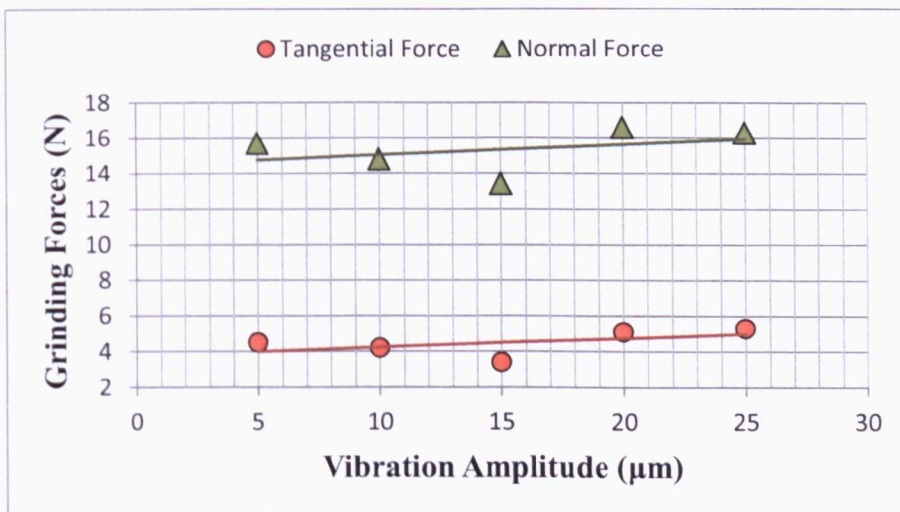


Figure 9. 16: Effect of Vibration Amplitude – Grinding Forces.



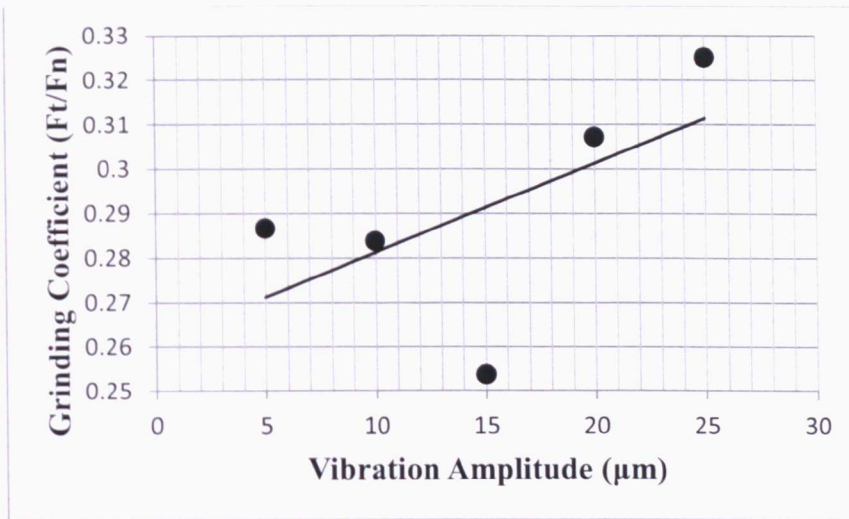


Figure 9. 17: Effect of Vibration Frequency - Grinding Coefficient.

This result shows an increase of grinding forces as the amplitude increases. According to the graph in Figure 9.16 an amplitude of 15 μm proved to be the optimal for this application as it secured the highest reduction in both normal and tangential forces. Coincidentally most of the experiments in this study were carried out using 15 μm vibration amplitude. At 15 μm , the lower grinding coefficient occurred, which also is a sign of less wheel wear.

9.6.2 Surface Roughness

The next set of results (Figure 9.18) show the variation of workpiece surface roughness with the vibration amplitude.

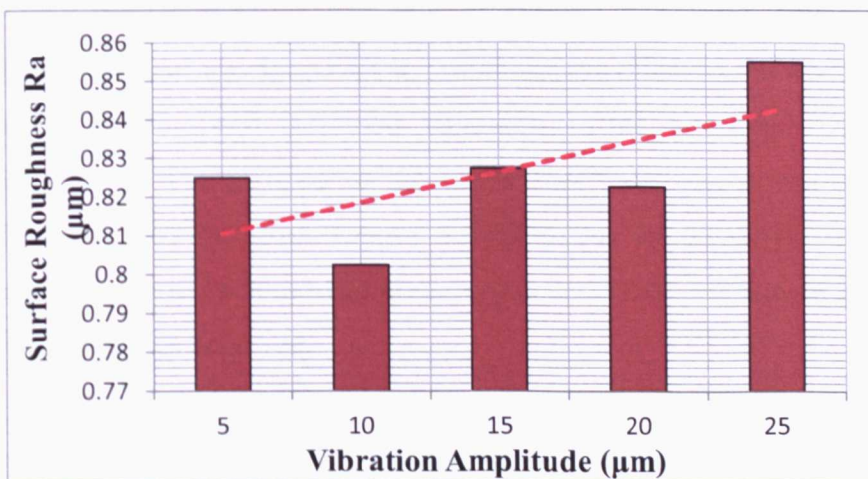


Figure 9. 18: Effect of Vibration Amplitude – Surface Roughness.



According to Figure 9.18 the highest reduction in workpiece surface roughness was achieved for 10 μm vibration amplitude. No significant change in surface quality was observed except that of 25 μm amplitude where it caused a burned surface. It is observed here that the surface roughness increased with the increase of the amplitude of vibration.

9.7 Remarks

The effects of each grinding parameter on vibration-assisted grinding process were examined in this chapter. The advantages of this novel method could easily be distinguished as it reduced the grinding forces, power and improved the surface quality of the workpiece. It was observed that for small depths of cut the application of vibration performed as conventional grinding but as the depths of cut increased the reduction of grinding forces and power was obvious.

The overall power of the system is the sum of grinding power and power needed to drive the amplifier of piezoelectric actuator. Thus, the superimposed vibration has a direct effect on the grinding power but the additional power of the amplifier remained constant. For that reason the system was operating at its resonance frequency in order to consume less power. Also, the surface roughness of the workpiece reduced with the application of vibration. Regarding the effect of work speed it could be seen that in most cases vibration-assisted grinding reduced the grinding forces and power. This reduction also became clearer at high work speeds where the load per grain increased.

An essential improvement was found while examining the effect of the wheel speed on the process. As the wheel speed increased vibration-assisted grinding outperformed the conventional grinding. The increase of the wheel speed and workspeed can only reach certain levels defined by the manufacturer. Lower forces were recorded for high wheel speed as the travel time of each individual grain was decreased. Moreover, at those speeds better surface quality was achieved.

Remarkable is the fact that vibration improved the process performance in each case and reduced the power consumption of the system. The major finding was that at 275 Hz -



resonant frequency of the vibrating rig - the process provided the best reduction of grinding forces and higher grinding coefficient than at other frequencies. The variation of vibration amplitude showed that high amplitudes more than 20 μm could lead to surface damage.



**Chapter 10: Effect of Grinding Wheels and Workpiece
Materials**



10.1 Introduction

During this experiment three different grinding wheels have been employed with three different workpiece materials. The aim was to investigate the performance of each wheel and each material. The grinding forces as well as the surface roughness for each workpiece were measured. Here, the real depth of cut was measured for each grinding trial and the volume of the material removed was calculated. The measurement of real depth of cut is described in detail later in this chapter. The following picture in Figure 10.1 shows the possible combinations of wheels and workpieces that were completed in this experiment.

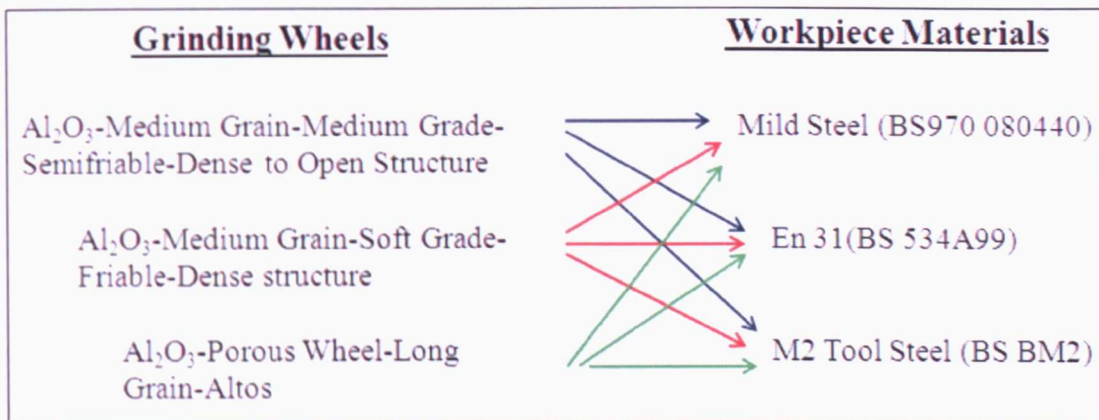


Figure 10. 1: Grinding Wheel – Workpiece Material Experimental Combinations.

The experimental parameters for all nine experiments are presented below in the Table 10.1.

Grinding Parameter	Value
Wheel Speed (Vs)	30 m/s
Work Speed (Vw)	50 mm/s
Grinding Condition	Dry
Wheel Feed	Traverse
Vibration Frequency	275 Hz
Vibration Amplitude	15 μ m (Peak)
Depth of Cut	15 μ m

Table 10. 1: Experimental Parameters – Three Grinding Wheels and Three Workpiece Materials.

The wheel speeds of 30 m/s was chosen due to the lowest amount of vibration produced to the spindle unit (Figures 7.7 & 7.8). The workspeed of 50 mm/s was chosen in a manner



that vibration produced negative clearance according to vibro-impact theory. Moreover, at that value the effect of vibration was not high and it was interesting to examine the performance of different wheels and workpieces at that workspeed.

10.2 Performance of Al_2O_3 (454A 601 L 7G V 3) Grinding Wheel

Six tests were performed in this section. The first three tests dealt with three different workpiece materials in conventional grinding and the other three during vibration-assisted grinding. This grinding wheel was an aluminium oxide (Al_2O_3), medium gain, medium grade wheel with dense to open structure. The three materials used were mild steel (MS), hardened EN31 and hardened M2 tool steel.

10.2.1 Grinding Forces

The trend of lowering the machining forces is also observed here as in the previous tests. The difference in performance between the conventional and vibration assisted grinding methods is illustrated below (Figures 10.2 and 10.3) in terms of normal and tangential forces for three types of materials.

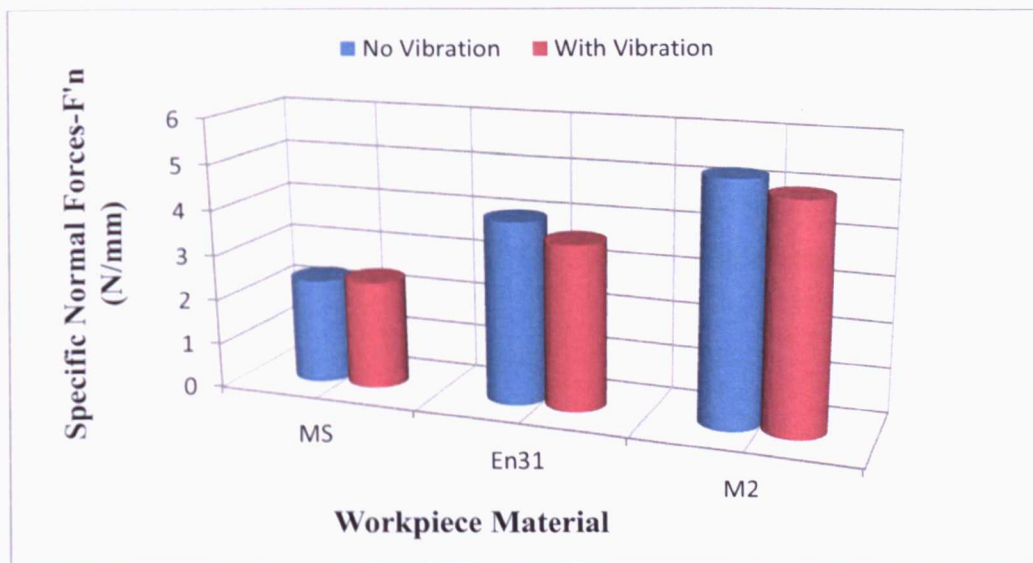


Figure 10. 2: Specific Normal Force for Al_2O_3 (454A 601 L 7G V 3) Wheel.



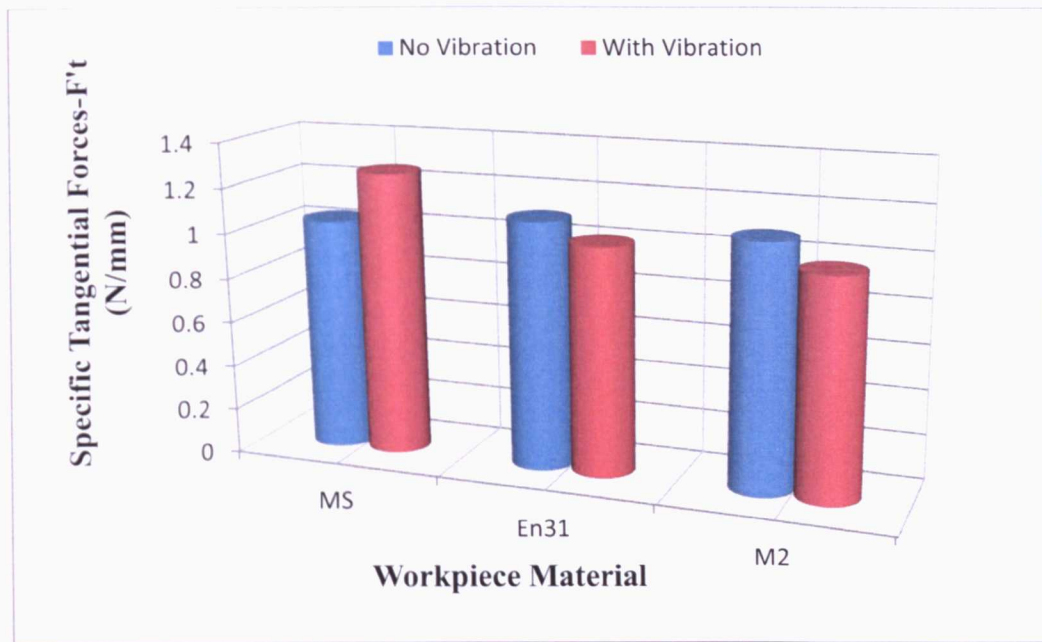


Figure 10. 3: Specific Tangential Force for Al_2O_3 (454A 601 L 7G V 3) Wheel.

Figures 10.2 and 10.3 suggest that vibration assisted grinding performed very well using a medium grain wheel to grind hard materials. Regarding the normal forces, the applied vibration provided a reduction of 10% for En31 and 5.7% for M2 tool steel. However, observation from the tangential force shows an increase with the medium grain wheel along with the application of vibration. The reason is that soft materials require harder grade wheels with coarse grain sizes. The increased force can be also attributed to the finding in Batako 2004 where it was shown that soft material do not provide a reduction in forces under impact loading however this idea does not hold for the next tests with a different wheel. The superimposed vibration on mild steel accelerated the wheel loading as it accelerated the accumulation of chips between the grains. In general, the application of vibration to the other materials provided on average similar magnitude of tangential grinding force.

10.2.2 Surface Roughness

The quality of machined surfaces is presented in Figure 10.4 below for all the materials during conventional and vibration-assisted grinding.



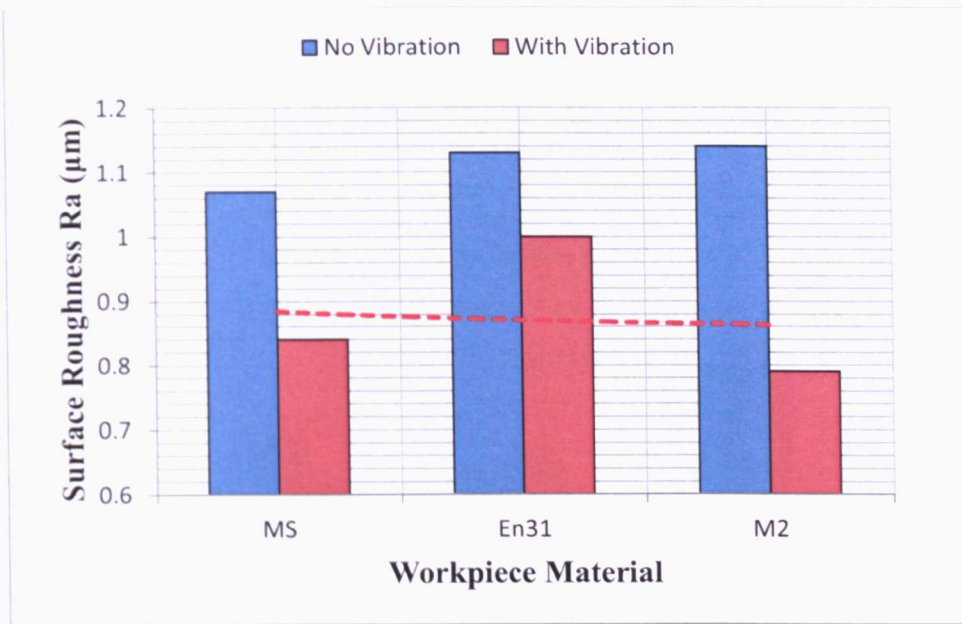


Figure 10. 4: Surface Roughness with Al_2O_3 (454A 601 L 7G V 3) Wheel.

Figure 10.4 illustrates the measured surface roughness for the three types of materials machined. It observed that superimposing vibration provides a better surface finish, achieving up to 30.7 % improvement in the hardest M2 tool steel and 21% for the mild steel. Also, in this case the wheel is semi-friable which means that it can produce high surface quality along with high stock removal. In friable wheels the abrasive grains break easier by the impact and generate the self sharpening process during grinding. Moreover, the vibration allowed the grains to cut in more edges due to the induced lapping process. Thus, this leads to a better surface finish in all three of workpiece materials.

10.3 Performance of Al_2O_3 (89A 60 K 5A V 217) Grinding Wheel

In this set of experiment, six tests were conducted with three different workpiece materials under conventional and vibration-assisted grinding. A second grinding wheel with different structure and properties was introduced for these tests. This wheel has medium grains but is graded as soft and also its structure is dense. Next is described how that wheel affected the process.



10.3.1 Grinding Forces

Figures 10.5 and 10.6 depict the grinding forces per width ground in conventional and vibration-assisted grinding.

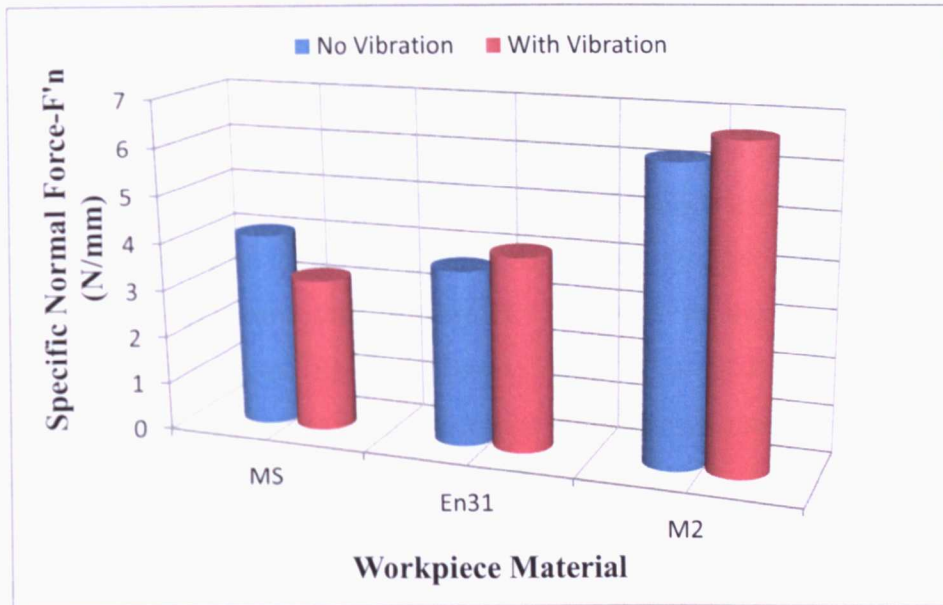


Figure 10. 5: Specific Normal Force for Al_2O_3 (89A 60 K 5A V 217) Wheel.

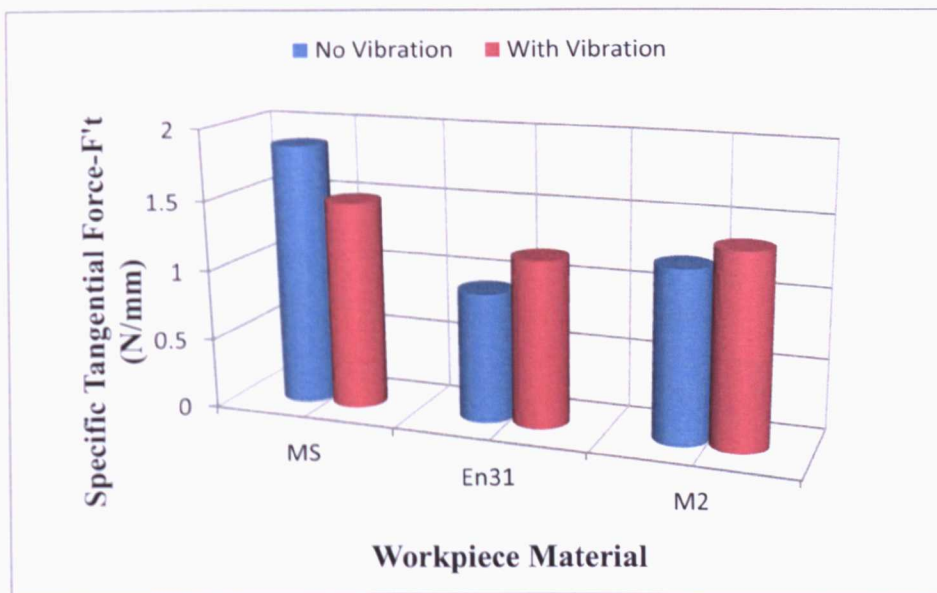


Figure 10. 6: Specific Tangential Force for Al_2O_3 (89A 60 K 5A V 217) Wheel.

In Figures 10.5 and 10.6 the replacement of the grinding wheel with a closed structure led to an overall increased cutting forces in both conventional and vibratory mode. This is explained by the fact that a closed wheel structure is easily clogged and this led to



increased rubbing rather than cutting. Only in the case of mild steel the vibration contributed positively to the process by reducing the normal force by 21.1% and tangential force by 20.1%. For harder material En31 and M2 the application of vibration resulted in fast dulling of the wheel with subsequent increase in cutting forces compared to conventional cutting. It is to be mentioned that ideally a softer grinding wheel is appropriate for grinding hard material. However, the structure of the bond and the grinding parameters play a significant role in achieving high product quality with lower grinding forces. This specific wheel was supposed to operate at higher speeds (e.g. 50 m/s) and apply small depths of cut as it was manufactured for light stock removal. During this test wheel manufacturer recommendations were not followed as the main purpose of this experiment was to investigate its performance. Thus, it proved that this wheel is not suitable for this application resulting in a rise of both normal and tangential forces comparing to the medium grade wheel (454A 601 L 7G V 3).

10.3.2 Surface Roughness

Figure 10.7 illustrates the measurements of surface roughness obtained during this test in conventional and vibration-assisted grinding.

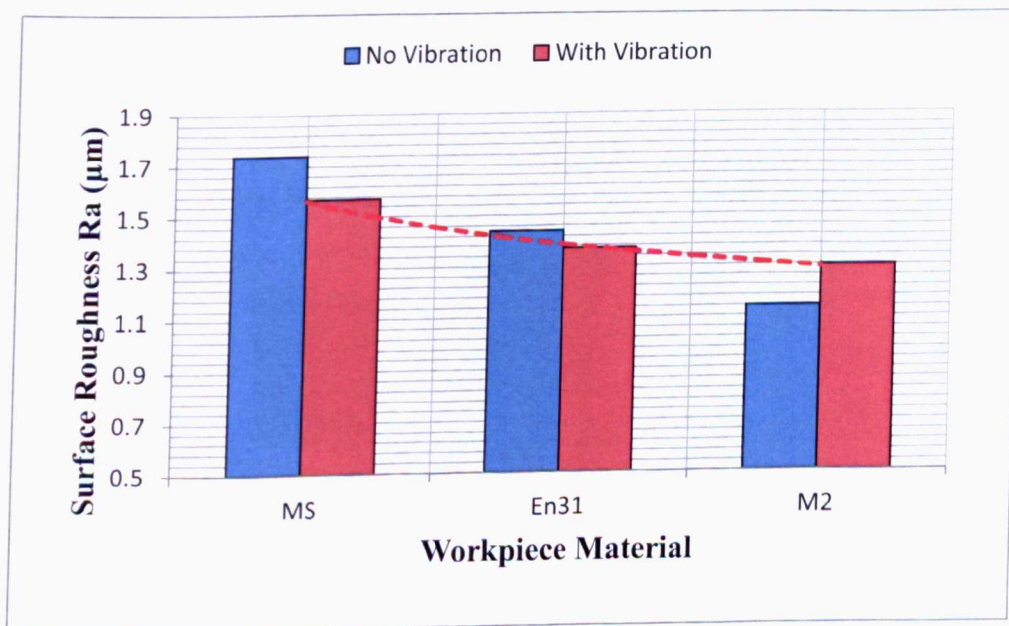


Figure 10. 7: Surface Roughness with Al_2O_3 (89A 60 K 5A V 217) Wheel.

As mentioned previously, a rise in both normal and tangential forces was observed relative to the results with the medium grade wheel (454A 601 L 7G V 3). This rise especially in normal forces affected the surface roughness of the workpiece and particularly the mild



steel workpiece as seen in Figure 10.7 producing a poor surface quality. However, the application of vibration improved the surface quality by reducing the surface roughness by 9.7% for mild steel and 4.8% for En31. It could be said that a closed wheel structure with medium to fine grit is inappropriate for grinding hard materials in vibratory mode. However, this finding suggests that it is possible to grind soft materials using vibration with lower power consumption and extended wheel life due to low normal forces. It is also observed that the surface roughness decreases as the work material gets harder.

10.4 Performance of Altos (Long Grain-Porous) Grinding Wheel

This type of wheel is also an Al_2O_3 long grain wheel with 54% porosity and 10:1 aspect ratio. It is friable and its full specifications are unknown as it is custom made for specific applications carried out in past experimental studies.

10.4.1 Grinding Forces

The performance of the Altos wheel in terms of grinding forces is shown below in Figures 10.8 and 10.9.

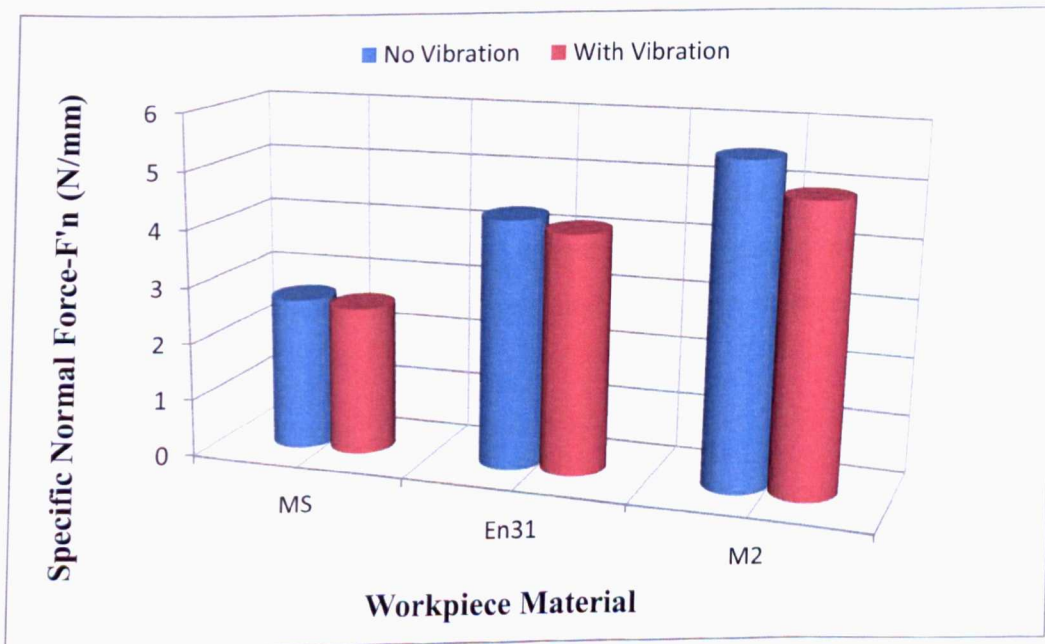


Figure 10. 8: Specific Normal Force for Altos Wheel.



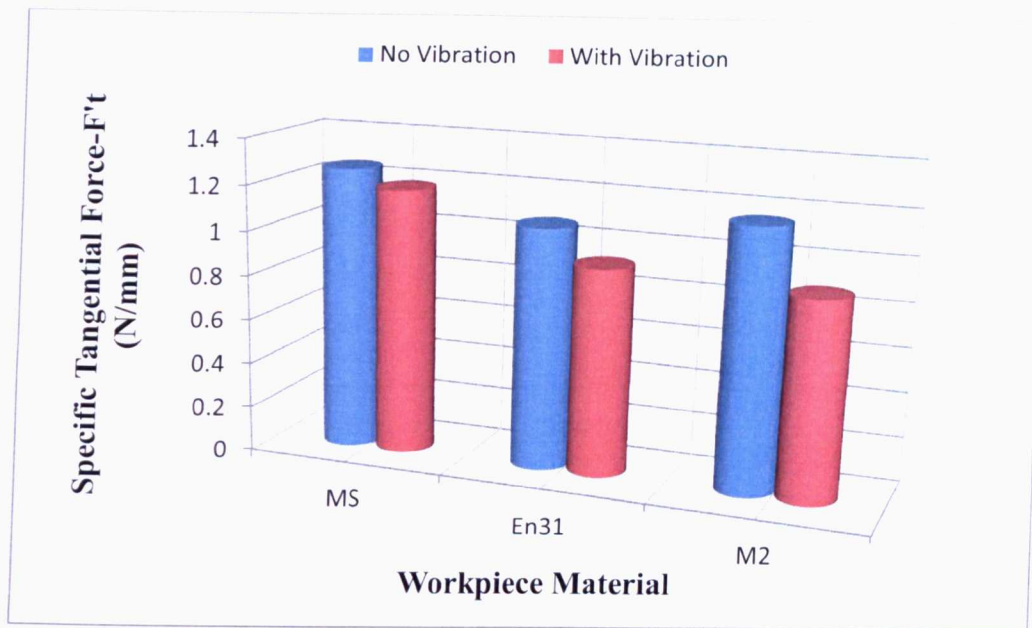


Figure 10. 9: Specific Tangential Force for Altos Wheel.

The use of the porous grinding wheel and the applied vibration led to the reduction of cutting grinding forces. From Figures 10.8 and 10.9 an overall reduction in cutting forces is observed. A better performance is seen when machining hardened materials, i.e. 10.4% reduction in normal forces and 23.6% reduction in tangential forces while grinding M2 hardened steel. However, mild steel did not respond well with the application of vibration as no significant reduction was observed in this test. This kind of response seems to be in line with the idea in (Batako, 2003) that soft material does not give greater advantage in vibro-machining. This may be explained by the ductility and the ability of the material to deform elastically to great extent without actual fracture. Furthermore, the high friability of the wheel causes fast and easy fracture of its grains. This type of wheels performs better with hard steel. Also, the vibration accelerated the grain fracture and thus the self-sharpening process.

It is equally noticed that in vibratory mode with the Altos wheel, the normal forces increased with the hardness of the material but the tangential cutting forces decreased with the hardness of the workpiece.



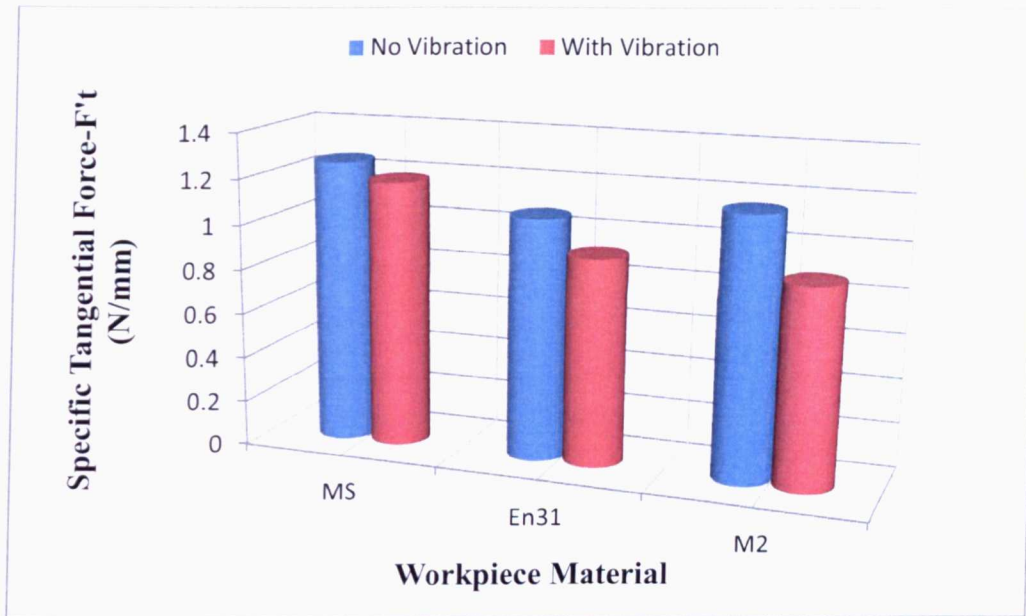


Figure 10. 9: Specific Tangential Force for Altos Wheel.

The use of the porous grinding wheel and the applied vibration led to the reduction of cutting grinding forces. From Figures 10.8 and 10.9 an overall reduction in cutting forces is observed. A better performance is seen when machining hardened materials, i.e. 10.4% reduction in normal forces and 23.6% reduction in tangential forces while grinding M2 hardened steel. However, mild steel did not respond well with the application of vibration as no significant reduction was observed in this test. This kind of response seems to be in line with the idea in (Batako, 2003) that soft material does not give greater advantage in vibro-machining. This may be explained by the ductility and the ability of the material to deform elastically to great extent without actual fracture. Furthermore, the high friability of the wheel causes fast and easy fracture of its grains. This type of wheels performs better with hard steel. Also, the vibration accelerated the grain fracture and thus the self-sharpening process.

It is equally noticed that in vibratory mode with the Altos wheel, the normal forces increased with the hardness of the material but the tangential cutting forces decreased with the hardness of the workpiece.



10.5 Process Performance by Removed Material

During this set of experiments, the real depth of cut was measured after each trial. The applied depth of cut was 15 μm using the dial of the machine tool handle but the other grinding parameters remained unmodified as described in Table 10.1 above. Each grinding test was performed in conventional and vibration mode. The true depth of cut was measured after each trial using a micrometer caliper. To keep consistency in the measurements, the ground workpieces were measured in-situ with the workpiece holder. After sparking out the workpiece the micrometer caliper was used to determine the zero reference point. Then the measurement was taken as illustrated in Figure 10.11 after the workpiece was ground.

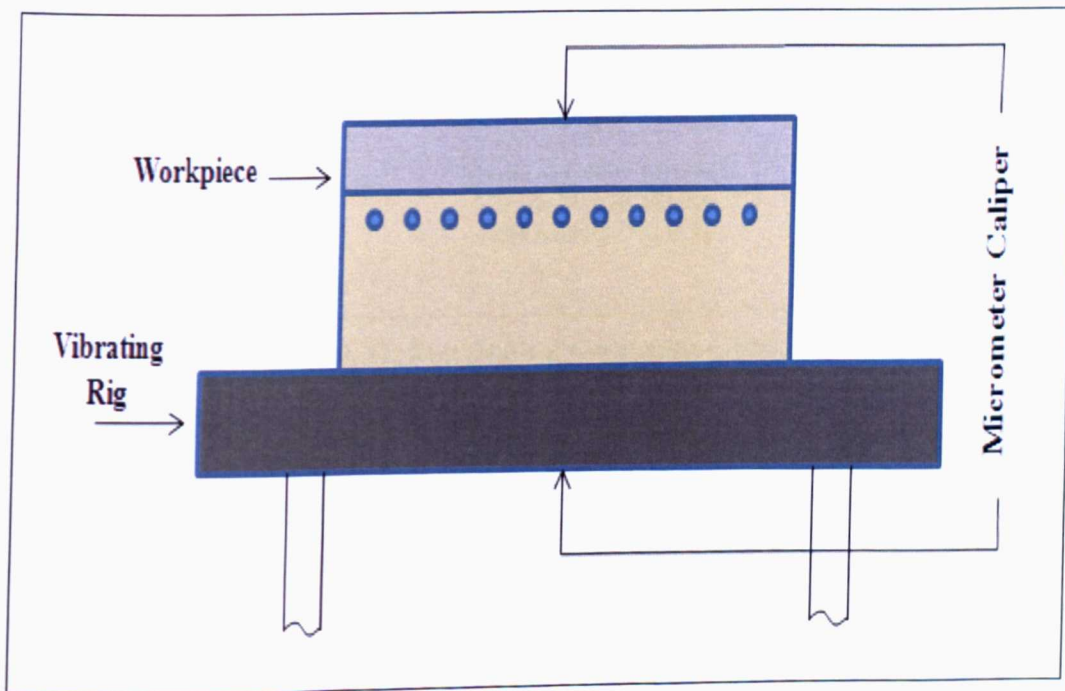


Figure 10. 11: Measurement of Real Depth of Cut Using a Micrometer Caliper.

Before any grinding trial the wheel was dressed and conditioned in order to maintain its initial condition and sharpness. The next set of results shows the performance of each workpiece material with different grinding wheels in terms of the measured real depth of cut achieved during each trial. These materials are presented with the following order: Mild Steel, En31 and M2 Tool Steel.



10.5.1 Wheel Performance in Mild Steel (BS970 080440, HRB 90.1)

The following graph in Figure 10.12 illustrates the real depth of cut achieved during conventional and vibration-assisted grinding of mild steel.

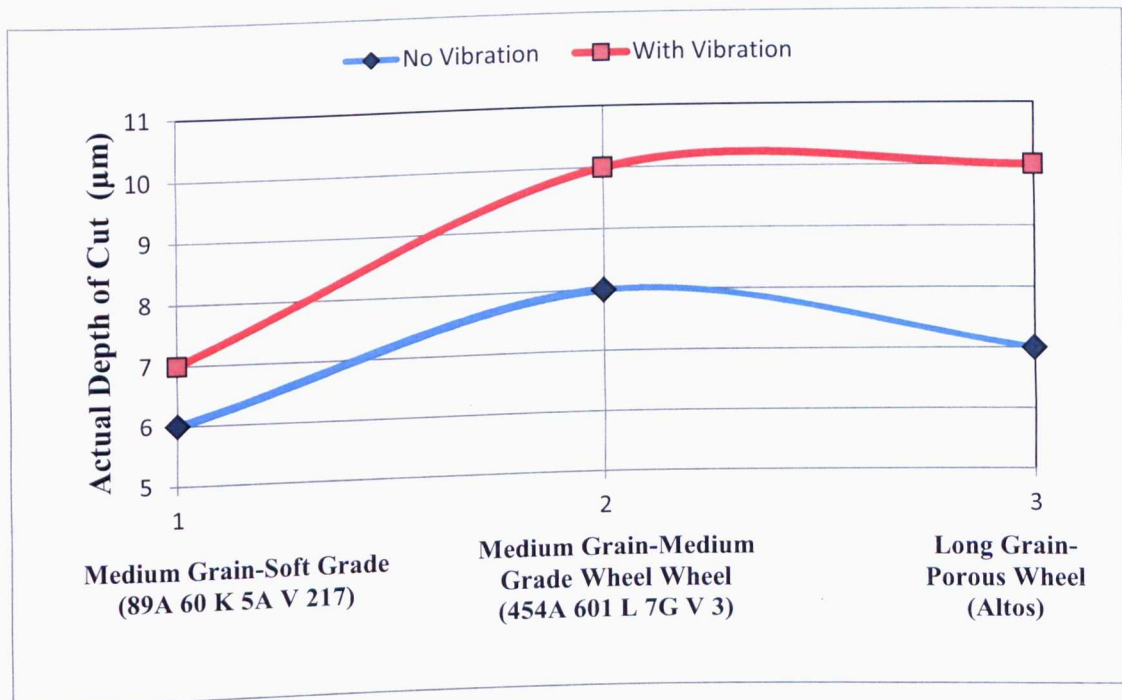


Figure 10.12: Real Depth of Cut Results – Mild Steel.

It is observed from the graph that vibration-assisted grinding provides an efficient cutting process contrary to the hypothesis in Batako, (2003). However, it can be argued that his view is right in terms of force but the increased cutting efficiency is attributed to the fact that each grit cuts with two edges i.e. forth and back. This leads to more material being removed per unit time in vibro-regime. Figure 10.12 show that the medium grain and medium grade wheel and the porous wheel while achieving the same material removal rate, secured the best performance in vibratory mode. In the first case the increase reached 25% and in the case of the porous wheel this percentage increased more to 42.8%. Moreover, grinding wheels with tougher grains result in higher removal rates. In occasions of stock removal grinding (SRG) where the surface finish and form are not the key objectives, the application of vibration can be particularly valuable. For the softer wheel the true depth of cut did not exceed 40% of the applied one. The contribution of vibration did not help in this specific case because these types of wheels are ideal for light stock removal.



10.5.2 Wheel Performance in En31 Workpiece (BS 534A99, HRC 64.2)

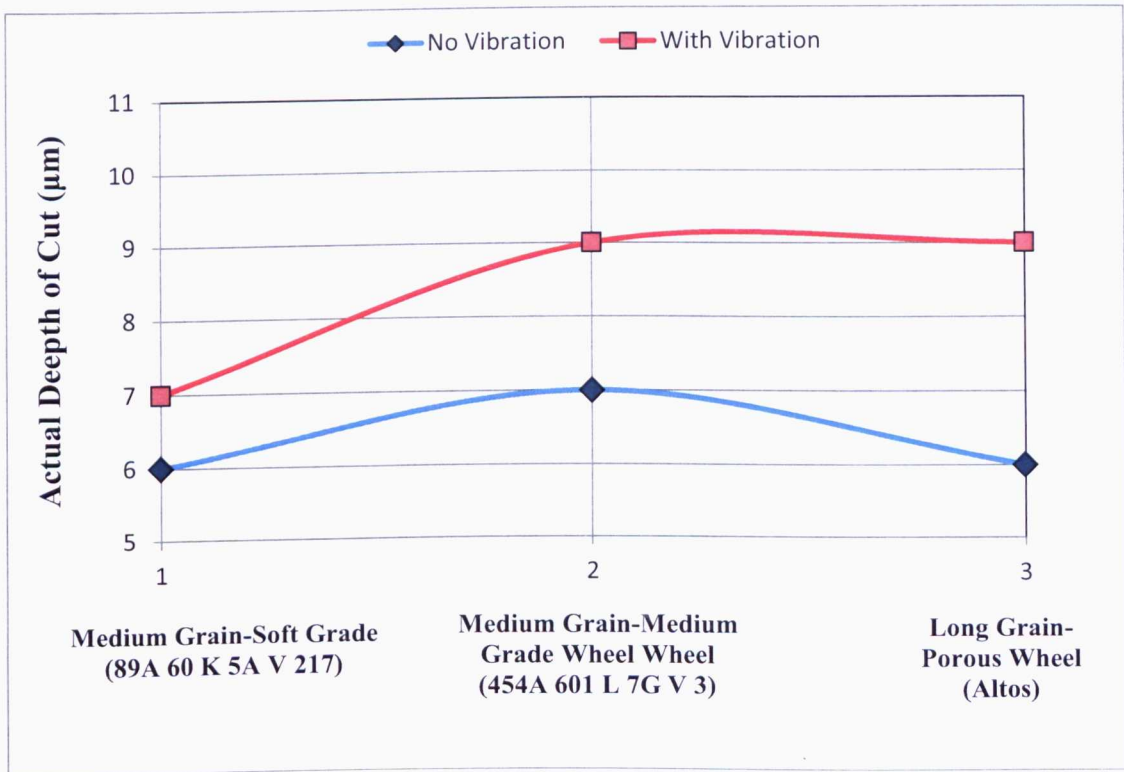


Figure 10. 13: Real Depth of Cut Results - En31.

In the graph in Figure 10.13, it is observed that the medium grade and the porous wheels produced the same results as in previous test in Figure 10.12. From these two sets of results it can be hypothesised that the application of vibration worked well with medium and porous wheels when machining hardened materials. Again similar results were detected for the soft grade wheel where no significant difference between conventional and vibration-assisted grinding occurred.



10.5.3 Wheel Performance in M2 Tool Steel (BS BM2, HRC 62)

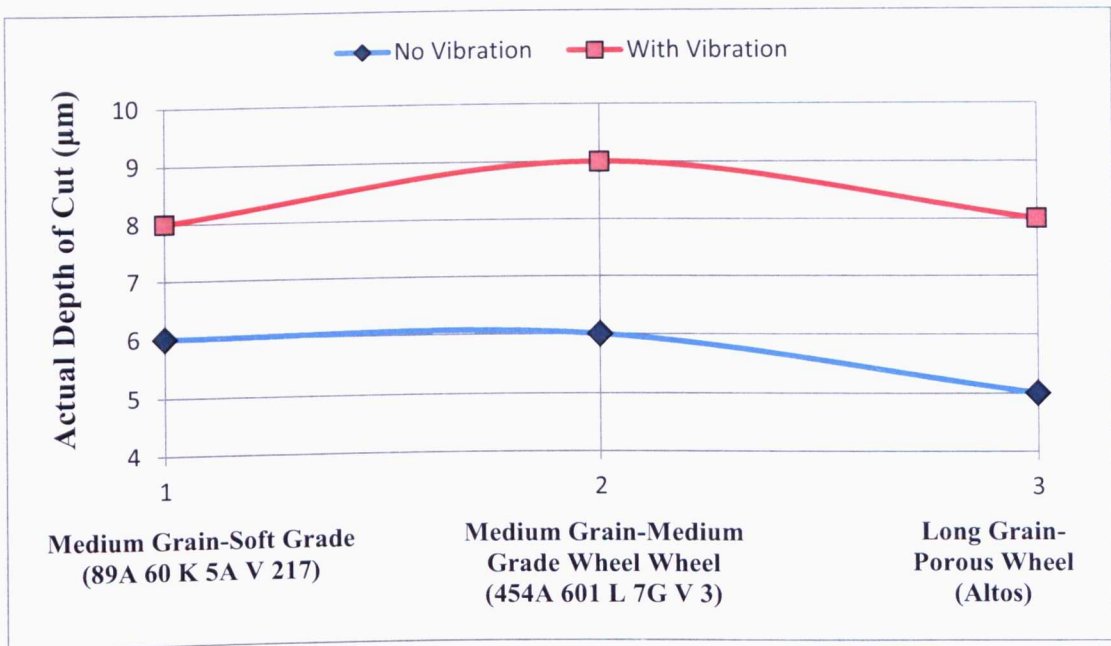


Figure 10. 14: Real Depth of Cut Results - M2.

Figure 10.14 gives the results of the hardest M2 tool steel. Comparing to results in Figure 10.12 and 10.13 it is seen that the medium grade wheel had the best performance when the soft grade and porous wheel secured same results in vibro-mode. However, the soft grade wheel also provided a good increase in depth of cut during vibration mode. Taking notice of the overall results of this experiment the key conclusion derived from this experiment is that low-frequency vibration of the workpiece could contribute to increase the material removal rate during the grinding process up to 50%.

10.6 Specific Material Removal Rate Results

The measured real depth of cut in the sets of experiments above was used to calculate the specific material removal rate (Q'_w) in both conventional and vibration-assisted grinding operation. As mentioned in the theory chapter, the material removal rate is a very important factor especially for industry as it describes the performance of the grinding wheel. The following results present how each grinding wheel performs with respect to the used workpiece materials.



10.6.1 Mild Steel (BS970 080440, HRB 90.1)

The following graph presents the material removal rate of the three wheels used to grind mild steel.

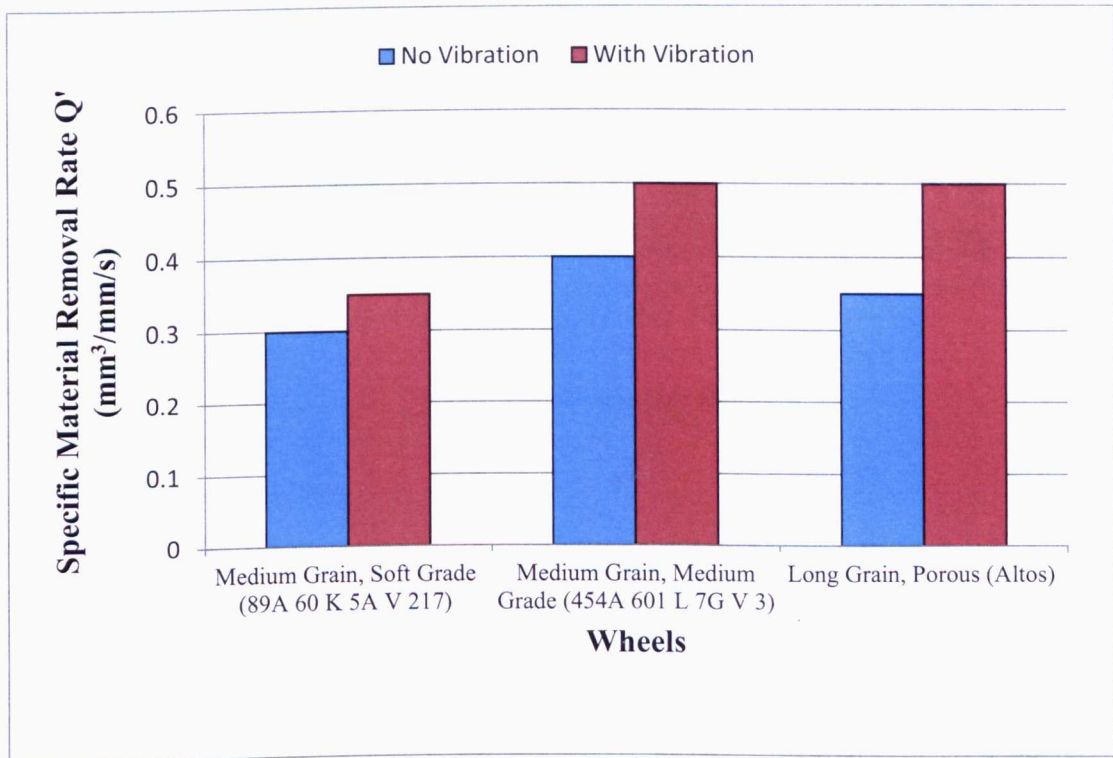


Figure 10. 15: Specific Material Removal Rate Results – Mild Steel.

As illustrated from the graph in Figure 10.15 the application of vibration increased the material removal rate for all three wheels. It is observed in this set of results when grinding mild steel that medium grade and porous wheels performed very well reaching up to 42.9% percentage improvement over conventional. Also, the nature of the wheel along with vibration increased the material removal rate as friable abrasives have large contact area. Large contact areas accomplish rapid stock removal. These wheels have the ability to expose new sharp edges more easily. The sharper the grain the better it cuts and it consequently produce higher material removal rates.

10.6.2 Hardened En31 (BS 534A99, HRC 64.2)

The next set of results concern the hardened En31 workpiece material.



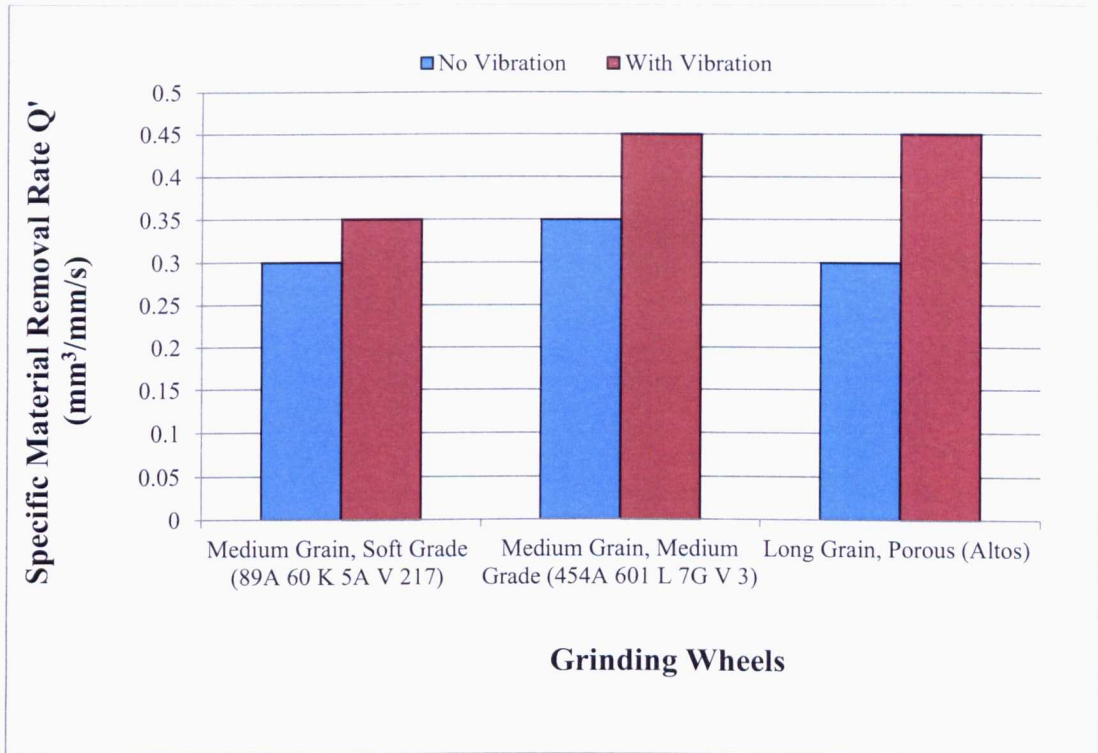


Figure 10. 16: Specific Material Removal Rate Results – En31.

In Figure 10.16 where the hardened En31 steel is machined, similar performance is observed. The superimposed vibration secured better cutting efficiency with the porous Altos wheel outperforming conventional by 50%. These results indicated that the medium grained-medium grade and porous wheels could be used for vibro-grinding for better performance.

10.6.3 Hardened M2 Tool steel (BS BM2, HRC 62)

During the hardness test, the M2 tool steel showed to be the hardest and this was expressed in terms of cutting forces and surface roughness. However, the vibration method proved that it can enhance the process by increasing the material removal rate as shown in the next graph (Figure 10.17).



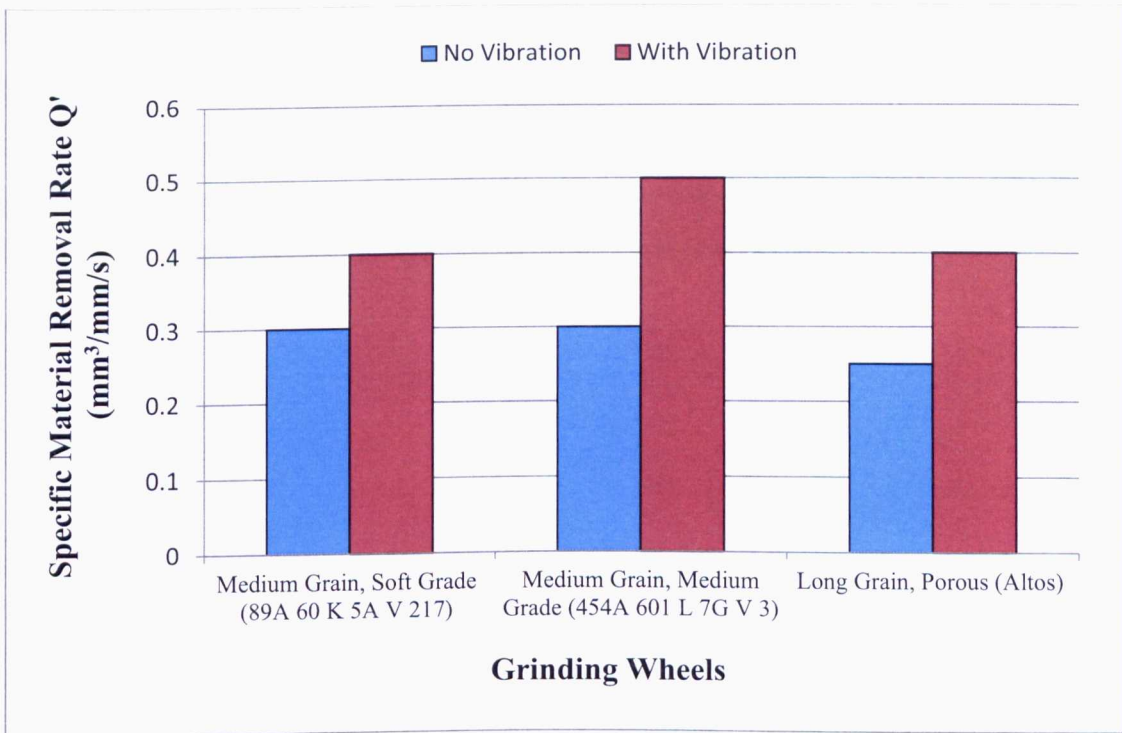


Figure 10. 17: Specific Material Removal Rate Results - M2.

During vibration assisted grinding much higher values of material removal rate were achieved regardless of the type of grinding wheel. In the present case the highest percentage of material removal increase was 66.6% and was detected during grinding with the medium grade wheel. The medium grade wheel is classified as semi-friable. Hence, its grains are not fractured very easily. The superimposed vibration allowed the grains to cut with two edges without breaking easy and achieve high material removal rate.

10.7 Remarks

During this experimental study three different materials and three grinding wheels were put into test and their performance was examined in conventional and vibration-assisted grinding processes. One of the key findings is that the induced vibration in almost all cases improved the performance of the process by decreasing the grinding forces, improving the workpiece surface quality and contributing to higher material removal rates. Lower forces mean lower power consumption and lower specific energy. Another essential finding was that the nature and properties of each abrasive wheel play a vital role in specific applications. Grain size, hardness and structure of each wheel should be taken into account



when targeting stock removal, form holding or workpiece surface quality. Each wheel is manufactured to work under certain circumstances and grinding parameters (wheel speed, work speed) and with specific workpiece materials. In this study it was found that even when the combination wheel-material-parameters were not the ideal, the application of vibration still secured an advantage over conventional processes.



Chapter 11: Wheel Wear



11.1 Introduction

This set of experiments was based on the effect of vibration on the wheel wear. Two different grinding wheels were tested and the G-ratio as well as the material removal rate (Q) was identified. A razor blade technique (Bhattacharyya & Moffatt, 1976) was employed to characterise the wheel wear and this is explained below.

11.2 Experimental Description

Each wheel was dressed before each grinding trial. 560 mm³ of workpiece material were removed gradually in several passes in conventional mode and with the application of vibration in order to achieve a considerable wheel wear. The real value of the removed material volume was found by measuring the workpiece at the end of each trial. This process has been described in details in Chapter 10.

Also, during this test the wear of the wheel was assessed in conventional and vibration-assisted grinding and the difference in performance was established. A razor blade was used to replicate the profile of the wheel wear (Figure 11.1) and a computerised surface texture measurement instrument was used to scan the blade edge reproducing the wheel surface profile (Figure 11.2). The procedure and the results are given in appendix D1 and D2 respectively.

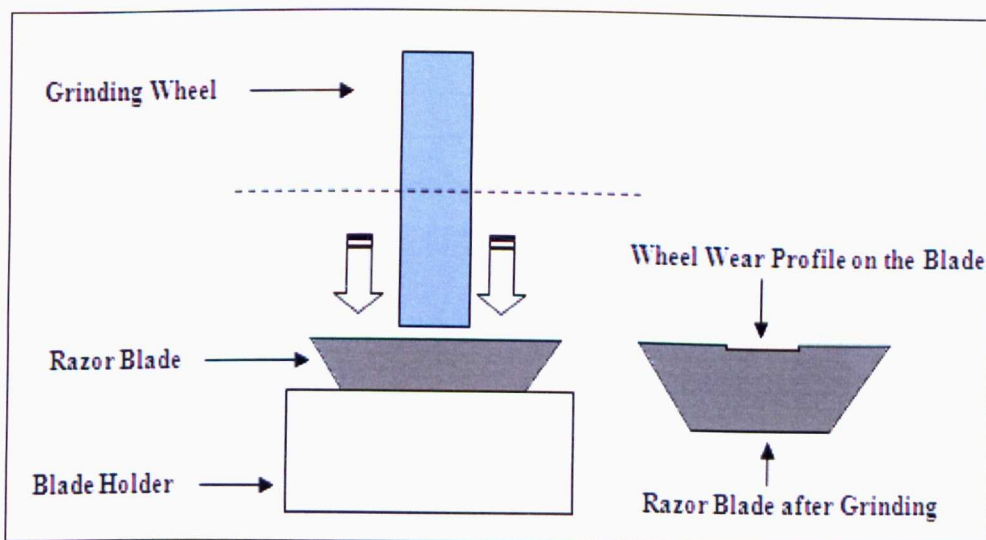


Figure 11. 1: Wheel Wear Test Using the Razor Blade Technique.



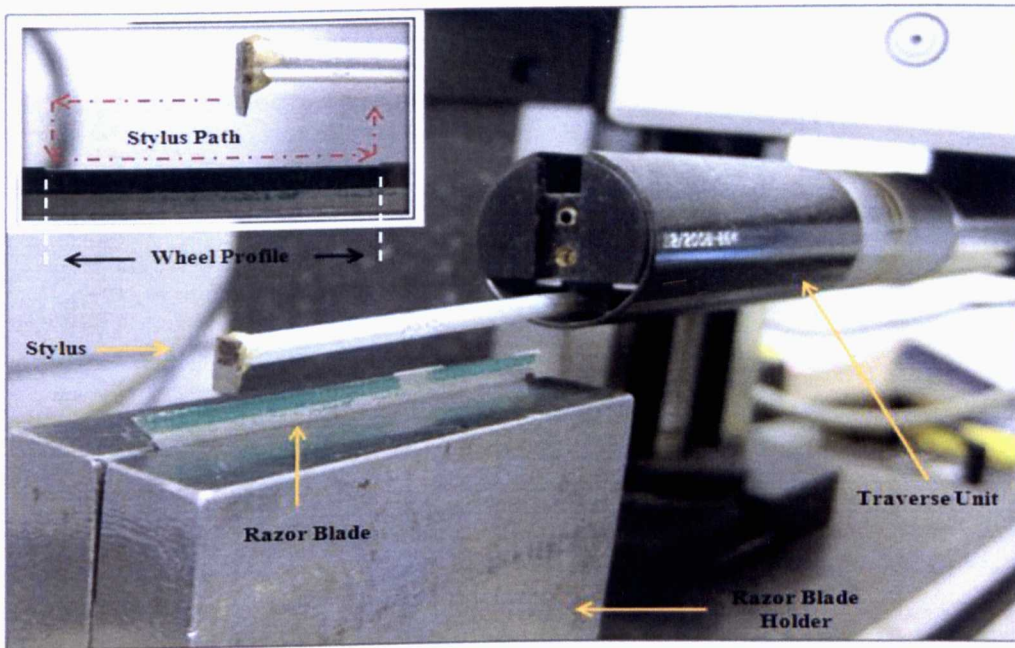


Figure 11. 2: Wheel Wear Test Measurement Configuration.

11.3 Wheel Wear

Two grinding wheels and two workpiece materials replicating extreme conditions were used for this specific experiment and the results for both conventional and vibration-assisted grinding are shown in Figure 11.3 for porous wheel and 11.4 for medium grain and medium grade wheel.

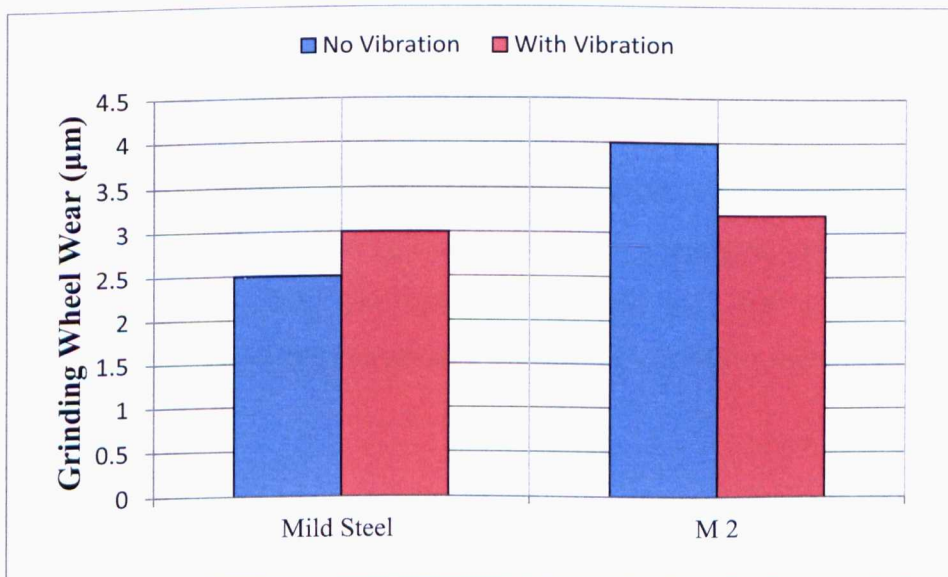


Figure 11. 3: Wheel Wear with Porous Grinding Wheel.



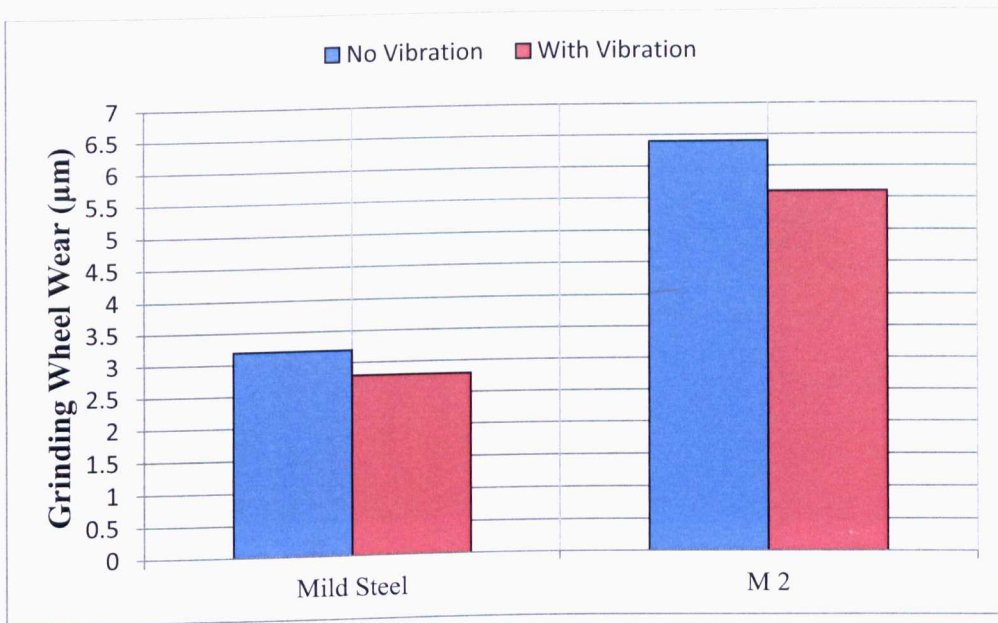


Figure 11. 4: Wheel Wear with Medium Grain Medium Grade Wheel (454A 601 L 7G V 3).

Figure 11.3 shows the performance of the porous wheel. In grinding the hardened M2 steel, the vibratory mode outperformed the conventional grinding with up to 20% decrease in wheel wear. However, the application of vibration when machining mild steel led to an increased wear of the wheel by 20%. It is well known in machining practice that soft materials are very hard to grind but vibration had worked well so far. The poor performance in this case is expected to be due to the effect of the type of grit and bond used. The Altos wheel was 54% porous with long needle grit design for inkonel 718 grinding. It was shown in Figure 10.9 that the cutting forces were higher. However, in Figure 10.12 the vibro-regime secured high actual depth of cut with subsequent higher removal rate. These factors contributed to high wear of the wheel.

It is observed from Figure 11.4 that the application of vibration led to reduced grinding wheel wear. In the case of mild steel ground with the medium grain wheel the decrease of the wheel wear reached 12.5%. However, grinding M2 tool steel which is harder, the performance of the wheel did not change and vibration secured the same decrease of wheel (12.5%).

The following pictures in Figure 11.5 illustrate the two different types of wheel grains. The first one is a needle grain with long aspect ratio (Altos) and the second one is the grain of a normal low aspect ratio grain.





Figure 11. 5: Types of Grains for Porous and Medium Wheel (Jackson, 2008).

On the other hand, the Altos wheel had high aspect ratio grains compared to normal grain. Therefore, the adhesion of the soft material to the grits and the added oscillation led to rapid breakage of the needle grain because the grains break faster as the ductile material is removed. This resulted into high wheel wear in Figure 11.3.

11.4 Material Removed

The following results present the material removed for both conventional and superimposed vibrational grinding. At the beginning of each grinding trial the wheel was dressed and conditioned. Successive small depths of cut were applied to the workpiece and material was removed sequentially. This process continued till the sum of these depths of cut reached 1 mm on the dial of the machine tool handle. The actual total depth of cut was measured and the volume of material removed was calculated. The following graphs in Figures 11.6 and 11.7 depict the removed material using a porous and medium grade grinding wheel during conventional and vibration-assisted grinding operation.



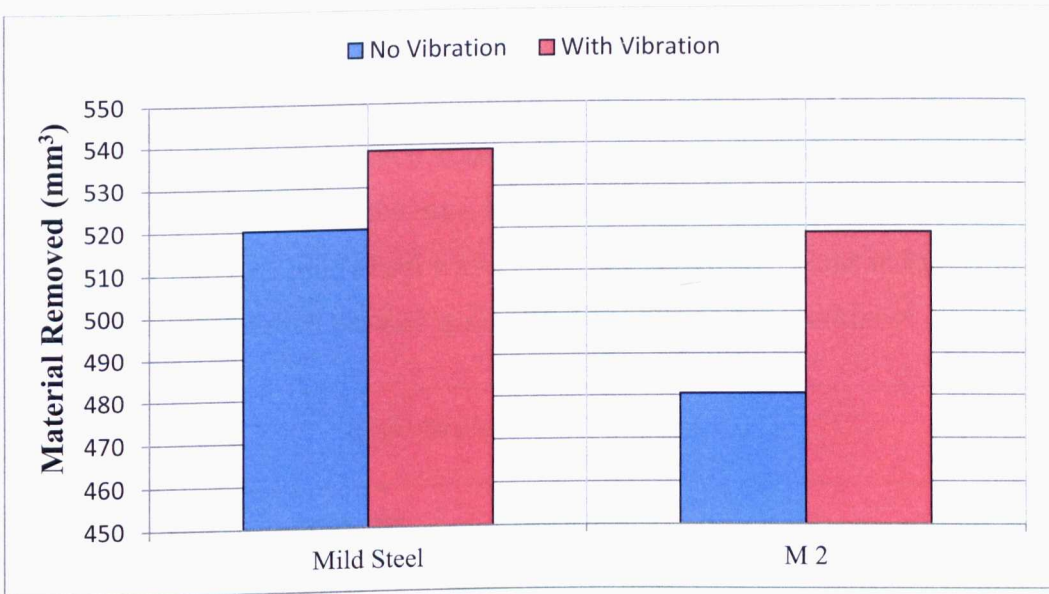


Figure 11. 6: Material Removed with Porous Grinding Wheel.

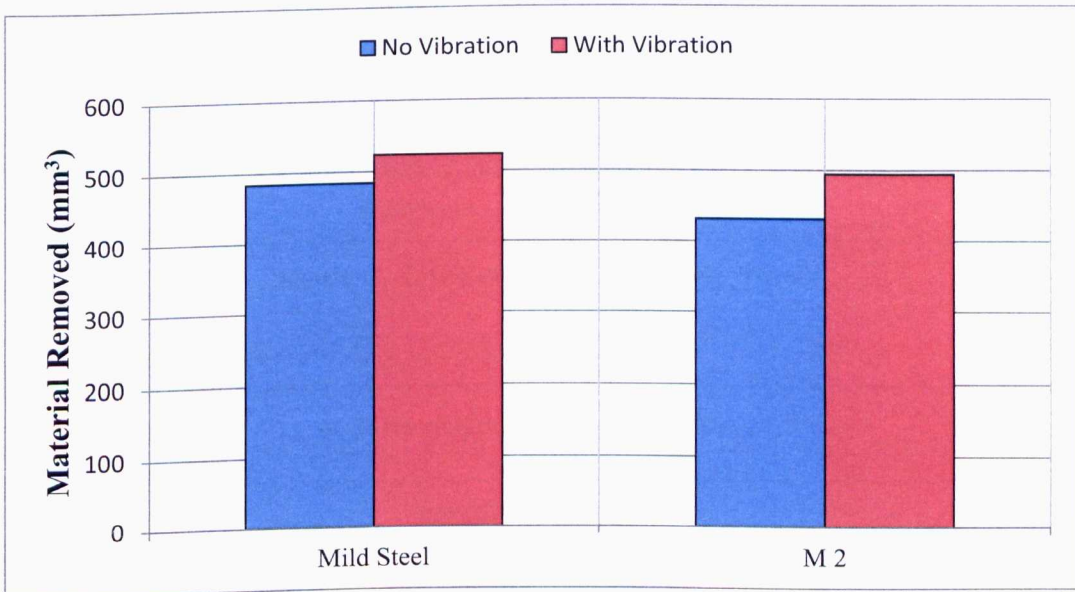


Figure 11. 7: Material Removed with Medium Grade (454A 601 L 7G V 3) Grinding Wheel.

The graphs in Figure 11.6 and 11.7 support the arguments given above for the reason of high wheel wear in vibratory regime. It is seen that the cutting efficiency is better in vibration mode as the achieved material removal is higher than in conventional grinding. Owing to the fact that the experiments were done in dry condition which is harsh for any grinding process, it is speculated that the superimposed vibration brings a net benefit.



11.4 G-Ratio Results

The G-ratio was calculated in each case during this experiment. As introduced in the chapter of theory, the G-ratio is the ratio of material ground per unit wheel width (U_w) to volume of wheel worn per unit wheel width (U_s). The following results in Figures 11.8 and 11.9 show the G-ratio of each process using different wheels and workpiece materials.

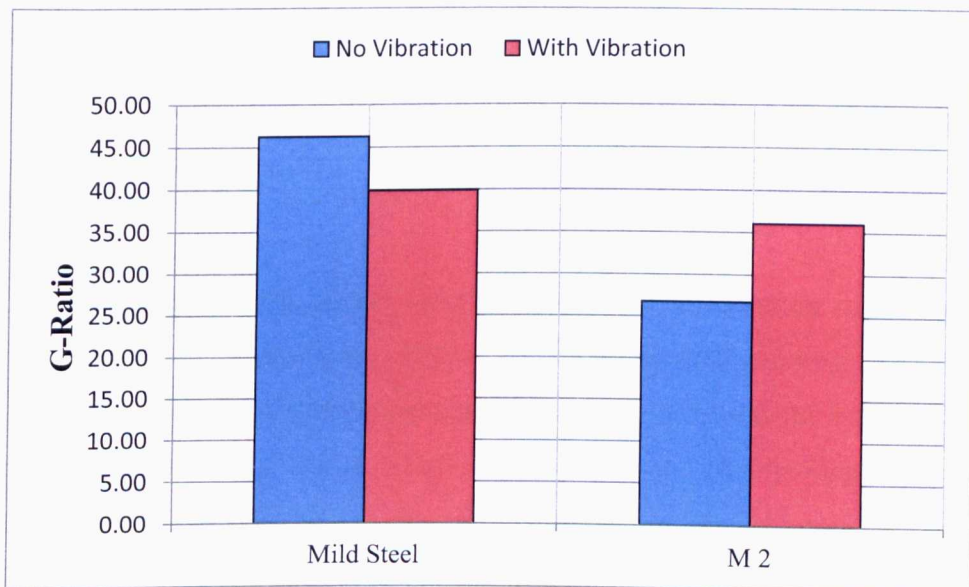


Figure 11. 8: G-Ratio-Porous Grinding Wheel.

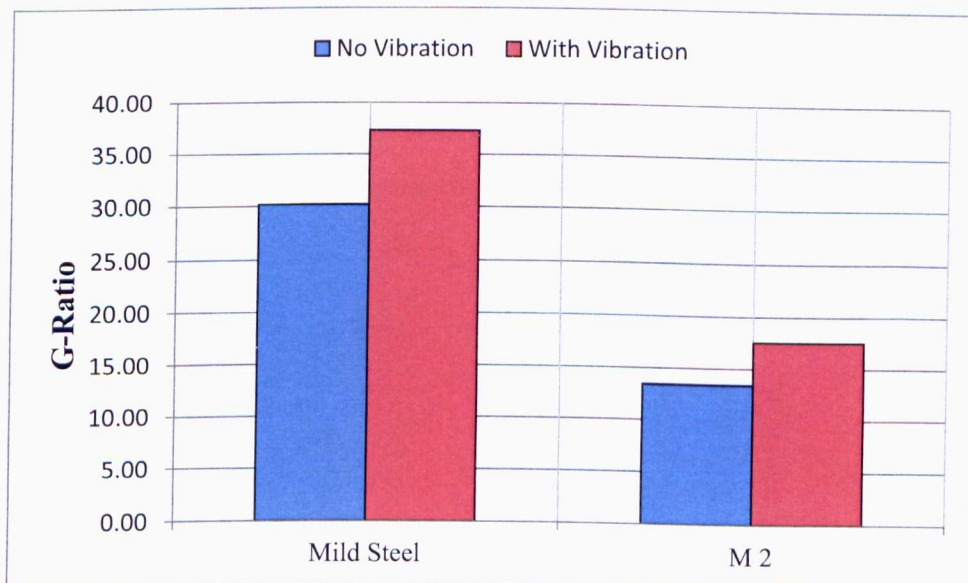


Figure 11. 9: G-Ratio-Medium Grain-Medium Grade (454A 601 L 7G V 3) Grinding Wheel.



As illustrated in Figures 11.8 and 11.9, the vibration-assisted method increased the G-ratio of the process in all cases. The exception is when the mild steel was ground with the porous grinding wheel where a decrease of 13.6% is observed for the reasons given in Figure 11.8 for wheel wear. This result proved that a wheel with high aspect ratio grit and soft of medium grade cannot be used to grind mild steel. However, if the cost of the wheel is not of concern and the removal rate is the prime target then using vibration would be beneficial to grind soft material. In all the other cases the increase of G-ratio was from 23.9% to 35% in the case of porous wheel and M2 tool steel.

11.5 Remarks

An overall view of the results shows clearly the benefits of vibration superimposition on the process in terms of wheel wear, material removal rate and grinding ratio. In all cases the superimposed vibration reduced the wheel wear and increased the volume of material removed. Moreover, the G-ratio increased contrary to conventional grinding. The improvement in percentage varied due to the nature of the grinding wheels and the properties of the workpiece materials. For example, the application of vibration did not prove beneficial when grinding mild steel with a porous wheel. Another, essential finding is observed in the last graph (Figure 11.9) where the G-ratio was found to be particularly lower when grinding M2 tool steel material with a medium grade wheel. This can be explained by the fact that for heavy stock removals harder wheels with tough grains are required. Also, for hard workpiece materials such as M2 sharper abrasives are preferable. However, even in this case, the vibration managed to raise the G-ratio by 30.9%.



Chapter 12: Effect of Closed-Loop Control System



12.1 Introduction

This set of experimental work deals with the control of vibration parameters during vibration – assisted grinding. In previous tests, the vibration parameters such as amplitude and frequency were set before the grinding process took place. However, during the grinding process it was not clear whether these parameters especially the amplitude of the vibration displacement were affected by the grinding forces. Therefore in this experiment, the system is driven at the desired frequency while controlling the amplitude of the displacement. For this purpose a closed loop control system was used.

12.2 Experiment Description

The diagram in Figure 12.1 represents the closed-loop system adopted in this experiment.

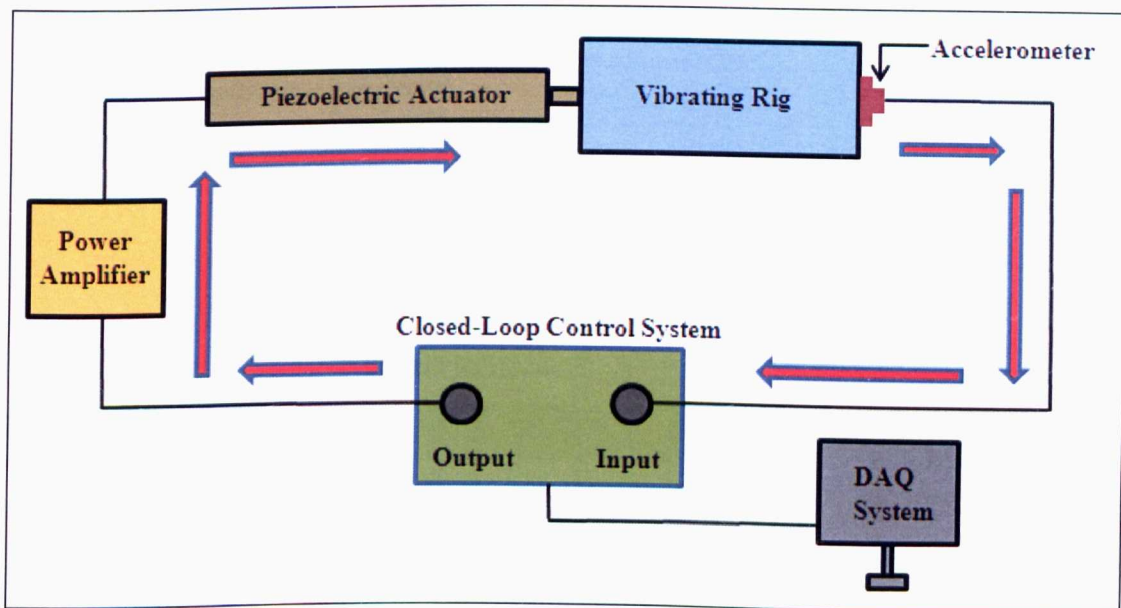


Figure 12. 1: Closed-Loop Control System Configuration.

The closed-loop control system was described in chapter 5. In this experiment, the control was the acceleration, which after double integration provided the feedback to the control loop. In the present experiment the displacement of vibration was set at $15 \mu\text{m}$. The control system then adjusted the amplitude of the excitation signal to the power amplifier in order



to maintain the 15 μm constant regardless of the grinding forces applied to the workpiece during grinding. Two different experimental tests were performed using this control system in terms of grinding wheel, workpiece material and grinding parameters and the results were compared to those of open-loop control and conventional grinding.

12.3 Preliminary Experiment- Medium Grade Wheel (454A 601 L 7G V 3) with Soft Steel

In this experiment, a medium grain and medium grade grinding wheel with dense structure was used to grind a mild steel workpiece material. Table 12.1 provides the details of the process configuration.

Grinding Parameter	Value
Grinding Wheel Type	Al ₂ O ₃ (454 A 601 L 7 G V3)
Wheel Speed (Vs)	35 m/s
Work Speed (Vw)	25 mm/s
Grinding Condition	Dry
Workpiece Material	Mild Steel (BS970 080440)
Wheel Feed	Traverse
Vibration Frequency (Vibration Mode)	275 Hz
Vibration Amplitude CLOSED-LOOP CONTROL	15 μm (Peak)
Depth of Cut	5-25 μm

Table 12. 1: Preliminary Experiment - Grinding Parameters.

12.3.1 Grinding Forces

The following graphs depict the variation of specific normal (Figure 12.2) and tangential (Figure 12.3) force during a conventional grinding process. Here two set of tests were undertaken. The oscillation was applied to the rig in an open ended at given amplitude and in a closed-loop where the amplitude of the vibration is kept constant. Acceleration from the process was used as feedback to the control system.



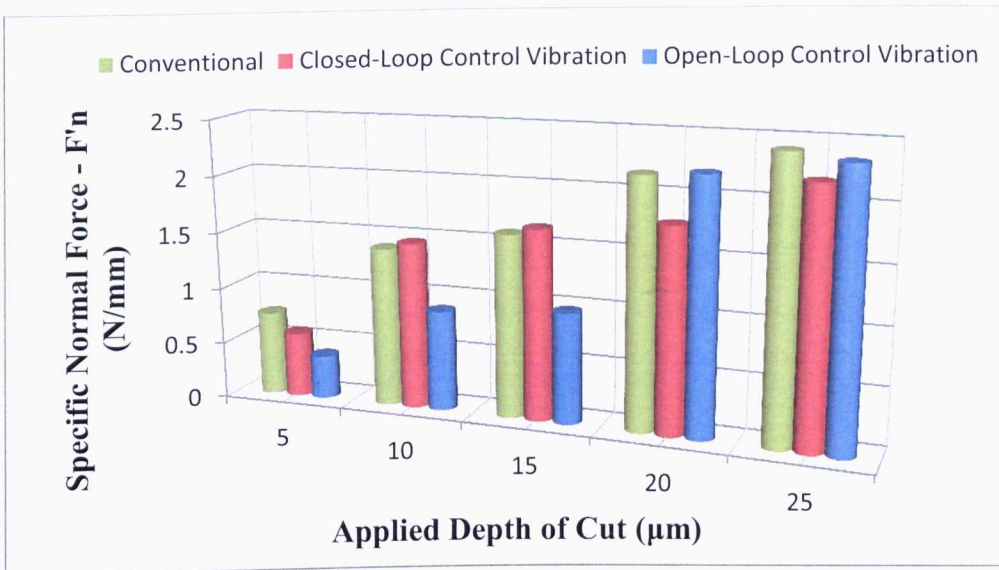


Figure 12. 2: Preliminary Experiment-Specific Normal Force Results.

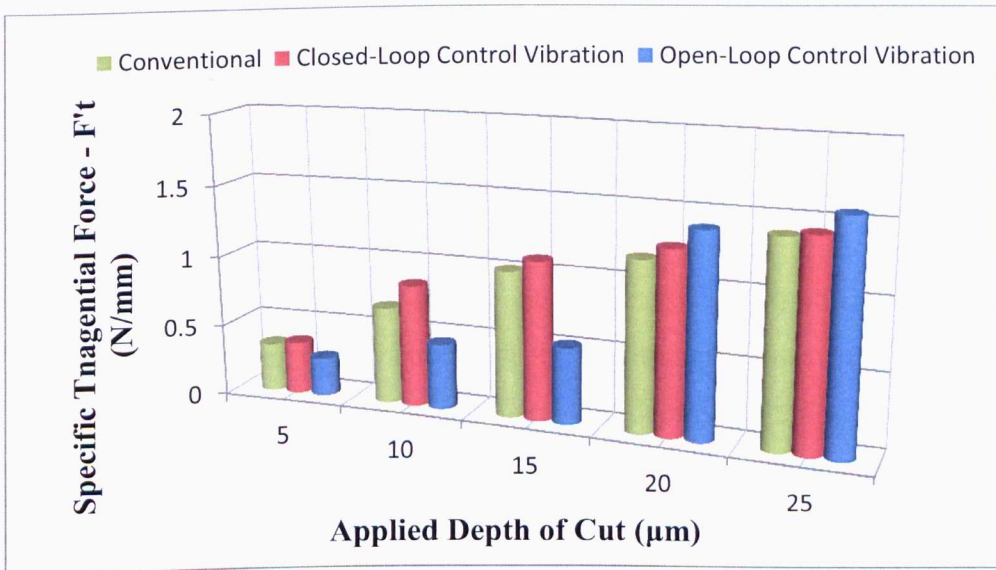


Figure 12. 3: Preliminary Experiment-Specific Tangential Force Results.

Taking notice of the normal force results graph, an obvious reduction is detected for higher values of depth of cut. This reduction reached 22% for normal forces compared to conventional grinding and 19% comparing to open-loop vibration control. Regarding the tangential force no essential reduction was observed. However, the closed-loop vibration control did not seem to increase significantly the grinding forces and it is seen that the closed-loop control system at time (small depth of cuts) produced similar cutting forces as in conventional grinding. In contrast open loop vibration secured lower cutting forces for a small depth of cut. From this result, it can be speculated that open loop vibration is desirable at small depths whereas close-loop control is effective with deeper cuts.



12.3.2 Surface Roughness

Figure 12.4 illustrates the surface roughness during each grinding trial using all three methods described above.

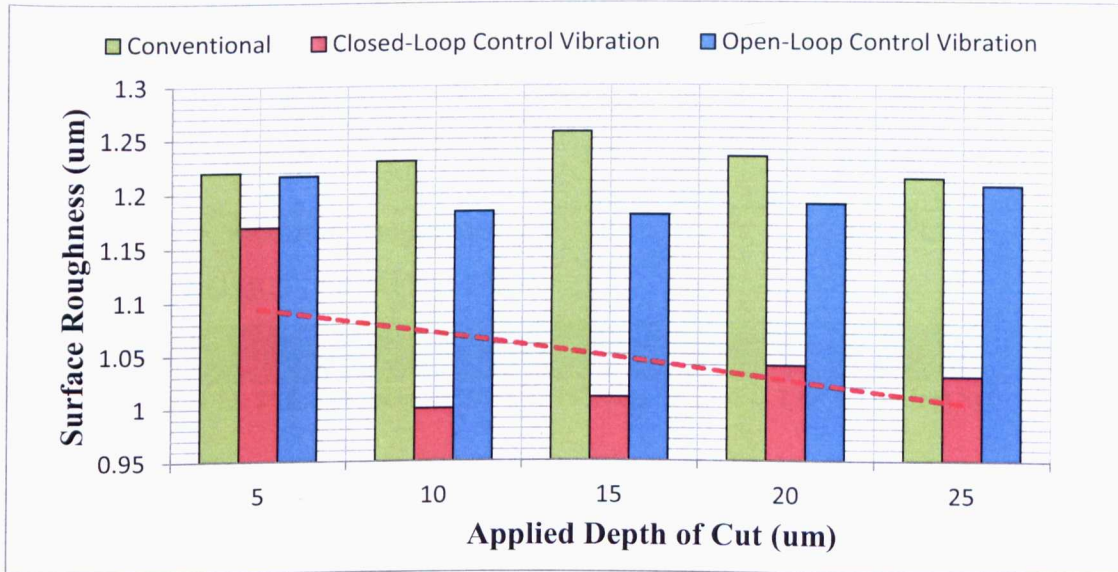


Figure 12. 4: Preliminary Experiment-Surface Roughness Results.

The improvement of surface quality during vibration assisted grinding with closed-loop control is obvious and tends to be better with the increasing depth of cut. The maximum improvement was observed at values higher than 5 μm depth of cut. For 15 μm depth of cut the reduction of surface roughness reached 14.4% of open-loop control and 19.8% of conventional grinding. Due to the nature of the workpiece material (soft steel) the surface roughness results were slightly higher than expected. However, the application of vibration showed that a significantly improvement of the quality could be achieved. The surface quality in open loop stayed invariant throughout this set of tests.

12.4 Soft Grade Wheel (VU33 A 602 HH 10 V B1) with Hardened Steel En31

In the present experiment an Al_2O_3 wheel suitable for grinding hardened steel at high speed was employed. The wheel had mixed size grains with an open structure. The following Table 12.2 shows the experimental parameters for these tests.



Grinding Parameter	Value
Grinding Wheel Type	Al ₂ O ₃ (VU33 A 602 HH 10 V B1)
Wheel Speed (Vs)	30 m/s
Work Speed (Vw)	200 mm/s
Grinding Condition	Dry
Workpiece Material	En31 (BS 534A99) HRC 64.2
Wheel Feed	Traverse
Vibration Frequency	275 Hz
Vibration Amplitude	15 μm (Peak)
CLOSED-LOOP CONTROL	
Depth of Cut	10-30 μm

Table 12. 2: Experimental Parameters Using CLOSED-LOOP Control System.

In this test the depth of cut varied from 10 to 30 μm in steps of 5 μm. The wheel speed was set to 30 m/s and the work speed was set to the maximum achievable by the grinding machine i.e. 200 mm/s. These parameters were set in an attempt to simulate the high efficiency grinding in terms of speed ratio Vs/Vw. The grinding wheel used for this experiment was a high performance dual grain count (mixed grain) abrasive aluminium oxide wheel with 50% of the grains being size 60 (medium grain) and 50% grit size 80 (fine grain). Also, it was a soft grade wheel with open structure operating speed at 65 m/s max. After each trial the real depth of cut was measured and the specific material removal rate was calculated. The following results show the differences between conventional, closed-loop and open loop vibration-assisted grinding.

12.4.1 Grinding Forces

The results in Figures 12.5 and 12.6 illustrate the system performance in terms of specific grinding forces.



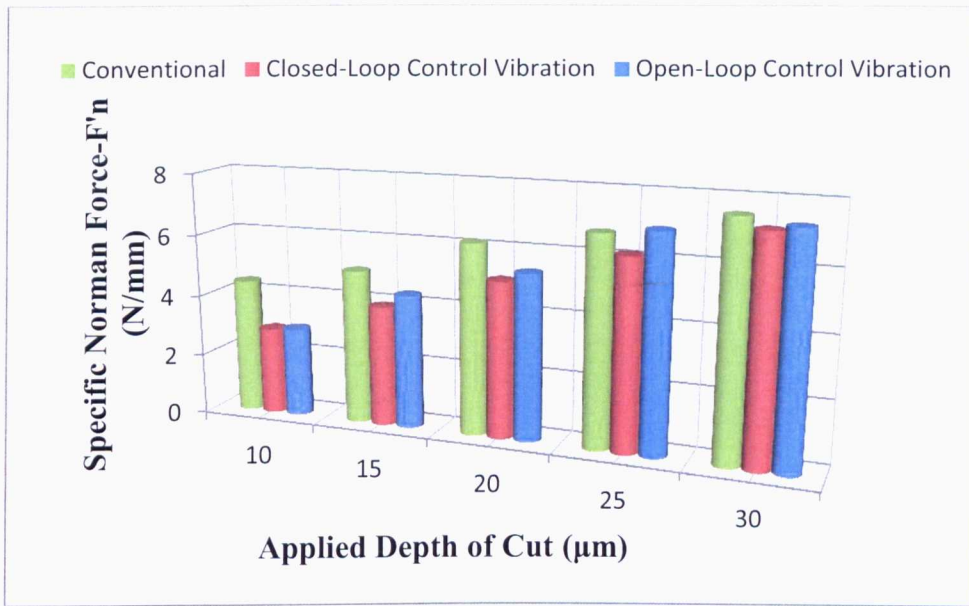


Figure 12. 5: Specific Normal Force Results.

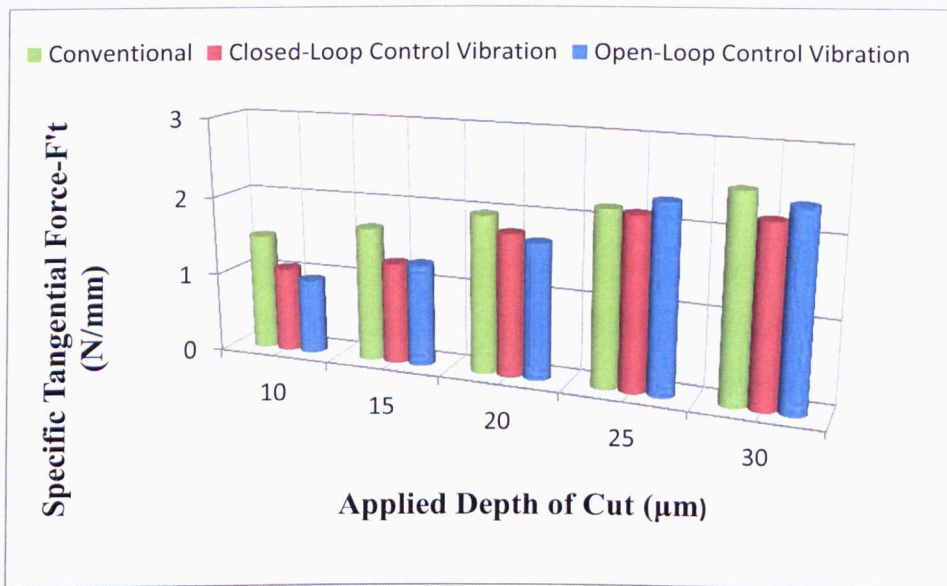


Figure 12. 6: Specific Tangential Force Results.

A reduction in grinding forces is observed between conventional and vibration-assisted grinding. The reduction exceeded 10.5% for normal forces, and 14.2% for tangential. In this case, with the closed-loop control process an additional 5.5 % reduction in grinding forces was achieved leading to a further decrease of power consumption during grinding.



12.4.2 Specific Energy

The graph in Figure 12.7 shows the power requirement of the process and illustrates the efficiency of each of the three methods used in this study.

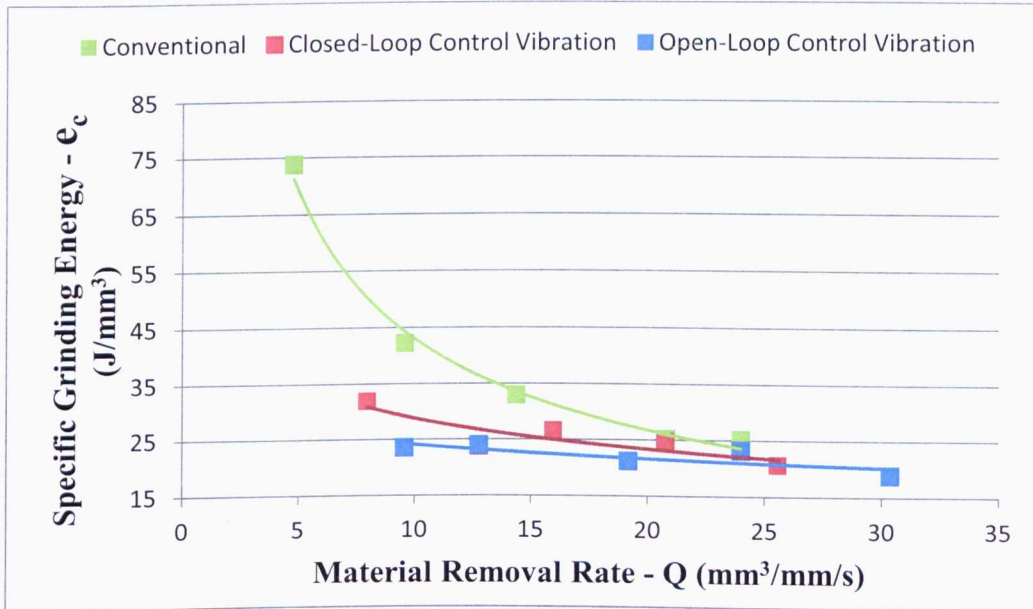


Figure 12. 7: Grinding Specific Energy.

Figure 12.7 gives the specific grinding energy (e_c) as a function of the material removal rate. It is seen in this graph that for the same grinding conditions the superimposed vibration led to an efficient cutting thus it secured a higher material removal rate than conventional.

Observation from Figure 12.7 suggests that the added vibration without feedback control (open-loop) was more energy efficient at it has lowest specific energies and removes more material than both conventional and closed-loop. This is an indication that random vibration could be applied. This may be linked with the random cutting process due to grain distribution.

Obviously the system consumed less grinding energy in vibratory mode. In closed-loop control, referring to Figure 12.5 and 12.6 it is agreeable that less force meant less power consumption because the power consumed is a function of the tangential force. However, the overall energy is a summation of grinding energy and energy spent by the amplifier of the piezoelectric actuator.



12.4.3 Surface Roughness

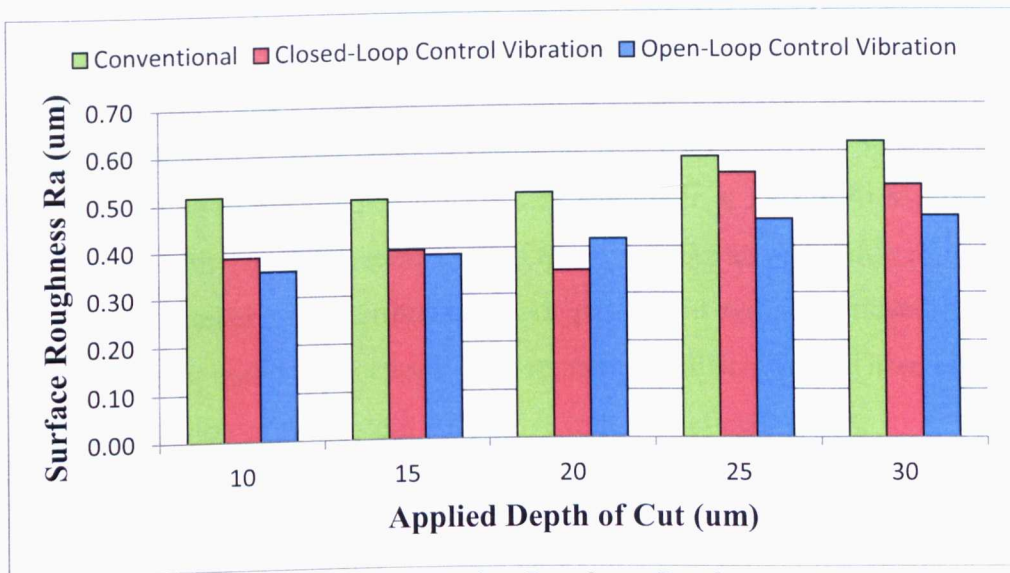


Figure 12. 8: Surface Roughness Results.

Figure 12.8 shows the improvement in workpiece surface quality accrued between conventional and vibration-assisted grinding. On the one hand the results in Fig 12.5 could be suggesting that open-loop control is beneficial at lower depth of cuts when the surface is of concern. On the other hand these results indicate that perhaps random vibration could be an option to consider due to the random nature of grain distribution in the cutting process. It is seen here that the average surface roughness is invariant with the superimposed vibration and the open-loop method secured the best surface quality.

12.5 Remarks

It was observed that, when the system was driven close to its natural frequency, the feedback loop was not fast enough to control the system. At some time the system became unstable and as measure of precaution built into the system, the process halted. During this experiment a further reduction of grinding forces was achieved compared to the open-loop vibration control process. This reduction led to further decrease of the system's power consumption. Nevertheless, the material removal rate was slightly decreased. This can be explained as the wheel properties did not allow for high stock removal and also the superimposed vibration along with the friability of the wheel grains caused rubbing instead of cutting.



One of the main advantages of the closed-loop control system was that it could control vibration parameters regardless of any externally applied force or disturbance. The first set of experiments showed a clear benefit of this system over the open-loop control whereas during the second set the closed-loop vibration control did not give the desired results. Taking into account the overall results it can be concluded that at low workspeeds the system had more time to control the displacement amplitude at 15 μm . At high workspeeds (second set of experiments) the system seemed to behave like an open-loop control system.. Due to the limit number of experimental work performed with the closed-loop control system it is clear that many of its capabilities remained undiscovered. Therefore, a further detailed implementation of the system could give more beneficial results.

Chapter 13: Discussion - Conclusions

13.1 Discussion

The main aim of this project was to investigate the effect of low-frequency superimposed vibration of the workpiece during surface grinding process. The target was to improve the performance of the process in terms of reducing the grinding forces, grinding energy, improving the surface quality of the workpiece and extending the life of the grinding wheel. After a comprehensive study of the literature, it was ascertained that there was a limited number of publications upon this subject. Most of the works that have been done in the past on the subject of vibration-assisted machining and especially grinding concerned different and complex designs, different ways of applying vibration as well as dissimilar grinding parameters. Particularly in grinding there is a limited number of publications which approached the present subject with satisfying results but with employing complex designs and difficult to exploit devices. Processed materials were not hardened steel but mainly silicon wafers where only a few microns were ground off.

The first step was to design a vibrating rig that would simultaneously accommodate and vibrate the workpiece during a surface grinding process. In order to achieve this target a number of different vibrating models were designed and simulated under varying loading conditions using the finite element method of some of the best simulation software packages such as SolidWorks and ANSYS. The simulation results revealed the high stress concentration areas for each model and the response of each one under the application of external forces.

The design aspect of the rig was to vibrate at its resonance frequency in order to achieve high displacement values with low power input. However, a number of other parameters should be taken into account before applying any specific value of frequency. That frequency should not much the natural frequency of the spindle unit in order to avoid harming the machine tool. For that reason, the spindle's natural frequency along with its static and dynamic stiffness was identified using different techniques, allowing for examination of the 'safe' frequency operational areas where spindle appeared the lowest displacements. That was the first parameter that played a vital role in the final design of the rig and its driving frequency bandwidth.

The second parameter was the vibration velocity. According to theory a vibro-impact condition was selected to follow in the present study where the vibration velocity does not exceed the workspeed and therefore the impact pair wheel-rig was under compression. The reason was that if there was clearance, the impact would damage the friable grains of the grinding wheel. Taking into consideration all these parameters the frequency bandwidth and the displacement amplitude was selected and based on them a novel design of vibrating rig was developed. It consisted of with two flat springs, ground to ensure perfect flatness between the moving parts. Prior to that a four flat spring system was developed and selected to undertake the preliminary experimental work but it was discarded due to a number of design irregularities.

The natural frequency of the two flat spring vibrating rig was found experimentally and these values were compared these with those of modal analysis performed in software. The impact test method was employed for this purpose and it was found that the natural frequency for the rig with was 290 Hz for the rig with two flat springs. There was a degree of discrepancy between the modal analysis, the analytical calculation and the impact test results. This error was higher in the case of the system with four springs as it appeared to be less stable than the new one. The reason for this divergence was due to boundary conditions and default assumptions in the software and its ability to handle complex structures. Therefore, the impact test results were selected for further experimental work with the vibrating rig mounted to the machine tool, attached to the piezoelectric actuator. In this case the entire system set up in its actual working configuration resonated at 275 Hz for the two flat spring system.

To test the initial design, a set of preliminary vibration-assisted grinding experiments were carried out using the four flat spring vibrating rig. No coolant was applied during these tests. The initial results showed a reduction in grinding forces when vibration was applied. Particularly, there was a 10.9% reduction in tangential grinding forces and for high depths of cut the reduction reached 21.7%. Moreover, the surface roughness was decreased during vibration-assisted grinding in all applied depths of cut.

The full scale of experimental work was conducted using a novel two flat spring vibrating rig. The reason was that the four spring rig could not achieve absolute flatness of the

workpiece and thus a lot of time was spent on the spark-out process resulting in the rapid wear of the wheel.

The effect of *depth of cut* on the process performance was examined. It was found that the superimposed vibration decreased the cutting forces with the increase of depth of cut. In some cases this decrease reached 22.5% in tangential forces for 25 μm depth of cut when grinding a hardened En 31 (HRC 64.2) workpiece material.

It was observed that for specific depths of cut the vibration affected positively the process by increasing the surface quality of the workpiece. That fact can be explained as the real depth of cut was not measured and thus it seemed that at these values of applied depth of cut, the superimposed vibration removed uncertain volume of material resulting in better or worse surface finish depending on the case.

The influence of the *workspeed* on the process was studied. Here it was also found that at higher workspeed the presence of vibration led to higher reduction of cutting forces and grinding power. A study of the contribution of the *wheelspeed* on the grinding process was undertaken. It was found that higher reductions in cutting forces were achieved at high wheelspeed. These reductions exceeded 19.3 % for normal forces and 20.8% for tangential. Alongside this reduction in cutting forces, a better surface finish of the workpiece was observed. The highest values of wheelspeed and workspeed were within the range of manufacturer's operational wheelspeed as well as the nature of the process and capabilities of the machine tool.

The performance of *grinding wheels* was studied with three different types: - 454A 60I L 7G V 3, 89A 60 K 5A V 217 and porous grain Altos. Three different workpiece materials (mild steel HRB 90, En31, HRC 64. and M2 HRC 62 were used during conventional and vibration-assisted grinding operations. In these experiments the actual depth of cut was measured and the material removal rate was obtained.

The results showed that the medium grain wheel seemed to work well with all three workpiece material during conventional and vibration mode. Almost all the results showed a reduction in grinding forces and improvement in surface roughness of the workpiece when vibration was applied. On the other hand, the applied vibration was not as successful

in grinding with the soft grade wheel. Especially, the hardened materials did not perform very well with the soft wheel due to increased rubbing instead of cutting.

Finally, the vibration provided excellent improvement in terms of forces and surface roughness when grinding the En31 material with the porous wheel. Grinding of M2 tool steel material resulted in a decrease of grinding forces in vibration-assisted mode, however, there was little gain in enhancing the surface roughness of the workpiece.

In vibration-assisted grinding higher values of actual depth of cut were achieved in all cases and particularly when medium and porous wheels were used. Hence, the specific material removal rates were improved reaching 50% increase in the case of porous wheel and En31 workpiece and 42.9% in the case of porous wheel and mild steel. This increase justifies the poor surface roughness of the workpiece recorded in this test. As expected, the lowest improvement was observed during grinding with the fine wheel. Because of the high friability of the wheel its grains were fractured rapidly with the application of vibration leading to wheel dullness.

The life of the grinding wheel was investigated in a set of experiments where two wheels were used (*454A 601 L 7G V 3* and *Altos*) to grind soft and hard materials (mild steel and M2 tool steel). Various combinations have been employed for the experiment and it was found that vibration decreased the wear of the wheel in all occasions except in the case of the porous wheel with a mild steel workpiece where vibration did not extend the life of the tool. The wear of the wheel in this case had an increase of 20%. However, the removed material in all cases was higher when vibration was applied. The calculation of G-ratio finally proved that vibration positively affected the process as an increase of 29-35% was observed. Nevertheless, in the case of the porous wheel cutting mild steel material the G-ratio dropped by 13.6% compared to conventional grinding.

The last set of experiments was carried out using a *closed-loop control system* for vibration-assisted grinding operation. This system is used to keep a desired vibration parameter constant regardless of any external factors that could possibly affect the process. During these tests the amplitude of vibration was kept constant at a specific value of 15 μm . The major difference between this test and the previous ones is the lack of knowledge about the actual vibration parameters during grinding process.

In all vibration-assisted machining processes the vibration parameters were set before the conduction of the experiment and it was assumed they remained constant. However, during the actual cutting or grinding the vibration parameters are affected by the cutting forces and feed rates. The closed-loop control system proved its ability to maintain the amplitude constant even when the system was driven at its natural frequency as occurred in the present study.

The results of this technique were compared to those of conventional grinding and vibration-assisted grinding with open-loop control. In closed-loop control, for higher depths of cut a reduction of 22% for normal forces compared to conventional grinding and 19% compared to open-loop vibration control was achieved. The closed-loop system did not perform very well for small depths of cut. Similar results were observed for tangential forces. Regarding the surface quality, the surface roughness of the ground workpieces decreased as the depth of cut increased in closed-loop control. However, in some cases the closed-loop control system seemed to pause and behaved like an open-loop control system due to the high values of workspeed that did not give the appropriate time for the system to respond to the sudden changes in the process.

Summarising, the benefits from vibration-assisted grinding is seen throughout the whole process. After an extensive study of the subject it can be said that vibration enhances the performance of the process depending on the machining configurations in terms of parameters and wheel workpiece material.

13.2 Conclusions

An initial approach to investigate the effect of low-frequency superimposed vibration of the workpiece during shallow surface grinding process has been carried out. After the development of a novel, simple and adaptable vibrating mechanism that could vibrate the workpiece in the direction coinciding with the workspeed a number of simulations and experimental tests the static and dynamic characteristics of the system were identified.

A study of the machine tool dynamics has been carried out and a detailed experimental investigation of the actual grinding machine in terms of its static and dynamic

characteristics has been completed. The analysis showed the stiffness of the spindle unit under static and dynamic loading conditions.

Furthermore, it was detected at which wheel speeds the spindle unit vibrates the most. It also revealed the range of vibration frequency values where the vibrating rig could be employed in order to avoid any resonance phenomena. The natural frequency of the spindle unit played an important role on the selection of the vibrating rig's stiffness and therefore its resonant frequency.

During the grinding tests the vibration was applied to the rig through a piezoelectric actuator. The vibration frequency was selected to match the resonant or near resonant frequency of the rig. In this way high values of amplitude were achieved with low voltage input and thus low power consumption.

Further to this, an innovative closed-loop control system was introduced to the process in order to maintain selected vibration parameters constant during grinding, regardless of the external applied forces from the cutting. Using this control system the displacement amplitude and frequency of vibration were constant in the actual grinding cycle. Resonant or near resonant frequency and the amplitude of displacement were the control targets in this study. At lower workspeeds the closed-loop control system performed better as it had more time to control the desired parameters.

The results from the main body of experimental work in vibration-assisted grinding proved that:

- ✓ The superimposed vibration reduced dramatically the grinding forces and grinding power, and improved the surface finish of the workpiece.
- ✓ High depths of cut, high workspeed and high wheelspeed along with the application of vibration drastically boost the performance of the process.
- ✓ The superimposed vibration reduced the wheel wear and increased the material removal rate.
- ✓ Applied vibration improved the surface quality of the workpiece contrary to conventional grinding.

- ✓ High porosity wheels with very soft material lead to poor G-ratio in vibratory mode.

This work has shown the appropriate and working combination of system configuration in terms of wheel, workpiece material and machining parameters. It is essential to clarify the fact that superimposed vibration decreased the grinding power consumption but not the overall power. The energy consumption of the power amplifier of the piezoelectric actuator has to be taken into account. However, because the system was driven at its resonant frequency the power consumption of the amplifier was at its lowest levels.

Chapter 14: Recommendations for Further Work

Though the presented work has covered the key parameters of vibration assisted grinding, still there are many aspects to investigate into in detail. A number of suggestions for future work are presented next.

- Different types of grinding wheels especially CBN wheels, should be used to study the performance of CBN wheels in the presence of vibration.
- Widen the range of processed workpiece materials. Difficult to grind materials such as nickel and titanium alloys should be investigated under vibration-assisted grinding.
- Introduce coolants and lubricants to the process. Minimum quantity lubrication (MQL) needs to be investigated as an alternative environment friendly process. This would provide a further understanding of the process and establish new relationships between the six methods; a) dry grinding, b) wet grinding, c) dry grinding and VAG, d) wet grinding and VAG, e) grinding with MQL, and f) MQL and VAG.
- Develop new oscillating rigs to vibrate the workpiece 2D or 3D. The second direction of vibration would be axial to the spindle unit and perpendicular to the tangential force. This method could allow the wheel grains to cut with more edges and therefore higher material removal rates could be achieved. The third direction should be perpendicular to the machining surface. Here, consideration should be given to the development of a device that could generate elliptical motion or if possible spherical oscillation. A synchronisation system should be in place to achieve an optimum output of the machining process.
- In terms of vibrating rig design, considerations should be given to the accommodation of large parts and easy adaptation to existing machine tools.
- Introduce vibration-assisted method to different types of grinding such as cylindrical creep-feed grinding and the HEDG process.

REFERENCES

- Albizuria, J., Fernandesb, M.H., Garitaonandiab, I., Sabalzac, X., Uribe-Etxeberriac, R., Hernandez, J.M. (2006) 'An active system of reduction of vibrations in a centerless grinding machine using piezoelectric actuators' *International Journal of Machine Tools & Manufacture*
- Alfares, M. & Elsharkawy, A. (2000) 'Effect of Grinding Forces on the Vibration of Grinding Machine Spindle System'. *International Journal of Machine Tools & Manufacture* 40, pp.2003–2030.
- Astathev, V. K., Babitsky, V. I., Kolovsky, M.Z. (2000), *Dynamics and Control of Machines*. Springer-Verlag, Berlin
- Ault, W. (1989), *Types of Grinding Wheels*. In: King, R.I. & Hahn, R.S. ed. Handbook of Modern Grinding Technology Chapman and Hall, New York pp.72-87.
- Babitsky, V.I. (1995) 'Autoresonant Mechatronic Systems' *Mechatronics* vol.5, No.5, pp.483-496
- Babitsky, V.I., Kalashnikov, A.N., Meadows, A., Wijesundara, A.A.H.P. (2003) 'Ultrasonically assisted turning of aviation materials' *Journal of Materials Processing Technology* v132 pp157–167
- Babitsky, V.I. (1998) '*Theory of Vibro-Impact Systems and Applications*' (Russian revised translation, Nauka, Moscow, 1978).
- Babitsky, V. I., Veprik, A. M. (1998), 'Universal Bumpered Vibration Isolator for Severe Environment' *Journal of Sound and Vibration*, 218(2) 269-292.
- Baines-Jones, V.A. (2010) '*Nozzle Design for Improved Useful Fluid Flow In Grinding*' LJMU Doctoral Dissertation, Record No. 000877481.
- Barczak, L.M., Batako, L.M., Morgan, M.N. (2010) 'A study of plane surface grinding under Minimum Quantity Lubrication (MQL) conditions' *International Journal of Machine Tools & Manufacture*.
- Batako, A.D. (2003) 'A self-exciting system for percussive rotary drilling' PhD Thesis, Loughborough University.

-
- Batako, A.D., Babitsky, V.I. & Halliwell, N.A. (2004) 'Modelling of Vibro-Impact Penetration of Self-Exciting Percussive-Rotary Drill Bit' *Journal of Sound and Vibration* 271, pp.209-225
 - Batako, A. D. L. & Koppal, S. (2007) 'Process monitoring in high efficiency deep grinding- HEDG' *Journal of Physics: Conference Series* 76 012061.
 - Batako, A. D., Rowe, W. B., Morgan, M. N. (2005) 'Temperature measurement in high efficiency deep grinding' *International Journal of Machine Tools & Manufacture*, 45 pp1231–1245
 - Bhattacharyya, S. K. & Moffatt, V.L. (1976) 'Characteristics of Micro Wheel Wear in Grinding' *Int. J. Mach. Tool Des. Res.* Vol. 16, pp. 325-334
 - Bowden, F.P. & Tabor, D. (1986) '*The Friction and Lubrication of Solids*' Clarendon Press, Oxford
 - Brandon, J.A., Al-Shareef, K.J.H. (1992) Optimization Strategies for Machine Tool Spindle-Bearing Systems: a Critical Review, *J. Eng. Ind.* 114 pp.244-253.
 - Brehl, D.E. & Dow, T.A. (2007) 'Review of vibration-assisted machining' *Precision Engineering Center*, North Carolina State University, United States.
 - Brinksmeier, E., Heinzl, C., Wittmann, M. (1999) 'Friction, Cooling and Lubrication in Grinding' *CIRP Annals-Manufacturing Technology*, vol.82 Issue 2 pp.581-598.
 - Chen, X. & Rowe, B.W. (1996) 'Analysis and Simulation of the Grinding Process. Part II: Mechanics of Grinding' *International Journal of Machine Tools and Manufacture*, v36, issue8, pp.883-896.
 - Chen, X., & Rowe, W.B. (1996) 'Analysis and Simulation of the Grinding Process' *International Journal of Machine Tools & Manufacturing*. 36 (8) 871-906
 - Chen, X., Rowe, W.B., Mills, B., Allanson, D.R. (1998) 'Analysis and Simulation of the Grinding Process, part IV: Effect of Wheel Wear', *International Journal of Machine Tools Manufacture* 38 (1–2) pp.41–49.
 - Cheng, C.H., Tony, L. Schmitz, G. Scott, D. (2007) 'Rotating Tool Point Frequency Response Prediction Using RCSA' *Machining Science and Technology*
 - Chern, G. L. & Chang Y-C, (2006) 'Using two-dimensional vibration cutting for micro-milling' *International Journal of Machine Tools & Manufacture* v46, pp. 659–666
-

-
- Chiu, N. & Malkin S. (1993) 'Computer simulation for cylindrical plunge grinding' University of Massachusetts-USA
 - Dagnall, H., (1997), '*Exploring Surface Texture*' Taylor and Hobson Publication, List No. 600-14/98.
 - Dapino, M.J., Flatau, A.B., Calkins, F.T. (2006) 'Statistical Analysis of Terfenol-D Material properties' *Journal of Intelligent Material Systems and Structures* v.17, 587
 - Dorf, R.C. & Bishop, R.H. '*Modern Control Systems*' (1998) Addison Wesley, USA
 - Ebbrell, S. (2003) '*Process Requirements For Precision Grinding*' (Doctoral Dissertation) Retrieved From John Moores University Library Database, Record Number: 000717781
 - Eiji, U. (1982) 'Theory of Cutting and Grinding', *Mechanical Engineering Publications*, Beijing.
 - Filiz, S., Cheng, C.H., Powell, K.B., Schmitz, T.L., Ozdoganlar, O. B. (2009) 'An Improved Tool-Holder Model for RCSA Tool-Point Frequency Response Prediction' *Precision Engineering* 33 pp. 26-36
 - Gao, Y., Tse, S. (2005) 'Evaluation of Dynamic Parameters for Underdamped Grinding Machines' *Key engineering materials* Vols.295-296 pp.631-636
 - Garcia-Gardea, E., Kapoor, S.G., Wu, S.M. (1980) 'Analysis of Grinding Dynamics by Dynamic Data System Methodology' *International Journal of Machine Tool Design and Research*, v.21 No.2 pp.99-108
 - Gawlak, G. (1984) 'Some Problems Connected with Balancing of Grinding Wheels' *Journal of Eng. Ind.* 106, pp 233-236.
 - Ge, P. Q., Li, J. F., Lu, C.H., Liu, Z. C. (2003), 'Performance Evaluation and Action Mechanism Analysis of Extreme Pressure Additives Used for Oil Based Cutting Fluids' *Key Engineering Materials* vol.250, pp. 281- 286.
 - Hanasaki, S., Fujivara, J., Wada, T., Hasegawa, Y. (1994) 'Vibratory creep feed grinding' *Trans. Japan Soc. Mech. Eng.*, 60 (573), 1829-1834.
 - Harris, C. M., (1988), '*Shock and Vibration Handbook*', McGraw-Hill, Inc, New York.
 - Howes, T. (1990) 'Assessment of the Cooling and Lubrication Properties of Grinding Fluids' *Ann. CIRP* 39, 1, pp.313-316.
-

-
- Huang, G. L. & Sun, C.T. (2006) 'The dynamic behaviour of a piezoelectric actuator bonded to an anisotropic elastic medium' *International Journal of Solids and Structures* v.43 pp.1291-1307
 - Inman, D. J. (1996) '*Engineering Vibration*' Prentice – Hall Inc., United States of America.
 - Jackson, A. (2008) '*An Investigation of Useful Fluid Flow in Grinding*' LJMU Doctoral Dissertation, Record No. 000820129
 - Jahanmir, S., Hwang, T., Whiteman, E.P., Job, L.S. & Evans, C.J. (1995) '*Measurement and Analysis of Forces in Grinding of Silicon Nitride*'. PD-Vol. 72, Tribology Symposium ASME
 - Jenkins, E. H., Kurfess, R. T. (1996) 'Dynamic Stiffness Implications for a Multi-Axis Grinding System' *Journal of Vibrations and Control*, v.3 pp.297-313
 - Jiang, Y.X., Tang, W.X., Zhang, G.L., Song, Q.H., Li, B.B., Du, B. (2007) 'An Experiment Investigation for Dynamics Characteristics of Grinding Machine' *Key engineering materials* Vol. 329 pp.767-772
 - Kalpakjian, S. & Schmid, S.R. (2010) '*Manufacturing Engineering and Technology*' Pearson Education Inc, USA.
 - Kang, Y., Chang, Y.P. Tsai, J.W., Chen, S.C., Yang, L.K. (2001) 'Integrated 'CAE Strategies for the Design of Machine Tool Spindle-Bearing Systems. *Finite Elements in Analysis and Design* 37 pp.485-511
 - Kermani, M.R., Patel, R., Moallem, M. (2005) 'Flexure Control Using Piezostack Actuators: Design and Implementation' *IEEE/ASME Transactions on Mechatronics* v.10, No 2.
 - King, R.I. & Hahn, R.S. (1986) '*Modern Grinding Technology*' Chapman and Hall, New York, USA.
 - Kirpitchenko, I., Zhang, N., Tchernykh, S., Liu, D.K. (2002) '*Dynamics and Control of Grinding Machines*' 6th International Conference on Motion and Vibration Control' Part 2, pp 1039-44
 - Kondo, K. (1997) 'Dynamic Behaviour of Terfenol-D' *Journal of Alloys and Compounds*, v.258 pp. 56-60
 - Lang, G. F. & Snyder, D. (2001) 'Understanding the Physics of Electrodynamic Shaker Performance' *Sound and Vibration*, Data Physics Corporation, San Jose, California
-

- Lee, H. S. & Furukawa, Y. (1988) 'On the Method to Determine the Stiffness of Grinding Machines' *Bull. Japan Soc. Of Prec. Engineering* Vol.22 No.2
- Liang, Z., Wu, Y., Wanga, X., Zhao, W. (2010) 'A new two-dimensional ultrasonic assisted grinding (2D-UAG) method and its fundamental performance in monocrystal silicon machining' *International Journal of Machine Tools & Manufacture*, v50 issue 8 pp728–736.
- Lo, C.C., (1969) 'Elastic contact of rough cylinders', *Int. J. Mech. Sci.*, 11 pp.105-115.
- Malkin, S. & Cook, N.H. (1971) 'The Wear of Grinding Wheels, part 1: Attritious Wear', *Transactions of ASME Journal of Engineering for Industry* 93, pp1120–1128.
- Malkin, S. & Guo, C. (2008) '*Grinding Technology-Theory and Applications of Machining with Abrasives*' Second Edition, Industrial Press Inc, New York.
- Malkin, S. (1989) '*Grinding Technology-Theory and Applications of Machining with Abrasives*' Ellis Horwood, Chichester
- Mannan, M.A., Fan, W.T., Stone, B. J., (1999) 'The Effects of Torsional Vibration on Chatter in Grinding' *Journal of Materials Processing Technology* 89–90 pp.303–309
- Marinescu, I. D., Hitchiner, M., Uhlmann, E., Rowe, B. W., Inasaki, I. (2007) '*Handbook of Machining with Grinding Wheels*' CRC Press, Taylor and Francis Group LLC, New York USA.
- Marinescu, I. D., Rowe B., Dimitrov, B., Inasaki, I. (2004) '*Tribology of Abrasive Machining Processes*' ISBN: 0-8155-1490-5 William Andrew, Inc. USA
- Markings for Identifying Grinding Wheels and Other Bonded Abrasives, American National Standard ANSI B74.13-1982.
- Masri, S. F. (1972), 'Forced Vibration of a Class of Non-Linear Two-Degree-of-Freedom Oscillators', *Int. J. Non-Linear Mechanics*. Vol. 7, 663-674
- Masuda, M. (1986) 'Ultraprecision Cutting of Steel with CBN Tools' *J. JSPE*, vol. 54, No.2, p384-389
- Mitrofanov, A.V., Babitsky, V.I., Silberschmidt, V.V. (2003) 'Finite element simulations of ultrasonically assisted turning' *Computational Materials Science* v28 pp 645–653

-
- Moriwaki, T. & Shamoto, E., (1991) 'Ultraprecision Diamond Turning of Stainless Steel by Applying Ultrasonic Vibration' Kobe University Japan vol.40 No.1
 - Movahhedy, M.R., Mosaddegh, P. (2006) 'Prediction of Chatter in High Speed Milling Including Gyroscopic Effects' *International Journal of Machine Tools & Manufacture*, 46(9): 996–1001.
 - Natsume, M., Shinmura, T., Sakaguchi K. (1998) 'Study of Magnetic Abrasive Machining by Use of Work Vibration System (Characteristics of plane finishing and application to the inside finishing of groove)', *Trans. Jpn. Soc. Mech. Eng.* 64 (627C) 4447-4452.
 - Oczos, K., Porzycki, J. Szlifowanie. (1986) Podstawy i technika, WNT, Warszawa,
 - Orynski, F. & Behcinski, G. (2003) 'Experimental research on the vibration surface grinding' *XXVI Naukowa Szcola Obrobki Sciernej*.
 - Orynski, F., Pawlowski, W. (2002) 'The mathematical description of dynamics of the cylindrical grinder' *International Journal of Machine Tools & Manufacture* 42 pp.773–780
 - Ostrovsky, V.I. (1981) 'The Theory of the Grinding Process' Leningrad State University, Leningrad,
 - Poletav, V.A. & Khrul'kov, V.A. (1990) 'Intermittent grinding with oscillation of the work' *Soviet Engineering Research*, v 10, n 1, p 134-136.
 - Pomirleanu, R. & Giurgiutiu, V. (2002) 'Full-Stroke Static and Dynamic Analysis of High-Power Piezoelectric Actuators' *Journal of Intelligent Material Systems and Structures* 13, 275
 - Qi, H.S. (1995) 'A contact length model for grinding wheel-workpiece contact' PhD Thesis. Liverpool John Moores University. UK.
 - Qi, H.S., Mills, B. & Rowe, W.B. (1994), 'An analysis of real contact length in abrasive machining processes using contact mechanics' *Wear* 176, pp 137-141.
 - Qi, H.S., Rowe, W.B., Mills, B. (1997) 'Experimental investigation of contact behaviour in grinding' *Tribology International*, vol. 30 No 4 pp 283-294
 - Qu, W., Wang, K., Miller, M.H., Huang, Y., Chandra, A. (2000) 'Using Vibration-Assisted Grinding to Reduce Subsurface Damage'. *Journal of the International Societies for Precision Engineering and Nanotechnology* v24 pp: 329-337.
 - Rowe, B.W. (2007) 'Principles of Modern Grinding Technology' William Andrew, Oxford United Kingdom
-

- Rowe, W.B., Qi, H.S., Morgan, M.N. & Zheng, H.W. (1993) *The Real Contact Length in Grinding Based on Depth of Cut and Contact Deflections*. Proc. Thirtieth International MATADOR Conference. UMIST, Macmillan. pp.187-193
- Schmitz, T., Ziegert, J., Stanislaus, C. (2004) A Method for Predicting Chatter Stability for Systems with Speed-Dependent Spindle Dynamics. SME technical paper TP04PUB182, *Transactions of NAMRI=SME*, 32: 17–24.
- Seto, W. W. (1964) *'Theory and Problems of Mechanical Vibrations'* Schaum Publishing Co. NY USA
- Shaw, C. M., (1996) *'Principles of Abrasive Processing'* Oxford University Press Inc., New York, USA
- Shinmura, T., & Takeshi, Y. (1997) 'Study of free form Surface Finishing by the Application of Magnetic Abrasive Machining. *Proceedings of JSME Annual Meeting (IV) Japanese* 220-221
- Smith, J.W. (1988) *'Vibration of Structures-Application in Civil Engineering Design'* ISBN: 0-412-28020-58 Chapman and Hall Ltd, London
- Spur G, & Holl S.E. (1997) 'Material Removal Mechanisms During Ultrasonic Assisted Grinding' *Production Engineering*. IV/2 pp.9-14
- Spur, G. & Holl, S.E. (1996) 'Ultrasonic Assisted Grinding of Ceramics' *Journal of Materials Processing Technology*. vol. 62 pp. 287-293.
- Srivastava, A. K., Sriram, K., Lal, G. K. (1985) 'A New Technique for Evaluating Wheel Loading' *Int. J. Mach. Tool Des. Res.* Vol. 25, No. 1, pp. 33-38,
- Syoji, K. (1999), 'Evolution in Grinding: Aiming for the maximum limits in efficiency and precision-from micron to nano, and from high speed to ultra high speed.' *Journal of the Japan Society for Precision Engineering*, 65:31.
- Taskesen, A. & Ercan, Y., (2003) *'Theoretical analysis and prediction of machine tool stability and chatter vibration during orthogonal metal cutting with a one degree of freedom model'*, 11th Machine Theory Symposium, Gazi University, Turkey
- Taskesen, A., & Ercan, Y. (2005) 'Computer aided nonlinear analysis of machine tool vibrations and a developed computer software' *Mathematical and Computational Applications*, Vol. 10, No. 3, pp. 377-385
- Taskesen, A., & Ercan, Y., (2003) *'Theoretical analysis and prediction of machine tool stability and chatter vibration during orthogonal metal cutting with a two*

- degrees of freedom model*', 11th Machine Theory Symposium, Gazi University, Turkey
- Tawakoli, T. & Azarhoushang, B. (2008) 'Influence of ultrasonic vibrations on dry grinding of soft steel' *International Journal of Machine Tools & Manufacture*, v48 pp1585– 1591 Institute of Grinding and Precision Technology (KSF), Furtwangen University, 78054VS-Schwenningen, Germany
 - Tawakoli, T. (1993) 'High Efficiency Deep Grinding' VDI-Verlag GmbH, *Mechanical Engineering Publications*, London
 - Tawakoli, T., Hadad, M.J., Sadeghi, M.H. (2010) 'Influence of oil mist parameters on minimum quantity lubrication – MQL grinding process' *International Journal of Machine Tools & Manufacture* v.50 pp521–531.
 - Tian, J., Hutton, S. (2001) 'Chatter Instability in Milling Systems with Flexible Rotating Spindles - a New Theoretical Approach' *Journal of Manufacturing Science and Engineering*, 123: 1–9.
 - Uhlmann, E. (1998) 'Surface Formation in Creep Feed Grinding of Advanced Ceramics with and without Ultrasonic Assistance' *Institute for Machine Tools and Factory Management*. Berlin Germany.
 - Venables, M. (2006) 'It's a grind [Grinding Technology]' *Manufacturing Engineering*, Volume 85, Issue 4, p.42–45
 - Wang, Y., Mason, M. T., (1992), 'Two-Dimensional Rigid-Body Collisions with Friction', *Journal of Applied Mechanics* Vol. 59, pp. 635-642.
 - Wang, Y., Moon, K.S., Miller, K.H., (1996) 'Micro-Actuation in Precision Grinding' *Proceedings of the ASME Dynamic Systems and Control Division*, Vol. 58, pp: 349-356
 - Xiao, G., Malkin, S. & Danai, K. (1992) 'Intelligent Control for Cylindrical Plunge Grinding' Proc. of American control conference. Chicago:391
 - Xiong, G.L., Yi, J.M., Zeng, C., Guo, H.K., Li, L.X. (2003) 'Study of the Gyroscopic Effect of the Spindle on the Stability Characteristics of the Milling system' *Journal of Materials Processing Technology*, 138: 379–384.
 - Yin, S. & Shinmura, T. (2007) 'Vibration-Assisted Magnetic Abrasive Polishing' *Key Engineering Materials* Vol.329 pp 207-212.

- Younis, M., Sadek, M.M., El-Wardani, T. (1987) 'A New Approach to Development of a Grinding Force Model', *Transactions of ASME Journal of Engineering for Industry* 109 pp.306–313.
- Zaruba, Z. (2005) '*Development of Grinding Strategy Incorporating Novel Methods for Controlling Waveshift and Wheel Run-Out*' (Doctoral Dissertation) Faculty of computing, Engineering and mathematical Sciences, University of Bristol.
- Zhang, B., & Meng, J. (2003) 'Grinding damage in fine Ceramics' *Journal of nanotechnology and Precision Engineering*. (1): pp25-30.
- Zhang, B., Hu, Z., Luo, H., Deng, Z. (2006) 'Vibration-Assisted Grinding – Piezotable Design and Fabrication' *Nanotechnology and Precision Engineering* Vol.4 No.4
- Zhang, H., Zhang, J., Huo, M. (2006) 'Study on ultrasonic Vibration Assisted Grinding in Theory' *Material Science Forum*. Vol. 532-533, pp 773-776
- Zhang, M., Kirpitchenko, I., Liu, D.K. (2005) 'Dynamic Model of Grinding Process' *Journal of Sound and Vibration*, 280 pp.425–432
- Zhang, P. & Miller, H. M. (2003) '*Grinding wheel loading with and without vibration assistance*' Proc. of the ASPE Annual Meeting pp 455-458 Michigan Technological University, Houghton, MI
- Zhong, Z. W., Yang, H. B. (2004) 'Development of a vibration Device for Grinding with Microvibration.' *Materials and Manufacturing Processes* 19:6, pp: 1121-1132
- Zhong, Z.W. & Rui, Z.Y. (2005) 'Grinding of Single-Crystal Silicon Using a Microvibration Device' *Materials and Manufacturing Processes*, 20 pp 687-696.
- Zhou, Z.X. & van Lutterwelt, C.A. (1992) '*The real contact length between grinding wheel and workpiece-A new concept and a new measuring method*' Ann CIRP 41, pp 387-391.

WEB-BASED SOURCES

- Ashley, S. (1996) '*Magnetostrictive actuators*' The American Society of Mechanical Engineers [online] Available at: <http://www.memagazine.org/backissues/membersonly/june98/features/magnet/magnet.html> [Accessed 3rd September 2008]
- Chan, A. L.S. (n.d) '*Equation of Motion: Natural Frequency*' [online]. Available at: <http://personal.cityu.edu.hk/~bsapplec/natural.htm> [Accessed 14th April 2008]
- EfunDA (2008) 'Damped Vibration of Free SDOF Systems' [online]. Available at: http://www.efunda.com/formulae/vibrations/sdof_free_damped.cfm [Accessed 7th April 2008].
- EfunDA (2010) 'Flat Surface Grinding' [online]. Available at: http://www.efunda.com/processes/machining/grind_flat_surface.cfm [Accessed 4th March 2010].
- Envirowise (2007) 'Sustainable Practices Sustainable Profits' [online] Available at: <http://www.envirowise.gov.uk/home.aspx> [Accessed 4th November 2007]
- GLOBALSPEC – The engineering Search Engine (2010) 'Shock and Vibration Testing Shakers' [online] Available at: http://www.globalspec.com/LearnMore/sensors_transducers_detectors/acceleration_vibration_sensing/shakers_vibration_shock_testing [Accessed 26th April 2010]
- Physik Instrumente-PI (2010) 'Fundamentals of Piezoelectric Actuators' [online] Available at: <http://www.physikinstrumente.com/en/products/prdetail.php?sortnr=400600.40> [Accessed 4th December 2010].
- Physik Instrumente-PI, (2010) 'Basic Designs of Piezoelectric Positioning Drives/Systems' [online] Available at: <http://www.physikinstrumente.com/en/products/prdetail.php?sortnr=400800.00> [Accessed 4th December 2010].
- Radical Departures-Advanced Techniques in Aerospace Manufacturing (2003) 'Grinding Roughs out a New Niche' [online]. Available at: <http://www.radical->

departures.net/2003/tyrolit.asp

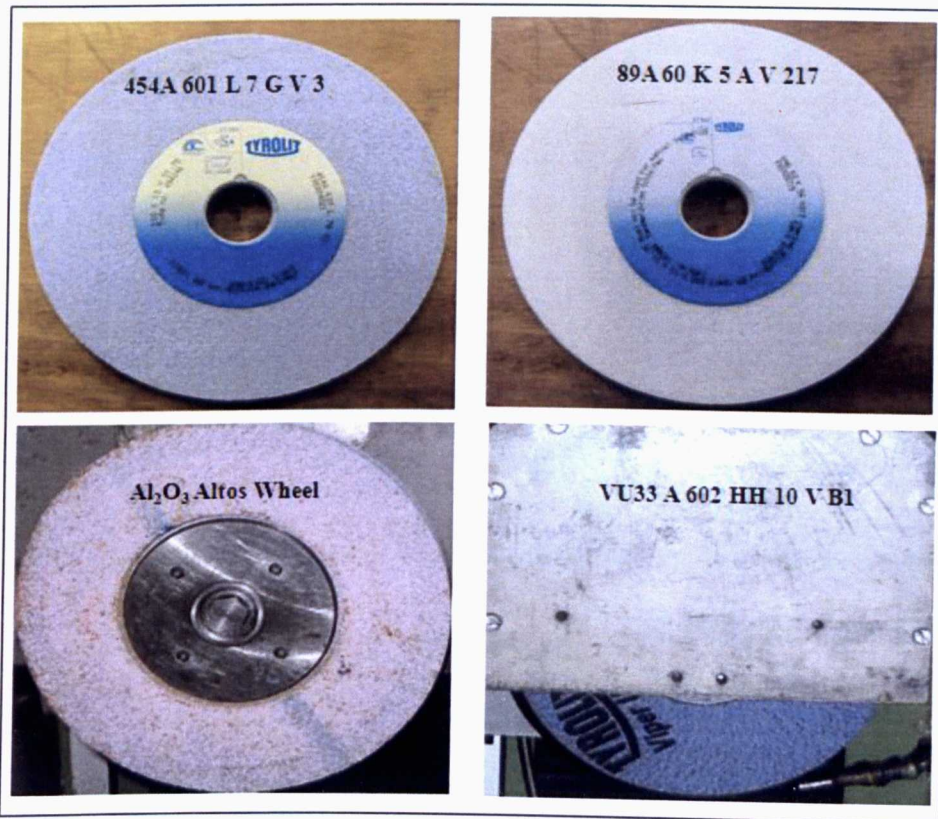
[Accessed 15th May 2010].

- Saint-Gobain Abrasives, (n.d.), '*Abrasive Cutting*' [online] Available at: <http://www.grindwellnorton.co.in/GrindingTech/pdfs/AbrasiveCutting.pdf> [Accessed 25th November 2007]
- THERMOTRON (2008) '*Fundamentals of Electrodynamic Vibration Testing Handbook*' [online] Available at: http://www.thermotron.com/resources/vibration_handbook.html [Accessed: 19th May 2009]
- Webster, J.A. (2008) '*In Grinding Coolant Application Matters*' [online] Available at: <http://www.sme.org/cgi-bin/find-articles.pl?&ME08ART19&ME&20080319&&SME&> [Accessed 25th October 2010]

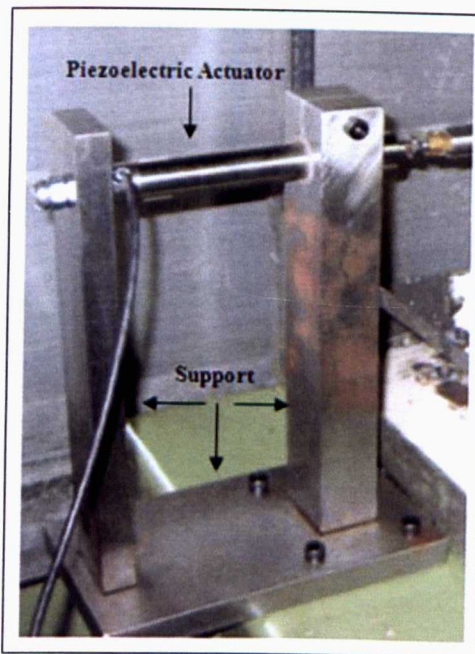
APPENDICES

APPENDIX - A

A-1 Grinding Wheels Used for the Experimental Work

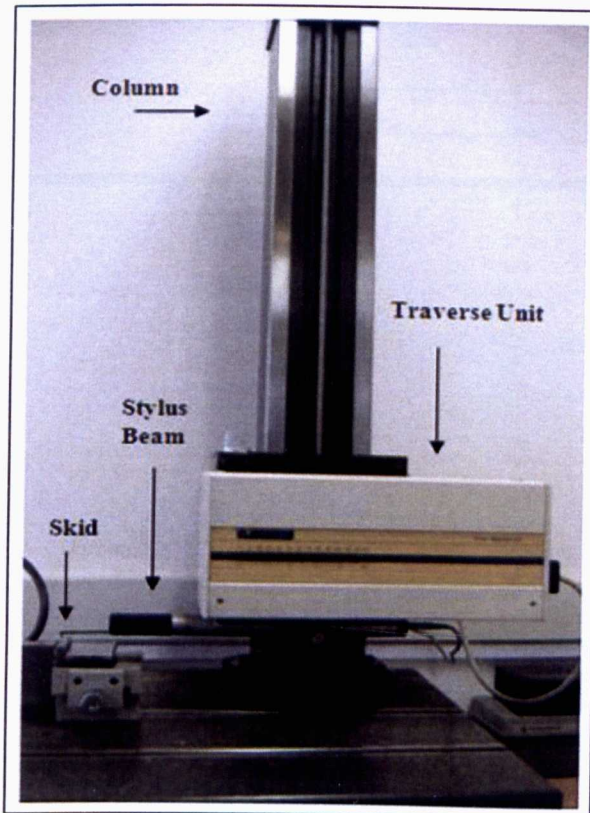
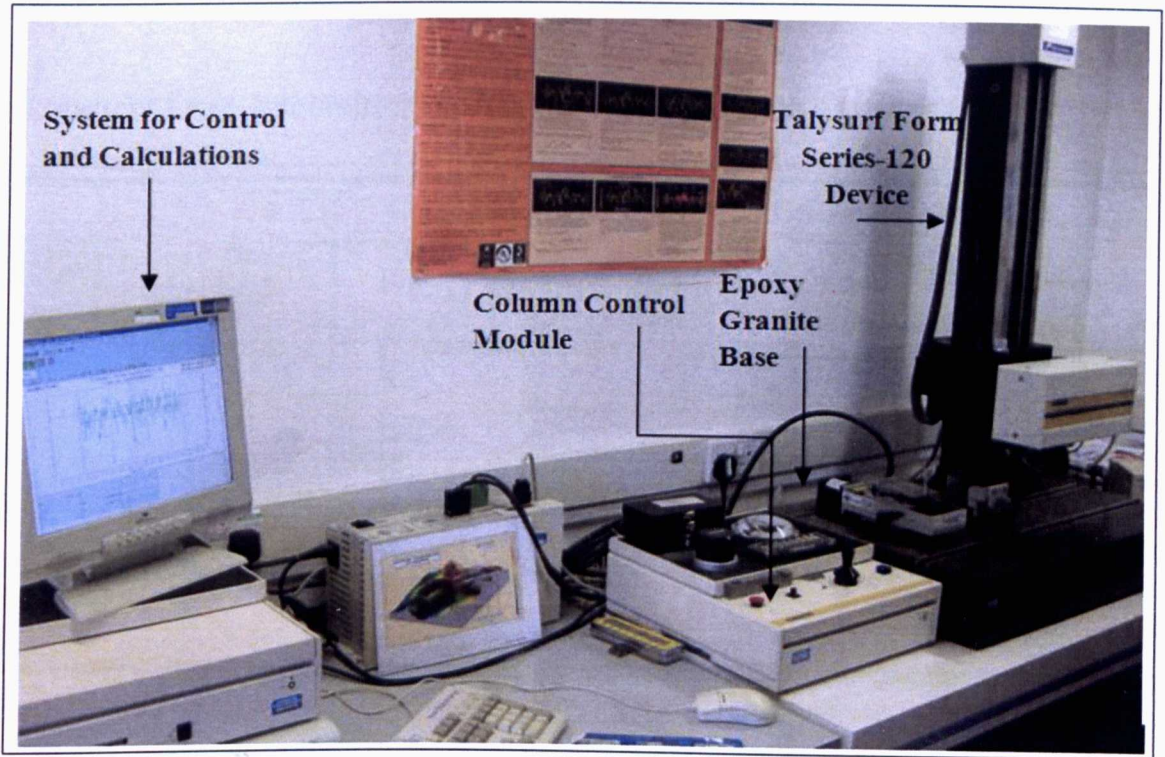


A-2 Piezoelectric Actuator and its Support

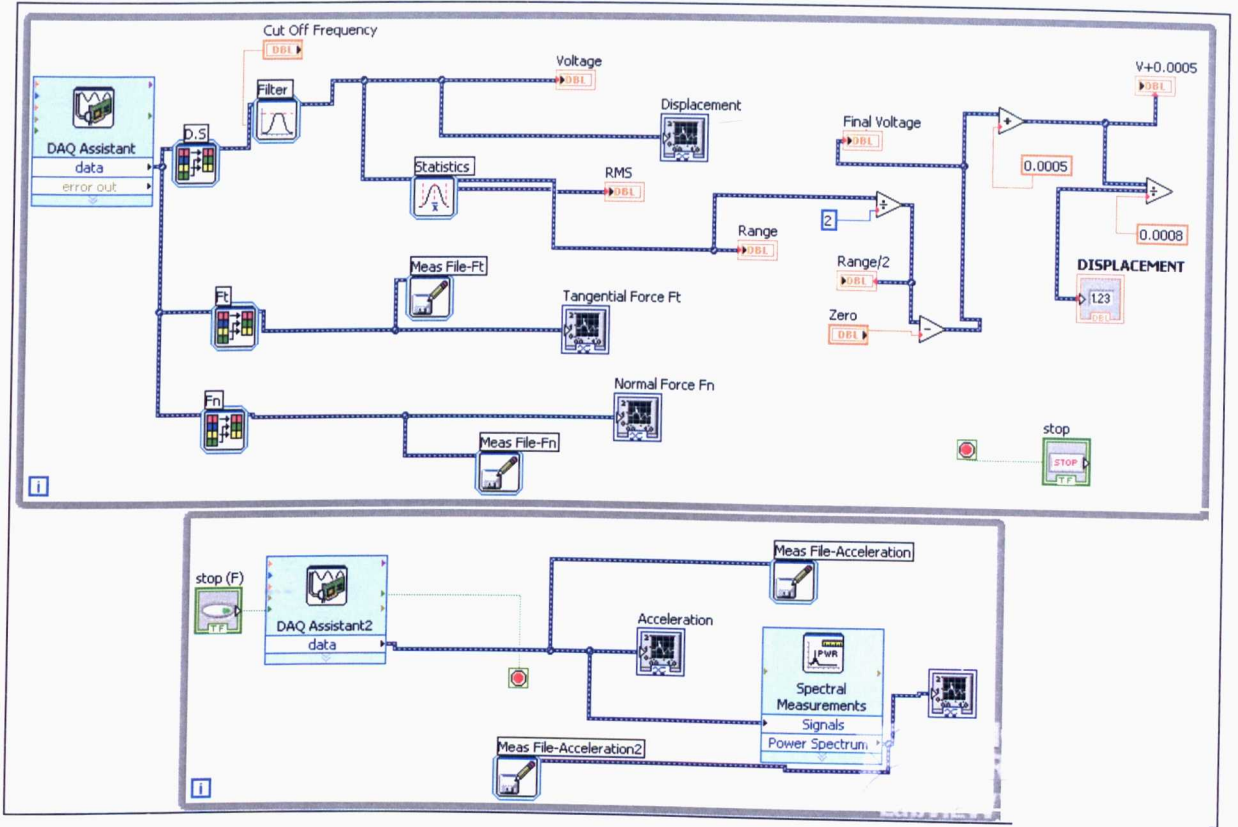


A-3 Talysurf Form - Surface Roughness Measurement Device



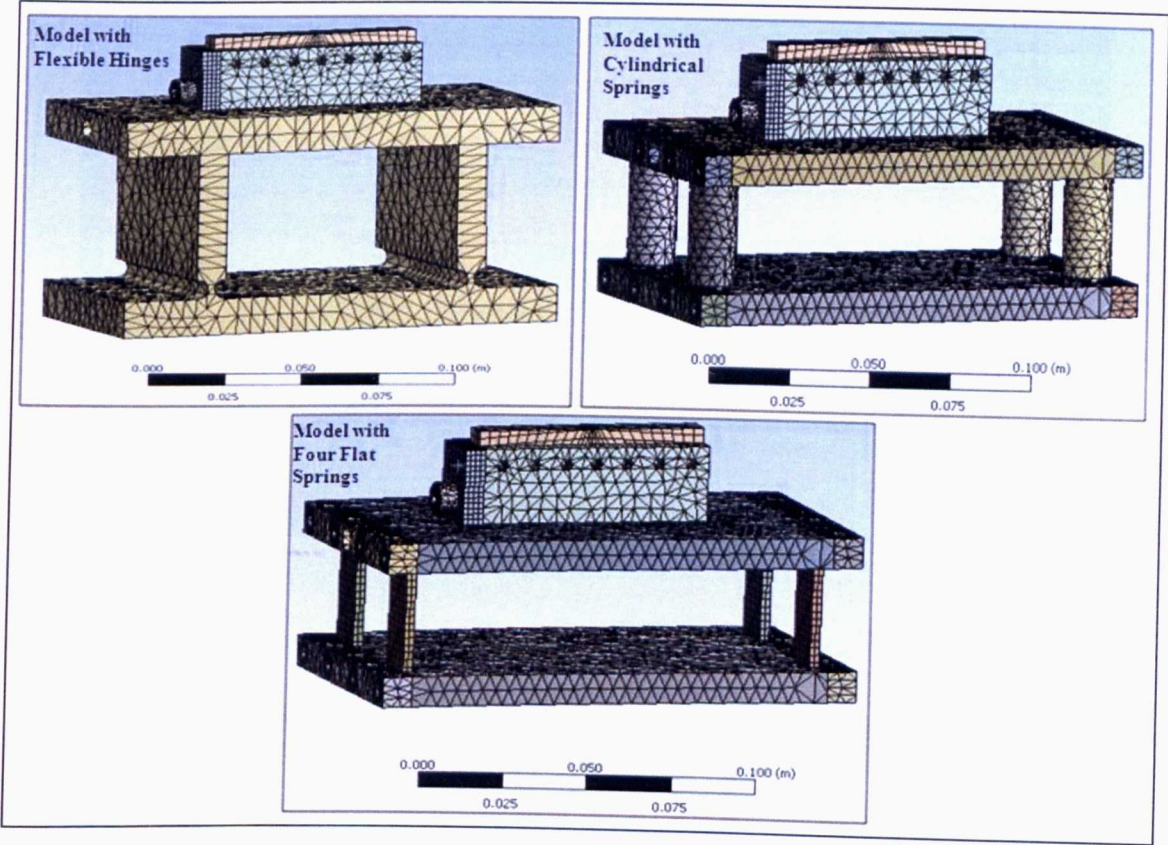


A-4 Labview Data Acquisition Software-Block Diagram

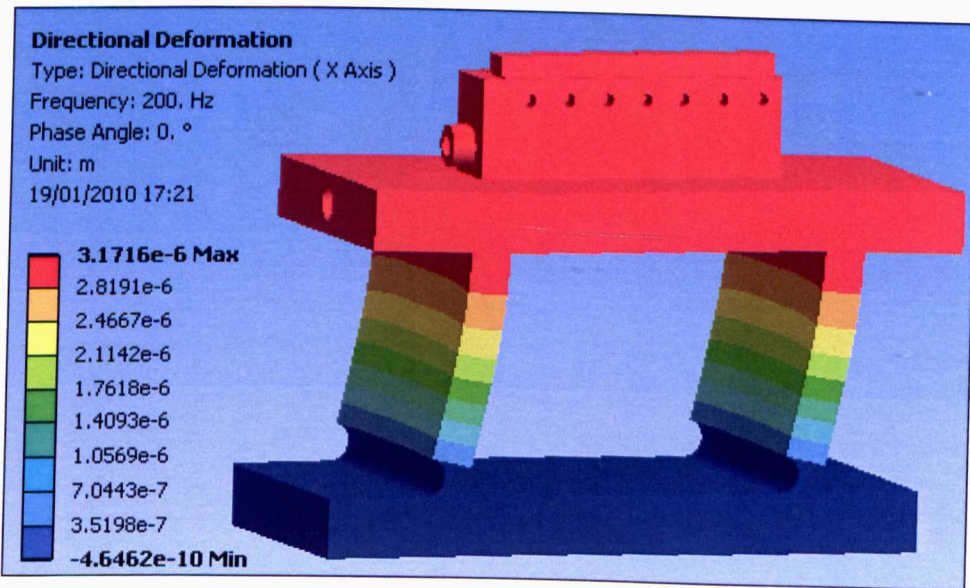


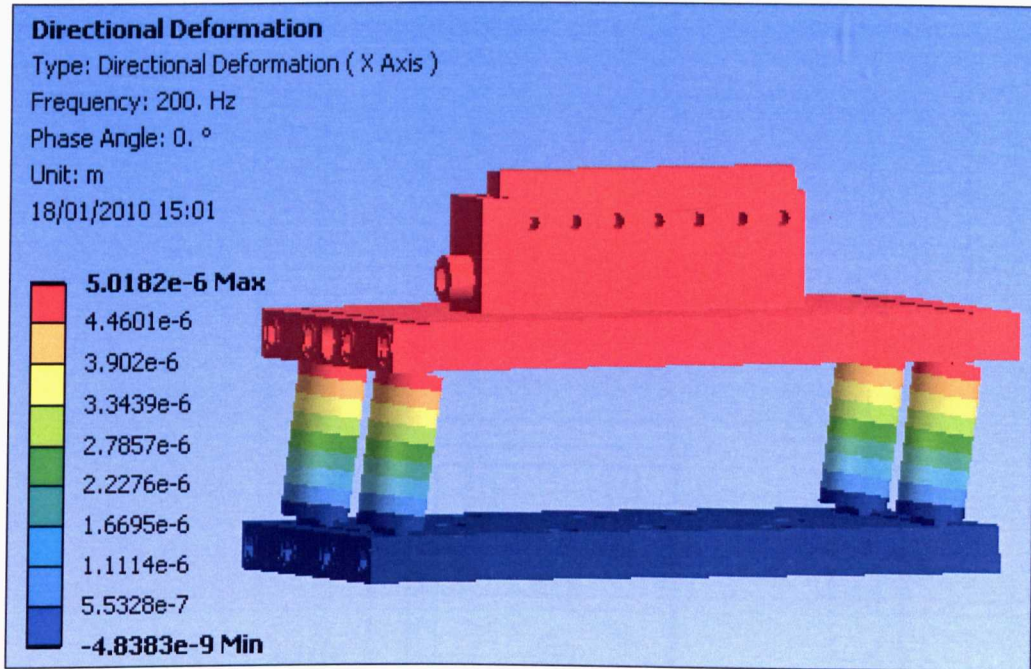
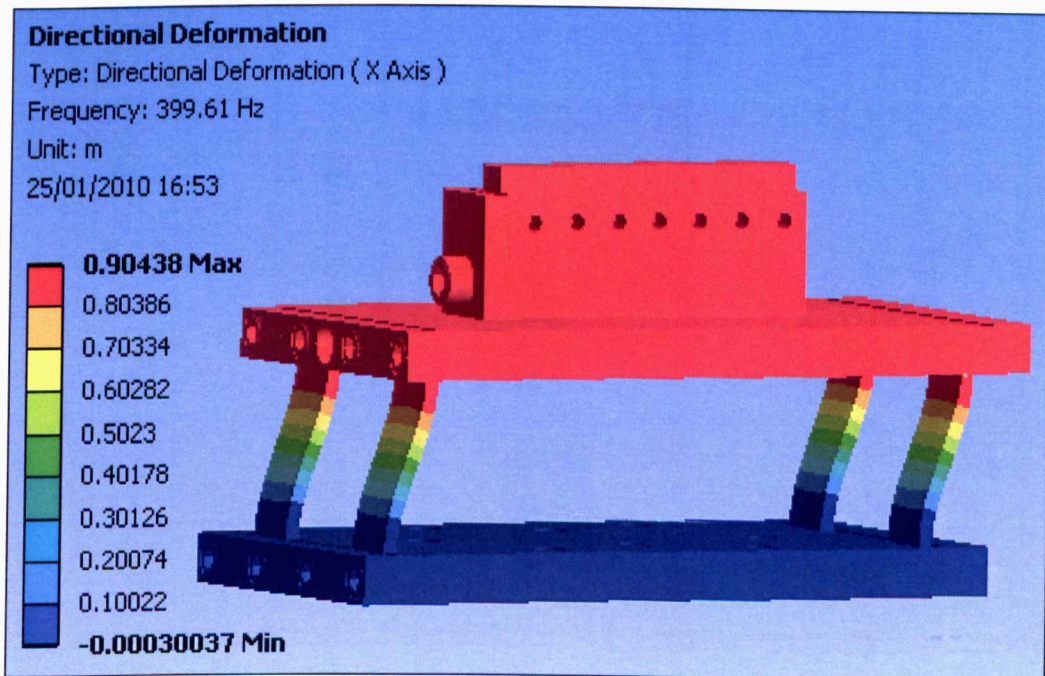
APPENDIX - B

B1- Dynamic Analysis Meshing Representation of all Models

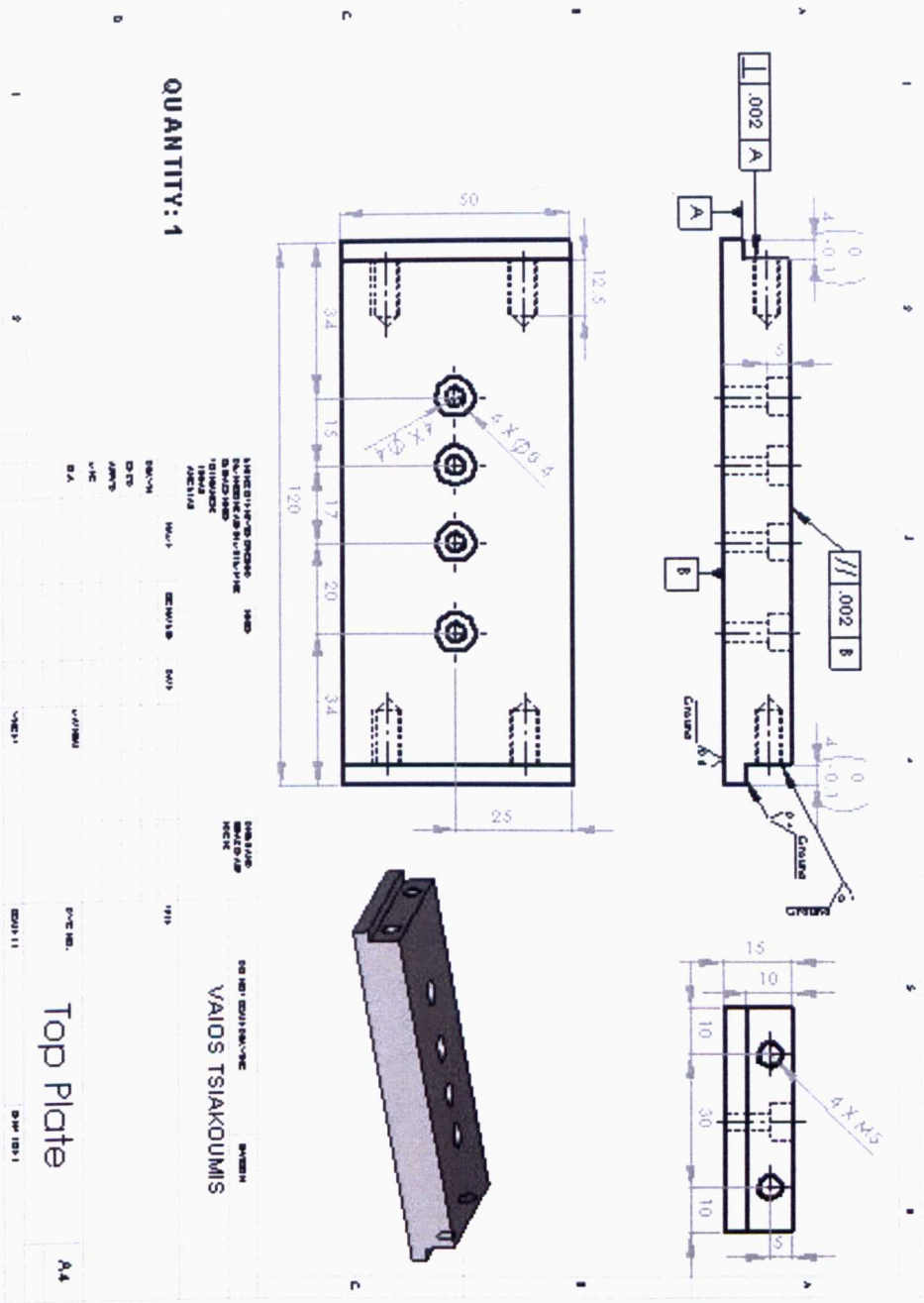


B2- Directional Deformation of the Model with Flexible Hinges

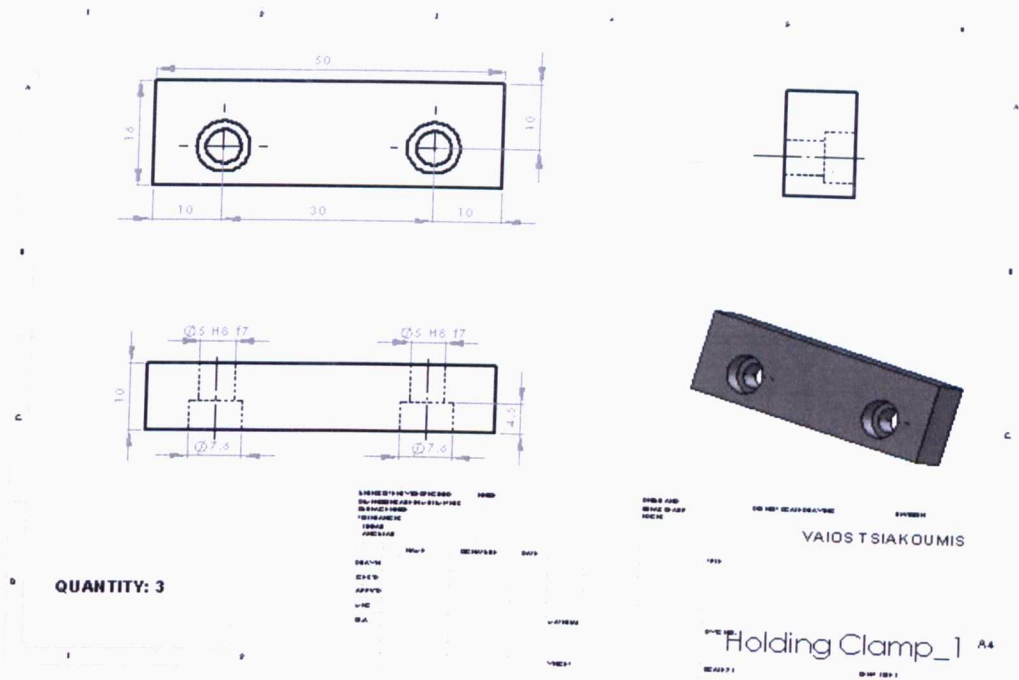


B3- Directional Deformation of the Model with Cylindrical Springs**B4-** Directional Deformation of the Model with Four Flat Springs

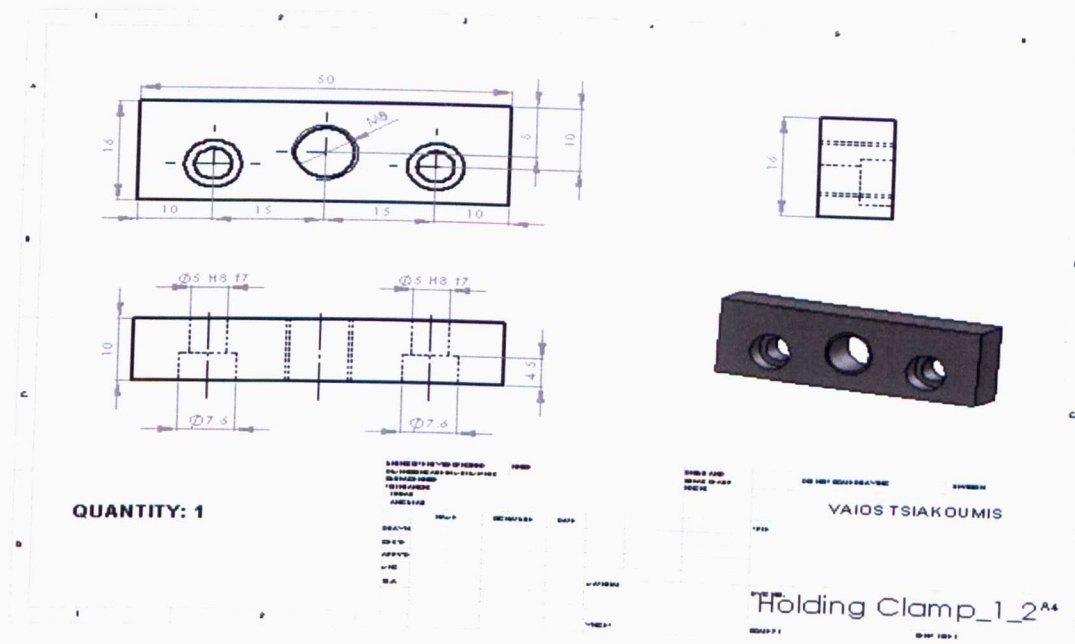
Bottom Plate



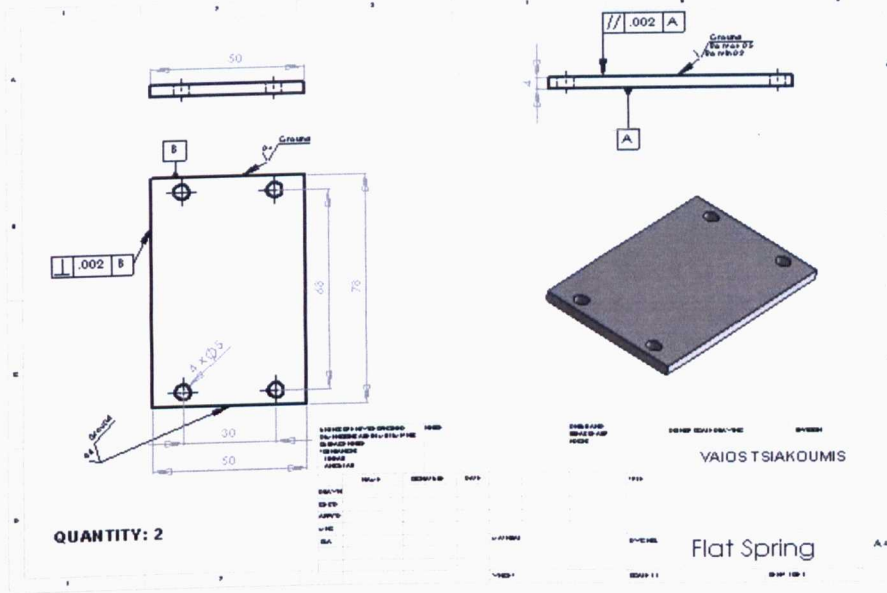
Holding Clamp-1



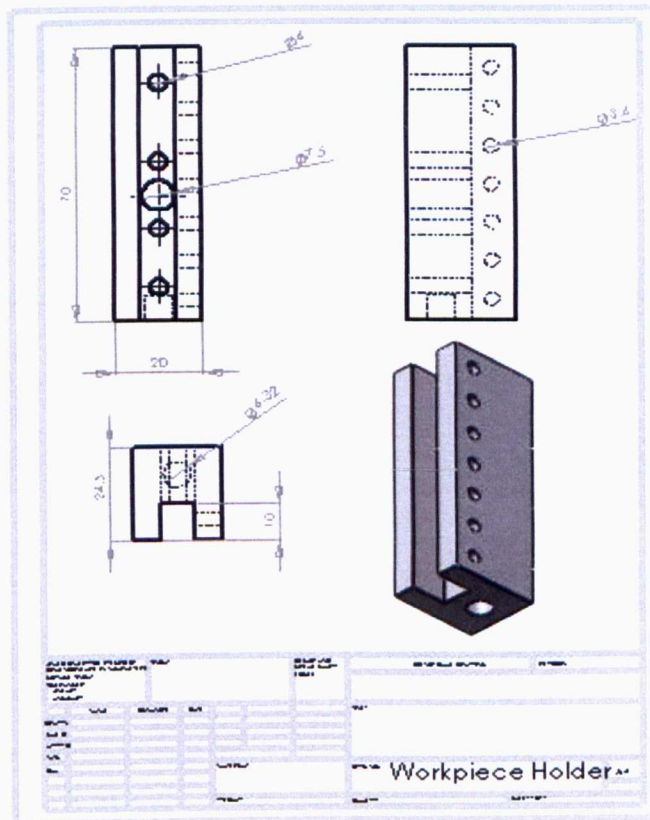
Holding Clamp-1-2



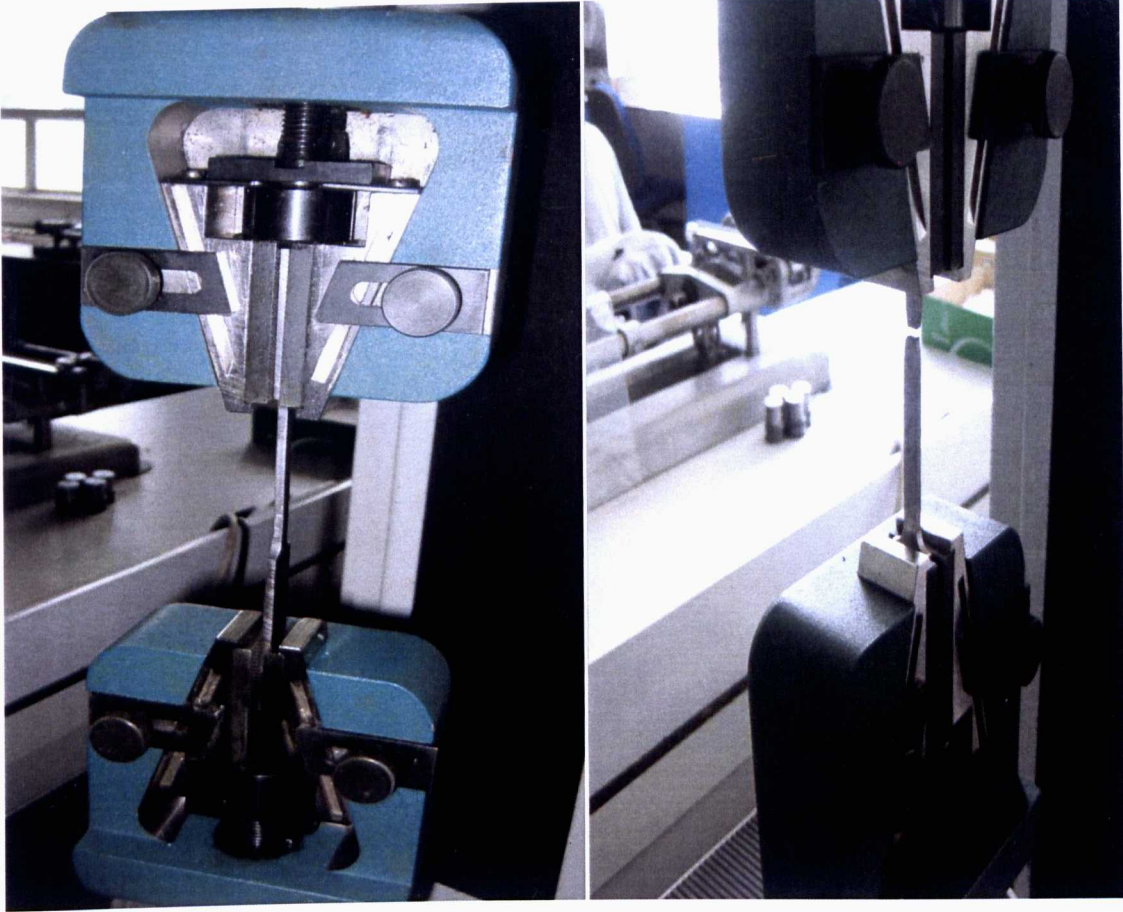
Flat Spring



Workpiece Holder

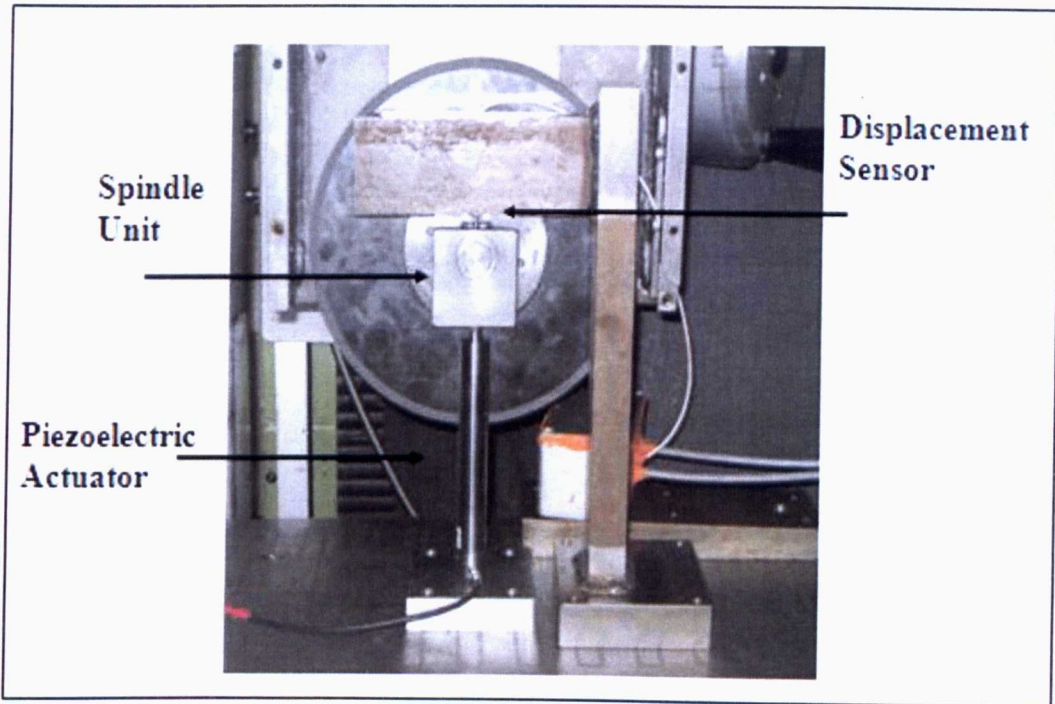


B6- Tensile Test

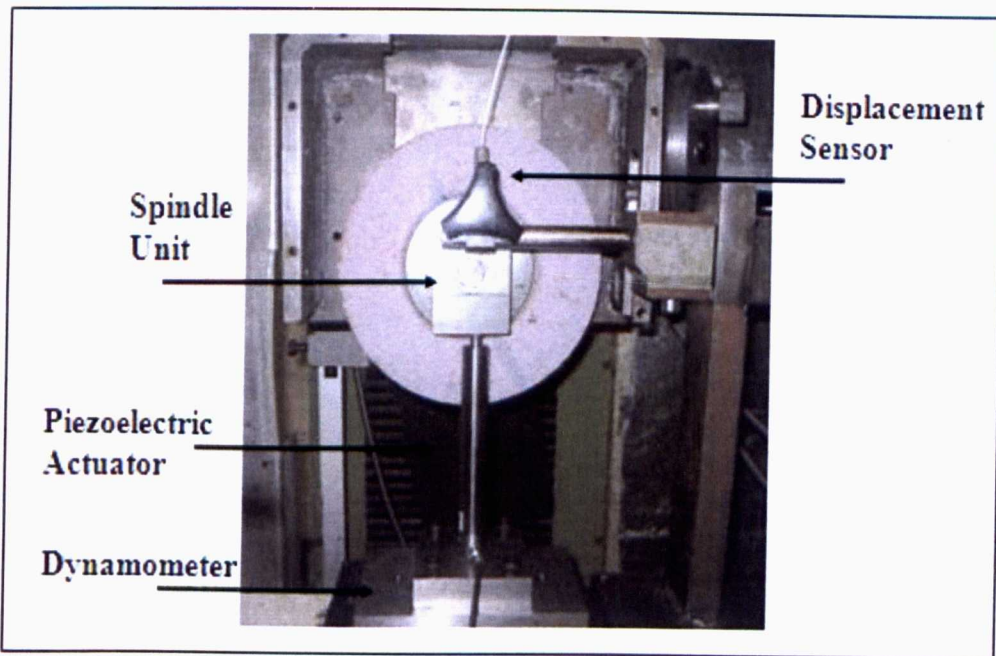


APPENDIX - C

C1-Sweep-Sine Test of the Spindle Unit

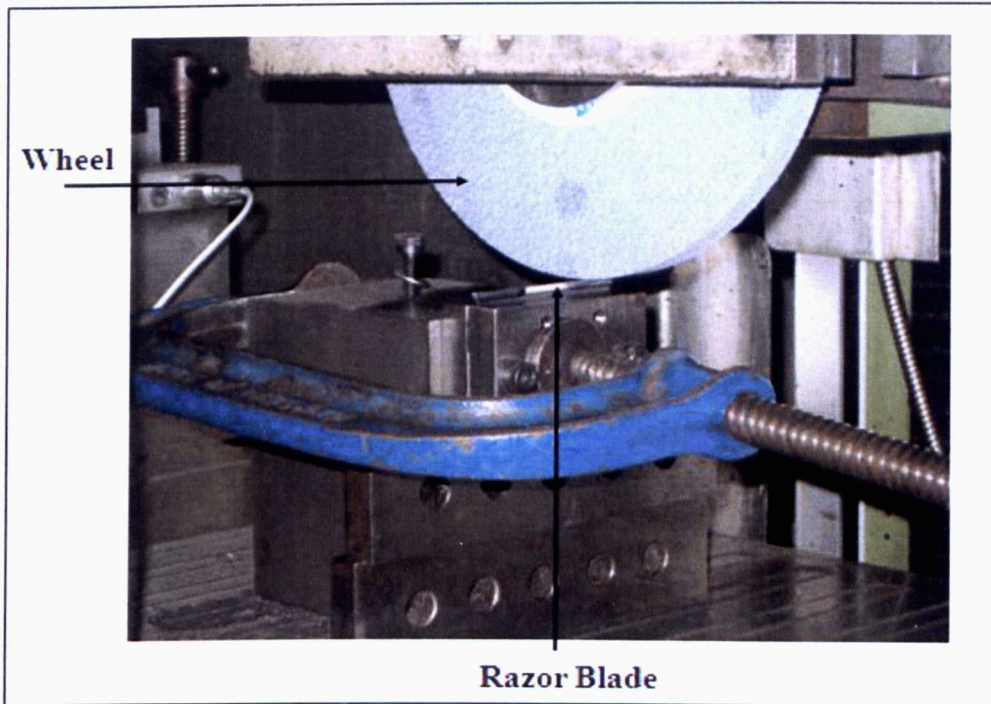


C2- Dynamic Stiffness Test Configuration

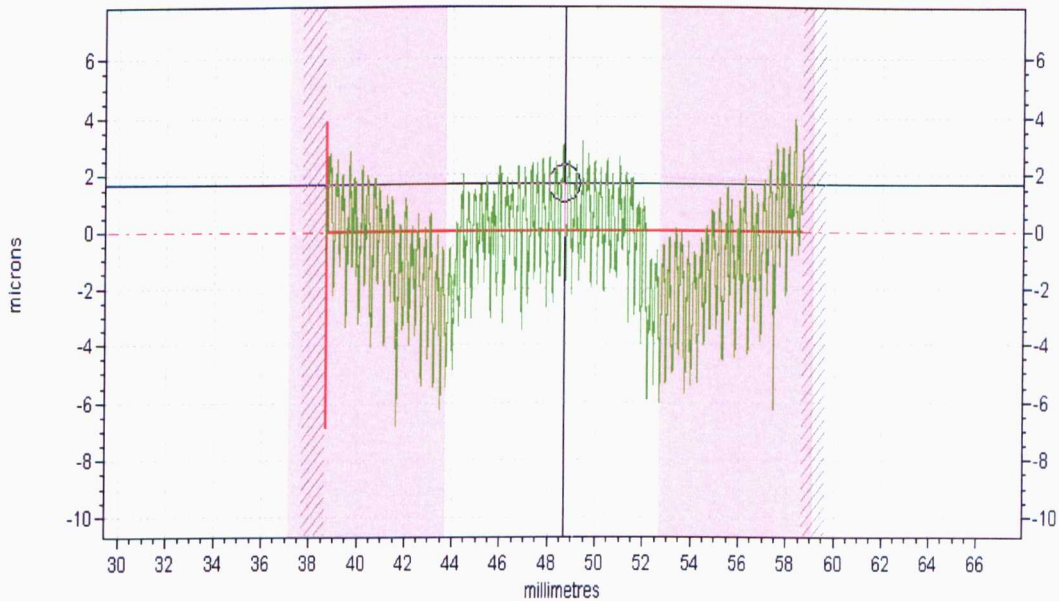


APPENDIX - D

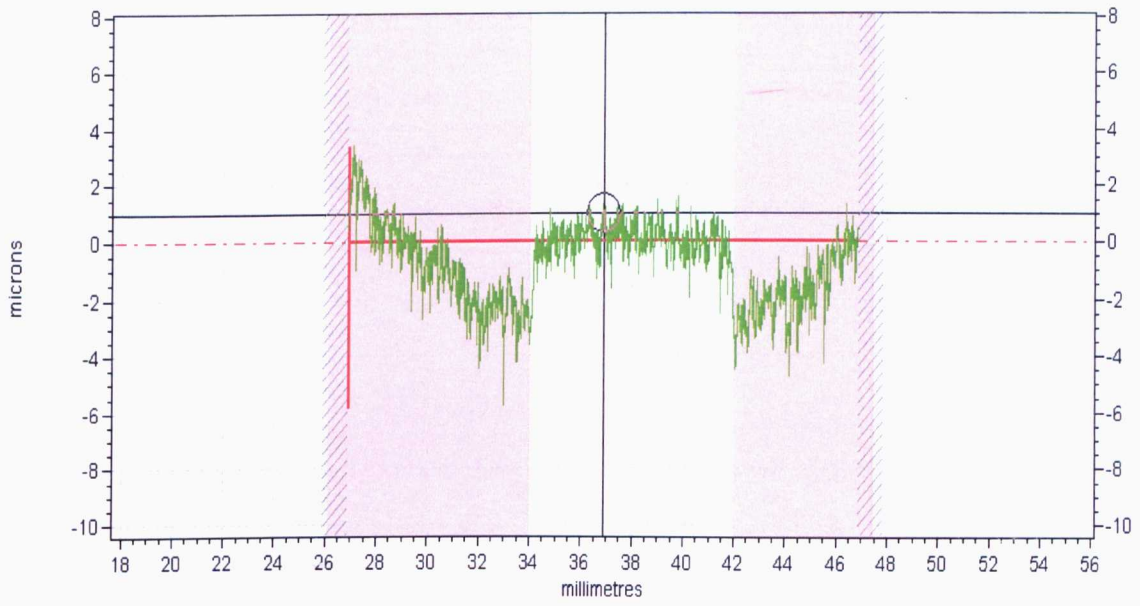
D1- Wheel Wear Test



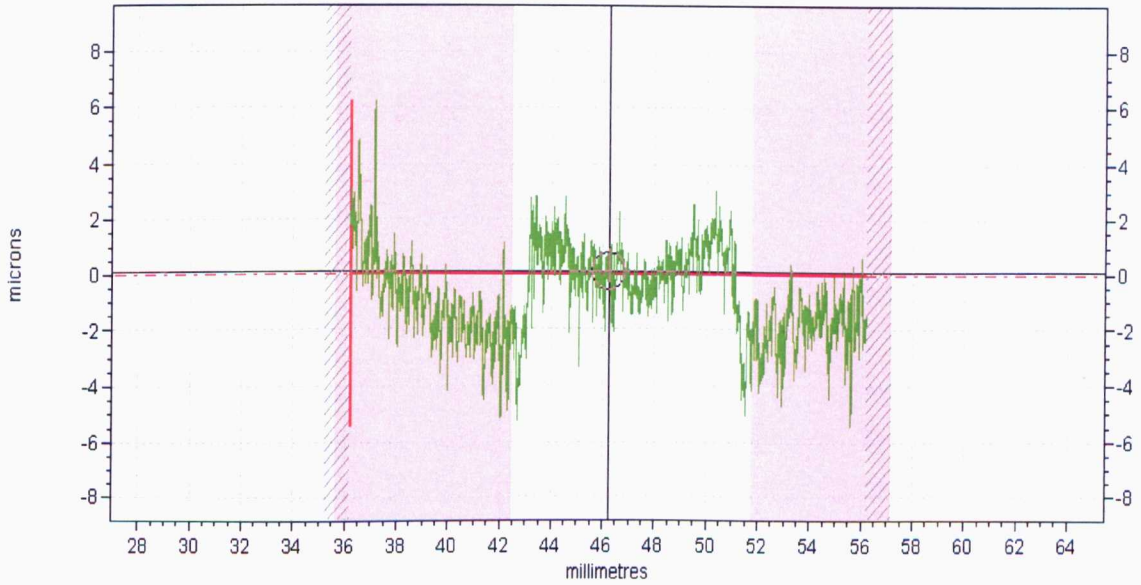
D2-Raw Profile of the Razor Blade

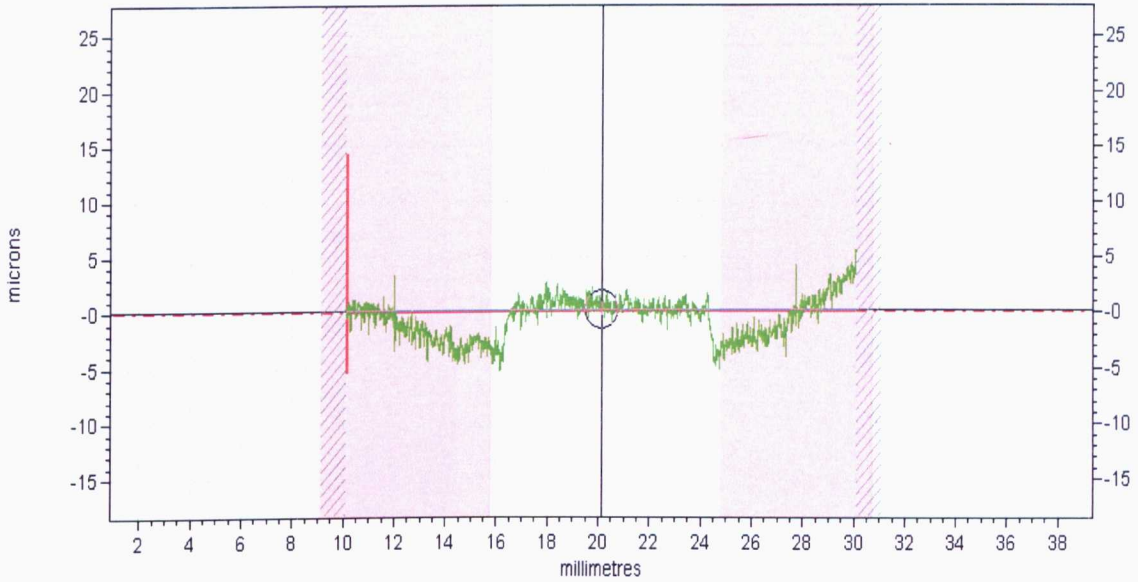
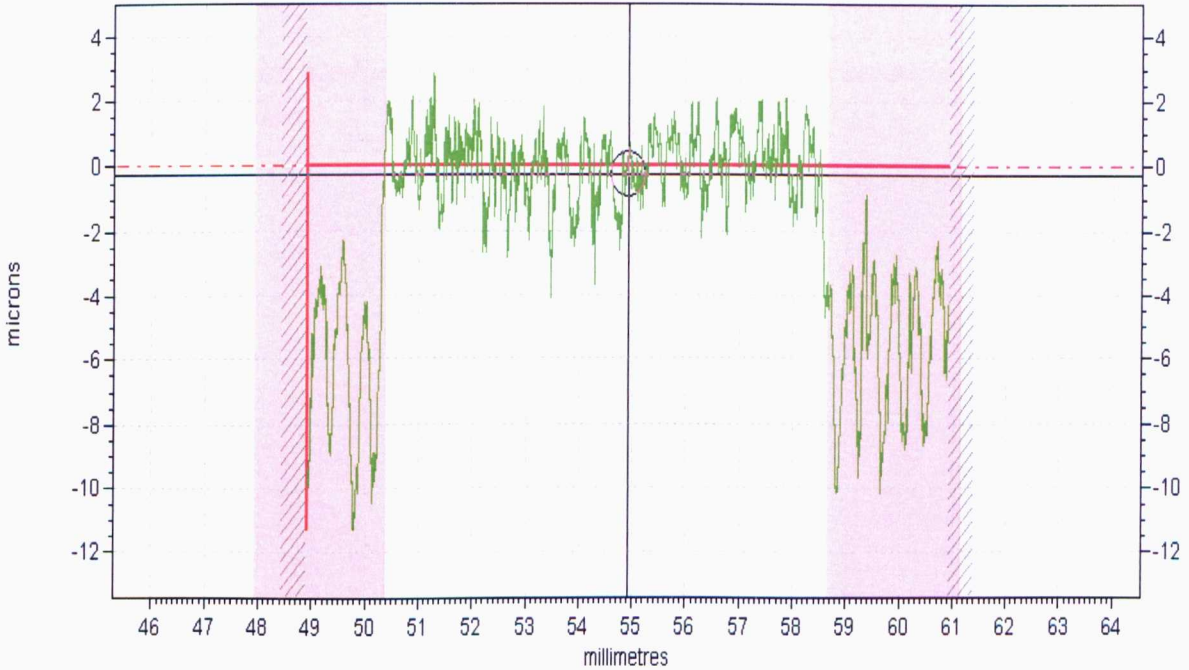
Altos Wheel-M2 Workpiece Material-No Vibration

Altos Wheel-M2 Workpiece Material-With Vibration

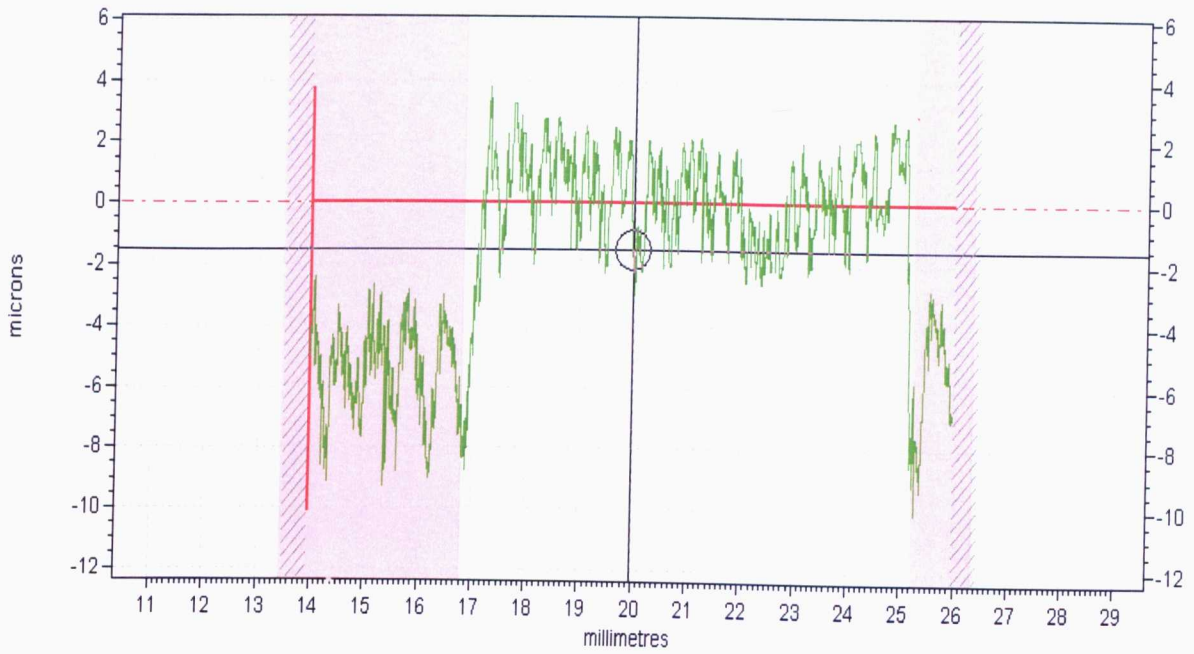


Altos Wheel-Mild Steel Workpiece Material-No Vibration

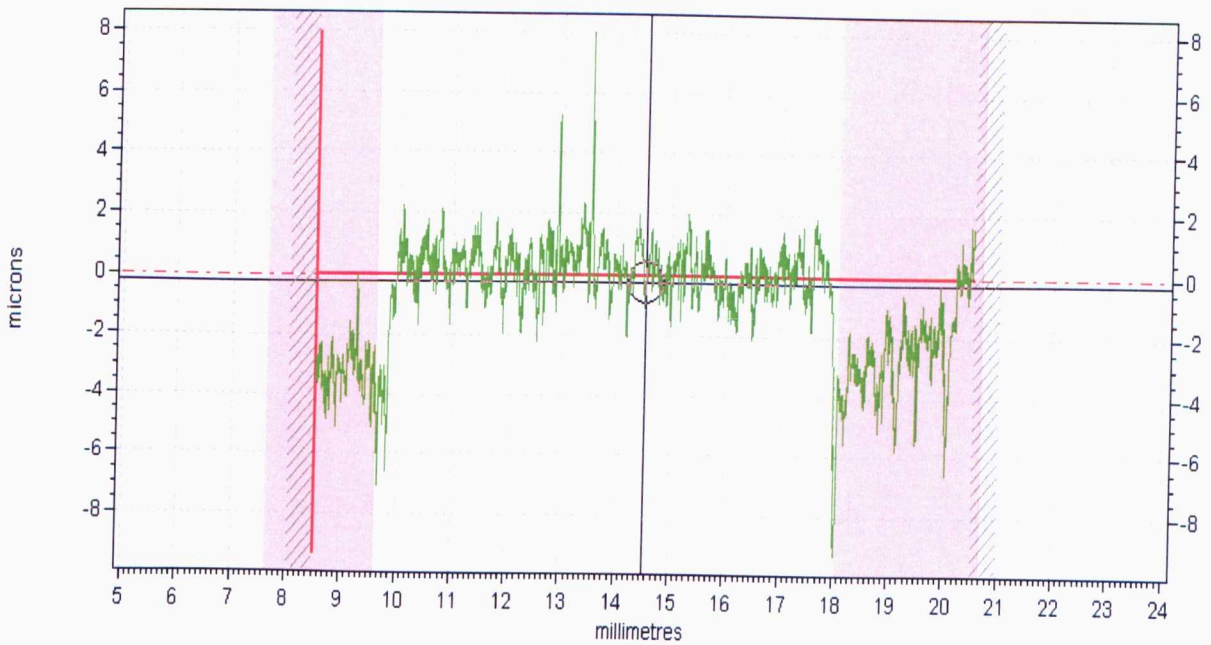


Altos Wheel-Mild Steel Workpiece Material-With Vibration*Al₂O₃ Medium Grain, Medium Grade (454A 601 L 7G V 3) Wheel-M2 Workpiece Material-No Vibration*

*Al₂O₃ Medium Grain, Medium Grade (454A 601 L 7G V 3) Wheel-M2 Workpiece
Material-With Vibration*



*Al₂O₃ Medium Grain, Medium Grade (454A 601 L 7G V 3) Wheel-Mild Steel Workpiece
Material-No Vibration*



*Al₂O₃ Medium Grain, Medium Grade (454A 601 L 7G V 3) Wheel-Mild Steel Workpiece
Material-With Vibration*

